

HIGHLY TUNABLE AND DEGRADABLE NANOGELS FOR DRUG DELIVERY

HIGHLY TUNABLE AND DEGRADABLE HYDROPHOBIZED NANOGELS FOR THE
INTRANASAL DELIVERY OF POORLY-WATER SOLUBLE ANTIPSYCHOTIC DRUGS
TO THE BRAIN

By MADELINE JENNA SIMPSON, H.B.Sc, B.A.Sc

A Thesis Submitted to the School of Graduate Studies in Partial Fulfilment of the
Requirements for the Degree Ph.D. of Chemical Engineering

McMaster University

© Copyright by Madeline Jenna Simpson, September 2020

McMaster University DOCTOR OF PHILOSOPHY (2020) Hamilton, Ontario (Chemical Engineering)

TITLE: Highly Tunable and Degradable Hydrophobized Nanogels for the Intranasal Delivery of Poorly-Water Soluble Antipsychotic Drugs to the Brain

AUTHOR: Madeline Jenna Simpson, H.B.Sc., B.A.Sc. (University of Ottawa)

SUPERVISOR: Professor Todd R. Hoare

NUMBER OF PAGES: xxvi, 288

Lay Abstract

Nanogels are soft, deformable polymer networks swollen in water with potential for drug delivery given their easy-to-tune physicochemical properties. However, the poor water solubility of many therapeutics, including antipsychotic drugs (APDs) used to treat schizophrenia, limits drug encapsulation within nanogels. In addition, conventional synthetic techniques produce materials that degrade into poorly-defined byproducts, causing toxicity concerns. This thesis presents novel strategies to incorporate hydrophobic domains and biodegradable bonds within poly(oligo ethylene glycol methacrylate) (POEGMA) nanogels. We demonstrate how these moieties affect nanogel swelling, degradability, cytocompatibility as well as the uptake and release of clinically prescribed APDs. Intranasal (IN) administration of drug-loaded nanogels is studied as a non-invasive delivery alternative to improve drug bioavailability. The proposed nanogel-based drug delivery systems can decrease drug dose, minimize adverse side effects, and improve patient adherence to therapeutic regimens relying on APDs, demonstrating their potential for clinical application.

Abstract

Nanogels are soft, deformable networks of cross-linked polymer swollen in water. Nanogels have the unique ability to swell in response to external physiological conditions. Their stimuli-responsive nature affects degradability, drug uptake and release, which can be exploited to create tunable drug delivery systems. The ability to alter the composition and structure of nanogels imparts advantageous characteristics for targeted drug delivery applications.

Antipsychotic drugs (APDs) used to treat schizophrenia, a chronic neuropsychiatric disorder, are typically hydrophobic. Prolonged dosing causes neurological and metabolic side effects due to the systemic administration of drug. Patient adherence to APD administration is low, causing complications that contribute to the substantial burden of disease. APDs would benefit from nanogel encapsulation through improved solubility and controlled release kinetics to reduce the adverse side effects associated with typical administration protocols.

This thesis presents the development of hydrophobized, biodegradable poly(oligoethylene glycol methacrylate) (POEGMA)-based nanogels to deliver APDs to the brain. Both an adaptation of conventional precipitation polymerization as well as a

spontaneous self-assembly technique are utilized to synthesize nanogels containing different hydrophobic domains. Incorporation of cross-linkers with different modalities of biodegradability enable stimuli-responsive degradation and drug release. The effects on nanogel swelling, biodegradability, and APD uptake and release kinetics are explored *in vitro*. The preclinical application of these APD-loaded nanogels is evaluated using the minimally invasive intranasal (IN) route for delivery. We show that these nanogel delivery systems have therapeutic effects in terms of significantly altering a range of rodent behaviours, including locomotion inhibition, the onset of catalepsy, and improvement in pre-pulse inhibition, over extended periods of time in relation to current administration strategies.

These drug-loaded nanogel delivery systems show potential to minimize the effective therapeutic dose by enhancing APD bioavailability via IN administration, thus reducing adverse outcomes and improving potential patient adherence to APD-based therapies in clinical use.

Acknowledgements

When I started grad school at McMaster, I did not anticipate finding myself surrounded by such a wonderful community that would support not only my research endeavours, but also provide many memorable personal moments. There are so many people who have made my journey incredible and I hope these words do justice to the immense gratitude I feel to everyone who has played an integral part in this degree.

I am incredibly grateful Dr. Todd Hoare opened the doors to his research group to me. He has been a fantastic graduate supervisor – encouraging, supportive and full of wisdom and advice. Dr. Hoare facilitated an abundance of opportunities that have enriched my grad school experience; I truly appreciate his willingness to promote my professional and personal development. From conferences and workshops to outreach and leadership, every year has consisted of a series of exciting events and milestones I continuously looked forward to. I appreciate his kindness (including pulling my luggage across Aachen, Germany while I travelled with a broken arm), his scientific insight (when I couldn't quite figure out an experimental issue), and his generosity (I have somehow managed to dip my toes in both the Atlantic and Pacific Oceans while attending conferences to present my research).

My graduate work would not have been possible without a wonderful collaboration with Dr. Ram Mishra and his research group. It has been a tremendous privilege to work with a knowledgeable and experienced expert in the field of neuroscience. I am grateful for Dr. Mishra's constructive input during committee meetings and willingness to facilitate a productive collaboration. The support from his graduate students (Ashley Bernardo, Brendan Fera, Judy Tran, Fahed Abu-Hijelh and Elvira Meleca) was crucial to the success of the projects I have undertaken. I am grateful for their advice, assistance and for spending hours in the CAF with me!

Dr. Robert Pelton has been an invaluable member of my supervisory committee. I have been lucky to receive suggestions and feedback from an immensely talented polymer and particle scientist. He approached my work with a unique perspective and often asked questions or suggested experiments that touched on a distinct aspect I had not yet considered, which led to further research and an enriched understanding of what I was studying. Thank you for your perceptive comments!

The Department of Chemical Engineering is full of impressive faculty, many of whom have played formative roles in my graduate school experience. I am incredibly grateful to Dr. Carlos Filipe, the department chair for the majority of my studies, who provided me with the opportunity to teach ChE 3L02. Thank you for trusting me with a course and enabling

me to contribute my own small piece to the education of the undergraduate students. I have also worked with many great professors and sessional instructors through my various teaching assistant positions; Dr. David Latulippe, Dr. Fran Lasowski, Dr. Prashant Mhaskar, Dr. Darko Ljubic, Dr. Heather Sheardown and Dr. Drew Higgins were all wonderful supervisors who helped me to develop my leadership, communication and technical skills as I undertook various roles as a lab, marking and tutorial TA. Dr. Jake Nease has also been a fantastic mentor and kind friend as I have navigated grad studies, TAs and my foray into teaching. Thank you all for your support and guidance – teaching and working with undergrads has been amongst my favourite activities as a grad student!

The support staff within Chem Eng has been vital to my grad school journey. Tim Stephens is a fantastic undergraduate lab coordinator and I enjoyed working in the undergrad lab as both a TA and an instructor. In particular, teaching 3L would not have been possible without Tim's patient guidance and tremendous work ethic. Mike Clarke is an instrument fixing wizard and I am grateful for the many, many times he repaired, replaced or resurrected a machine or computer. His technical expertise also enabled 3L to run smoothly and his quick response to issues has been invaluable. Doug Keller has been an incredible resource as a lab manager and I am very grateful for his health and safety knowledge, and the fact that if he can't fix a problem, he knows the person on campus who can! Our departmental office is full of smart, friendly and funny ladies who know how to get a job done! Linda Ellis was helpful on innumerable occasions – sending packages across borders, booking rooms and fixing the many errors in my expense reports. Michelle Whalen was always on top of scholarship applications to ensure the best possible chances of securing new funding and making sure that all my graduate milestones were complete and up to date. Kristina Trollip was my go-to for anything involving finances – from grad pay, to allocating funds for student-run conferences and events, she was always generous with her time and the funds she provided! Thank you all for making the little details easily and seamlessly come together!

This brings me to the most overwhelming group of people I have to express my gratitude to – my peers, who quickly became my friends and in many cases, my teammates. I was introduced to Emilia Paron during my interview and she was the final piece of the puzzle that convinced me to join Dr. Hoare's group. Her immense passion and genuine enthusiasm about her research and the group still resonate with me today. Emilia imparted so much practical advice - she encouraged me to say yes to every opportunity presented to me; whether it was attending and presenting at conferences, volunteering for info nights or participating on ChEGSS, she always wanted to be helpful and involved. She is a wonderful friend and continues to provide me with so much insight and perspective. I had the good fortune to be mentored by Daryl Sivakumaran upon joining

the lab. Daryl is force of good wherever he is found – in the lab he is proficient and helpful, as a friend he is inclusive and funny, and as a teammate, you’re glad he is not your opponent! Daryl was an impeccable mentor during my first several months in the lab – I watched him balance research, thesis writing, sports and activities alongside friendships and family, with what appeared to be ease, but what I now know to be immense thoughtfulness. I have aspired to embody that same approach and I am grateful to have had the opportunity to learn from such a talented individual. I was lucky to be given a desk next to Scott Campbell – a great researcher, hilarious friend with diverse music tastes and owner of some of the most ridiculous novelty items I have ever seen. His close proximity in the office meant he was my default question answerer, and I relied on him and trusted him to give me honest, direct feedback on pretty much everything that came to mind in the office. Scott was the biggest promoter of intramural sports, specifically innertube water polo and softball, and trivia nights and I am grateful for all his efforts to include me in activities that have given me some of my best grad school memories! Trevor Gilbert rounds out this cohort of Ph.D. students who contributed to my formative years in the Hoare group. Trevor is a genuinely kind and thoughtful person whose puns, memes and gifs have made me belly laugh on too many occasions to count. I have immensely enjoyed all the cottage weekends he hosted each summer and all the cookies he baked and shared! Thank you for trying to help me become a softball player, even though it was a lost cause, and always looking out for the best interests of everyone around you!

It has truly been a privilege to work alongside some astoundingly talented individuals, particularly the intelligent women I am lucky to call friends. My “polymer girls” Emilia, Stephanie Kedzior and Sabrina Hogson made days a bit brighter and the workload feel a bit lighter with every trip to Starbucks. Steph has an incredible work ethic and her commitment to achieving her best with whatever she undertakes is one of the most admirable qualities about her. She motivates me to excel at all that I do and I loved making lots of incredible memories with her from Sweden to Calgary. Sabrina is a beautiful soul – I watched her face immense challenges head on and act with grace while dealing with some of life’s toughest moments. Her goofy sense of humour and sweet attitude always makes me smile and I feel so grateful for her friendship. Kelli-anne Johnson and Nicola Muzzin are two of my dearest friends and I love that we share mutual passions outside of school and work. From going to yoga, barre and lyrical dance classes, I have loved sharing so much of what makes me happy with the two of you. Ridhidhi Dave brought fresh perspective and a keen attitude to our group. I am particularly grateful for our evening walks and ice cream dates that gave me a break and distraction while writing my thesis during a pandemic. Finally, my grad school experience has been tremendously positively influenced by my friendship with Eva Mueller, my conference buddy, travel companion, hair stylist and so much more. She has consistently been a bright ray of sunlight as we have navigated multiple cities, countries and research adventures together. Grad school

would not have been half as fun without her friendship and I know she will continue to be a kind and helpful leader within the Hoare lab as she pursues her Ph.D.

The Hoare lab has been home to a fantastic (and sometimes rowdy) group of smart, outgoing (gentle?)men. Jonathan Dorogin was a tremendously thoughtful and helpful friend who kindly devoted a lot of time to helping me with laborious experiments. His perspective on life and knowledge on the most unique topics have taught me a lot. Ali Babar also provided an immense amount of time and extensive support while developing behavioural models and despite the hard work, it was always fun working alongside him and I am grateful for his immeasurable patience. Ali Affar was a constant source of chemistry support and his unique sense of humour provided excellent entertainment during our hallway hangouts. Matt Campea brought wonderful positive energy and a sense of optimism to both our research lab and his work as a TA in 3L. His great attitude made it easy to work alongside him. Doren Singh's baking creations certainly rival some of my own, which I think is because he is such a great chemist! Michael Kiriakou has been a pleasure to work alongside in our lab pod and I am constantly motivated by his work ethic (and his no-nonsense approach to getting people to complete their cleaning tasks)! Nate Dowdall and Andrew Lofts have been wonderful, hard-working additions to our lab in recent years. I graduate knowing that under their careful maintenance, all three of our freeze dryers may actually work simultaneously one day!

The Hoare lab has also been lucky to host a great group of post-docs during my tenure as a grad student. Although Niels Smeets was only there for a short time at the beginning of my degree, he taught me a lot of great chemistry and provided the foundation for many of the materials I worked with! Lukas Sadowski was a great chemist and even better conference buddy. He definitely did the bulk of the work kayaking while I pointed at seals popping up in the Pacific Ocean! Somiraa Said was extremely kind and generous with her time and was always willing to work through an experiment design problem or provide advice. Xiaoyun Li is very organized and thoughtful and I have been grateful for her help in tackling stubborn drug release!

The grad students in McMaster's Chem Eng department have always been a fun group to socialize with. I was lucky to befriend many neighbours across the hall in the Sheardown lab. Cheryl Bachan, Alysha Spadafora, Nicole Amaral and Mitch Ross have been great scientific buddies and I am grateful for the many small ways they have contributed to this thesis, from lending equipment and chemicals, to keeping me entertained during long synthesis and purification days, and sharing lots of motivation and support! Ryan LaRue has also been a great office buddy – we've exchanged a lot of soup, baked goods, recipes and great conversation between our cubicles in the office. I also enjoyed serving on ChEGSS alongside many students who I would not have otherwise had the opportunity to

meet and work with – it was always very fun planning and attending events and I will miss many of our traditional activities that marked each season and semester! Serving on the PolyMac organizing committee was another great way to meet grad students in different departments that I would not have otherwise gotten to know and it was a wonderful conference that brought so many people together!

The work in this thesis would not have been possible without the hard work and diligence of two tremendous young women – Ana Arezina and Ugonwa Echendu. I am touched that Ana trusted me as a supervisor, for not only one, but three summers! Her willingness to try things, eagerness to learn and great attitude brought a lot of this work to fruition. Ugonwa's friendly demeanor brought great energy to the lab. Her impressive work ethic, organization, and meticulous approach to completing her thesis truly made an abundance of difference to the work we completed together. Many, many undergrads have passed through this research group during my tenure and I have always enjoyed the energy and excitement they have brought to our work!

The friendships that have evolved during grad school have given me some of my best memories over the last several years. Meeting Sarah Biberhofer, Christine Gabardo, Laura Nease, Diane Sivakumaran, and Devon Jones, I think mostly through Chem Eng sports teams, brought a lot of fun activities, weekend's away and special celebrations together. Biebs has been a great, supportive friend, even recently from the far away island of Scotland, although I have missed her on too many occasions to count since she has moved. Christine's kindness, ability to empathize, and the fact that she is always ready for a spin class followed by brunch has kept me going (and healthy!) whenever I needed a pick me up. Diane's love for all things kitty cat and sparkly, and willingness to go the extra mile to make things special and memorable is truly unmatched. I couldn't ask for a more genuine and thoughtful friend than Laura - her wit, humour and outgoing personality are qualities I admire more than anything. Devon Jones was my soccer teammate for a nanosecond (before we both succumbed to major injuries in summer 2018), and then I was lucky to have her on my team of TAs during 3L. Not only was she a really hard worker in the lab, I have learned that follows her everywhere, including our outdoor, safely physically-distanced pandemic workouts, that brought me much needed movement, fresh air and accountability to not stay glued to my desk chair. My friends from undergrad have remained a constant source of support throughout my Ph.D. Trips back to Ottawa to see Zoe Reaume have been welcomed breaks on many occasions and I always appreciate her hospitality and our time spent together. I somehow managed to follow Jennifer Klowak from Ottawa to Hamilton/McMaster and end up as her neighbour (mostly because she helped me find a place to live). From baking, to studying, to working out together, not much has changed since our undergrad days (besides our acquired pets!) and having a friend close by as soon as I moved really helped me to get to know my new

home. Perrine Corman has been truly supportive over the years and I have great memories from the summer she spent in Hamilton! Jane Lian and Tracy Debi, who have been my friends since high school (well over a decade now!), have always been my closest confidantes and can make me laugh over just about anything. We've been on a lot of fantastic trips together that have helped me escape the rigours of grad school and return with fresh perspective. Every opportunity to get together, especially when we have lived cities, provinces or countries apart, has brought me a lot of joy!

My grad school journey would not have possible without support for my amazing family. My sister Fiona is a trailblazer and she has always motivated me to pursue my goals. I admire her intelligence and I am grateful for the helpful guidance she provided me while contemplating my decision to attend grad school. My Mom and Dad have consistently been my biggest supporters throughout my Ph.D. (and life). I am grateful that their home is always open to me as a welcoming sanctuary. From the home cooked dinners and laundry facilities they provided every Sunday evening, their babysitting services for my cat Biff whenever I travelled, and their constant willingness to listen to me talk about struggles and challenges I needed to get off my chest, I could not have been successful in grad school without them. They have provided me with much needed perspective on many occasions and I am so lucky to have parents who believe in me against all odds. I love you so much and could not have completed this degree (or the two before that led me here) without you!

Table of Contents

Lay Abstract.....	iii
Abstract.....	iv
Acknowledgements.....	vi
Table of Contents.....	xii
List of Figures	xv
List of Tables.....	xix
List of Abbreviations and Symbols.....	xxii
Declaration of Academic Achievement.....	xxv
Chapter 1 : Introduction	1
1.1 Schizophrenia.....	1
1.2 Preclinical Pharmacological Models of Schizophrenia.....	12
1.3 Antipsychotic Drugs	20
1.4 Administration of APDs.....	29
1.5 Nanoparticles for Targeted Drug Delivery to the Brain	45
1.6 Thesis Objectives.....	63
1.7 References.....	67
Chapter 2 : Evaluating the Therapeutic Efficacy and Biological Transport of Hydrophobized Poly(oligoethylene glycol methacrylate)-Based Nanogels for the Delivery of Lurasidone	82
2.1 Abstract.....	83
2.2 Introduction	84
2.3 Experimental	88
2.4 Results and Discussion	96
2.5 Conclusions	111
2.6 Acknowledgements.....	112
2.7 References.....	113

Chapter 3 : Degradable, Hydrophobized Poly(oligoethylene glycol methacrylate)-Based Nanogels for Intranasal Delivery of Haloperidol to the Brain	118
3.1 Abstract	119
3.2 Introduction	120
3.3 Experimental	126
3.4 Results and Discussion	134
3.5 Conclusions	153
3.6 Acknowledgements.....	154
3.7 References.....	155
S3.1 Supporting Information.....	161
Chapter 4 : Narrowly Dispersed, Degradable, and Scalable Poly(oligoethylene glycol methacrylate)-Based Nanogels via Thermal Self-Assembly	163
4.1 Abstract	164
4.2 Introduction	165
4.3 Experimental	171
4.4 Results and Discussion	177
4.5 Conclusions	197
4.6 Acknowledgements.....	200
4.7 References.....	201
S4.1 Supporting Information.....	207
Chapter 5 : Thermally Self-Assembled Poly(oligoethylene glycol methacrylate)-co-Poly(oligolactic acid methacrylate) Nanogels for the Intranasal Delivery of Olanzapine to the Brain.....	217
5.1 Abstract	218
5.2 Introduction	219
5.3 Experimental	226
5.4 Results and Discussion	239
5.5 Conclusions	264
5.6 Acknowledgements.....	265
5.7 References.....	266
S5. Supporting Information.....	275

Chapter 6 : Conclusions and Future Work	278
6.1 Summary and Conclusions	278
6.2 Future Work	283

List of Figures

Chapter 1: Introduction

Figure 1.1: Prevalence of schizophrenia by country	2
Figure 1.2: Model of schizophrenia showing genetic and environmental contributions to its pathophysiology and expressed symptoms.....	4
Figure 1.3: Neurotransmitter pathways and receptors regulating the dopaminergic system	9
Figure 1.4: Chemical structures of first and second generation antipsychotic drugs used to treat schizophrenia.	28
Figure 1.5: Intranasal (IN) drug delivery showing direct transport to the brain and indirect transport to systemic circulation.	38
Figure 1.6: Drug delivery pathways through the nasal epithelium to the brain.	41
Figure 1.7: Summary of possible pathways drugs and/or nanoparticles may traverse to reach the brain and/or circulation.....	44
Figure 1.8: Nanoparticles used for the delivery of APDs.	51
Figure 1.9: <i>In vitro</i> performance of PNIPAM nanogels for olanzapine delivery	62
Figure 1.10: Synthesis of poloxamer-407-co-AMPS nanogels and <i>in vitro</i> dissolution behaviour	62

Chapter 2: Evaluating the Therapeutic Efficacy and Biological Transport of Hydrophobized Poly(oligoethylene glycol methacrylate)-Based Nanogels for the Delivery of Lurasidone

Figure 2.1: Logarithmic intensity-based size distribution from DLS of (A) BMA nanogels or (B) MMA nanogels containing different mol% of hydrophobic comonomer (0-15%).	98
Figure 2.2: Degradation and stability of EGDMA cross-linked 10% BMA nanogels.	102

Figure 2.3: Particle size distribution of nanogels incubated in mimics of physiological conditions using nanoparticle tracking analysis (NTA).	103
Figure 2.4: SH-SY5Y neuronal cell viability measured via an MTT assay	104
Figure 2.5: Locomotor activity of male Wistar Hans rats dosed 1.33 hr prior to movement tracking.....	108
Figure 2.6: Biodistribution of Cy5 fluorescently-labeled 10% BMA nanogels administered intranasally at a concentration of 15 wt%	111
Chapter 3 : Degradable, Hydrophobized Poly(oligoethylene glycol methacrylate)-Based Nanogels for Intranasal Delivery of Haloperidol to the Brain	
Figure 3.1: Logarithmic intensity-based particle size distribution (from DLS) of 10% BMA nanogels fabricated using varying ratios of M(EO) ₂ MA:OEGMA ₅₀₀	138
Figure 3.2: Transmission electron microscopy image (magnification 100 000×) of 0.1 wt% 10% BMA 100:0 nanogel stained with 1% uranyl acetate.	139
Figure 3.3: Degradation of 10% BMA 100:0 nanogels measured by DLS	141
Figure 3.4: Characterization of nanogels after 24 hour exposure to various mimics of physiological conditions using (A) nanoparticle tracking analysis (NTA) and (B) gel permeation chromatography (GPC).....	143
Figure 3.5: Cumulative <i>in vitro</i> release of HLP from 10% BMA 100:0 nanogels.....	146
Figure 3.6: Nanogel cytotoxicity to SH-SY5Y neuronal cells	148
Figure 3.7: Locomotor activity of rats over a 2.5 hour period.....	150
Figure 3.8 Cataleptic response following intranasal administration of haloperidol	153
Figure S3.1 Stability of 10% BMA 100:0 nanogels measured by DLS at 37°C over 12 h.....	162

Chapter 4 : Narrowly Dispersed, Degradable, and Scalable Poly(oligoethylene glycol methacrylate)-Based Nanogels via Thermal Self-Assembly

Figure 4.1: Lower critical solution temperature behavior of 1 wt% POA, POH, NIPAM-Ald and NIPAM-Hzd polymer solutions in DIW.....	179
Figure 4.2: Effect of POH polymer content on nanogel diameter and polydispersity (1 wt% core pre-polymer solution concentration).	183
Figure 4.3. Effect of self-assembly temperature (at the core pre-polymer LCST, 5°C above the core pre-polymer LCST, and 10°C above the core pre-polymer LCST) on nanogel diameter and polydispersity (1 wt% core pre-polymer solution concentration).....	187
Figure 4.4. Effect of core solution concentration (0.5 or 1 wt%, POH or POA core) on nanogel diameter and polydispersity	189
Figure 4.5. Representative example of the effect of the cross-linker:core ratio on the diameter of 1 wt% POH core nanogels assembled at 10°C above the LCST of the core POH polymer	191
Figure 4.6. Component weightings of average diameter (red), standard deviation of average diameter (green), and polydispersity (blue) from Principle Component Analysis of the response variables.	192
Figure 4.7: Contribution of different reaction composition and condition parameters on the diameter of self-assembled nanogels.....	194
Figure 4.8: Suspensions produced by scaling up of three different synthetic conditions	196
Figure 4.9: Logarithmic intensity-based nanogel size distribution of small (6.5 mL - red) and large (50 mL - green) batches of self-assembled 1 wt% POH core and 0.2 wt% POA cross-linked nanogels produced at 10°C above the core polymer LCST.	197
Figure S4.1: Logarithmic intensity-based size distributions of self-assembled nanogels prepared using the latent variable model-predicted synthetic conditions to minimize the overall polydispersity.	214

Figure S4.2: Transmission electron microscopy image (120 000× magnification) of self-assembled 1 wt% POH core/0.2 wt% POA cross-linked nanogels produced at 10°C above the core polymer LCST 215

Figure S4.3: Nanogel particle size distributions measured using DLS (1 wt% POH core/0.2 wt% POA cross-linked nanogels produced at 10°C above the core polymer LCST).....216

Chapter 5: Thermally Self-Assembled Poly(oligoethylene glycol methacrylate)-co-Poly(oligolactic acid methacrylate) Nanogels for the Intranasal Delivery of Olanzapine to the Brain

Figure 5.1: Lower critical solution behaviour of nanogel precursor polymers..... 241

Figure 5.2: Physiochemical properties of self-assembled nanogels..... 244

Figure 5.3: Accelerated degradation of self-assembled nanogels..... 247

Figure 5.4: Characterization of intact nanogel and degraded nanogels using nanoparticle tracking analysis (NTA)..... 248

Figure 5.5: Comparison of molecular weights of nanogel precursor polymers and degradation products..... 249

Figure 5.6: Characterization of degraded nanogels at intracellular pH using nanoparticle tracking analysis (NTA)..... 251

Figure 5.7: Comparison of nanogel diameter (from DLS) before (empty nanogel: P0, P4 and P8) and after olanzapine loading (P0-OLZ, P4-OLZ, P8-OLZ) 254

Figure 5.8: Cumulative *in vitro* release of olanzapine in different physiologically-relevant conditions..... 256

Figure 5.9: Cytotoxicity of precursor polymers and nanogels to SH-SY5Y cells 257

Figure 5.10: Pre-pulse inhibition in MK-801-induced rat models of schizophrenia 261

Figure S5.1: Nanogel degradation and stability monitored using DLS 276

Figure S5.2: Multimodal intensity-based size distributions at t=0 h (solid line) and t=12 h (dashed line) (from DLS) 277

List of Tables

Chapter 1: Introduction

Table 1.1: Physicochemical properties of first and second generation antipsychotic drugs used to treat schizophrenia. 29

Chapter 2: Evaluating the Therapeutic Efficacy and Biological Transport of Hydrophobized Poly(oligoethylene glycol methacrylate)-Based Nanogels for the Delivery of Lurasidone

Table 2.1: Chemical synthesis of nanogels containing different mol% ratios of BMA and MMA. 90

Table 2.2: Effective particle diameter, polydispersity (PD) (from DLS) and electrophoretic mobility (from PALS) of nanogels containing various amounts of BMA comonomer 97

Table 2.3: Effective particle diameter, polydispersity (PD) (from DLS) and electrophoretic mobility (from PALS) of nanogels containing various amounts of MMA comonomer..... 97

Table 2.4: Drug loading capacity (DLC) and encapsulation efficiency (EE) of lurasidone in nanogels prepared with 0-15 mol% BMA or MMA..... 99

Chapter 3: Degradable, Hydrophobized Poly(oligoethylene glycol methacrylate)-Based Nanogels for Intranasal Delivery of Haloperidol to the Brain

Table 3.1: Effective diameter (from DLS) and electrophoretic mobility (from PALS) of 100:0 POEGMA nanogels prepared with various amounts of BMA comonomer 136

Table 3.2: Effective diameter (from DLS) and electrophoretic mobility (from PALS) of 100:0 POEGMA nanogels prepared with various amounts of MMA comonomer 137

Table 3.3 Effective diameter (from DLS) and electrophoretic mobility (from PALS) of 10% BMA nanogels prepared with varying POEGMA monomer ratios 137

Table 3.4: Drug loading capacity (DLC) and encapsulation efficiency (EE) of haloperidol in BMA and MMA nanogels as a function of their hydrophobic comonomer content..... 144

Table 3.5: Drug loading capacity (DLC) and encapsulation efficiency (EE) of haloperidol in 10% BMA nanogels as a function of their OEGMA₅₀₀ contents..... 145

Table S3.1: Chemical synthesis of BMA nanogels.....	161
Table S3.2: Chemical synthesis of MMA nanogels.....	161
Chapter 4: Narrowly Dispersed, Degradable, and Scalable Poly(oligoethylene glycol methacrylate)-Based Nanogels via Thermal Self-Assembly	
Table 4.1: Chemical characterization of linear polymer precursors.....	179
Table 4.2: Comparison of nanogel diameter and polydispersity achieved via small scale (6.5 mL) and large scale (50 mL) self-assembly conditions	197
Table S4.1: Hydrodynamic diameters and size distributions of 0.5 wt% POH core nanogels.	2097
Table S4.2: Hydrodynamic diameters and size distributions of 0.5 wt% POA core nanogels.	21008
Table S4.3: Hydrodynamic diameters and size distributions of 1.0 wt% POH core nanogels.	21109
Table S4.4: Hydrodynamic diameters and size distributions of 1.0 wt% POA core nanogels.	2120
Table S4.5: Optimized synthetic conditions to produce nanogel populations with desired size and population distributions.....	2141
Table S4.6: Comparison of predicted versus actual particle sizes and polydispersities of nanogels assembled using model-predicted optimal recipes for each optimization case studied.	2142
Table S4.7: Optimized synthetic conditions to produce nanogel populations with desired size and population distributions.....	214
Table S4.8: Comparison of predicted versus actual particle sizes and polydispersities of nanogels assembled using model-predicted optimal recipes for each optimization case studied.....	214

Chapter 5: Thermally Self-Assembled Poly(oligoethylene glycol methacrylate)-co-Poly(oligolactic acid methacrylate) Nanogels for the Intranasal Delivery of Olanzapine to the Brain

Table 5.1: Physicochemical properties of linear POEGMA polymers.....	242
Table 5.2: Dynamic light scattering (hydrodynamic diameter/polydispersity) and phase analysis light scattering (electrophoretic mobility) measurements of self-assembled nanogels.....	244
Table 5.3: GPC characterization of molecular weight (number average M_n) and dispersity (\bar{D}) of untreated precursor polymers and nanogel degradation products after 24 hours of treatment with 100 mM HCl.....	249
Table 5.4: Drug loading capacity (DLC) and encapsulation efficiency (EE) of olanzapine in P0, P4 and P8 nanogels.....	253
Table S5.1 Recipes of POH-OLAMA polymers containing 20 mol% OLAMA.....	273

List of Abbreviations and Symbols

¹ H-NMR	Proton nuclear magnetic resonance
AA	Acrylic acid
ADH	Adipic acid dihydrazide
Ald	Aldehyde
AIBMe	2,2-azobisisobutyric acid dimethyl ester
AMP	Amphetamine
AMPS	2-acrylamido-2-methylpropane sulfonic acid
AMT	Absorptive-mediated transport
ANOVA	Analysis of variance
APD	Antipsychotic drug
APO	Apomorphine
ATRP	Atom-transfer radical polymerization
BBB	Blood-brain barrier
BCS	Biopharmaceutical Classification System
BMA	Butyl methacrylate
CDCl ₃	Deuterated chloroform
CMT	Carrier-mediated transport
CNS	Central nervous system
CSF	Cerebrospinal fluid
Cy5	Cyanine5
Đ	Dispersity
DA	Dopamine
DALY	Disability-Adjusted Life Year
DIW	Deionized water
DLC	Drug loading content
DLS	Dynamic light scattering
DMAEMA	2-(dimethylamino)ethyl methacrylate
DMAEMAm	<i>N</i> -(2,2-dimethylaminoethyl)methacrylamide
DMEMAm	<i>N</i> -(2,2-dimethoxyethyl)methacrylamide
DMEM	Dulbecco's Modified Eagle's Medium-high glucose
DOX	Doxorubicin
DSM	Diagnostic & Statistical Manual of Mental Disorders
DTT	D,L-dithiothreitol
EDC	<i>N</i> '-ethyl- <i>N</i> -(3-dimethylaminopropyl)-carbodiimide
EE	Encapsulation efficiency
EGDMA	Ethylene glycol dimethacrylate
EPS	Extrapyramidal symptom
FBS	Fetal bovine serum

FDA	Food and Drug Administration
GABA	γ -aminobutyric acid
Glu	Glutamate
GPC	Gel permeation chromatography
GSH	Glutathione
HCl	Hydrochloric acid
HEDSDA	2-hydroxyethyl disulfide diacrylate
HLP	Haloperidol
HPLC	High performance liquid chromatography
Hzd	Hydrazide
ICD	International Classification of Diseases
IM	Intramuscular
IN	Intranasal
IP	Intraperitoneal
IV	Intravenous
KCl	Potassium chloride
KCPS	Kilocounts per second
KPS	Potassium persulfate
LAI	Long-acting injectable
LCST	Lower critical solution temperature
logP	Hydrophobic partitioning coefficient
LUR	Lurasidone
MBA	<i>N,N'</i> -methylene bisacrylamide
M(EO) ₂ MA	Diethylene glycol methacrylate
MK-801	Dizocilpine
MMA	Methyl methacrylate
MTS	3-(4,5-dimethylthiazol-2-yl)-5-(3-carboxymethoxyphenyl)-2-(4-sulfophenyl)-2H-tetrazolium
MTT	3-(4,5-dimethylthiazol-2-yl)-2,5-diphenyltetrazolium bromide
M _n	Number average molecular weight
M _w	Weight average molecular weight
MWCO	Molecular weight cutoff
NaCl	Sodium chloride
NaOH	Sodium hydroxide
NHS	N-hydroxysuccinimide
NMDA	<i>N</i> -methyl-D-aspartate
NP	Nanoparticle
NTA	Nanoparticle tracking analysis
OLAMA	Oligo(lactic acid methacrylate)

OLB	Olfactory bulb
OLZ	Olanzapine
O(M)NE	Olanzapine (mucoadhesive) nanoemulsions
ORN	Olfactory receptor neuron
NMR	Nuclear magnetic resonance spectroscopy
PO	POH nanogel
P4	POH-OLAMA ₄ nanogel
P8	POH-OLAMA ₈ nanogel
PALS	Phase aligned light scattering
PAMAM	Polyamidoamine
PBS	Phosphate buffered saline
PCL	Poly(ϵ -caprolactone)
PCP	Phencyclidine
PDI	Polydispersity index
PEG	Poly(ethylene glycol)
PET	Positron emission tomography
PLS	Projection to latent structures
PISA	Polymerization-induced self-assembly
PFC	Prefrontal cortex
PLGA	Poly(lactic-co-glycolic acid)
PNIPAM	Poly(<i>N</i> -isopropylacrylamide)
PO	Per os (oral)
POEGMA	Poly(oligo ethylene glycol methacrylate)
POA	Aldehyde-functionalized POEGMA
POH	Hydrazide-functionalized POEGMA
PPI	Pre-pulse inhibition
RAFT	Reversible addition-fragmentation transfer
RMT	Receptor-mediated transport
SDS	Sodium dodecyl sulfate
SLN	Solid lipid nanoparticle
TEM	Transmission electron microscopy
TGA	Thioglycolic acid
UCST	Upper critical transition temperature
UV-vis	Ultraviolet-visible
VPTT	Volume phase transition temperature
WHO	World Health Organization
YLD	Years Lived with Disability

Declaration of Academic Achievement

The majority of the work presented in this thesis was designed, executed, analysed, interpreted and written by the author, in consultation with Dr. Todd Hoare, with the exception of the following:

Chapter 2: Brendan Fera and I executed the locomotion behavior experiments together; we both contributed to the development of the behavioural model including drug dosing, timeline of data collection as well as data analysis and interpretation. Jonathan Dorogin and Ashley Bernardo led the organ excision work for the biodistribution study, with support from CAF staff, and Jonathan Dorogin also helped prepare the tissue samples for fluorescent analysis. Fahed Abu-Hijelh contributed to tissue sectioning and aided in the execution of the cell viability study. Dr. Niels Smeets provided the synthetic procedure for nanogel synthesis that was adapted to create the implemented formulations.

Chapter 3: Ugonwa Echendu synthesized and characterized the various nanogel formulations and conducted preliminary drug loading studies as part of her undergraduate thesis. Ali Babar assisted in the execution of the pharmacodynamics studies. Dr. Niels Smeets provided the recipe and protocol for the synthesis of the disulfide cross-linker as well as the original recipe/protocol for the 15 mol% hydrophobic comonomer nanogels.

Chapter 4: Ana Arezina aided in polymer synthesis, conducted self-assembly reactions and collected the corresponding characterization data on the assembled nanogels. Dr. Brendan Corbett performed the multivariate statistical analysis and led the writing of the relevant sections of the manuscript.

Chapter 5: Ana Arezina contributed to polymer synthesis and characterization of polymers. She also conducted preliminary self-assembly reactions and characterization of the resulting nanogels. Judy Tran assisted with the execution of the cell viability studies.

Chapter 1 : Introduction

1.1 Schizophrenia

1.1.1 Epidemiology

Schizophrenia is a universally occurring, chronic, debilitating neuropsychiatric disorder. Globally, the prevalence of schizophrenia is approximately 0.3-0.7 % of the population (Figure 1.1);¹⁻² with the number of cases increasing from 13.1 million in 1990 to 20.9 million in 2016.³⁻⁴ There is a substantial burden on patients, caregivers and society associated with this disease, causing it to rank as the 12th most disabling disease out of 310 disorders and injuries examined in a 2016 study.¹ The onset of schizophrenia is typically in late adolescence to early adulthood with equal rates of occurrence in men and women, although men tend to present at a younger age with more severe symptoms.⁴⁻⁵ Schizophrenia is characterized by a group of complex symptoms, none of which are pathogenic; however, the chronic nature and difficulties in effectively managing the disease result in afflicted individuals having higher rates of comorbid illnesses such as heart and respiratory diseases, stroke, diabetes and cancer. As such, a diagnosis of schizophrenia leads to a decreased life expectancy of ~10 years.^{4, 6-7}

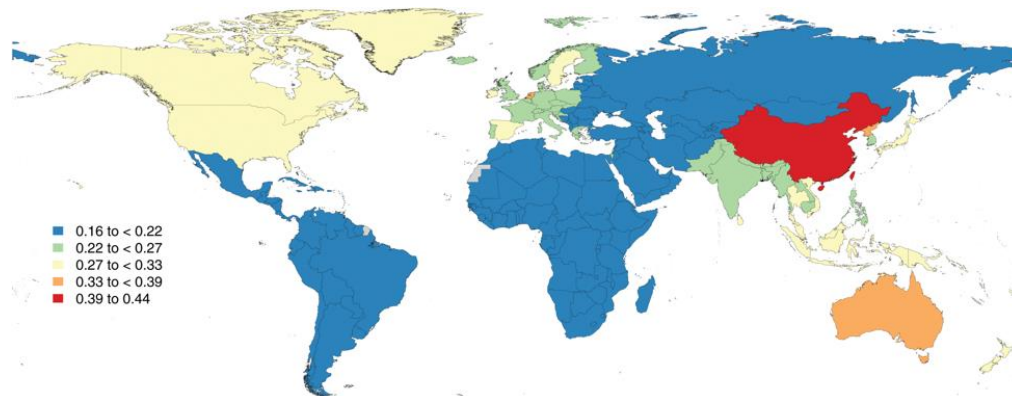


Figure 1.1: Prevalence of schizophrenia by country. Adapted with permission from Charlson et al., 2018 [4].

1.1.2 Economic Burden of Disease

The substantial economic impact of schizophrenia can be attributed to the characteristics of the disease; its early onset, chronic nature, symptomology, typically low adherence to treatment regimens, and high rate of disability all contribute to its costly burden. ⁶ Even when patients have access to the best combination of treatments available, including medication, therapy and rehabilitation, approximately two-thirds of the afflicted population experience persistent and fluctuating symptoms, leading to high levels of mental and social disability.¹ In this context, maintenance of a normal lifestyle is challenging; frequent hospital admissions, early retirement, and excess mortality all contribute to the economic impacts of disease. The Global Burden of Disease Study determined that schizophrenia accounts for 1.1% of disability-adjusted life years (DALYs), making schizophrenia the eighth leading cause of DALYs worldwide in individuals aged 15-

24 according to the World Health Organization (WHO).⁶ Schizophrenia also contributes to 2.8% of years lived with disability (YLD) which is equivalent to 13.4 million YLD.¹

This high level of disability results in large direct and indirect costs associated with schizophrenia. The WHO estimates that schizophrenia accounts for 1.6-2.6% of total healthcare expenditures globally.² In Canada, the direct healthcare costs associated with providing care for afflicted individuals amounted to 2.02 billion CAD in 2004 while the indirect costs (such as loss of productivity, disability, unemployment, premature death, and burden on caregivers) was estimated to be 4.83 billion CAD.⁸ The disease burden associated with schizophrenia is expected to escalate in Canada as the population grows and life expectancy increases, unless effective treatments can be developed.⁴

1.1.3 Pathophysiology

Schizophrenia is a complex disease influenced by genetic, neurodevelopmental, and environmental factors. The exact mechanisms and pathways determining the disease physiology have not been fully elucidated at this time due to the extensive and complex circuitry present within the brain. Risk factors for schizophrenia include brain injury, drug use, prenatal infection, malnutrition, social isolation, and marginalization.⁹ Early onset detection and diagnosis of schizophrenia is challenging as there is no biological test or psychometric trait marker available for screening due to its polygenic transmission and locus heterogeneity.^{3, 9} However, the social, motor and cognitive developmental

trajectory in children does show some correlation in individuals who later develop schizophrenia (Figure 1.2).^{3,6} Currently, physicians rely on the diagnostic criteria outlined in the Diagnostic and Statistical Manual of Mental Disorders (DSM, Version 5, 2013) and the International Classification of Diseases (ICD, Version 11, 2018).

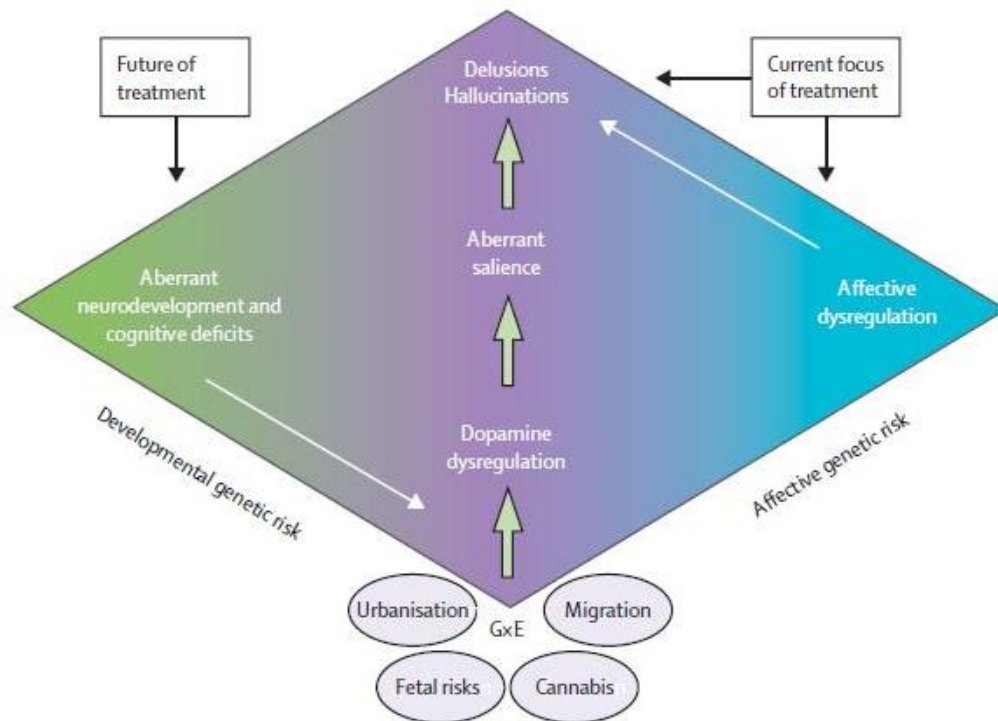


Figure 1.2: Model of schizophrenia showing genetic and environmental contributions to its pathophysiology and expressed symptoms. Affective dysregulation and aberrant neurodevelopment and cognitive deficits both directly and indirectly contribute to the occurrence of schizophrenia. Adapted with permission from van Os and Kapur, 2009 [2].

Dopamine Hypothesis

The dopamine hypothesis, initially proposed by Van Rossum, postulates that an increase in central dopamine neurotransmission produces the psychotic symptoms of schizophrenia.¹⁰ This hypothesis was based on the discovery in the early 1950s that

neuroleptic drugs were able to suppress psychotic symptoms.¹¹⁻¹⁴ By 1974, dopamine implication in the physiology of schizophrenia was ascertained when the antipsychotic activity of neuroleptic drugs was attributed to the blockade of dopamine D₂ receptors due to a high level of receptor occupancy in patients treated with different APDs.¹⁵⁻¹⁶ The dysregulation of dopamine within the brains of patients with schizophrenia is attributed to two outcomes: (1) dopamine supersensitivity; and (2) over-activity of dopamine transmission. Both drug-naïve and treated patients show supersensitivity to dopamine-like compounds compared to healthy control subjects.¹⁷ Treatment with dopamine agonists or dopamine-releasing compounds (such as amphetamine) cause the presentation of psychotic behaviours that closely resemble the symptoms associated with schizophrenia.¹⁸⁻¹⁹ Positron emission tomography (PET) studies of schizophrenia patients actively experiencing episodes revealed the release of more endogenous dopamine when patients were treated with amphetamine compared to both individuals in clinical remission and healthy controls,²⁰ further supporting the hypothesis.

The overarching rationale that this hypothesis relies upon is that dopamine dysregulation within the brain contributes to both the symptoms embodied by individuals with schizophrenia as well as the treatment outcomes elicited by neuroleptic drugs. As schizophrenia presents with diverse symptomology, the dysregulation hypothesis has expanded to explain the occurrence of positive, negative and cognitive changes.

Hyperactive dopamine transmission through the mesolimbic pathway of the brain is associated with the positive symptoms; psychosis is linked with an increased release of dopamine in the subcortical regions with high densities of D₂ receptors such as the striatum and basal ganglia, as observations of individuals with schizophrenia during a psychotic episode have concluded that there are higher levels of D₂ receptor occupancy within the striatum compared to healthy controls.^{18-19, 21}

Elevated levels of dopamine receptors have also been proposed as the cause of increased dopamine activity.¹⁸ In comparison to healthy controls, striatal dopamine D₂ receptor densities have been observed to be elevated by 5.8% in drug-naïve patients and persist in patients with a long duration of illness who have undergone chronic treatment with APDs.^{18, 22} As D₂ receptor agonists induce comparable psychotic symptoms and antagonists mitigate psychotic episodes, D₂ receptor occupancy is clearly implicated in the regulation of the positive symptoms of schizophrenia.^{21, 23} However, treatment with drugs that have a high affinity for dopamine D₂ receptors does not sufficiently address the negative or cognitive symptoms of schizophrenia, suggesting that there are alternative molecular targets involved.^{9, 19}

Currently, the negative and cognitive symptoms of schizophrenia are associated with a hypoactive mesocortical system. Specifically, brain imaging studies have established

hypofunctionality in the prefrontal cortex (PFC),^{21, 24} resulting in decreased neurotransmission due to hypostimulation of the dopamine D₁ receptor and thus decreased subcortical dopamine activity that induces negative symptoms and cognitive deficits.¹⁹ Interestingly, in animal models, simultaneous dopamine hyperactivity in the mesolimbic system and hypoactivity in the mesocortical system can occur. As such, a revised hypothesis suggesting the two activities are concurrently possible is widely accepted today.²⁵ However, the cause of aberrant dopamine activity in the brain has yet to be elucidated, indicating that further investigation is required to fully explain the cause of dopamine dysregulation.

N-methyl-D-aspartate Receptor Hypofunction Hypothesis

N-methyl-D-aspartate (NMDA) receptors are ion channels found throughout the central nervous system (CNS) and are a subtype of glutamate receptors required to modulate glutamate activity.²⁶⁻²⁷ Glutamate is a major excitatory neurotransmitter in the mammalian nervous system²⁸ implicated in influencing behavior, memory, motor function, emotion, and executive functioning,²⁹ all of which are impaired in patients with schizophrenia (and thus indicative of the likelihood of their involvement in the characterization of the disease). Like the dopamine hypothesis, the NMDA hypofunction theory of psychosis is based on observations that the administration of NMDA antagonists such as phencyclidine (PCP) and ketamine triggers psychosis in healthy individuals and exacerbates the symptoms of individuals with schizophrenia.^{9, 30} Models that lack NMDA

receptors also display schizophrenia phenotypes and behaviours.²⁶ The majority of the effects associated with NMDA receptor hypofunction are attributed to deficits in cortical glutamate activity that lead to variations in glutamate signalling and changes in prefrontal connectivity,^{20, 31} inducing both negative and cognitive symptoms of schizophrenia.³² Faulty NMDA receptors in the PFC, anterior cingulate cortex, and/or cerebral cortex allow for excessive glutamate efflux and thus overstimulation of postsynaptic glutamate neurons, subsequently altering the activity of dopamine in the mesolimbic and mesocortical systems³³ to induce the heterogeneous symptomology of schizophrenia.³⁴ As more evidence examining the aberrant behaviour of monoamine molecules and neurotransmitters in patients with schizophrenia is accumulated, the dopamine dysregulation and NMDA receptor hypofunction theories have become intertwined (Figure 1.3).²¹ It has been proposed that dopamine dysregulation contributes to changes in NMDA receptor activity and thus ultimately glutamate transmission, thereby resulting in the spectrum of symptoms embodied in patients with schizophrenia.²⁰

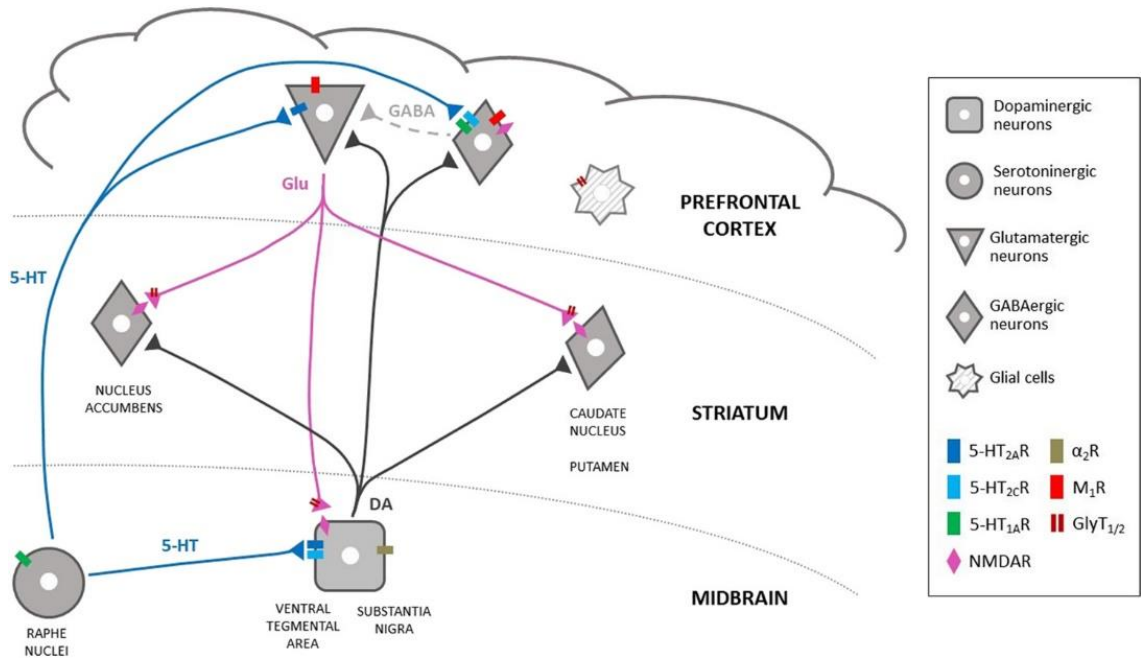


Figure 1.3: Neurotransmitter pathways and receptors regulating the dopaminergic system. Dopamine (DA) transmission from neurons within the midbrain projects to neurons within the striatum and prefrontal cortex. Transmission of γ -aminobutyric acid (GABA, glutamate (Glu), and serotonin (5-HT) influence dopaminergic activity via direct and indirect pathways using glutamatergic, serotonergic, and GABAergic neurons. Muscarinic (M_1R), NMDA (NMDAR), noradrenergic (α_2R), and serotonergic ($5-HT_xR$) receptors as well as glycine transporters ($GlyT_{1/2}$) are expressed in different neuronal populations. Adapted with permission from Aringhieri *et al.*, 2018 [21].

1.1.4 Symptoms

The heterogeneous nature of schizophrenia symptoms can render correct diagnosis challenging, resulting in misdiagnosis or prolonged periods without diagnosis (prodromal period). There are two accepted resources used to diagnose schizophrenia: the Diagnostic and Statistical Manual of Mental Disorders (DSM, Version 5, 2013) and the International Classification of Diseases (ICD, Version 11, 2018). Schizophrenia is diagnosed based on

the presence of positive and negative symptoms as well as cognitive deficits. These clinical manifestations make it difficult for patients to manage emotions, think clearly and relate to those around them, which has a substantial impact on their quality of life.³¹ A psychotic episode typically prompts investigation into the possibility of schizophrenia; however, such episodes are not solely confined to this particular disease. As such, other criteria such as duration, dysfunction, and presence of depression, mania or delusions, as well as associated substance use have to be considered.² Disturbances in cognition, communication, motivation and sleep often precede clinical diagnosis by weeks, months or years.³⁵ However, given that the onset of schizophrenia often coincides with hormonal changes experienced by adolescents and young adults, in the absence of psychosis they are not clinically significant enough to substantiate alternative causes.

Positive Symptoms

Psychotic symptoms and thought disorganization are often grouped under the term positive symptoms.²⁰ These symptoms can include hallucinations (which may be visual, auditory, olfactory or somatic), delusions, paranoia, and disorganized thought and speech.³⁶ Hallucinations are produced by defects in source monitoring; errors in processing result in incorrect attribution of internal sensations to external stimuli. Delusions are caused by vivid, excess thoughts that are mis-attributed to a sense of urgency and certainty, leading to conviction of their validity. Unconventional discourse and poor communication stem from disordered thoughts.⁹ These symptoms often result

in uncontrolled outbursts and ultimately are the behaviours that lead to the pursuit of a clinical diagnosis.

Negative Symptoms

Deficits in normal behaviour are classified as negative symptoms.³⁷ This can include decreased motivation (volition), apathy, and pleasure (anhedonia) as well as changes in social behaviour (withdrawal).²⁰ Deficits in expression, including blunted affect and paucity of speech, are part of this symptomology.^{1, 37} Apathy, avolition and anhedonia are linked to aberrations in reinforced learning caused by the inability to associate value with different rewards.³⁷ Oscillations in mood are associated with social isolation and withdrawal.⁹ Blunted affect can be a lack of displayed feeling or an inappropriate or bizarre response, in both facial expressions and tone of voice, in emotional contexts.^{36, 38} Although these symptoms appear more discrete than the array of positive symptoms, they are amongst the most difficult to effectively treat.

Cognitive Deficits

Cognitive deficits are generally evident years prior to the first psychotic episode but are typically not adequately addressed due to a lack of established protocols for early onset detection.²⁶ Attention and memory problems, alterations to executive functioning and decision-making skills, and perturbed linguistic capabilities are all indicators of reduced cognitive abilities.² Impairments in verbal, visual and working memory can be affected by

processing issues.⁹ Issues maintaining focus and a decreased ability to rationally reason and problem solve often persist even during instances of clinical response or remission. These deficits are the basis for substantial limits on the working and social functioning of patients with schizophrenia.³⁶

1.2 Preclinical Pharmacological Models of Schizophrenia

As schizophrenia presents with an abundance of clinical symptomology, reliable means to reproduce these behaviours are necessary to screen proposed treatments for the disease. Animal models are necessary tools to define the pathogenesis and treat human disease.³⁹ However, it is difficult to create adequate models of complex neuropsychiatric disorders, especially for a disease like schizophrenia in which the etiology and pathophysiology are not fully elucidated.³⁹ It is particularly challenging to produce models with cognitive deficits, since the animals used are less cognitively developed.⁴⁰ Indeed, identifying quantifiable brain phenotypes for drug efficacy and side effects is one of the major challenges in translating psychiatric research between species (ie. from rodents, to monkeys, to humans).⁴¹ Animals models do not exhibit all behavioural abnormalities, just as patients with schizophrenia do not always clinically manifest every symptom of the disease.³⁹ As such, current animal models of schizophrenia should not be considered as the animal equivalent of the human manifestation of the disease but rather a tool useful to test a specific causative or mechanistic hypotheses regarding schizophrenia.⁴⁰ There

are three criteria of validity that an animal model must provide in order to be a relevant disease model: (1) predictive validity describes how well the animal performance aligns with human presentation of schizophrenia, requiring the model to be specific and sensitive to detect pharmacological effects;^{40, 42} (2) construct validity refers to how the model replicates the neurobiological mechanism of schizophrenia, required to provide a sound theoretical rationale for its use,^{40, 42} and (3) face validity, the most challenging criteria to satisfy, examines the similarities in behavioural changes between the model and the disease state, requiring accurate reproduction of the symptoms embodied by humans to be transferred to animal models.^{40, 42} In this context, below we examine the preclinical pharmacological models of schizophrenia that are induced by psychomimetic drugs.⁴² These models have reasonable predictive validity and some construct value but limited face validity, as they use drugs that are known to enhance schizophrenia-like symptoms in rodents based on an understanding of how such drugs alter neurotransmitter systems.⁴⁰ In all cases, administration of these drugs produces certain behavioural changes in rodent models that are both measurable and reversible through intervention with antipsychotic drugs (APDs).⁴²

1.2.1 Dopamine Receptor Agonists

Attempts to model aspects of schizophrenia in animals have primarily focused on drugs that affect the dopaminergic systems.⁴³ Such drugs include amphetamine (AMP) and

apomorphine (APO), two dopamine receptor agonists that enhance dopamine release.⁴⁴ AMP produces psychotic symptoms in humans caused by presynaptic hyperactivity that induces increased dopamine release.⁴⁰ In rodents, AMP is able to mimic the positive symptoms of schizophrenia by causing hyperlocomotion and stereotypy.³⁹ APO also induces hyperlocomotion and other stereotyped behaviours.⁴⁵ AMP and APO have also been used to induce deficits in sensorimotor gating in both humans and rats.⁴⁶ Pre-administration of APDs can reduce hyperlocomotion and restore deficits in PPI induced by either AMP or APO in rodents.⁴⁰

1.2.2 NMDA Receptor Antagonists

As the NMDA hypofunction hypothesis has gained supporting evidence, the use of NMDA receptor antagonists to induce preclinical models has become more common. Such antagonists, including phencyclidine (PCP), ketamine and dizocilpine (MK-801), provide selective, non-competitive receptor antagonism³⁹ that results in the full range of positive, negative and cognitive symptoms of schizophrenia in normal human patients.^{42, 47-48} In humans, PCP causes hallucinations, delusions, social withdrawal, paucity of speech, and impaired cognitive performance.⁴⁴ PCP administration can thus enable the evaluation of positive symptoms using open-field locomotion studies, negative symptoms using social interaction and forced swim test experiments, and cognitive deficits in different maze-based behavioural assays using rodents.⁴⁷ In comparison to AMP, which stimulates

dopamine release from D₂ receptors, PCP produces phenotypically similar positive symptoms but a better mimic of the negative/cognitive symptoms given that PCP antagonism of NMDA receptors reduces glutamate transmission in the PFC and thus contributes to the negative and cognitive deficits.⁴⁰ Ketamine is a derivative of PCP that has diminished toxicity and fewer side effects associated with its use. It is most often used to study cognitive deficits in rodents given that it reduces sensorimotor gating and spatial learning while causing memory impairment due to increased dopamine release in the PFC; however, it does induce hyperlocomotion due to increased dopamine turnover in the striatum and cortex. Atypical APDs can block the effects of ketamine in both rodents and humans.⁴⁷ MK-801 is an analogue of PCP but is more selective and potent than either PCP or ketamine due to its potential to enable a longer blockade of the NMDA receptor ion channel.^{44, 47} MK-801 works preferentially on GABAergic interneurons and disturbs glutamatergic neurotransmission, leading to hyperexcitation in the PFC neural circuit.^{44,47} Systemic administration of MK-801 also stimulates mesolimbic dopamine neurons, causing dopamine efflux within the striatum, medial PFC, and nucleus accumbens.⁴⁹ In rodents, such stimulation results in hyperlocomotion, decreased social interaction, and deficits in sensorimotor gating and memory^{44,46-47} that can be reversed upon administration of a dopamine receptor antagonist due to depletion of dopamine; this reversibility indicates that the behavioral effects of MK-801 are dopamine-dependent despite its strong affinity for NMDA receptors.⁴⁹ In fact, dopamine D₁ and D₂ receptors as

well as serotonin 5-HT_{1A} and 5-HT_{2A} and adrenergic α_1 -receptors are all reported to be involved in MK-801 induced behaviours.⁴³ This broad receptor activity makes MK-801 an excellent option for the investigation of novel APDs with unconventional receptor binding profiles given that it can induce a wide range of schizophrenia-like symptoms in rodents.

1.2.3 Behavioural Studies

Pharmacological preclinical models enable the presentation of characteristic behaviours induced upon administration of a dopamine receptor agonist or NMDA receptor antagonist. Individual rodent behaviours are not complete animal models of schizophrenia; rather, they are experimental studies used to develop and validate animal models of the disease state. Measurable behavioural abnormalities can be quantified directly in rodents due to conservation of the neural circuitry underlying a behaviour between rodents and humans.³⁹ The efficacy of drug formulation pharmacodynamics requires assessment using behavioural testing.⁵⁰ Herein, three different behavioural experiments are presented that are relevant to the drugs studied within this thesis.

Open-Field Locomotion

As patients with schizophrenia can exhibit psychomotor agitation, hyperlocomotion is used as a behavioural test to provide translational relevance to positive symptoms of schizophrenia.^{39, 44} All five of the drugs discussed above are able to induce rodent

hyperactivity that can subsequently be decreased by administration of both typical and atypical APDs.³⁹ As hyperlocomotion is associated with increased dopaminergic activity in the mesolimbic system,⁵¹ some typical APDs such as haloperidol can suppress rodent locomotion in the absence of drug-induced hyperactivity due to their high binding affinity for D₂ receptors.⁵²⁻⁵³ Conversely, drug-induced models of schizophrenia are required to induce hyperlocomotion to show attenuation by atypical APDs, which typically have less affinity for D₂ receptors since their primary mechanism of action involves serotonin (5-HT) receptors.²¹ The advantage of open-field locomotion is that it utilizes chambers equipped with cameras and/or light beams that allow automated tracking of three-dimensional movement, enabling rapid and reliable analysis of rodent behaviour with good reproducibility.⁴² Although it has low face validity, locomotion is a useful test for screening APD treatments in preclinical models of schizophrenia.

Pre-Pulse Inhibition

Pre-pulse inhibition (PPI) is an operational measure of sensorimotor gating that enables regulation of environmental inputs and selectively allocates attentional resources to salient stimuli.⁴⁶ PPI is the normal reduction in the startle response due to exposure to a low intensity non-startling stimulus (pre-pulse) prior to a large startle stimulus (pulse).⁴⁹ As PPI provides an almost identical response in humans and rodents alike, it is a frequently used test due to its cross-species conservation.^{39, 54} PPI is thought to correlate with both

positive symptoms (psychosis and disordered thoughts)⁵⁴ and cognitive deficits (distractability and impaired processing)⁴² associated with schizophrenia because it is the process by which large batches of information can be screened or filtered from one's surrounding.^{39, 49, 54} In healthy individuals (both rodents and humans), pre-exposure to a weak stimulus attenuates the startle response;⁴⁸ deficits in PPI are observed in both treated and drug-naïve patients with schizophrenia⁵⁵ as they are unable to moderate their startle response due to oversensitivity to sensory stimulation, causing overload that correlates with cognitive fragmentation.⁵⁶ In rodents, deficits in PPI can be induced by the administration of either dopamine receptor agonists or NMDA receptor antagonists;^{46, 57} however, the correct pharmacological agent must be selected depending on the APD being tested. Typical APDs are unable to reverse NMDA receptor antagonist deficits in PPI; for example, haloperidol (HLP) cannot reverse MK-801-induced deficits but can restore APO-induced PPI.⁵⁷ Similarly, NMDA receptor antagonism is able to distinguish between typical and atypical APDs.⁴² PPI may be affected by: (1) increased dopamine sensitivity in the mesolimbic system (which regulates whether dopamine receptor antagonism can reverse PPI deficits); or (2) glutamatergic mechanisms (which regulate whether selective antagonism of the NMDA receptor can reverse PPI deficits).⁵⁴ Deficits in sensorimotor gating have been linked to emotional/visceral centers of the limbic system and PFC as well as regions associated with motor control and coordination, like the striatum. In these regions, dopamine and glutamate transmission promote

sensorimotor gating, indicating that different pharmacological models and different APDs can both induce deficits and reverse them, respectively.⁵⁵ Quantification of startle response requires computerized chambers equipped with platforms that can detect movement.⁴² Movement amplitude is monitored for different tests (pre-pulse alone, startle response alone and pre-pulse/startle combined trials) to enable the calculation of startle attenuation.

Catalepsy

Catalepsy is characterized by the inability to initiate voluntary motor activity due to a lack of response to external stimuli. It is embodied as the retention of limbs in whatever awkward or uncomfortable posture they are placed due to muscular rigidity.⁵⁸ Unlike the two abovementioned behavioural tests, catalepsy does not correlate with a schizophrenia-like symptom demonstrated in humans. However, the test does produce a motor side-effect that can predict the probability of a drug to induce Parkinson-like behaviours, correlating with the occurrence of extrapyramidal side effects (EPS) in humans. This test has high predictive validity, making it a reliable tool to examine dosing effects. In addition, the doses administered in rodents that cause APD intervention to move from therapeutic to undesired side effect correlate well with doses that cause extrapyramidal symptoms (EPS) in humans, making catalepsy a good screening tool for monitoring dose-dependent side effects.⁴² Catalepsy testing can also be easily carried out

using very basic equipment consisting of a mounted horizontal bar and a stop watch; the amount of time that a rodent remains in an unperturbed unnatural position is measured and scored, with values >20 s typically indicating the onset of catalepsy.⁵³

1.3 Antipsychotic Drugs

Effective treatment of schizophrenia relies upon four crucial elements: medication (APDs), psychological therapy, rehabilitation, and social support.⁵⁹ Due to the long prodromal period prior to clinical diagnosis, intervention is typically not implemented until significant deterioration has occurred, making it difficult to define a protocol that can restore the prior quality of life of a patient with schizophrenia. Ideally, the goal of treatment should be to identify the neuropsychiatric condition as early as possible, treat the symptoms, provide tools to caregivers for support, maintain/modify intervention to prevent relapse, and reintegrate the patient into society.⁶ APDs are the first line of pharmacological treatment options and are the mainstay for both acute and long-term treatment of schizophrenia given that they reduce symptom severity and hospitalization, and improve socialization and rehabilitation in society.^{1,21,59} Clinical studies evaluate APDs based on their efficacy, quality of life, tolerability, drop out rates, and side effects.²¹ Currently, APDs are split into two groups typical (or first generation) APDs are classified by their chemical structure while atypical (or second generation) APDs are classified according to their pharmacology and are grouped according to their clinical mechanism

of action.^{3, 60} Each APD has a unique receptor binding profile, ability to modify behaviour and side effect profile.⁴¹

1.3.1 Typical Antipsychotic Drugs

Typical APDs have distinctive chemical backbones, with all typical APDs being analogs of phenothiazine, butyrophenone, thioxanthene, dibenzoaxazepine, dihydroindole, or diphenylbutylpiperidine.⁶⁰⁻⁶¹ The commonality shared by drugs in this group is the antagonism of dopamine D₂ receptors being their primary mode of action.⁴¹ Interaction with this receptor correlates with the antipsychotic efficacy of these drugs and is believed to alleviate the positive symptoms of schizophrenia by releasing dopamine into the striatum and increasing presynaptic synthesis.^{16, 41} The extent of D₂ receptor occupancy is a critical characteristic for predicting the treatment outcomes of these drugs; multiple imaging studies suggest 60-70% occupancy provides an optimal therapeutic window but greater than 80% occupancy increases the risk of EPS.^{19, 62} Adverse side effects are also correlated with the rate at which the drug-receptor complex is displaced in response to changes in dopamine levels; slow disassociation prevents dopamine binding and produces insurmountable antagonists contributing to higher incidence of EPS.²¹ Although typical APDs offer potent relief from the positive symptoms of schizophrenia, poor patient compliance due to the adverse side effects associated with both acute and long term use represent key clinical limitations. Parkinsonism is one of the EPS caused by typical APDs, inducing symptoms including resting tremor, muscular rigidity, akinesia, or bradykinesia.

According to the WHO pharmacovigilance database, drug-induced Parkinsonism is the second most common cause of Parkinsonism, with the highest risk associated with APDs acting as dopamine D₂ antagonists; in particular, the first-generation APD haloperidol alone accounted for 9.4% of drug-induced Parkinsonism cases.⁶³ Tardive dyskinesia, an involuntary movement disorder, is also associated with typical APD therapy. This side effect can be irreversible and has a worryingly high incidence rate of 5% per year.⁶⁴ These problematic side effects are also attributed to off-site actions at other receptors⁶⁰ given that dopamine receptors are not just restricted to the CNS but are also present on peripheral organs.²¹ Thus, systemic administration of these drugs can lead to off-target interactions that likely contribute to the problematic side effects. In addition, 25-60% of schizophrenia patients are either largely resistant or only partially responsive to typical APD treatment, further contributing to the low efficacy of typical APDs in treating negative symptoms and deficits in cognition.⁶⁰

Haloperidol

Haloperidol (HLP, 4-[4-(p-chlorophenyl)-4-hydroxypiperidino] 4'-fluorobutyrophenone, Figure 1.4A) is a phenyl-piperidinyl-butyrophenone typical (first generation) APD that was initially clinically prescribed for the treatment of schizophrenia in 1967.⁶⁵ It is currently listed on the WHO List of Essential Medicines for the treatment of psychotic symptoms including schizoaffective and bipolar disorders.⁶⁶ Haloperidol is also prescribed to control motor and verbal tics in individuals with Tourette syndrome. The drug is only prescribed

to children who display hyperactive or explosive, aggressive behaviours. Haloperidol has low solubility and high permeability, resulting in its designation as a class II drug in the Biopharmaceutical Classification System (BCS).⁶⁷ Like most typical APDs, haloperidol's primary mechanism of action is antagonism of the dopamine D₂ receptors found in the mesolimbic and mesocortical systems;⁶⁸ haloperidol is able to compete with endogenous dopamine at the orthosteric site and block excessive dopamine neurotransmission in the brain.⁶⁹ When administered at low doses, haloperidol binds to D₂ receptors and α_1 -adrenergic receptors to modulate positive symptoms; when administered at high doses, haloperidol binds to 5-HT₂ receptors to moderately regulate negative symptoms.^{68,70-71} Haloperidol also has fast binding association and slow dissociation kinetics to striatal D₂ receptors, which are associated with the negative side effects of the drug.^{68, 72} Indeed, there is an extensive list of adverse outcomes associated with haloperidol including both anti-cholinergic effects (e.g. dry mouth, constipation, blurred vision) and cardiovascular effects (e.g. tachycardia, hypo and hypertension, ventricular arrhythmia).⁷³ The most prevalent side effects are neurological and include extrapyramidal symptoms (EPS), Parkinsonism, akathisia and dystonia.⁷⁴ Long-term use is associated with tardive dyskinesia that may persist even after treatment is withdrawn. Haloperidol clearance and degradation can further lead to neurotoxic hepatic metabolites that have increased potency towards causing EPS.^{71, 75} As such, despite its essential role in the management

of psychosis worldwide, haloperidol also suffers from several drawbacks that need to be addressed to improve its safety and efficacy profiles.

For chronic treatment, haloperidol is most commonly prescribed orally (PO) and is commercially available in tablet form as Haldol (Table 1.1). Frequent low doses are typically prescribed to help mitigate side effects.⁷⁶ A slow release form is also available as an intramuscular (IM) injection in the form of haloperidol decanoate which is released over a period of four weeks,⁷⁷ helping to improve adherence to the drug treatment regimen for non-compliant patients. However, the need for an intramuscular injection limits the number of patients that can practically benefit from such a controlled release approach.

1.3.2 Atypical Antipsychotic Drugs

Atypical APDs first evolved as a class of drugs that have alternate chemical structures to typical APDs. As more drugs were developed, this definition expanded to include drugs that have equivalent antipsychotic efficacy without EPS, superior antipsychotic efficacy for treatment resistant patients, or the ability to address the negative and cognitive deficits.⁶⁰ This second generation of drugs can be divided mechanistically depending on the drug's receptor binding profile. Some atypical APDs are powerful antagonists of both dopamine D₂ receptors and serotonin 5-HT_{2A} receptors, while a separate group interacts with these and other neuroreceptors.⁶⁰ Moderate doses of atypical APDs produce higher

5-HT_{2A} receptor occupancy than D₂ receptors,⁴¹ an alternative pharmacological binding profile to typical APDs that is thought to contribute to the lower incidence of Parkinsonism and tardive dyskinesia (the latter of which is 2-10× less for atypical APDs).⁴¹ However, an understanding both the pharmacodynamics and pharmacokinetics of an atypical APD is required to develop the complete therapeutic profile because it is difficult to determine efficacy based on single receptor affinities or receptor affinity ratios.^{21, 41} While the side effects of atypical APDs are generally less severe than those of typical APDs, they still have adverse outcomes associated with their use. In particular, metabolic symptoms including weight gain, hyperlipidemia and increased insulin resistance are prevalent in patients who take atypical APDs, indicating that the diverse receptor binding profile leads to alternative side effects not otherwise seen with only the D₂ receptor antagonism provided by typical APDs.⁷⁸⁻⁷⁹ However, the improved social and cognitive outcomes associated with treatment regimens utilizing atypical APDs indicates that a broader receptor binding profile does have beneficial outcomes that improve the full spectrum of symptoms associated with schizophrenia while also mitigating the adverse neurological side effects.

Olanzapine

Olanzapine (OLZ) is a thienobenzodiazepine compound (2-methyl-4-(4-methyl-1-piperazinyl)-10H-thieno[2,3-b][1,5]benzodiazepine, Figure 1.4B) that is classified as an atypical (second generation) APD. Like haloperidol, it is a BCS class II drug.⁶⁷ Olanzapine is prescribed to individuals diagnosed with schizophrenia as well as bipolar disorder and can

also be used in combination with other medications to treat depression. Olanzapine can simultaneously antagonize dopamine D₁ and D₂ receptors in the striatal tissue of the mesolimbic/mesocortical systems as well as serotonin (5-HT_{2A} and 5-HT_{2C}), muscarinic (M₁), and α_1 and α_2 adrenergic receptors found in the frontal cortex.^{54, 70, 80-82} Olanzapine is able to reduce both positive and negative symptoms due to its wide receptor binding affinity.⁸²⁻⁸⁴ At low doses, olanzapine selectively inhibits behaviours mediated by the mesolimbic and mesocortical systems; at higher doses, it also inhibits behaviours mediated by the nigrostriatal system.⁸⁵ Olanzapine has been clinically prescribed for the treatment of schizophrenia since 1996 and is commercially available as Zyprexa. The optimal therapeutic dose for olanzapine ranges from 20-60 ng/mL, but the recommended daily dose is 10-20 mg.⁸⁶⁻⁸⁷ The discrepancy in values can be attributed to the low aqueous solubility causing poor dissolution in gastro-intestinal fluids coupled with extensive first-pass metabolism and efflux by P-glycoproteins.⁸⁸⁻⁸⁹ The drug's half-life in humans is reported to range between 21-54 hr, which enables steady state concentrations within one week after daily dosing. The most common adverse side effects are metabolic; olanzapine can cause weight gain (leading to obesity), hyperglycemia, dyslipidemia, elevated plasma glucose, triglycerides and liver enzyme levels, and/or diabetes.^{21, 78-79} Although rare compared to first generation APDs, chronic treatment with olanzapine leading to D₂ receptor occupancy >80% can produce highly undesirable negative symptoms such as Parkinsonian-like EPS and an increased risk of tardive dyskinesia.^{21, 70,}

⁸⁶ Olanzapine is also available in a long-acting injectable (LAI) format as a pamoate salt that is administered every two to four weeks as a deep intramuscular injection.⁹⁰ However, like with haloperidol, the need to inject this formulation limits its large-scale practical utility in all but the least compliant/most affected patient populations.

Lurasidone

Lurasidone (LUR, (3aR,4S,7R,7aS)-2-[(1R,2R)-2-[4-(1,2-benzisothiazol-3-yl)piperazin-1-ylmethyl] cyclohexylmethyl]hexahydro-4,7-methano-2H-isoindole-1,3-dione, Figure 1.4C) is an azapirone derivative recently approved for the treatment of schizophrenia.⁹¹ It is an atypical APD and similarly categorized as a BCS class II drug; however, it is much less soluble than either HLP or OLZ, with exceptionally poor aqueous solubility and even minimal solubility in alcohols and other organic solvents (Table 1.1). Lurasidone has a particularly unique receptor binding profile; while it does bind to D₂ receptors, it also has strong affinity for serotonin 5-HT_{2A}, 5-HT₇, and 5-HT_{1A} receptors and noradrenaline α_{2C} receptors.⁹² Interactions with 5-HT_{2A} are thought to minimize D₂ antagonism-induced adverse EPS, while its partial agonist activity of 5-HT_{1A} can have anxiolytic and antidepressant value. Interactions with 5-HT₇ also elicit antidepressant effects in addition to procognitive benefits that are supplemented by its antagonism of α_{2A} receptors.⁹³ These distinctive pharmacological features enable lurasidone to address the full spectrum of schizophrenia symptoms (positive, negative and cognitive). The broad receptor activity also enables lurasidone to be prescribed for the treatment of depression associated with

bipolar disorder, as well as anxiety.⁹² However, the low solubility of lurasidone results in very poor bioavailability after oral administration (9-19%) due to its slow dissolution and poor absorption.³⁶ To enhance absorption, the prescription of Latuda (the oral tablet form of lurasidone) is accompanied with directions to consume with at least 350 kcal of food within 30 min of dosing, a key drawback given that poor compliance to drug dosing regimens is a known challenge of APD therapy.^{36, 94} A wide range of doses (20-160 mg/day) is recommended depending on the patient's age, preferred time of dosing, and extent of illness.⁹⁴ However, if the delivery challenge can be overcome, lurasidone has much more minimal adverse side effects, as only 60% receptor occupancy is needed for therapeutic efficacy but >75% occupancy is required to produce adverse outcomes.⁹⁵⁻⁹⁶ Akathisia and somnolence are apparent dose-related side effects, while nausea, sedation, and Parkinsonism have also been reported.⁹¹ However, there is a substantially lower likelihood that neurological (EPS) and metabolic (weight gain) side effects commonly associated with typical and atypical APDs, respectively, will occur.²¹

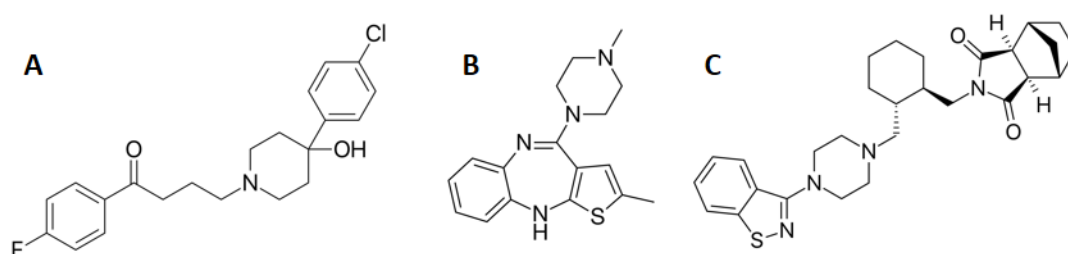


Figure 1.4: Chemical structures of first and second generation antipsychotic drugs used to treat schizophrenia. (A) haloperidol (typical); (B) olanzapine (atypical) and (C) lurasidone (atypical).

Table 1.1: Physiochemical properties of first and second generation antipsychotic drugs used to treat schizophrenia.

	Haloperidol	Olanzapine	Lurasidone
Commercial Name	Haldol	Zyprexa	Latuda
Drug Type	Typical	Atypical	Atypical
BCS Classification	II	II	II
Chemical Formula	C ₂₁ H ₂₃ ClFNO ₂	C ₁₇ H ₂₀ N ₄ S	C ₂₈ H ₃₆ N ₄ O ₂ S
Molecular Weight (g/mol)	375.9	312.4	429.7
Aqueous Solubility (µg/mL)	14	94	8
Log P	4.3	3.6	5.6
Typical Dose	0.5-5 mg/8-12 hr	10-20 mg/day	20-160 mg/day
Bioavailability (%)	60-70	60-65	9-19
Half-life (hr)	14.5-36.7	21-54	18

Despite the unique and varied pharmacological profiles of each of the three APDs described above and summarized in Table 1.1, these and other clinically prescribed APDs only reduce 13% of the disease burden of schizophrenia. Even if patient compliance to regimens showed better adherence, three-quarters of the burden would remain unavoidable based on the extensive limitations of the available therapies. This clearly demonstrates the need to continue to invest in basic and applied research to further elucidate the etiology of the disease in order to advance the efficacy of therapeutic intervention for effective schizophrenia treatment.

1.4 Administration of APDs

1.4.1 Blood-Brain Barrier

The central nervous system (CNS) is comprised of the brain and the spinal cord, two vital and functionally complex regulatory organs,⁹⁷ and is one of the most challenging areas to

effectively and safely access in the body. APDs must enter the brain to produce their desired therapeutic outcome, making schizophrenia difficult to treat given that access to the brain is strictly regulated by the blood-brain barrier (BBB).⁹⁸⁻⁹⁹ The BBB consists of brain capillary endothelial cells connected by tight junctions with no fenestrations and is responsible for maintaining brain tissue health and function as well as protecting against dangerous exogenous materials such as pathogens and toxins.^{97, 100} The BBB acts as a semipermeable interface to regulate the passage of necessary substances from the circulatory system into the brain.¹⁰¹ Access to the brain through the BBB is controlled by the chemical structure of the drug and its ability to bypass efflux pumps.¹⁰⁰ Typically, only small, neutral, lipophilic molecules can freely pass through the BBB, with polar or charged molecules and larger peptides and proteins much less likely to penetrate the BBB given that (1) the tight junctions act as physical barrier to passage of more hydrophilic therapeutics and (2) integrated enzymes within the membrane, such as P-glycoproteins, act as metabolic barriers that can recognize and degrade or pump out larger hydrophobic molecules (300-4000 Da in size).^{98, 102-103} Ultimately, the BBB excludes 98% of molecules from the CNS, severely limiting the ability of drugs and biologics to permeate the brain and provide diagnostic information and/or therapeutic intervention.^{100, 104}

Several transport mechanisms exist across the BBB. Small, non-polar, lipophilic substances can passively diffuse (the reason for their enhanced transportability) while

other lipophilic agents can pass through the endothelial membrane via a transcellular pathway. Typically, APDs rely on this mode of transport to access the brain due to their small size and hydrophobicity. The cells within the endothelial layer of the BBB also possess receptors that aid in the active transport of other nutrients and compounds. Carrier-mediated transport (CMT) can be exploited by chemically modifying drugs to mimic substrates of specific transporters, while receptor-mediated transport (RMT) utilizes vesicular transfer upon recognition of a specific binding ligand to facilitate endocytosis and transcytosis of molecules. In the latter case, specific transport systems exist for essential nutrients like glucose, amino acids, purine bases, nucleosides, and other hydrophilic substances as well as large endogenous molecules such as hormones and lipoproteins; as such, mimics of these molecules as well as prodrug formulations including such molecules can help to enable this route of entry. Adsorptive-mediated transport (AMT) delivers drugs by binding cationic molecules through the electrostatic interactions with the negative charge of the BBB membrane. This is a unique strategy that does not affect endogenous cellular process in the way that other drug delivery strategies might, but is not popular due to off-target effects and toxicity. Although APDs have not been modified to exploit these mediated routes of transport into the brain, they are useful strategies that can be applied to enable the transport of different types of drug carriers across the blood-brain barrier.^{98, 101}

There are several potential drug delivery methods that can be utilized to bypass the highly selective BBB. Perhaps the most obvious option is direct entry to the CNS using an intracranial injection or an intrathecal injection, which places drug solution directly into the cerebrospinal fluid (CSF). However, these techniques are highly invasive must be performed by specially trained personnel to prevent infection and edema. In addition, the formulation must be specifically designed to avoid the use of additives and preservatives that are found in other injectable drugs as it is being introduced into a highly sensitive area.¹⁰² Another drawback is that drugs administered to the CSF are rapidly cleared, thus limiting time for diffusion into the brain.⁹⁸ As such, current intervention with APDs relies on more traditional routes of administration.

1.4.2 Oral drug delivery

Oral (per os, PO) tablets are the most accepted and preferred form of drug administration due to low cost and ease of administration.¹⁰⁵ However, the poor water solubility of most APDs (including those used in this thesis, Table 1.1) limits the rate of dissolution in gastric fluids and minimizes absorption. Enzymatic degradation within the gastrointestinal tract and hepatic first pass metabolism that prematurely sequesters the drug also contribute to the low bioavailability of APDs.¹⁰⁶ In order to ensure sufficient bioavailability of APDs by the time the circulatory system delivers the drug to the brain, large doses must be taken to overcome clearance mechanisms.¹⁰⁷ Disintegrating tablets are easier for patients to take and have faster absorption, but ultimately have similar bioavailability.¹⁰⁸ Despite

the faster onset of action, administration challenges remain when a patient is acutely agitated, has difficulty swallowing, or exhibits treatment avoidance (refusal to swallow/hiding pill).¹⁰⁸ Due to the route of delivery and the substantial dose that must be ingested, chronic dosing of APDs PO is more likely to result in significant negative side effects that can be neurological or metabolic depending on the APD.^{50, 106} Adverse side effects lead to poor patient adherence and demoralization, introducing an additional set of issues associated with this type of administration. Dose alterations due to variations in administration can produce adverse effects, leading to a 5-fold risk of relapse and hospitalization. Introduction of atypical APDs was hoped to boost adherence rates due to the absence of the severe neurological side effects, but patient compliance to prescription of this class of APD remains poor.¹⁰⁹

1.4.3 Intravenous drug delivery

Intravenous (IV) administration is an off-label application of APDs; to-date there are no Food and Drug Administration (FDA) approved formulations of IV-administered APDs.¹¹⁰⁻
¹¹¹ However, in cases where patients present in emergency departments experiencing psychosis or agitation, IV administration of haloperidol lactate and olanzapine pamaote has been used for sedation. As with PO administration, low solubility in aqueous solution limits the dose that can be administered in aqueous IV suspensions.⁵⁰ IV administration of 5-10 mg OLZ results in sedation within 10 minutes in 50-68% of patients (comparable

to other sedative drugs) but results in potential hypoxia, mandating an the ability to continue monitoring the patient when off-label drug administration occurs.¹¹² IV administration is not always feasible as it requires access and cannulation, which may not be possible depending on the patient's state upon admittance to the emergency department; the safety of both the patient and attending staff must be considered.¹¹⁰⁻¹¹¹ Currently, expert consensus is to avoid IV treatments in the assessment and management of agitation in psychiatry given that use of IV APDs is controversial in the absence of appropriate safety and efficacy evaluations. Further investigation is needed in order to secure FDA approval of IV APDs for treatment of acute agitation.¹¹¹

1.4.4 Intramuscular/depot drug delivery

Long-acting injectable (LAI) formats of several typical and atypical APDs have been approved to help circumvent some of the issues associated with PO administration. LAIs are provided as deep tissue intramuscular (IM) injections once every 2-4 weeks. Such injections avoid first-pass metabolism and are able to reduce the fluctuations of drug concentrations in plasma levels compared to PO, thus providing steady state delivery of APD with more consistent and predictable outcomes over extended times. IM injections can also employ the minimum effective dose, which has a lower incidence of side effects and decreases the risk of overdose relative to doses required for PO delivery; coupled with a reduction in dose deviation enabled by the controlled release properties of the injections (removing the need to remember to take a pill 1-3× daily), fewer instances of

acute exacerbations of the disease state are typically observed using IM injections, thus improving patient quality of life. Correspondingly, LAIs have lower rates of relapse, hospitalization and mortality than PO APDs as well as better adherence.^{109, 113-115} IM administration of LAI APDs is also superior to placebo and has a small but significant benefit compared to PO APDs in terms of improving psychosocial function, such as the execution of daily and socio-occupational tasks as well as self-reported well-being, satisfaction, and quality of life.¹¹⁶

Two of the drugs used in this thesis have long-acting IM formulations commercially available. Haloperidol decanoate, the LAI format of haloperidol, was approved in 1967 as an IM injection. It is provided as a prodrug in which the haloperidol molecule is attached to a long-chain aliphatic ester and formulated in sesame oil. Upon injection, it forms a depot of drug that is slowly dissolved by endogenous plasma esterase in the blood to release the drug over a period of 2-4 weeks, which is a substantial reduction in the frequency of administration compared to 1-3× daily PO tablets. The maximal plasma concentration is observed on day 7, and the elimination half-life is about 3 weeks.^{77, 117} Alternately, olanzapine pamoate is the LAI formula for olanzapine (approved in 2007 for IM injection) consisting of a microcrystalline salt of OLZ and pamoic acid suspended in aqueous solution. Upon injection, the salt complex slowly dissolves into OLZ and pamoic

acid with a half-life of 30 days. The LAI is used for maintenance treatment, while another immediate-release IM injectable is available for the treatment of acute agitation.^{113, 117}

Although LAIs do have substantial benefits, there are certain disadvantages that cause patients with schizophrenia to reject this treatment option. IM injections are highly invasive and painful at the site of administration due to drug leakage causing irritation or lesions, with the occurrence of nodules, fibrosis and abscesses representing the primary reason for patients to opt-out of LAIs.¹⁰⁹ There is also substantial infrastructure associated with administration; injections must be administered by a medical professional in a setting that is able to maintain safe storage and discard options for needles. In Norway, there is a mandatory 3 hour observational period after IM injection due to the risk of delirium/sedation syndrome that occurs in 0.04% of patients receiving LAIs. Some patients also associate stigma with repeated visits to doctor's offices and prefer the option to privately self-administer APDs. Due to the slow release nature of LAIs, the time required to reach steady state is prolonged; however, the extended release can also be problematic when the medication needs to be tapered or stopped if adverse effects need to be addressed.¹¹³⁻¹¹⁴ In this respect, an extended release formulation that could be self-administered but persists for a shorter period of time (i.e. one week instead of one month, such that any side-effects could be more efficiently corrected) may be more beneficial.

The ability of LAIs to attenuate side effects, improve patient adherence, and decrease the risks of relapse, hospitalization, and mortality shows that extended release formulas have an inherent benefit to APD treatment regimens. However, the invasive nature of IM injections substantially limit the desire to pursue this avenue of treatment, especially when chronic dosing for a lifetime is required. As such, a route of administration that continues to exploit the advantages of this type of injection, but removes the problematic invasiveness is highly desirable and warrants pursuit to further improve the clinical outcomes of APDs.

1.4.5 Intranasal drug delivery

Intranasal (IN) drug delivery is an alternate route of administration for APD delivery to the brain that can enhance patient compliance and tolerance.⁵⁰ It offers the advantage of having a rapid onset of action and being considerably less invasive than IM injection.⁹⁸ The substantial benefit of IN delivery is the ability to bypass the BBB entirely, enabling direct nose-to-brain transport that considerably enhances APD bioavailability (Figure 1.5). IN delivery can also avoid hepatic first pass metabolism or systemic clearance, allowing much lower doses to be delivered in comparison to PO. This substantially minimizes dose-related neurological and metabolic side effects by minimizing interactions with peripheral receptors at non-target sites.¹¹⁸ In order to avoid mucociliary clearance mechanisms within the nasal cavity, the anterior portion of the cavity (which is devoid of ciliated cells)

is typically targeted to provide an effective amount of neurologic therapeutic agent directly to the olfactory epithelium through absorption.¹¹⁹ Delivery to the brain can occur through two different pathways, which are described in detail in the following sections.

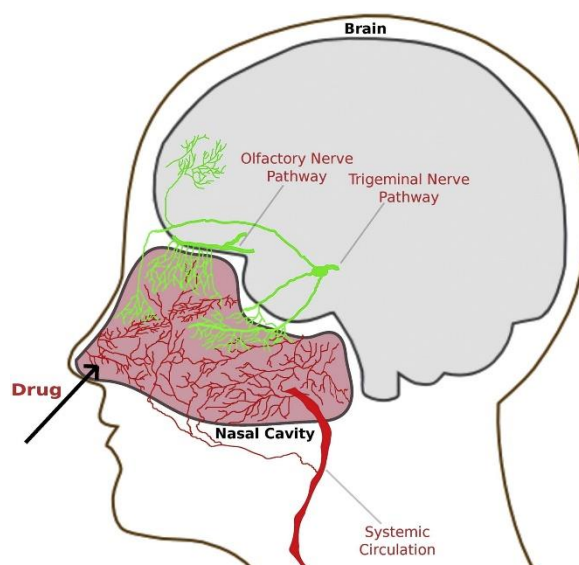


Figure 1.5: Intranasal (IN) drug delivery showing direct transport to the brain and indirect transport to systemic circulation. Nerves and nerve endings are depicted in green, while blood vessels are depicted in red. Adapted with permission from Katare *et al.*, 2017 [50].

Direct pathway

The direct pathway enables drug to be transported rapidly to the brain via different transit routes depending on the drug's chemical and physical properties; for 29 of 82 drugs tested, more than 80% of the administered drug dose was transported to the brain via the direct pathway.¹²⁰ Direct nose-to-brain transport can be divided into two distinct

groups: (1) intracellular transport via either the olfactory or trigeminal nerves that provide a direct connection between the nasal cavity and the brain; or (2) extracellular transport that relies upon various types of transcellular or paracellular mechanisms for drugs to enter the brain (Figure 1.6).¹²¹

The olfactory nerve pathway provides access to the cerebrospinal fluid (CSF) or brain parenchyma in the subarachnoid space, or by crossing the synaptic junctions and entering the output neurons of the olfactory bulbs (OLBs).¹²² Drugs must traverse the olfactory epithelium by internalization into olfactory receptor neurons (ORNs) that are interspersed amongst support cells.¹²¹ Uptake occurs through endocytosis or pinocytosis. The dendrites of the ORNs extend into the mucus layer while the axons extend through the lamina propria. Drugs travel along the axon and traverse perforations in the cribriform plate via the nerve bundle to enter the cranial cavity, which is in contact with the subarachnoid space; the axons terminate on mitral cells of the OLB for subsequent distribution into the olfactory tract, piriform cortex and hypothalamus of the brain.¹²¹⁻¹²³ Olfactory nerves deposit drug into the rostral (anterior/front) region of the brain. This transneuronal pathway relies on passive diffusion, RMT, and absorptive endocytosis and is thus very slow, with drug appearing in the CNS 24 hours after IN administration.¹²⁴ Direct transport is also possible following the trigeminal nerve pathway, although it has been newly identified and is mechanistically less understood. Trigeminal nerve receptors

are found in the olfactory and respiratory epithelium of the nasal cavity. The perineural space of the cranial trigeminal nerve interacts with the subarachnoid space, while the trigeminal nerve deposits in the caudal (posterior/back) of the brain with a small portion terminating in the OLB.¹²¹ This route requires 17-56 hours for drug to appear in the CNS.¹⁰³ Neither of these processes can explain the rapid appearance of drugs in the CSF and brain commonly observed for small, lipophilic drug and are therefore not likely the predominant mode of drug transport.¹²¹

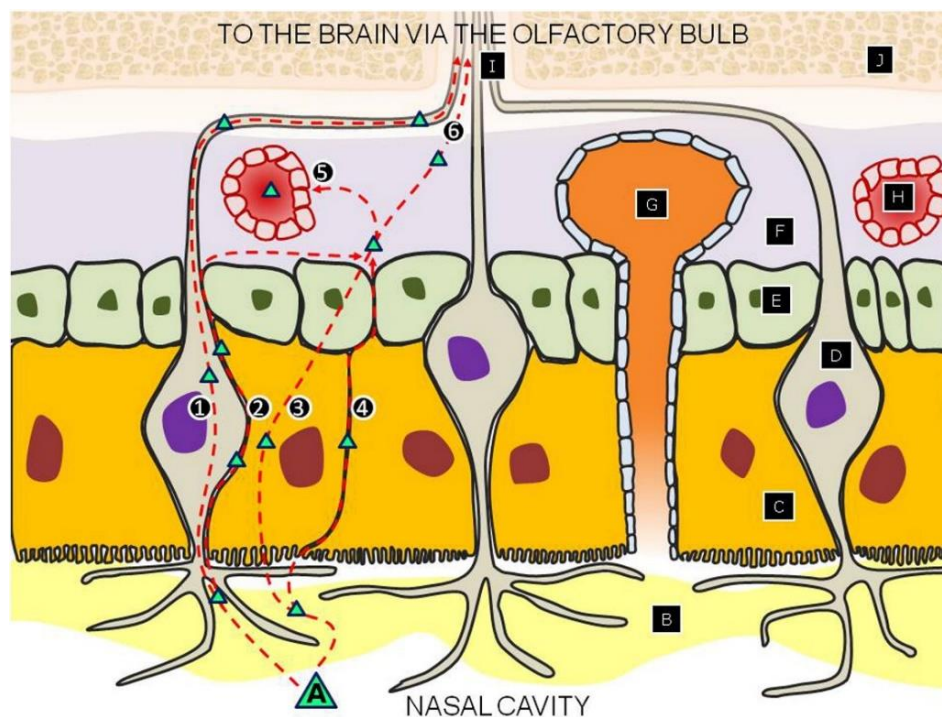


Figure 1.6: Drug delivery pathways through the nasal epithelium to the brain. Drugs or drug-loaded nanocarriers (compounds) (A) are administered through the intranasal route, where they encounter the nasal cavity and mucus (B). Olfactory epithelial cells (C; small dark red circles denote the nucleus) surround and support olfactory sensory neurons (D; purple circles represent the nucleus) project cilia into (B). In Pathway (1), compounds are transported intracellularly into the olfactory sensory neuron and reach the brain (via the olfactory bulb) by travelling along the axon. Compounds can also travel (Pathway 2) between olfactory sensory neurons (paracellularly) and (C). Olfactory epithelial cells can uptake compounds (Pathway 3) and transport them transcellularly across the epithelium. Compounds can also cross the epithelium by travelling between olfactory epithelial cells paracellularly (Pathway 4). Once across, they can be transported into blood vessels (H) and enter systemic circulation (Pathway 5). To reach the brain (Pathway 6) they can travel through the lamina propria (F) and extracellularly through perineural or perivascular channels to reach the brain. (E) Basal cells (small dark green circles represent the nucleus); (G) Bowman's gland; (I) olfactory tract and (J) cribriform plate. Adapted with permission from Katare *et al.*, 2017 [50].

Extracellular transport uses mechanisms that enable rapid movement between the nasal epithelial cells and the OLB and other regions.¹²¹ Transcellular transport (used by lipophilic agents) occurs through the sustentacular cells to the lamina propria. Diffusion or convection into compartments associated with the nerve bundle perineural space leads to entry into cranial compartments. Transcellular movement relies on CMT, RMT, endocytosis or passive diffusion (the latter of which is most likely for hydrophobic drugs).^{103, 124} Alternately, paracellular aqueous diffusion is the most common external transport mechanism for water-soluble agents, enabling transport through epithelial tight junctions and between neighbouring sustentacular cells and/or olfactory neurons by passive diffusion or solvent drag.^{123, 125} Drugs are first absorbed across the olfactory sustentacular epithelial cells to reach the submucosa and subsequently enter into the perineural space through loose perineural epithelium or epithelial cell junctions, after which drug can penetrate the cribriform plate.¹²³⁻¹²⁴ Extracellular pathways enable drug detection in the CNS within 0.5-2.5 hours of IN administration.¹⁰³ It is also likely that drugs are able to permeate the brain using more than one pathway, enabling an expansion of the duration of therapeutic onset. Nanoparticles can use these pathways to enter the brain, provided their size, composition and surface chemistry are designed to facilitate uptake by one of the mechanisms listed above. Both the intracellular and extracellular pathways have been shown to support nanocarrier transport to the brain. Small nanocarriers (<100 nm) or the presence of specific surface ligands that target receptors

can be exploited to facilitate nanoparticle uptake by these pathways. Additionally, the use of mucoadhesive excipients to promote retention of drug delivery systems within the nasal mucosa is thought to enhance the likelihood of nose-to-brain transport by prolonging the residence time of nanoparticles within the nasal cavity.⁵⁰

Indirect pathway

The indirect pathway is an alternate route facilitated by IN administration. Although it is not the desired primary mechanism for APD delivery to the brain, this route is often exploited for other drugs that require enhanced bioavailability but not necessarily entry to the brain to execute their function. If drug is able to remain in the nasal cavity and avoid enzymatic degradation and mucociliary clearance (which occurs approximately every 15-20 minutes)¹⁰³ but does not participate in a direct pathway, its ultimate fate is absorption into the bloodstream via absorption into the capillary blood vessels underlying the nasal mucosa (Figure 1.7).^{121, 123-124} Once in the bloodstream, the drug is exposed to systemic circulation, ultimately leading to complete elimination.¹²¹ However, there is a possibility that drug absorbed into systemic circulation can be transported across the BBB and enter the brain to execute its intended function.¹²³⁻¹²⁴ Counter-current transfer whereby drugs enter the venous blood supply in the nasal cavity and get transferred to the carotid arterial blood supply for the brain and spinal cord is also possible, although rare.¹²¹ Given that drug will first pass through hepatic and renal clearance mechanisms

and induce off-target side effects through peripheral tissue exposure following the indirect route, this pathway is generally not favorable for APD delivery; indeed, it typically facilitates lower drug bioavailability and slower onset than IV administration, albeit with the benefit of avoiding invasive administration. As such, IN delivery of APDs predominantly exploits the direct pathway of extracellular transport to initiate therapeutic intervention. A very small fraction of nanocarriers has been reported to indirectly access the brain, with the likelihood of such transport increased for particles <50 nm and again facilitated by surface chemistry (including targeting ligands such as lectins or transferrins that enhance uptake using AMT or RMT).⁵⁰

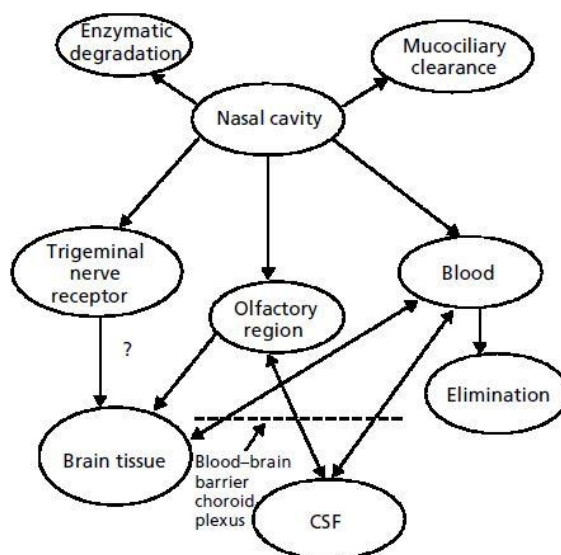


Figure 1.7: Summary of possible pathways drugs and/or nanoparticles may traverse to reach the brain and/or circulation. Circumvention of enzymatic degradation and mucociliary clearance enables the direct passage of drug to the brain via the trigeminal or olfactory routes. Indirect transport through the blood and/or cerebrospinal fluid (CSF) may also occur. Ultimate elimination occurs upon entry into systematic circulation through the blood. Adapted with permission from Illum, 2004 [124].

1.5 Nanoparticles for Targeted Drug Delivery to the Brain

IN delivery of APDs to the brain is an attractive route of administration because it can bypass the BBB and minimize drug dose through improved bioavailability, thereby decreasing the risk of adverse side effects using a minimally invasive alternative for drug intervention. However, there are two factors that IN administration alone does not address. The first limitation is the poor aqueous solubility of most APDs, which limits the concentration of drug that can be administered to the nasal cavity using tissue-compatible solutions; for example, the administration of oils or low pH solutions required to solubilize hydrophobic APDs can cause significant irritation and/or permanent damage to the nasal mucosa and epithelial cells.¹²⁶⁻¹²⁷ The second limitation is the lack of sustained release, an issue potentially exacerbated with the fast transport of drug into the brain via the direct IN route. This limitation is particularly critical to address given the low patient compliance associated with APD administration. Indeed, IM injections that create depots of APD have favourable clinical outcomes because the minimum effective dose can be administered and is accompanied by slow drug dissolution to provide long-term intervention, in turn improving patient compliance and decreasing the occurrence of side effects. In this context, nanoparticles are attractive drug carriers to: (1) enhance drug encapsulation by improving drug solubility, enabling large quantities of drug to be dispersed in solution at concentrations not otherwise accessible; (2) control drug release kinetics by acting as a barrier to release, enabling drug to remain concentrated in its active

form at the intended target and thereby maintaining drug concentrations within the required therapeutic window;⁹⁸ (3) improve the clinical efficacy of therapeutics by targeting drugs to specific tissues and cell types, thereby minimizing drug doses and reducing negative side effects; and (4) enable easy administration of drug into the nose via low-viscosity solutions using conventional IN administration techniques (e.g. spray or aerosolization).

A variety of different nanocarrier formulations can be used as controlled drug delivery vehicles. Dendrimers, micelles, solid lipid nanoparticles (SLNs), and other polymeric nanoparticles comprised of either natural or synthetic materials have the potential for large drug uptake while improving spatial and temporal drug release kinetics through targeting (Figure 1.10).⁹⁸ There are several key characteristics nanoparticles must possess to be administered IN and persist *in vivo* for prolonged drug delivery. The first key design consideration is size. Current strategies can engineer particles to precise dimensions with high monodispersity, which is very important for consistent drug uptake and particle distribution *in vivo*. Nanoparticles with average diameters of ~100 nm have the ability to access specific tissues, while particles that are too small or too large are more easily identified by the body's clearance mechanisms and thus accumulate in non-target organs such as the liver, spleen and kidney. Permeation of the BBB is typically considered a size-restricted process, with a large majority of the literature reporting that particles <100 nm

have a greater potential to gain entry to the brain.^{98, 100, 128-130} However, particles up to 300 nm have been shown to enable drug delivery to the brain,¹³¹⁻¹³² although data does not always clearly portray whether the nanoparticles themselves permeate into the brain or simply provide a depot for extended free drug diffusion into the brain.^{78, 133-135} As such, while size does play a critical role in *in vivo* behaviour, the influence of nanoparticle composition, structure, and therapeutic uptake are also relevant considerations for drug delivery system design. Particle morphology is also a tunable parameter that can affect drug delivery.¹³⁶ Spherical nanocarriers are most commonly used for BBB targeted delivery as they can be easily synthesized and have high surface area to volume ratios for drug uptake.¹³⁷ In comparison to rod-shaped particles, which have larger aspect ratios, spheres show less accumulation in the liver and lungs.¹³⁸ Computer simulations of particle transport in a blood vessel have demonstrated that rods have greater binding interactions due to a larger contact area, thereby increasing the likelihood of off-target associations.¹³⁹ Rod-shaped particles can also cause disrupted cytoskeleton organization and interfere with cell adhesion, leading to reduced cell viability;¹⁴⁰ it hypothesized this effect is attributed to the preferred localization of rod-shaped nanoparticles in the cell nucleus upon uptake, in contrast to spherical micelles and vesicles that tend to remain in the cytoplasm.¹⁴¹ Spheres also show better apparent permeation of the BBB in comparison to rods, as it is hypothesized that the extracellular transport mechanisms are more effective for spherical particles.¹⁴²

Particle stability is another important parameter to maintain prolonged drug release. For effective transport, particles cannot aggregate or dissociate upon exposure to mucus, serum, or blood as this can reduce nanoparticle mobility.¹⁴³⁻¹⁴⁴ Numerous strategies have been developed to help maintain nanoparticle stability. The most popular solution is the incorporation of an inert, hydrophilic, non-immunogenic polymer, such as poly(ethylene glycol) (PEG), at the nanoparticle surface that acts as a protein-repellent shield to prevent mucoadhesion and facilitate transport through mucus for uptake into cells.^{8, 143, 145-147} Polyvinyl alcohol and polyvinyl pyrrolidone are other inert polymers commonly used as capping agents, particularly to mitigate the high surface energies of metallic particles to prevent aggregation.¹⁴⁸ Surface coatings consisting of biological agents have also been utilized, including polysaccharides such as chitosan,¹⁴⁹ hyaluronic acid,¹⁵⁰ and heparin¹⁵¹ that typically have good stability in biological fluids, proteins such as albumin, keratin,¹⁵² transferrin,¹⁵³ and lactoferrin¹⁵⁴ that are stable under physiological conditions and endow both steric and electrostatic stability,¹⁵⁵ and naturally-occurring lipids such as phosphatidylcholine¹⁵⁶, cholesterol¹⁵⁷ or exosome-derived lipids¹⁵⁸⁻¹⁶⁰ that are both non-immunogenic and non-toxic.

While stability is an important parameter to ensure the drug delivery vehicle reaches its target area, degradability is necessary for regulating drug release kinetics while also

ensuring clearance once the particle has completed its intended activity. Drug release is often dependent on the kinetics of particle degradation and, as such, the biodegradability of the particle is an important design consideration. Ideally, the method of degradation will be responsive to the environment in which the drug will be released, avoiding or minimizing drug leakage in which the drug pre-emptively releases during circulation to result in inefficient accumulation of therapeutic at the target tissue. A tunable drug release profile can be controlled via the selection of cross-linker or degradable bonds incorporated into the nanoparticle structure.^{136, 161-162} Poly(lactic-co-glycolic acid) (PLGA) nanoparticles are commonly selected because the polyester backbone of the polymer is hydrolytically degradable as well as cleavable upon exposure to esterase and lipase,¹⁶³⁻¹⁶⁴ prolonging drug release compared to free drug diffusion.¹⁰⁶ The incorporation of labile bonds that respond to physiological conditions is also highly attractive for drug delivery systems. Cleavage of disulfide bonds using either glutathione (GSH) or dithiothreitol (DTT) is popular because the reduction of these bonds occurs via a bio-orthogonal reaction; for example, both DTT¹⁶⁵ and GSH-mediated¹⁶⁶ degradation has been shown to enhance release of doxorubicin from disulfide-cross-linked PNIPAM microgels. Particle degradation can also be mediated by exposure to the acidic environment of lysosomes, thereby triggering drug release following endocytosis; for example, acid-catalyzed hydrolysis of the ester bonds within oligo(ethylene glycol methacrylate) micelles has been demonstrated to enable increased rate of doxorubicin release under intracellular pH

relative to neutral pH conditions.¹⁶⁷ By exploiting unique cellular conditions to trigger degradation and enhance drug release, better site-specific drug delivery can be achieved.

The chemical and physical properties of nanoparticles can be tuned to enhance the uptake of therapeutics of interest; this ensures high drug encapsulation and lowers the amount of material required to deliver the drug. This is particularly important for highly hydrophobic APDs given that their poor aqueous solubility prevents drug dissolution in physiologically-compatible solutions, limiting the available routes of administration for drug delivery.¹⁶⁸ Increased solubilization of hydrophobic drugs within nanoparticles is a key attribute of drug delivery vehicles.^{89, 169} Formation of nanoparticles consisting of hydrophobic building blocks such as lipids and hydrophobic polymers can improve APD entrapment. The lipid core of solid lipid nanoparticles provides ideal conditions to solubilize hydrophobic APDs and prolong drug release based on the diffusion coefficient of drug through the lipid matrix. In particular, glyceryl monostearate (HLP¹⁷⁰ and LUR¹⁷¹) and glyceryl tristearate (OLZ¹⁷²) have been used to solubilize APDs. Emulsions have also been formed using anise oil,¹⁷³ soybean oil¹⁷⁴ or Capmul medium chain monoglyceride¹⁷⁵ to enable enhanced solubilization of LUR and, by extension, higher drug loading and prolonged drug release. Polymeric nanoparticles can also be used in this context, with the optimization of hydrophobic comonomer content within nanoparticles having been investigated for enabling APD uptake. For example, increasing the L:G ratio within PLGA

nanoparticles to favour the more hydrophobic lactic acid has been used to increase HLP¹⁷⁶⁻¹⁷⁷ and OLZ loading¹⁰⁶ and minimize burst release.¹⁷⁸

Several different nanoparticle-based materials have been proposed for the IN delivery of HLP, OLZ or LUR (Figure 1.8). Each formulation has its own benefits and drawbacks, as discussed in the sections below.

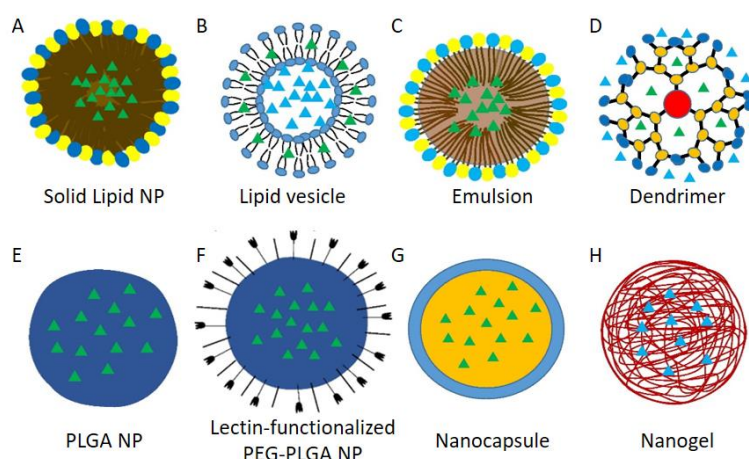


Figure 1.8: Nanoparticles used for the delivery of APDs. (A) Solid lipid nanoparticles with a solid lipids (brown circle) in the core and different surfactants with hydrophilic heads (blue and yellow circles) and hydrophobic tails in the core. (B) Lipid vesicles comprised of a phospholipid bilayer (hydrophilic heads are represented by blue circles and hydrophobic tails by lines). (C) Oil (brown circle) in water (O/W) nanoemulsion stabilized with different types of surfactants comprised of a hydrophilic head (blue and yellow circles) and hydrophobic tail (brown lines). (D) Dendrimers with a hydrophobic core (red circle) and branches (orange circles), and a hydrophilic surface (blue circles). (E) PLGA nanoparticle consisting of solid polymer core (blue). (F) PEG (black lines)-PLGA nanoparticle surface-functionalized with lectin (pitchforks) for targeting and mucoadhesion. (G) Nanocapsules with a hydrophobic core (orange circle) and hydrophilic shell (blue circumference). (H) Nanogels made of a water-swollen network of cross-linked hydrophilic or amphiphilic polymer chains. Adapted with permission from Katare *et al.*, 2017 [50].

1.5.1 Lipid-Based Nanoparticles

Lipids are a common material for APDs because they easily solubilize this class of therapeutic. For example, HLP has been encapsulated in the dense lipid core of solid lipid nanoparticles (SLNs, Figure 1.8A) based on glyceryl monostearate; IN delivery using the small (~150 nm) SLNs produced greater and faster HLP concentration in the brain relative to IP administration.¹⁷⁰ Nanostructured lipid carriers with a similar size (200 nm) containing LUR administered intranasally also facilitated a much higher drug concentration; 8× more LUR was detected in the brain and the half-life of elimination was more than doubled the compared to a PO drug solution, showing the clear advantage of a nanocarrier in prolonging drug release *in vivo*.¹⁷⁹ In contrast, much larger (~400 nm diameter) transfersomal vesicles of phosphatidylcholine consisting of a lipid bilayer containing surfactant molecules surrounding an aqueous compartment (Figure 1.8B) enabled more OLZ to access the brain when administered IV compared to IN, a result attributed to the moderate inflammation detected in the nasal cavity that likely led to rapid carrier clearance to prevent drug penetration.¹⁸⁰ Collectively, these results show that the size of the drug carrier affect the permeability into the brain, with larger vesicles showing less effective drug delivery.

1.5.2 Emulsions

Emulsions are another popular type of nanoscale drug carrier because they also readily facilitate solubilization of lipophilic compounds into their formulations (Figure 1.8C).

Nanoemulsions are kinetically¹⁸¹ and thermodynamically¹⁸² stable and produce small globule sizes that are ideal for nose-to-brain transport. Mucoadhesive HLP miniemulsions (~200 nm) administered IN resulted in drug delivery to the brain at a rate 6× faster and at a concentration 2-fold greater than facilitated by the equivalent formulation IV.¹⁸² Nanoemulsions containing OLZ (ONE) and optionally coated with mucoadhesive chitosan (OMNE) resulted in high brain/blood ratios for up to 8 hours that were markedly greater than that achieved via IV administration.¹⁴⁹ For the first hour, the ONE showed higher brain/blood ratios, demonstrating rapid permeation of the mucosa; subsequently, from 2-8 hours, the mucoadhesive formulation produced larger ratios, showing the ability of mucoadhesion to retain drug-releasing emulsions at the target. Formulation of LUR-containing nanoemulsions resulted in ~50 nm particles with enhanced drug release *in vitro* compared to drug solution, demonstrating the solubilizing effects of the nanoemulsion.¹⁸¹ Spontaneous locomotor activity was examined using each of these formulations (HLP, OLZ and LUR) to characterize the pharmacodynamics of the IN administered drug. Only acute time points were collected; data collection began 10-30 minutes after drug dosing and was only monitored for 5-10 minutes thereafter. The data collected shows that IN administration enables rapid onset of therapeutic intervention but does not assess additional long-term time points to demonstrate sustained release and prolonged intervention.

1.5.3 Dendrimers

The Mishra group has reported the use dendrimers (Figure 1.8D) based on polyamidoamine (PAMAM) for haloperidol delivery.⁵² The tiny (~15 nm), five-generation dendrimers solubilized 100-fold more HLP compared to the drug's aqueous solubility; correspondingly, IN delivery of the HLP-dendrimer formulations required ~6× less drug than an IP injection of drug solution to produce comparable pharmacological outcomes. However, the inability to further concentrate the dendrimer dispersions due to aggregation, coupled with carrier toxicity concerns flagged as potential concerns about long-term or higher dose use of this carrier, may limit the clinical relevance of this approach.

1.5.4 Polymer Nanoparticles

Polymer nanoparticles are solid, colloidal systems based on water-insoluble polymers that can be produced using different synthetic techniques. PLGA nanoparticles (Figure 1.8E) have been used to fabricate OLZ drug delivery vehicles with sustained *in vitro* drug release kinetics and encouraging *ex vivo* toxicity studies;¹⁰⁶ however, this work lacked supporting *in vivo* pharmacokinetic and pharmacodynamics data. Work from our group has also utilized nanoparticles comprised of PEG-PLGA for the intranasal delivery of HLP.⁵³ PEG-PLGA particles functionalized with lectin groups to promote mucoadhesion (Figure 1.8F) showed up to a 3-fold increase in HLP concentrations in the brain compared to PEG-PLGA

nanoparticles or IP administration. However, pharmacodynamics data collected used conventional doses of drug employed IP that did not reinforce the enhanced bioavailability of drug administered IN. Two mucoadhesive formulations have also been reported for IN delivery of OLZ. Chitosan nanoparticles showed slow release kinetics *in vitro* but problematic dose-dependent toxicity towards RPMI nasal epithelial cells *in vitro*.¹⁸³ Alternately, amphiphilic nanocapsules (Figure 1.8G) based on hydrophilic poly(ϵ -caprolactone) and hydrophobic methyl methacrylate, and surface-functionalized with 2-(dimethylamino)ethyl methacrylate (DMAEMA) to promote mucoadhesion showed improvement in PPI within 45 minutes of IN administration using a very low dose of OLZ (100 μ g) in an APO-induced model of schizophrenia. However, the rapid *in vitro* release kinetics resulted in 80% drug release in the first 4 hours and complete drug release within 12 hours, indicating that prolonged therapeutic intervention with these nanocapsules is unlikely.¹⁸⁴

1.5.5 Micro/nanogels

Nanogels are dynamic, soft, deformable, gel-like structures consisting of cross-linked water-soluble polymers (Figure 1.8H). Thus, nanogels have an interior matrix that renders them highly permeable and able to swell, making them fascinating structures for drug delivery.¹⁸⁵ Their highly tunable properties include high colloidal stability in aqueous conditions, flexibility, functionality, and biodegradability.¹⁸⁶ Nanogel size can be

controlled during synthesis by adjusting the concentration of initiator, surfactant, and/or the ratio of co-monomers, the extent of cross-linking, the solvent and/or the reaction temperature.¹⁸⁷ Size significantly affects bioavailability, with moderate sizes between 70-200 nm ideal for avoiding clearance by various *in vivo* mechanisms.¹⁸⁸ Physical dimensions are also strongly influenced by the balance between osmotic pressure and polymer elasticity; cross-linking, which may be through chemical bonds or physical interactions, helps the formation of discrete particles by driving polymer collapse and also controlling swellability.¹⁸⁹⁻¹⁹⁰ Nanogel colloidal stability is also attributed to cross-linking as it ensures that the nanogel structure is retained without undergoing dissolution in a favourable solvent (such as aqueous physiological conditions).^{185, 188, 191-192} The most unique characteristic that distinguishes nanogels from other nanoparticles is the ability to swell, creating a pliable, elastic structure that leads to longer *in vivo* retention times and reduced accumulation in the liver.¹³⁶ Swelling behaviour, which allows nanogels to adapt their size and shape, is influenced by the chemical composition of the nanogel, the architecture of the matrix (degree of cross-linking), and external triggers imparted by the surrounding environment.^{185, 189, 191} The stimuli-responsive nature of nanogels is in particular a unique property of this particle type. Response to changes in solvent, pH, ionic strength, redox potential, temperature, and/or light (amongst other factors) can be integrated into the chemistry of nanogels to manipulate physiochemical properties such as swelling, permeability, flexibility, and hydrophilic/hydrophobic balance;¹⁹² in turn,

these changes can be employed as a strategy to enable drug uptake, control drug release, and facilitate nanogel degradation.¹⁶⁹

For drug delivery applications, high loading capacity and sustained release profiles are integral properties of the nanogel system. The interior mesh-like network of polymer is ideal for encapsulation, which can be enhanced by nanogel swelling to provide an enlarged cargo space for drug encapsulation.^{189, 193} Nanogels enable high drug loading capacity because their composition can be tuned to improve a molecule's affinity for the particle; spontaneous drug loading through electrostatic, van der Waals or hydrophobic interactions can be promoted by selecting appropriate functional groups for incorporation into the polymer backbone.^{186, 189} For APD delivery, the incorporation of hydrophobic pockets within the nanogel structure can solubilize the drug within an otherwise highly hydrophilic structure.^{189, 192} Drug release occurs by different mechanisms, with some combination of diffusion, nanogel degradation, and/or external stimuli regulating release kinetics.¹⁸⁹ Incorporation of labile bonds into the polymer backbone or cross-links can facilitate degradation in response to external triggers, leading to both nanogel erosion (essential for ultimate clearance) and triggered drug release.^{189, 191} Nanogels also offer key properties to promote the delivery of therapeutic cargos through physiological barriers.^{186, 191} For the purpose of APD delivery via the IN route, a nanogel that can maintain the appropriate hydrophilic/hydrophobic balance is crucial to

prevent entrapment within the nasal mucosa while also promoting affinity for the cell membrane to enable embedment within the lipid bilayer of the epithelium,^{146, 194-197} ultimately promoting drug release within the target area and minimizing off-site interactions to reduce the likelihood of adverse side effects.

Nanogels have been used for the encapsulation of hydrophobic drugs such as the anti-convulsant phenytoin¹⁹⁸, anti-cancer drugs temoporfin,¹⁹⁹ doxorubicin (DOX),²⁰⁰⁻²⁰¹ paclitaxel,²⁰² and curcumin^{150, 203} as well as fluorescent molecules used for imaging such as pyrene²⁰⁴. In most cases, incorporation of a hydrophobic moiety within the otherwise hydrophilic nanogel structure was utilized to improve drug affinity for the nanogel; for example, naphthalene physically cross-linked into nanogels based on the glucan schizophyllan²⁰⁰ and PEG-*b*-PGA polymers hydrophobically modified by conjugating L-phenylalanine methyl ester hydrochloride and cross-linking with cystamine to create a hydrophobic ionic core²⁰¹ have both been demonstrated to enable effective DOX encapsulation. Using a similar approach, 11-amino-1-undecanethiol hydrochloride was conjugated to the hyaluronic acid backbone to create an amphiphilic nanogel capable of loading curcumin and modulating controlled release through cleavage of a disulfide bond,¹⁵⁰ acetylation of a self-assembled ulvan nanogel was demonstrated to enhance curcumin solubility,²⁰³ and the addition of isopropylidenglycerol to a self-assembled PEG-based nanogel was demonstrated to improve the solubility of PTX.²⁰² Finally,

incorporation of phenytoin and pyrene both relied on the physical structure of their respective nanogel; increased cross-link density within a PNIPAM nanogel entrapped phenytoin¹⁹⁸, while pyrene preferentially localized within the hydrophobic core of a star cross-linked nanogel.²⁰⁴ More complex strategies for enhancing drug affinity have also been reported. For example, a specific designer peptide sequence was conjugated to a polyglycerol-based nanogel synthesized using nanoprecipitation to facilitate temoporfin encapsulation¹⁹⁹ Although different molecules are selected depending on the target molecule, the strategy to create reservoirs for drug uptake by altering the chemical or physical properties of the nanogel are shared.

IN delivery of nanogels has also been explored for CNS conditions such as Alzheimer's,²⁰⁵⁻²⁰⁶ depression,²⁰⁷ and lymphoma²⁰⁸. Insulin delivery for Alzheimer's has been reported using poly(*N*-vinyl pyrrolidone)-co-acrylic acid nanogels prepared using electron beam irradiation of aqueous polymer solutions. Insulin was conjugated to the nanogel using EDC/sulfo-NHS chemistry to facilitate amide bond formation.²⁰⁵⁻²⁰⁶ An *in vitro* BBB model showed that free insulin, nanogels, and insulin-loaded nanogels could traverse brain endothelial cells,²⁰⁵ while pharmacokinetics studies show localization of fluorescently-labelled insulin in the olfactory bulb, cortex and hippocampus 30-60 minutes post-IN administration of loaded nanogels.²⁰⁶ Alternately, ionic gelation was used to prepare alginate/calcium nanogels using an inverse emulsion templating approach to encapsulate

the anti-depressant icariin; suspension of these nanogels in poloxamer solutions helped to control both icariin and nanogel release kinetics, leading to gradual entry into the brain as confirmed by fluorescence tracking.²⁰⁷ Ionic gelation was also utilized to create cationic chitosan/pentasodium triphosphate electrostatically cross-linked nanogels containing methotrexate for lymphoma treatment via IN delivery. Quantification of the drug administered with and without nanogel in the brain revealed that the nanogel enhanced drug entry into the brain compared to the free solution, suggesting that the nanogel helped to retain the drug at the target site.²⁰⁸ The IN route is also popular for vaccine administration using nanogels.^{194, 209-211} Cationic cholesterol group-bearing pullulan has been extensively utilized to generate nanogels formed via physical interactions that can deliver a variety of antigens and adjuvants through hydrophobic interactions. The cationic charge facilitates adherence to the nasal epithelium to prolong nanogel retention and enhance antigen/adjuvant uptake.^{194, 209-211}

Despite the promising findings from the above studies utilizing nanogels to aid in IN delivery of various therapeutics, there have only been two reported two instances of nanogels used for the encapsulation of APDs (specifically olanzapine),^{134, 212} neither of which examined IN administration as the intended route for therapeutic intervention. Both nanogels were chemically cross-linked using *N,N'*-methylene bisacrylamide (MBA), a conventional, non-biodegradable cross-linker. The PNIPAM nanogel had a low OLZ

loading content of 2 wt% and showed biphasic release with a burst of 40% within the first 2 hours and complete release within 2 days (Figure 1.9A). Although the nanogels appeared non-cytotoxic towards NH 3T3 fibroblasts (Figure 1.9B), the lack of well-defined degradation products formed is problematic for clinical applications.²¹² The most recently proposed nanogel formulation utilizes poloxamer-407 co-polymerized with 2-acrylamido-2-methylpropane sulfonic acid (AMPS) (Figure 1.10A). Increased OLZ loading was observed as the concentrations of each nanogel component were increased, while increasing the cross-linker concentration reduced nanogel swelling and decreased drug uptake (Figure 1.10 B). Dissolution studies confirmed the enhanced solubility of OLZ in the nanogels compared to OLZ tablets (Figure 1.10 C), and no cytotoxicity or weight gain was associated with administration after two weeks of daily 40 mg/kg doses compared to a control cohort.¹³⁴ However, the absence of controlled release data, a clear mechanism to enable degradation, and *in vivo* behavioral data demonstrating effective transport of drug to the brain over an extended period limits the translation of these formulations.

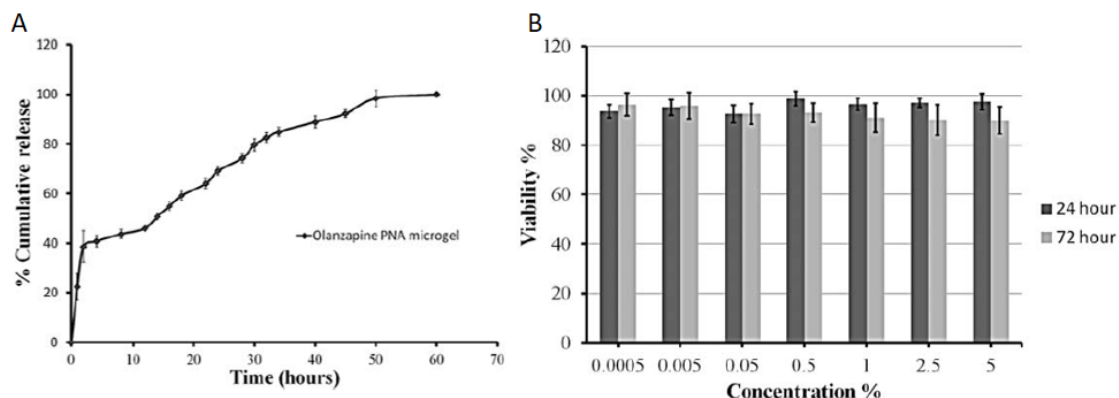


Figure 1.9: *In vitro* performance of PNIPAM nanogels for olanzapine delivery. (A) *In vitro* OLZ release in 37°C PBS pH 7.4 stirred at 100 rpm. (B) Evaluation of NH 3T3 mouse embryonic fibroblast cell viability using the MTT assay after 24 and 72 hours of OLZ-nanogel treatment. Adapted from Pervaiz *et al.*, 2016 [212].

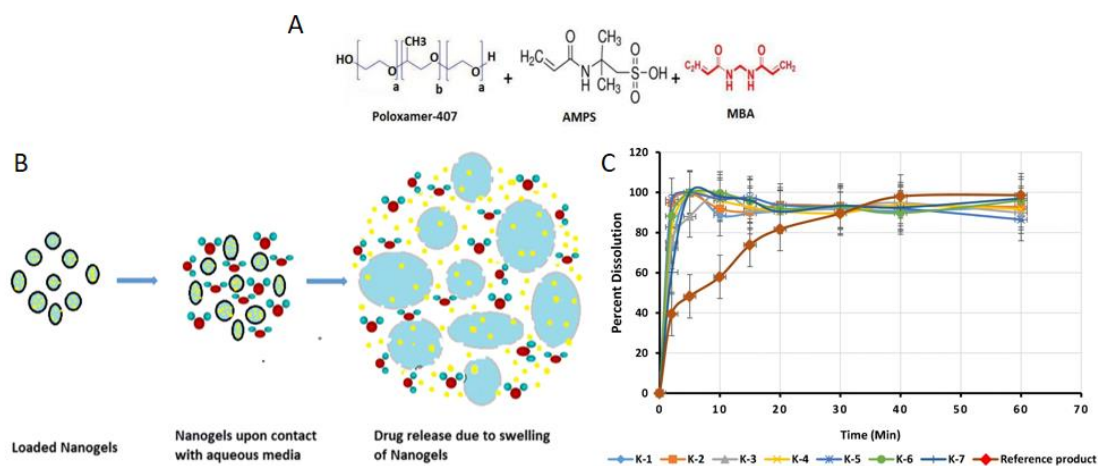


Figure 1.10: Synthesis of poloxamer-407-co-AMPS nanogels and *in vitro* dissolution behaviour. (A) Schematic of nanogel components including poloxamer-407 (polymer), AMPS (monomer) and MBA (cross-linker). (B) *In vitro* swelling upon dissolution in aqueous media prompts OLZ release. (C) OLZ dissolution from nanogel formulations (K1-K7) compared to OLZ tablet (reference product). Adapted with permission from Khan *et al.*, 2020 [134].

Although these studies provide preliminary evidence for the potential of nanogels to act as APD delivery systems, they lack particular design considerations to circumvent the known limitations of nanogels such as hydrophilicity and degradability. In addition, there is a clear lack of data in the literature on the transport of nanogels following IN delivery as well as their potential to enable prolonged therapeutic efficacy. As such, we believe there is a significant opportunity to implement novel modifications to improve APD intervention using nanogel-based delivery systems, a topic this thesis aims to address.

1.6 Thesis Objectives

The distinct properties of nanogels that distinguish them from conventional nanoparticle drug delivery systems can be leveraged to create powerful drug delivery systems for APDs. The opportunity to improve the bioavailability of poorly-water soluble APDs using a non-invasive route of administration, combined with the possibility to minimize the dose required for treatment and thus reduce the risk of adverse side effects associated with these therapies, is a significant benefit of nanoscale drug delivery systems. In addition, the advantage of sustained drug release imparted by a nanogel will be investigated to determine if prolonged therapeutic intervention is possible. The proposed drug delivery systems have the potential to improve patient adherence to drug regimens relying on APDs for the effective treatment of schizophrenia and will be investigated using preclinical animal models to determine their safety and efficacy for potential translation to clinical applications.

Chapter 2 describes the precipitation polymerization of poly(oligoethylene glycol methacrylate) (POEGMA) nanogels containing hydrophobic domains based on co-polymerization with either butyl methacrylate (BMA) or methyl methacrylate (MMA). These nanogels are synthesized using ethylene glycol dimethacrylate (EGDMA) as the cross-linker to impart pH-responsive degradability. Nanogels containing various amounts of either hydrophobic co-monomer are investigated for the uptake of lurasidone, aiming to enhance its solubility and improve its bioavailability by using an alternative route of administration that does not require gut-mediated absorption. The nanogel formulation showing the highest drug loading capacity is examined *in vitro* for biodegradability and cytotoxicity. *In vivo* pharmacodynamics studies are then conducted to evaluate the efficacy of LUR-loaded nanogels to attenuate locomotor hyperactivity in a rodent model of schizophrenia. Nanogel pharmacokinetics are investigated to determine nanogel fate *in vivo*.

Chapter 3 explores our ability to improve the stimuli-responsive nature of the hydrophobized POEGMA nanogels. The disulfide-containing cross-linker 2-hydroxyethyl disulfide diacrylate is used to introduce a redox responsive moiety within the cross-linker and is investigated for its potential to augment biodegradability and enhance drug release kinetics. Additional nanogel formulations are synthesized to further elucidate the role of hydrophilic/hydrophobic balance in nanogel-based delivery systems. Haloperidol

encapsulated within three distinct nanogel formulations was then used to examine the dose-dependent response of IN administered HLP-containing nanogels in two pharmacodynamics studies, tracking both locomotion and catalepsy. Encapsulation and delivery of haloperidol, which has previously been delivered IN using different nanoparticle-based systems, demonstrates the advantages of using a nanogel to lower drug dose and prolong therapeutic intervention compared to more conventional “hard” nanoparticle drug delivery systems for hydrophobic drugs.

Chapter 4 explores a different technique to synthesize degradable POEGMA nanogels for biomedical applications. Thermoresponsive POEGMA polymers with aldehyde or hydrazide functionality are utilized for the rapid, all-aqueous self-assembly of hydrazone cross-linked nanogels. The ability to control nanogel size and population dispersity is investigated by interchanging the core and cross-linking polymers and varying the quantity of core polymer, cross-link ratio, and reaction temperature relative to the core polymer’s lower critical solution temperature. Multivariate statistical analysis is used to analyze the nanogels’ properties in response to these variables. The ability to scale up the self-assembly process and retain nanogels with ideal properties for biomedical applications is demonstrated.

Chapter 5 utilizes the optimized variables established in Chapter 4 to synthesize POEGMA nanogels with hydrophobic domains derived via the co-polymerization of oligo(lactic acid methacrylate) (OLAMA) into the hydrazide-functionalized precursor polymer. The precursor hydrazide-functionalized polymers containing OLAMA are first optimized to have lower critical solution temperature (LCST) values in an accessible range for self-assembly. The self-assembled nanogels are loaded with olanzapine via both post-synthesis soaking and direct loading via nanogel self-assembly and analyzed based on their degradability, drug release potential, and cytocompatibility. Delivery of olanzapine demonstrates how the unique soft and elastic characteristics of nanogels enable APD delivery to the brain using larger (>100 nm) nanoparticles than typically reported for this application. The therapeutic efficacy of the IN administration of self-assembled OLZ-loaded nanogels is evaluated by quantifying rodent PPI response in a MK-801 induced model of schizophrenia. As this behavioural response is highly conserved between rodents and humans, the ability to restore PPI using olanzapine, a clinically-prescribed APD, reinforces the potential for clinical translation of this novel technology.

Chapter 6 summarizes the overall conclusions derived from the research described herein and proposes future experiments that can further the potential of this work in the field of nanogel-based drug delivery systems.

1.7 References

- (1) Saha, S.; Chant, D.; Welham, J.; McGrath, J., A Systematic Review of the Prevalence of Schizophrenia. *PLoS Med.* **2005**, *2* (5), 413-433.
- (2) van Os, J.; Kapur, S., Schizophrenia. *Lancet* **2009**, *374* (9690), 635-645.
- (3) Jablensky, A., Epidemiology of Schizophrenia: The Global Burden of Disease and Disability. *Eur. Arch. Psych. Clin. Neurosci.* **2000**, *250* (6), 274-285.
- (4) Charlson, F. J.; Ferrari, A. J.; Santomauro, D. F.; Diminic, S.; Stockings, E.; Scott, J. G.; McGrath, J. J.; Whiteford, H. A., Global Epidemiology and Burden of Schizophrenia: Findings from the Global Burden of Disease Study 2016. *Schizophrenia Bull.* **2018**, *44* (6), 1195-1203.
- (5) Segarra, R.; Ojeda, N.; Zabala, A.; García, J.; Catalán, A.; Eguíluz, J. I.; Gutiérrez, M., Similarities in Early Course Among Men and Women with a First Episode of Schizophrenia and Schizophreniform Disorder. *Eur. Arch Psychiatry Clin. Neurosci.* **2012**, *262* (2), 95-105.
- (6) Rossler, W.; Salize, H. J.; van Os, J.; Riecher-Rossler, A., Size of Burden of Schizophrenia and Psychotic Disorders. *Eur. Neuropsychopharmacol.* **2005**, *15* (4), 399-409.
- (7) McGrath, J.; Saha, S.; Chant, D.; Welham, J., Schizophrenia: A Concise Overview of Incidence, Prevalence, and Mortality. *Epidemiol. Rev.* **2008**, *30* (1), 67-76.
- (8) Goeree, R.; Farahati, F.; Burke, N.; Blackhouse, G.; O'Reilly, D.; Pyne, J.; Tarride, J. E., The Economic Burden of Schizophrenia in Canada in 2004. *Curr. Med. Res. Opin.* **2005**, *21* (12), 2017-2028.
- (9) Seeman, M. V.; Seeman, P., Is Schizophrenia a Dopamine Supersensitivity Psychotic Reaction? *Prog. Neuropsychopharmacol. Biol. Psychiatry* **2014**, *48*, 155-160.
- (10) van Rossum, J. M., The Significance of Dopamine-Receptor Blockade for the Mechanism of Action of Neuroleptic Drugs. *Archives Int. Pharmacodyn. Ther.* **1966**, *160* (2), 492-494.
- (11) Seeman, P., Dopamine Receptors and the Dopamine Hypothesis of Schizophrenia. *Synapse (New York, N.Y.)* **1987**, *1* (2), 133-152.
- (12) Delay, J., Utilisation Therapeutique Psychiatrique d'une Phenothiazine d'Action Centrale Lective. *Ann. Med. Psychol.* **1952**, *110*, 112-115.
- (13) Delay, J., Traitement des Etats d'Excitation et Agitation par une Methode Medicamenteuse Derive de l'Hibernotherapie. *Ann. Med. Psychol.* **1952**, *110*, 267-275.
- (14) Hamon, J., Remaques sur l'Action du 4560 RP sur l'Agitation Maniaque. *Ann. Med. Psychol.* **1952**, *110*, 331-335.
- (15) Seeman, P.; Lee, T., The Dopamine-Releasing Actions of Neuroleptics and Ethanol. *J. Pharmacol. Exp. Ther.* **1974**, *190* (1), 131-40.
- (16) Seeman, P.; Lee, T.; Chau-Wong, M.; Wong, K., Antipsychotic Drug Doses and Neuroleptic/Dopamine Receptors. *Nature* **1976**, *261* (5562), 717-719.
- (17) Lieberman, J. A.; Kane, J. M.; Alvir, J., Provocative Tests with Psychostimulant Drugs in Schizophrenia. *Psychopharmacology* **1987**, *91* (4), 415-33.
- (18) Farde, L., Brain Imaging of Schizophrenia—The Dopamine Hypothesis. *Schizophr. Res.* **1997**, *28* (2), 157-162.

- (19) Toda, M.; Abi-Dargham, A., Dopamine Hypothesis of Schizophrenia: Making Sense of it All. *Curr. Psychiat. Reports* **2007**, *9* (4), 329-336.
- (20) Laruelle, M.; Abi-Dargham, A.; Gil, R.; Kegeles, L.; Innis, R., Increased Dopamine Transmission in Schizophrenia: Relationship to Illness Phases. *Biol. Psychiat.* **1999**, *46* (1), 56-72.
- (21) Aringhieri, S.; Carli, M.; Kolachalam, S.; Verdesca, V.; Cini, E.; Rossi, M.; McCormick, P. J.; Corsini, G. U.; Maggio, R.; Scarselli, M., Molecular Targets of Atypical Antipsychotics: From Mechanism of Action to Clinical Differences. *Pharmacol. Therapeut.* **2018**, *192*, 20-41.
- (22) Seeman, P., Schizophrenia and Dopamine Receptors. *Eur. Neuropsychopharm.* **2013**, *23* (9), 999-1009.
- (23) Grunder, G.; Cumming, P., The Dopamine Hypothesis of Schizophrenia: Current status. In *The Neurobiology of Schizophrenia*, Abel, T.; Nickl-Jockschat, T., Eds. Academic Press: United Kingdom, 2016; pp 109-124.
- (24) Okubo, Y.; Suhara, T.; Suzuki, K.; Kobayashi, K.; Inoue, O.; Terasaki, O.; Someya, Y.; Sassa, T.; Sudo, Y.; Matsushima, E.; Iyo, M.; Tateno, Y.; Toru, M., Decreased Prefrontal Dopamine D1 Receptors in Schizophrenia Revealed by PET. *Nature* **1997**, *385* (6617), 634-636.
- (25) Featherstone, R. E.; Kapur, S.; Fletcher, P. J., The Amphetamine-Induced Sensitized State as a Model of Schizophrenia. *Prog. Neuropsychopharmacol. Biol. Psychiatry* **2007**, *31* (8), 1556-1571.
- (26) Balu, D. T., The NMDA Receptor and Schizophrenia: From Pathophysiology to Treatment. *Adv. Pharmacol.* **2016**, *76*, 351-382.
- (27) Löscher, W.; Hönack, D., The Behavioural Effects of MK-801 in Rats: Involvement of Dopaminergic, Serotonergic and Noradrenergic Systems. *Eur. J. Pharmacol.* **1992**, *215* (2), 199-208.
- (28) Dyck, B. A.; Skoblenick, K. J.; Castellano, J. M.; Ki, K.; Thomas, N.; Mishra, R. K., Synapsin II Knockout Mice Show Sensorimotor Gating and Behavioural Abnormalities Similar to Those in the Phencyclidine-Induced Preclinical Animal Model of Schizophrenia. *Schizophr. Res.* **2007**, *97* (1-3), 292-3.
- (29) Logue, S. F.; Gould, T. J., The Neural and Genetic Basis of Executive Function: Attention, Cognitive Flexibility, and Response Inhibition. *Pharmacol. Biochem. Be.* **2014**, *123*, 45-54.
- (30) Olney, J. W.; Newcomer, J. W.; Farber, N. B., NMDA Receptor Hypofunction Model of Schizophrenia. *J. Psychiat. Res.* **1999**, *33* (6), 523-533.
- (31) Basu, D.; Tian, Y.; Hui, P.; Bhandari, J.; Johnson, R. L.; Mishra, R. K., Change in Expression of Vesicular Protein Synapsin II by Chronic Treatment with D2 Allosteric Modulator PAOPA. *Peptides* **2015**, *66*, 58-62.
- (32) Millan, M. J., N-Methyl-D-Aspartate Receptor-Coupled GlycineB Receptors in the Pathogenesis and Treatment of Schizophrenia: A Critical Review. *CNS Neurol. Disord. – DR.* **2002**, *1* (2), 191-213.
- (33) Moghaddam, B.; Adams, B.; Verma, A.; Daly, D., Activation of Glutamatergic Neurotransmission by Ketamine: A Novel Step in the Pathway from NMDA Receptor

- Blockade to Dopaminergic and Cognitive Disruptions Associated with the Prefrontal Cortex. *J.Neurosci.* **1997**, *17* (8), 2921-2927.
- (34) Deutch, A. Y.; Tam, S. Y.; Freeman, A. S.; Bowers, M. B., Jr.; Roth, R. H., Mesolimbic and Mesocortical Dopamine Activation Induced by Phencyclidine: Contrasting Pattern to Striatal Response. *Eur. J. Pharmacol.* **1987**, *134* (3), 257-264.
- (35) Larson, M. K.; Walker, E. F.; Compton, M. T., Early Signs, Diagnosis and Therapeutics of the Prodromal Phase of Schizophrenia and Related Psychotic Disorders. *Expert Rev. Neurother.* **2010**, *10* (8), 1347-1359.
- (36) Greenberg, W. M.; Citrome, L., Pharmacokinetics and Pharmacodynamics of Lurasidone Hydrochloride, a Second-Generation Antipsychotic: A Systematic Review of the Published Literature. *Clin. Pharmacokinet.* **2017**, *56* (5), 493-503.
- (37) Veerman, S. R. T.; Schulte, P. F. J.; de Haan, L., Treatment for Negative Symptoms in Schizophrenia: A Comprehensive Review. *Drugs* **2017**, *77* (13), 1423-1459.
- (38) Peralta, V.; De Leon, J.; Cuesta, M. J., Are There More Than Two Syndromes in Schizophrenia?: A Critique of the Positive-Negative Dichotomy. *Br. J. Psychiatry* **2018**, *161* (3), 335-343.
- (39) Powell, C. M.; Miyakawa, T., Schizophrenia-Relevant Behavioral Testing in Rodent Models: A Uniquely Human Disorder? *Biol. Psychiatry* **2006**, *59* (12), 1198-1207.
- (40) Marcotte, E. R.; Pearson, D. M.; Srivastava, L. K., Animal Models of Schizophrenia: A Critical Review. *J. Psychiatry Neurosci.* **2001**, *26* (5), 395-410.
- (41) Tollens, F.; Gass, N.; Becker, R.; Schwarz, A. J.; Risterucci, C.; Künnecke, B.; Lehardt, P.; Reinwald, J.; Sack, M.; Weber-Fahr, W.; Meyer-Lindenberg, A.; Sartorius, A., The Affinity of Antipsychotic Drugs to Dopamine and Serotonin 5-HT(2) Receptors Determines Their Effects on Prefrontal-Striatal Functional Connectivity. *Eur. Neuropsychopharmacol.* **2018**, *28* (9), 1035-1046.
- (42) Gobira, P. H.; Ropke, J.; Aguiar, D. C.; Crippa, J. A. S.; Moreira, F. A., Animal Models for Predicting the Efficacy and Side Effects of Antipsychotic Drugs. *Braz. J. Psychiatry* **2013**, *35*, S132-S139.
- (43) Tenn, C. C.; Kapur, S.; Fletcher, P. J., Sensitization to Amphetamine, but Not Phencyclidine, Disrupts Prepulse Inhibition and Latent Inhibition. *Psychopharmacology* **2005**, *180* (2), 366-376.
- (44) Winship, I. R.; Dursun, S. M.; Baker, G. B.; Balista, P. A.; Kandratavicius, L.; Maia-de-Oliveira, J. P.; Hallak, J.; Howland, J. G., An Overview of Animal Models Related to Schizophrenia. *Can. J. Psychiatry* **2019**, *64* (1), 5-17.
- (45) Ellenbroek, B. A.; Cools, A. R., Apomorphine Susceptibility and Animal Models for Psychopathology: Genes and Environment. *Behav. Genet.* **2002**, *32* (5), 349-361.
- (46) Bubenikova, V.; Votava, M.; Horacek, J.; Palenicek, T.; Dockery, C., The Effect of Zotepine, Risperidone, Clozapine and Olanzapine on MK-801-Disrupted Sensorimotor Gating. *Pharmacol. Biochem. Behav.* **2005**, *80* (4), 591-596.
- (47) Lee, G.; Zhou, Y., NMDAR Hypofunction Animal Models of Schizophrenia. *Front. Mol. Neurosci.* **2019**, *12*, 185.
- (48) Daya, R. P.; Bhandari, J.; Kooner, S. K.; Ho, J.; Rowley, C. D.; Bock, N. A.; Farncombe, T.; Mishra, R. K., The Dopamine Allosteric Agent, PAOPA, Demonstrates Therapeutic

- Potential in the Phencyclidine NMDA Preclinical Rat Model of Schizophrenia. *Front. Behav. Neurosci.* **2018**, *12*, 302-302.
- (49) Zangrando, J.; Carvalho, R.; Labbate, G.; Medeiros, P.; Longo, B. M.; Melo-Thomas, L.; Barbosa Silva, R. C., Atypical Antipsychotic Olanzapine Reversed Deficit on Prepulse Inhibition of the Acoustic Startle Reflex Produced by Microinjection of Dizocilpine (MK-801) into The Inferior Colliculus in Rats. *Behav. Brain Res.* **2013**, *257*, 77-82.
- (50) Katare, Y. K.; Piazza, J. E.; Bhandari, J.; Daya, R. P.; Akilan, K.; Simpson, M. J.; Hoare, T.; Mishra, R. K., Intranasal Delivery of Antipsychotic Drugs. *Schizophr. Res.* **2017**, *184*, 2-13.
- (51) SamsDodd, F., Effect of Novel Antipsychotic Drugs on Phencyclidine-Induced Stereotyped Behaviour and Social Isolation in the Rat Social Interaction Test. *Behav. Pharmacol.* **1997**, *8* (2-3), 196-215.
- (52) Katare, Y. K.; Daya, R. P.; Gray, C. S.; Luckham, R. E.; Bhandari, J.; Chauhan, A. S.; Mishre, R. K., Brain Targeting of a Water Insoluble Antipsychotic Drug Haloperidol via the Intranasal Route using PAMAM Dendrimer. *Mol. Pharm.* **2015**, *12* (9), 3380-3388.
- (53) Piazza, J.; Hoare, T.; Molinaro, L.; Terpstra, K.; Bhandari, J.; Selvaganapathy, P. R.; Gupta, B.; Mishra, R. K., Haloperidol-Loaded Intranasally Administered Lectin Functionalized Poly(Ethylene Glycol)-Block-Poly(D,L)-Lactic-Co-Glycolic Acid (PEG-PLGA) Nanoparticles for the Treatment Of Schizophrenia. *Eur. J. Pharm. Biopharm.* **2014**, *87* (1), 30-39.
- (54) Bakshi, V. P.; Swerdlow, N. R.; Braff, D. L.; Geyer, M. A., Reversal of Isolation Rearing-Induced Deficits in Prepulse Inhibition by Seroquel And Olanzapine. *Biol. Psychiatry* **1998**, *43* (6), 436-445.
- (55) Martin, R. S.; Secchi, R. L.; Sung, E.; Lemaire, M.; Bonhaus, D. W.; Hedley, L. R.; Lowe, D. A., Effects of Cannabinoid Receptor Ligands on Psychosis-Relevant Behavior Models in the Rat. *Psychopharmacology* **2003**, *165* (2), 128-135.
- (56) Braff, D. L.; Geyer, M. A., Sensorimotor Gating and Schizophrenia. Human and Animal Model Studies. *Arch. Gen. Psychiatry* **1990**, *47* (2), 181-188.
- (57) Cilia, J.; Reavill, C.; Hagan, J. J.; Jones, D. N. C., Long-term Evaluation of Isolation-Rearing Induced Prepulse Inhibition Deficits in Rats. *Psychopharmacology* **2001**, *156* (2-3), 327-337.
- (58) Meyer, J. S., Chapter 22 - Behavioral Assessment in Developmental Neurotoxicology: Approaches Involving Unconditioned Behaviors Pharmacologic Challenges in Rodents. In *Handbook of Developmental Neurotoxicology*, Slikker, W.; Chang, L. W., Eds. Academic Press: San Diego, 1998; pp 403-426.
- (59) Azmanova, M.; Pitto-Barry, A.; Barry, N. P. E., Schizophrenia: Synthetic Strategies and Recent Advances in Drug Design. *Medchemcomm* **2018**, *9* (5), 759-782.
- (60) Mailman, R. B.; Murthy, V., Third Generation Antipsychotic Drugs: Partial Agonism or Receptor Functional Selectivity? *Curr. Pharm. Des.* **2010**, *16* (5), 488-501.
- (61) Chokhawala, K.; Stevens, L., Antipsychotic Medications. In *StatPearls*, StatPearls Publishing Copyright © 2020, StatPearls Publishing LLC.: Treasure Island (FL), 2020.
- (62) Yilmaz, Z.; Zai, C. C.; Hwang, R.; Mann, S.; Arenovich, T.; Remington, G.; Daskalakis, Z. J., Antipsychotics, Dopamine D2 receptor Occupancy and Clinical Improvement in Schizophrenia: A Meta-Analysis. *Schizophr. Res.* **2012**, *140* (1), 214-220.

- (63) de Germay, S.; Montastruc, F.; Carvajal, A.; Lapeyre-Mestre, M.; Montastruc, J.-L., Drug-Induced Parkinsonism: Revisiting the Epidemiology Using the WHO Pharmacovigilance Database. *Parkinsonism Relat. Disord.* **2020**, *70*, 55-59.
- (64) Correll, C. U.; Leucht, S.; Kane, J. M., Lower Risk for Tardive Dyskinesia Associated with Second-Generation Antipsychotics: A Systematic Review of 1-year Studies. *Am. J. Psychiatry* **2004**, *161* (3), 414-425.
- (65) Thaakur, S. R.; Jyothi, B., Effect of Spirulina Maxima on the Haloperidol Induced Tardive Dyskinesia and Oxidative Stress in Rats. *J. Neural Transm.* **2007**, *114* (9), 1217-1225.
- (66) World Health Organization, World Health Organization Model List of Essential Medicines, 21st List, 2019. World Health Organization: Geneva, 2019.
- (67) Golfar, Y.; Shayanfar, A., Prediction of Biopharmaceutical Drug Disposition Classification System (BDDCS) by Structural Parameters. *J. Pharm.* **2019**, *22* (1), 247-269.
- (68) Schotte, A.; Janssen, P. F. M.; Megens, A. A. H. P.; Leysen, J. E., Occupancy of Central Neurotransmitter Receptors by Risperidone, Clozapine And Haloperidol, Measured Ex Vivo by Quantitative Autoradiography. *Brain Res.* **1993**, *631* (2), 191-202.
- (69) Kapur, S.; Seeman, P., Antipsychotic Agents Differ in How Fast They Come Off the Dopamine D2 Receptors. Implications for Atypical Antipsychotic Action. *J. Psychiatry Neurosci.* **2000**, *25* (2), 161-166.
- (70) Hou, Y.; Yang, J. Y.; Wu, C. F.; Huang, M., Effects of Clozapine, Olanzapine And Haloperidol on Ethanol-Induced Ascorbic Acid Release in Mouse Striatum. *Prog. Neuropsychopharmacol. Biol. Psychiatry* **2005**, *29* (1), 83-89.
- (71) Igarashi, K.; Kasuya, F.; Fukui, M.; Usuki, E.; Castagnoli, N., Studies on the Metabolism of Haloperidol (HP) - the Role of Cyp3a in the Production of the Neurotoxic Pyridinium Metabolite HPP+ found in Rat-Brain Following IP Administration of HP. *Life Sci.* **1995**, *57* (26), 2439-2446.
- (72) Sykes, D. A.; Moore, H.; Stott, L.; Holliday, N.; Javitch, J. A.; Lane, J. R.; Charlton, S. J., Extrapyramidal Side Effects of Antipsychotics are Linked to Their Association Kinetics at Dopamine D2 Receptors. *Nat. Commun.* **2017**, *8* (1), 763.
- (73) Fyfe, T. J.; Kellam, B.; Sykes, D. A.; Capuano, B.; Scammells, P. J.; Lane, J. R.; Charlton, S. J.; Mistry, S. N., Structure–Kinetic Profiling of Haloperidol Analogues at the Human Dopamine D2 Receptor. *J. Med. Chem.* **2019**, *62* (21), 9488-9520.
- (74) Moller, H. J.; Kissling, W.; Lang, C.; Doerr, P.; Pirke, K. M.; Vonzerssen, D., Efficacy and Side-Effects of Haloperidol in Psychotic-Patients - Oral Versus Intravenous Administration. *Am. J. Psychiat.* **1982**, *139* (12), 1571-1575.
- (75) Murata, T.; Maruoka, N.; Omata, N.; Takashima, Y.; Igarashi, K.; Kasuya, F.; Fujibayashi, Y.; Wada, Y., Effects of Haloperidol and Its Pyridinium Metabolite on Plasma Membrane Permeability and Fluidity in the Rat Brain. *Prog. Neuropsychopharmacol. Biol. Psychiatry* **2007**, *31* (4), 848-857.
- (76) Kudo, S.; Ishizaki, T., Pharmacokinetics of Haloperidol. *Clin. Pharmacokinet.* **1999**, *37* (6), 435-456.
- (77) Takahashi, M.; Uehara, T.; Nonaka, M.; Minagawa, Y.; Yamazaki, R.; Haba, M.; Hosokawa, M., Synthesis and Evaluation Of Haloperidol Ester Prodrugs Metabolically Activated by Human Carboxylesterase. *Eur. J. Pharm. Sci.* **2019**, *132*, 125-131.

- (78) Joseph, E.; Reddi, S.; Rinwa, V.; Balwani, G.; Saha, R., Design and In Vivo Evaluation of Solid Lipid Nanoparticulate Systems of Olanzapine for Acute Phase Schizophrenia Treatment: Investigations on Antipsychotic Potential and Adverse Effects. *E. J. Pharm. Sci.* **2017**, *104*, 315-325.
- (79) Lord, C. C.; Wyler, S. C.; Wan, R.; Castorena, C. M.; Ahmed, N.; Mathew, D.; Lee, S.; Liu, C.; Elmquist, J. K., The Atypical Antipsychotic Olanzapine Causes Weight Gain by Targeting Serotonin Receptor 2C. *J. Clin. Invest.* **2017**, *127* (9), 3402-3406.
- (80) Moore, N. A.; Tye, N. C.; Axton, M. S.; Risius, F. C., The Behavioral Pharmacology of Olanzapine, a Novel "Atypical" Antipsychotic Agent. *J. Pharmacol. Exp. Ther.* **1992**, *262* (2), 545-551.
- (81) Bymaster, F. P.; Calligaro, D. O.; Falcone, J. F.; Marsh, R. D.; Moore, N. A.; Tye, N. C.; Seeman, P.; Wong, D. T., Radioreceptor Binding Profile of the Atypical Antipsychotic Olanzapine. *Neuropsychopharmacology* **1996**, *14* (2), 87-96.
- (82) Li, X. M.; Perry, K. W.; Wong, D. T.; Bymaster, F. P., Olanzapine Increases In Vivo Dopamine and Norepinephrine Release in Rat Prefrontal Cortex, Nucleus Accumbens and Striatum. *Psychopharmacology* **1998**, *136* (2), 153-161.
- (83) Firdous, S.; Aman, T.; Nisa, A. U., Determination of Olanzapine by UV Spectrophotometry and Non-Aqueous Titration. *J. Chem. Soc. Pak.* **2005**, *27* (2), 163-167.
- (84) Renkoglu, P.; Celebier, M.; Arica-Yegin, B., HPLC Determination of Olanzapine and Carbamazepine in their Nicotinamide Cocrystals and Investigation of the Dissolution Profiles of Cocrystal Tablet Formulations. *Pharm. Dev. Technol.* **2015**, *20* (3), 380-384.
- (85) Ninan, I.; Kulkarni, S. K., Preferential Inhibition of Dizocilpine-Induced Hyperlocomotion by Olanzapine. *Eur. J. Pharmacol.* **1999**, *368* (1), 1-7.
- (86) Badshah, A.; Subhan, F.; Rauf, K., Controlled Release Matrix Tablets of Olanzapine: Influence of Polymers on the In Vitro Release and Bioavailability. *AAPS PharmSciTech.* **2010**, *11* (3), 1397-1404.
- (87) Gupta, N. V.; Gowda, D. V.; Balamuralidhara, V.; Khan, S. M., Formulation and Evaluation of Olanzapine Matrix Pellets for Controlled Release. *DARU* **2011**, *19* (4), 249-256.
- (88) Dixit, M.; Kini, A. G.; Kulkarni, P. K., Enhancing the Aqueous Solubility and Dissolution of Olanzapine Using Freeze-Drying. *Braz. J. Pharm. Sci.* **2011**, *47* (4), 743-749.
- (89) Abdelbary, G. A.; Tadros, M. I., Brain Targeting of Olanzapine via Intranasal Delivery of Core-Shell Difunctional Block Copolymer Mixed Nanomicellar Carriers: In Vitro Characterization, Ex Vivo Estimation of Nasal Toxicity and In Vivo Biodistribution Studies. *Int. J. Pharm.* **2013**, *452* (1), 300-310.
- (90) Bushe, C. J.; Falk, D.; Anand, E.; Casillas, M.; Perrin, E.; Chhabra-Khanna, R.; Detke, H. C., Olanzapine Long-Acting Injection: A Review of First Experiences of Post-Injection Delirium/Sedation Syndrome in Routine Clinical Practice. *BMC Psychiatry* **2015**, *15* (1), 65.
- (91) Samalin, L.; Garnier, M.; Llorca, P. M., Clinical Potential of Lurasidone in the Management of Schizophrenia. *Therap. Clin. Risk Manag.* **2011**, *7*, 239-250.
- (92) Ishibashi, T.; Horisawa, T.; Tokuda, K.; Ishiyama, T.; Ogasa, M.; Tagashira, R.; Matsumoto, K.; Nishikawa, H.; Ueda, Y.; Toma, S.; Oki, H.; Tanno, N.; Saji, I.; Ito, A.;

- Ohno, Y.; Nakamura, M., Pharmacological Profile of Lurasidone, A Novel Antipsychotic Agent with Potent 5-Hydroxytryptamine 7 (5-HT7) and 5-HT1A Receptor Activity. *J. Pharmacol. Exp. Ther.* **2010**, *334* (1), 171-181.
- (93) Horisawa, T.; Ishiyama, T.; Ono, M.; Ishibashi, T.; Taiji, M., Binding of Lurasidone, A Novel Antipsychotic, to Rat 5-HT7 Receptor: Analysis by H-3 SB-269970 Autoradiography. *Prog. Neuropsychopharmacol. Biol. Psychiatry* **2013**, *40*, 132-137.
- (94) Kantrowitz, J. T.; Citrome, L., Lurasidone for Schizophrenia: What's Different? *Expert Rev. Neurother.* **2012**, *12* (3), 265-273.
- (95) Tarazi, F. I.; Riva, M. A., The Preclinical Profile of Lurasidone: Clinical Relevance for the Treatment of Schizophrenia. *Expert. Opin. Drug Discov.* **2013**, *8* (10), 1297-1307.
- (96) Freyberg, Z.; Aslanoglou, D.; Shah, R.; Ballon, J. S., Intrinsic and Antipsychotic Drug-Induced Metabolic Dysfunction in Schizophrenia. *Front. Neurosci.* **2017**, *11*, 432.
- (97) Jacob, A.; Alexander, J. J., Complement and Blood-Brain Barrier Integrity. *Mol. Immunol.* **2014**, *61* (2), 149-152.
- (98) Hwang, S. R.; Kim, K., Nano-Enabled Delivery Systems Across the Blood-Brain Barrier. *Arch. Pharm. Res.* **2014**, *37* (1), 24-30.
- (99) Sahoo, S. K.; Labhassetwar, V., Nanotech Approaches to Delivery and Imaging Drug. *Drug Discov. Today* **2003**, *8* (24), 1112-1120.
- (100) Liu, D.; Lin, B.; Shao, W.; Zhu, Z.; Ji, T.; Yang, C., In Vitro and In Vivo Studies on the Transport of PEGylated Silica Nanoparticles Across the Blood-Brain Barrier. *ACS Appl. Mater. Interfaces* **2014**, *6* (3), 2131-2136.
- (101) Mukherjee, S.; Madamsetty, V. S.; Bhattacharya, D.; Roy Chowdhury, S.; Paul, M. K.; Mukherjee, A., Recent Advancements of Nanomedicine in Neurodegenerative Disorders Theranostics. *Adv. Funct. Mater.* **2020**, *30* (35), 2003054.
- (102) Gao, H. L.; Pang, Z. Q.; Jiang, X. G., Targeted Delivery of Nano-Therapeutics for Major Disorders of the Central Nervous System. *Pharm. Res.* **2013**, *30* (10), 2485-2498.
- (103) Lochhead, J. J.; Thorne, R. G., Intranasal Delivery of Biologics to the Central Nervous System. *Adv. Drug Deliv. Rev.* **2012**, *64* (7), 614-628.
- (104) Pardridge, W. M., The Blood-Brain Barrier: Bottleneck in Brain Drug Development. *NeuroRx* **2005**, *2* (1), 3-14.
- (105) Jawahar, N.; Hingarh, P. K.; Arun, R.; Selvaraj, J.; Anbarasan, A.; S, S.; G, N., Enhanced Oral Bioavailability of an Antipsychotic Drug Through Nanostructured Lipid Carriers. *Int. J. Biol. Macromol.* **2018**, *110*, 269-275.
- (106) Seju, U.; Kumar, A.; Sawant, K. K., Development and Evaluation of Olanzapine-Loaded PLGA Nanoparticles for Nose-to-Brain Delivery: In Vitro and In Vivo Studies. *Acta Biomater.* **2011**, *7* (12), 4169-4176.
- (107) Oosthuizen, P. P.; Emsley, R. A.; Maritz, J. S.; Turner, J. A.; Keyter, N., Incidence of Tardive Dyskinesia in First-Episode Psychosis Patients Treated with Low-Dose Haloperidol. *J. Clin. Psychiatry* **2003**, *64* (9), 1075-1080.
- (108) Montgomery, W.; Treuer, T.; Karagianis, J.; Ascher-Svanum, H.; Harrison, G., Orally Disintegrating Olanzapine Review: Effectiveness, Patient Preference, Adherence, and Other Properties. *Patient Prefer. Adherence* **2012**, *6*, 109-125.

- (109) Bera, R. B., Patient Outcomes Within Schizophrenia Treatment: A Look at the Role of Long-Acting Injectable Antipsychotics. *J. Clin. Psychiatry* **2014**, *75* (2), 30-33.
- (110) Chan, E. W.; Knott, J. C.; Taylor, D. M.; Kong, D. C. M., Intravenous Olanzapine for Acute Agitation in the Emergency Department. *J. Pharm. Pract. Res.* **2011**, *41* (2), 135-138.
- (111) Khorassani, F.; Saad, M., Intravenous Olanzapine for the Management of Agitation: Review of the Literature. *Ann. Pharmacother.* **2019**, *53* (8), 853-859.
- (112) Martel, M. L.; Klein, L. R.; Rivard, R. L.; Cole, J. B., A Large Retrospective Cohort of Patients Receiving Intravenous Olanzapine in the Emergency Department. *Acad. Emerg. Med.* **2016**, *23* (1), 29-35.
- (113) Ranković, A.; Jankovic, S., Problems with the Administration of Antipsychotic Drugs in Depot Formulations in the Treatment of Schizophrenia. *Acta Fac. Med. Naiss.* **2018**, *35*, 65-72.
- (114) Tveito, M.; Smith, R. L.; Molden, E.; Haslemo, T.; Refsum, H.; Hartberg, C.; Correll, C. U.; Høiseth, G., Age Impacts Olanzapine Exposure Differently During Use of Oral Versus Long-Acting Injectable Formulations: An Observational Study Including 8,288 Patients. *J. Clin. Psychopharmacol.* **2018**, *38* (6), 570-576.
- (115) Leucht, C.; Heres, S.; Kane, J. M.; Kissling, W.; Davis, J. M.; Leucht, S., Oral Versus Depot Antipsychotic Drugs for Schizophrenia--A Critical Systematic Review and Meta-Analysis of Randomised Long-Term Trials. *Schizophr. Res.* **2011**, *127* (1-3), 83-92.
- (116) Olagunju, A. T.; Clark, S. R.; Baune, B. T., Long-Acting Atypical Antipsychotics in Schizophrenia: A Systematic Review and Meta-Analyses of Effects on Functional Outcome. *Aus. NZ. J. Psychiat.* **2019**, *53* (6), 509-527.
- (117) Park, E. J.; Amatya, S.; Kim, M. S.; Park, J. H.; Seol, E.; Lee, H.; Shin, Y. H.; Na, D. H., Long-Acting Injectable Formulations of Antipsychotic Drugs for the Treatment of Schizophrenia. *Arch. Pharm. Res.* **2013**, *36* (6), 651-659.
- (118) Scigliano, G.; Ronchetti, G., Antipsychotic-Induced Metabolic and Cardiovascular Side Effects in Schizophrenia: A Novel Mechanistic Hypothesis. *CNS Drugs* **2013**, *27* (4), 249-257.
- (119) Hanson, L. R.; Frey, W. H., Intranasal Delivery Bypasses the Blood-Brain Barrier to Target Therapeutic Agents to the Central Nervous System and Treat Neurodegenerative Disease. *BMC Neurosci.* **2008**, *9* (3), 1-4.
- (120) Kozlovskaya, L.; Abou-Kaoud, M.; Stepensky, D., Quantitative Analysis of Drug Delivery to the Brain via Nasal Route. *J. Control. Release* **2014**, *189*, 133-140.
- (121) Dhuria, S. V.; Hanson, L. R.; Frey, W. H., Intranasal Delivery to The Central Nervous System: Mechanisms and Experimental Considerations. *J. Pharm. Sci.* **2010**, *99* (4), 1654-1673.
- (122) Mathison, S.; Nagilla, R.; Kompella, U. B., Nasal Route for Direct Delivery of Solutes to the Central Nervous System: Fact or Fiction? *J. Drug Target.* **1998**, *5* (6), 415-41.
- (123) Illum, L., Transport of Drugs from the Nasal Cavity to the Central Nervous System. *Eur. J. Pharm. Sci.* **2000**, *11* (1), 1-18.
- (124) Illum, L., Is Nose-to-Brain Transport of Drugs in Man a Reality? *J. Pharm. Pharmacol.* **2004**, *56* (1), 3-17.

- (125) Bahadur, S.; Pathak, K., Physicochemical and Physiological Considerations for Efficient Nose-to-Brain Targeting. *Expert. Opin. Drug. Deliv.* **2012**, *9* (1), 19-31.
- (126) Quadir, M.; Zia, H.; Needham, T. E., Toxicological Implications of Nasal Formulations. *Drug Deliv.* **1999**, *6* (4), 227-242.
- (127) Pires, P. C.; Santos, A. O., Nanosystems in Nose-to-Brain Drug Delivery: A Review of Non-Clinical Brain Targeting Studies. *J. Control. Release* **2018**, *270*, 89-100.
- (128) Saraiva, C.; Praça, C.; Ferreira, R.; Santos, T.; Ferreira, L.; Bernardino, L., Nanoparticle-Mediated Brain Drug Delivery: Overcoming Blood-Brain Barrier to Treat Neurodegenerative Diseases. *J. Control. Release* **2016**, *235*, 34-47.
- (129) Vinogradov, S. V.; Batrakova, E. V.; Kabanov, A. V., Nanogels for Oligonucleotide Delivery to the Brain. *Bioconj. Chem.* **2004**, *15* (1), 50-60.
- (130) Shilo, M.; Sharon, A.; Baranes, K.; Motiei, M.; Lellouche, J.-P. M.; Popovtzer, R., The Effect of Nanoparticle Size on the probability to Cross The Blood-Brain Barrier: An In-Vitro Endothelial Cell Model. *J. Nanobiotechnology* **2015**, *13* (1), 19.
- (131) Wohlfart, S.; Gelperina, S.; Kreuter, J., Transport of Drugs Across the Blood-Brain Barrier by Nanoparticles. *J. Control. Release* **2012**, *161* (2), 264-73.
- (132) Ceña, V.; Játiva, P., Nanoparticle Crossing of Blood–Brain Barrier: a Road to New Therapeutic Approaches to Central Nervous System Diseases. *Nanomedicine* **2018**, *13* (13), 1513-1516.
- (133) Chen, Y. C.; Hsieh, W. Y.; Lee, W. F.; Zeng, D. T., Effects of Surface Modification of PLGA-PEG-PLGA Nanoparticles on Loperamide Delivery Efficiency Across The Blood-Brain Barrier. *J. Biomater. Appl.* **2013**, *27* (7), 909-922.
- (134) Khan, K. U.; Akhtar, N.; Minhas, M. U., Poloxamer-407-Co-Poly (2-Acrylamido-2-Methylpropane Sulfonic Acid) Cross-Linked Nanogels for Solubility Enhancement of Olanzapine: Synthesis, Characterization, and Toxicity Evaluation. *AAPS PharmSciTech.* **2020**, *21* (5), 141.
- (135) Joseph, E.; Saha, R. N., Investigations on Pharmacokinetics and Biodistribution of Polymeric and Solid Lipid Nanoparticulate Systems of Atypical Antipsychotic Drug: Effect of Material Used and Surface Modification. *Drug. Dev. Ind. Pharm.* **2017**, *43* (4), 678-686.
- (136) Blanco, E.; Shen, H.; Ferrari, M., Principles of nanoparticle design for Overcoming Biological Barriers to Drug Delivery. *Nat. Biotechnol.* **2015**, *33* (9), 941-951.
- (137) Navya, P. N.; Daima, H. K., Rational Engineering of Physicochemical Properties of Nanomaterials for Biomedical Applications with Nanotoxicological Perspectives. *Nano Converg.* **2016**, *3* (1), 1.
- (138) Kolhar, P.; Anselmo, A. C.; Gupta, V.; Pant, K.; Prabhakarandian, B.; Ruoslahti, E.; Mitragotri, S., Using Shape Effects to Target Antibody-Coated Nanoparticles to Lung and Brain Endothelium. *PNAS* **2013**, *110* (26), 10753-10758.
- (139) Tan, J.; Shah, S.; Thomas, A.; Ou-Yang, H. D.; Liu, Y., The Influence of Size, Shape and Vessel Geometry on Nanoparticle Distribution. *Microfluid. Nanofluidics* **2013**, *14* (1), 77-87.

- (140) Huang, X.; Teng, X.; Chen, D.; Tang, F.; He, J., The Effect of the Shape of Mesoporous Silica Nanoparticles on Cellular Uptake and Cell Function. *Biomaterials* **2010**, *31* (3), 438-448.
- (141) Hinde, E.; Thammasiraphop, K.; Duong, H. T. T.; Yeow, J.; Karagoz, B.; Boyer, C.; Gooding, J. J.; Gaus, K., Pair Correlation Microscopy Reveals the Role of Nanoparticle Shape in Intracellular Transport and Site of Drug Release. *Nat. Nanotechnol.* **2017**, *12* (1), 81-89.
- (142) Brown, T. D.; Habibi, N.; Wu, D.; Lahann, J.; Mitragotri, S., Effect of Nanoparticle Composition, Size, Shape, and Stiffness on Penetration Across the Blood–Brain Barrier. *ACS Biomater. Sci. Eng.* **2020**, *6* (9), 4916–4928
- (143) Suk, J. S.; Xu, Q.; Kim, N.; Hanes, J.; Ensign, L. M., PEGylation as a Strategy for Improving Nanoparticle-Based Drug and Gene Delivery. *Adv. Drug Deliv. Rev.* **2016**, *99*, 28-51.
- (144) Lai, S. K.; Wang, Y.-Y.; Hanes, J., Mucus-Penetrating Nanoparticles for Drug and Gene Delivery to Mucosal Tissues. *Adv. Drug Deliv. Rev.* **2009**, *61* (2), 158-171.
- (145) Tang, B. C.; Dawson, M.; Lai, S. K.; Wang, Y.-Y.; Suk, J. S.; Yang, M.; Zeitlin, P.; Boyle, M. P.; Fu, J.; Hanes, J., Biodegradable Polymer Nanoparticles that Rapidly Penetrate the Human Mucus Barrier. *PNAS* **2009**, *106* (46), 19268-19273.
- (146) Wang, Y.-Y.; Lai, S. K.; Suk, J. S.; Pace, A.; Cone, R.; Hanes, J., Addressing the PEG Mucoadhesivity Paradox to Engineer Nanoparticles that “Slip” Through the Human Mucus Barrier. *Angew. Chem. Int. Ed.* **2008**, *47* (50), 9726-9729.
- (147) Yang, M.; Lai, S. K.; Wang, Y.-Y.; Zhong, W.; Happe, C.; Zhang, M.; Fu, J.; Hanes, J., Biodegradable Nanoparticles Composed Entirely of Safe Materials that Rapidly Penetrate Human Mucus. *Angew. Chem. Int. Ed.* **2011**, *50* (11), 2597-2600.
- (148) Ajitha, B.; Kumar Reddy, Y. A.; Reddy, P. S.; Jeon, H.-J.; Ahn, C. W., Role of Capping Agents in Controlling Silver Nanoparticles Size, Antibacterial Activity and Potential Application as Optical Hydrogen Peroxide Sensor. *RSC Adv.* **2016**, *6* (42), 36171-36179.
- (149) Kumar, M.; Misra, A.; Mishra, A. K.; Mishra, P.; Pathak, K., Mucoadhesive Nanoemulsion-Based Intranasal Drug Delivery System of Olanzapine for Brain Targeting. *J. Drug. Target.* **2008**, *16* (10), 806-814.
- (150) Pedrosa, S. S.; Goncalves, C.; David, L.; Gama, M., A Novel Crosslinked Hyaluronic Acid Nanogel for Drug Delivery. *Macromol. Biosci.* **2014**, *14* (11), 1556-1568.
- (151) Argyo, C.; Cauda, V.; Engelke, H.; Rädler, J.; Bein, G.; Bein, T., Heparin-Coated Colloidal Mesoporous Silica Nanoparticles Efficiently Bind to Antithrombin as an Anticoagulant Drug-Delivery System. *Chem.-Eur. J.* **2012**, *18* (2), 428-432.
- (152) Thilagam, R.; Gnanamani, A., Preparation, Characterization and Stability Assessment of Keratin and Albumin Functionalized Gold Nanoparticles for Biomedical Applications. *Appl. Nanosci.* **2020**, *10* (6), 1879-1892.
- (153) Chang, J.; Jallouli, Y.; Kroubi, M.; Yuan, X. B.; Feng, W.; Kang, C. S.; Pu, P. Y.; Betbeder, D., Characterization of endocytosis of transferrin-coated PLGA Nanoparticles by the Blood–Brain Barrier. *Int. J. Pharm.* **2009**, *379* (2), 285-292.
- (154) Huang, R.; Ke, W.; Han, L.; Liu, Y.; Shao, K.; Ye, L.; Lou, J.; Jiang, C.; Pei, Y., Brain-Targeting Mechanisms of Lactoferrin-Modified DNA-Loaded Nanoparticles. *Journal of Cereb. Blood Flow Metab.* **2009**, *29* (12), 1914-1923.

- (155) Limongi, T.; Canta, M.; Racca, L.; Ancona, A.; Tritta, S.; Vighetto, V.; Cauda, V., Improving Dispersal of Therapeutic Nanoparticles in the Human Body. *Nanomedicine* **2019**, *14* (7), 797-801.
- (156) Dumontel, B.; Canta, M.; Engelke, H.; Chiodoni, A.; Racca, L.; Ancona, A.; Limongi, T.; Canavese, G.; Cauda, V., Enhanced Biostability and Cellular Uptake of Zinc Oxide Nanocrystals Shielded with a Phospholipid Bilayer. *J. Mater. Chem. B* **2017**, *5* (44), 8799-8813.
- (157) Fenart, L.; Casanova, A.; Dehouck, B.; Duhem, C.; Slupek, S.; Cecchelli, R.; Betbeder, D., Evaluation of Effect of Charge and Lipid Coating on Ability of 60-nm Nanoparticles to Cross an In Vitro Model of the Blood-Brain Barrier. *J. Pharmacol. Exp. Ther.* **1999**, *291* (3), 1017-1022.
- (158) Srivastava, A.; Amreddy, N.; Babu, A.; Panneerselvam, J.; Mehta, M.; Muralidharan, R.; Chen, A.; Zhao, Y. D.; Razaq, M.; Riedinger, N.; Kim, H.; Liu, S.; Wu, S.; Abdel-Mageed, A. B.; Munshi, A.; Ramesh, R., Nanosomes Carrying Doxorubicin Exhibit Potent Anticancer Activity Against Human Lung Cancer Cells. *Sci. Rep.* **2016**, *6* (1), 38541.
- (159) Illes, B.; Hirschle, P.; Barnert, S.; Cauda, V.; Wuttke, S.; Engelke, H., Exosome-Coated Metal–Organic Framework Nanoparticles: An Efficient Drug Delivery Platform. *Chem. Mater.* **2017**, *29* (19), 8042-8046.
- (160) Khongkow, M.; Yata, T.; Boonrungsiman, S.; Ruktanonchai, U. R.; Graham, D.; Namdee, K., Surface Modification of Gold Nanoparticles with Neuron-Targeted Exosome for Enhanced Blood–Brain Barrier Penetration. *Sci. Rep.* **2019**, *9* (1), 8278.
- (161) Chen, Y.; Liu, L. H., Modern Methods for Delivery of Drugs Across the Blood-Brain Barrier. *Adv. Drug Deliv. Rev.* **2012**, *64* (7), 640-665.
- (162) Yin, J.; Chen, Y.; Zhang, Z. H.; Han, X., Stimuli-Responsive Block Copolymer-Based Assemblies for Cargo Delivery and Theranostic Applications. *Polymers* **2016**, *8* (7), 29.
- (163) Kemme, M.; Prokesch, I.; Heinzl-Wieland, R., Comparative Study on the Enzymatic Degradation Of Poly(Lactic-Co-Glycolic Acid) by Hydrolytic Enzymes Based on the Colorimetric Quantification of Glycolic Acid. *Polym. Test.* **2011**, *30* (7), 743-748.
- (164) Lee, S. H.; Kim, I. Y.; Song, W. S., Biodegradation of Polylactic Acid (PLA) Fibers Using Different Enzymes. *Macromol. Res.* **2014**, *22* (6), 657-663.
- (165) Cui, R.; Zhang, Z.; Nie, J.; Du, B., Tuning the Morphology, Network Structure, and Degradation of Thermo-Sensitive Microgels by Controlled Addition of Degradable Cross-Linker. *Colloid Polym. Sci.* **2017**, *295* (4), 665-678.
- (166) Chen, J.; Wu, M.; Veroniaina, H.; Mukhopadhyay, S.; Li, J.; Wu, Z.; Wu, Z.; Qi, X., Poly(N-isopropylacrylamide) Derived Nanogels Demonstrated Thermosensitive Self-Assembly and GSH-Triggered Drug Release for Efficient Tumor Therapy. *Polym. Chem.* **2019**, *10* (29), 4031-4041.
- (167) Zhao, S.; Yang, H.; Zuo, C.; Sun, L.; Ma, L.; Wei, H., PH-Sensitive Drug Release of Star-Shaped Micelles with OEG Brush Corona. *RSC Adv* **2016**, *6* (112), 111217-111225.
- (168) Ferris, D. P.; Lu, J.; Gothard, C.; Yanes, R.; Thomas, C. R.; Olsen, J.-C.; Stoddart, J. F.; Tamanoi, F.; Zink, J. I., Synthesis of Biomolecule-Modified Mesoporous Silica Nanoparticles for Targeted Hydrophobic Drug Delivery to Cancer Cells. *Small* **2011**, *7* (13), 1816-1826.

- (169) Malmsten, M., Soft Drug Delivery Systems. *Soft Matter* **2006**, *2* (9), 760-769.
- (170) Yasir, M.; Sara, U. V. S., Solid Lipid Nanoparticles for Nose to Brain Delivery of Haloperidol: In Vitro Drug Release and Pharmacokinetics Evaluation. *Acta. Pharm. Sin. B.* **2014**, *4* (6), 454-463.
- (171) Patel, M. H.; Mundada, V. P.; Sawant, K. K., Fabrication of Solid Lipid Nanoparticles of Lurasidone HCl for Oral Delivery: Optimization, In Vitro Characterization, Cell Line Studies and In Vivo Efficacy in Schizophrenia. *Drug Dev. Ind. Pharm.* **2019**, *45* (8), 1242-1257.
- (172) Vivek, K.; Reddy, H.; Murthy, R. S. R., Investigations of the Effect of the Lipid Matrix on Drug Entrapment, In Vitro Release, and physical stability of Olanzapine-Loaded Solid Lipid Nanoparticles. *AAPS PharmSciTech.* **2007**, *8* (4), 16-24.
- (173) Dondapati, D.; Srimathkandala, M. H.; Sanka, K.; Bakshi, V., Improved Solubility and Dissolution Release Profile of Lurasidone by Solid Self-Nanoemulsifying Drug Delivery System. *Anal. Chem. Lett.* **2016**, *6* (2), 86-97.
- (174) Basalious, E. B.; Abdallah Ahmed, M., Phospholipid Based Self-Nanoemulsifying Self-Nanosuspension (P-SNESNS) as a Dual Solubilization Approach for Development Of Formulation with Diminished Food Effect: Fast/Fed In Vivo Pharmacokinetics Study in Human. *Eur. J. Pharm. Sci.* **2017**, *109*, 244-252.
- (175) Miao, Y.; Sun, J.; Chen, G.; Lili, R.; Ouyang, P., Enhanced Oral Bioavailability of Lurasidone by Self-Nanoemulsifying Drug Delivery System in Fasted State. *Drug Dev. Ind. Pharm.* **2016**, *42* (8), 1234-40.
- (176) Budhian, A.; Siegel, S. J.; Winey, K. I., Haloperidol-Loaded PLGA nanoparticles: Systematic Study of Particle Size and Drug Content. *Int. J. Pharm.* **2007**, *336* (2), 367-75.
- (177) Budhian, A.; Siegel, S. J.; Winey, K. I., Controlling the In Vitro Release Profiles for a System of Haloperidol-Loaded PLGA Nanoparticles. *Int. J. Pharm.* **2008**, *346* (1-2), 151-159.
- (178) Bohrey, S.; Chourasiya, V.; Pandey, A., Factorial Design Based Preparation, Optimization, Characterization and In Vitro Drug Release Studies of Olanzapine Loaded PLGA Nanoparticles. *Mater. Res. Express* **2016**, *3* (12), 125403.
- (179) Jazuli, I.; Annu; Nabi, B.; Moolakkadath, T.; Alam, T.; Baboota, S.; Ali, J., Optimization of Nanostructured Lipid Carriers of Lurasidone Hydrochloride using Box-Behnken Design for Brain Targeting: In Vitro and In Vivo Studies. *J. Pharm. Sci.* **2019**, *108* (9), 3082-3090.
- (180) Salama, H. A.; Mahmoud, A. A.; Kamel, A. O.; Abdel Hady, M.; Awad, G. A. S., Brain Delivery of Olanzapine by Intranasal Administration of Transfersomal Vesicles. *J. Liposome. Res.* **2012**, *22* (4), 336-345.
- (181) Patel, M. R.; Patel, R. B.; Thakore, S. D.; Solanki, A. B., Brain Targeted Delivery of Lurasidone HCl via Nasal Administration of Mucoadhesive Nanoemulsion Formulation for the Potential Management of Schizophrenia. *Pharm. Dev. Technol.* **2020**, *25* (8), 1018-1030.
- (182) El-Setouhy, D. A.; Ibrahim, A. B.; Amin, M. M.; Khowessah, O. M.; Elzanfaly, E. S., Intranasal Haloperidol-Loaded Miniemulsions for Brain Targeting: Evaluation of Locomotor Suppression and In Vivo Biodistribution. *Eur. J. Pharm. Sci.* **2016**, *92*, 244-254.

- (183) Ruby, J. J.; Pandey, V. P., Formulation and Evaluation of Olanzapine Loaded Chitosan Nanoparticles for Nose-to-Brain Targeting an In Vitro and Ex Vivo Toxicity Study. *J. App. Pharm. Sci.* **2016**, *6* (9), 34-40.
- (184) Fonseca, F. N.; Betti, A. H.; Carvalho, F. C.; Gremiao, M. P.; Dimer, F. A.; Guterres, S. S.; Tebaldi, M. L.; Rates, S. M.; Pohlmann, A. R., Mucoadhesive Amphiphilic Methacrylic Copolymer-Functionalized Poly(Epsilon-Caprolactone) Nanocapsules for Nose-to-Brain Delivery of Olanzapine. *J. Biomed. Nanotechnol.* **2015**, *11* (8), 1472-1481.
- (185) Karg, M.; Pich, A.; Hellweg, T.; Hoare, T.; Lyon, L. A.; Crassous, J. J.; Suzuki, D.; Gumerov, R. A.; Schneider, S.; Potemkin, I. I.; Richtering, W., Nanogels and Microgels: From Model Colloids to Applications, Recent Developments, and Future Trends. *Langmuir* **2019**, *35* (19), 6231-6255.
- (186) Cuggino, J. C.; Blanco, E. R. O.; Gugliotta, L. M.; Alvarez Igarzabal, C. I.; Calderón, M., Crossing Biological Barriers with Nanogels to Improve Drug Delivery Performance. *J. Control. Release* **2019**, *307*, 221-246.
- (187) Agrawal, G.; Agrawal, R., Functional Microgels: Recent Advances in Their Biomedical Applications. *Small* **2018**, *14* (39), 1801724.
- (188) Vashist, A.; Kaushik, A.; Vashist, A.; Bala, J.; Nikkhah-Moshaie, R.; Sagar, V.; Nair, M., Nanogels as potential drug nanocarriers for CNS drug delivery. *Drug Discov Today* **2018**, *23* (7), 1436-1443.
- (189) Kabanov, A. V.; Vinogradov, S. V., Nanogels As Pharmaceutical Carriers: Finite Networks of Infinite Capabilities. *Angew. Chem. Int. Ed.* **2009**, *48* (30), 5418-5429.
- (190) Downey, J. S.; McIsaac, G.; Frank, R. S.; Stöver, H. D. H., Poly(divinylbenzene) Microspheres as an Intermediate Morphology between Microgel, Macrogel, and Coagulum in Cross-Linking Precipitation Polymerization. *Macromolecules* **2001**, *34* (13), 4534-4541.
- (191) Aderibigbe, B. A.; Naki, T., Design and Efficacy of Nanogels Formulations for Intranasal Administration. *Molecules* **2018**, *23* (6), 1241.
- (192) Shah, S.; Rangaraj, N.; Laxmikeshav, K.; Sampathi, S., Nanogels as Drug Carriers - Introduction, Chemical Aspects, Release Mechanisms and Potential Applications. *Int. J. Pharm.* **2020**, *581*, 119268.
- (193) Town, A. R.; Giardiello, M.; Gurjar, R.; Siccardi, M.; Briggs, M. E.; Akhtar, R.; McDonald, T. O., Dual-Stimuli Responsive Injectable Microgel/Solid Drug Nanoparticle Nanocomposites for Release Of Poorly Soluble Drugs. *Nanoscale* **2017**, *9* (19), 6302-6314.
- (194) Nochi, T.; Yuki, Y.; Takahashi, H.; Sawada, S.; Mejima, M.; Kohda, T.; Harada, N.; Kong, I. G.; Sato, A.; Kataoka, N.; Tokuhara, D.; Kurokawa, S.; Takahashi, Y.; Tsukada, H.; Kozaki, S.; Akiyoshi, K.; Kiyono, H., Nanogel Antigenic Protein-Delivery System for Adjuvant-Free Intranasal Vaccines. *Nat. Mater.* **2010**, *9* (7), 572-578.
- (195) Curtis, E. M.; Bahrami, A. H.; Weikl, T. R.; Hall, C. K., Modeling Nanoparticle Wrapping or Translocation in Bilayer Membranes. *Nanoscale* **2015**, *7* (34), 14505-14514.
- (196) Fukuyama, Y.; Yuki, Y.; Katakai, Y.; Harada, N.; Takahashi, H.; Takeda, S.; Mejima, M.; Joo, S.; Kurokawa, S.; Sawada, S.; Shibata, H.; Park, E. J.; Fujihashi, K.; Briles, D. E.; Yasutomi, Y.; Tsukada, H.; Akiyoshi, K.; Kiyono, H., Nanogel-Based Pneumococcal Surface

- Protein A Nasal Vaccine Induces MicroRNA-Associated Th17 Cell Responses with Neutralizing Antibodies Against Streptococcus Pneumoniae in Macaques. *Mucosal Immunol.* **2015**, *8* (5), 1144-1153.
- (197) Yuki, Y.; Kong, I.; Sato, A.; Nochi, T.; Mejima, M.; Kurokawa, S.; Hiroiwa, T.; Fukuyama, Y.; Sawada, S.; Takahashi, H.; Akiyoshi, K.; Kiyono, H., Adjuvant-Free Nanogel-Based PspA Nasal Vaccine for the Induction of Protective Immunity Against Pneumococcus (166.7). *J. Immunol. Res.* **2012**, *188* (1) .
- (198) Li, Z.; Van Zee, N. J.; Bates, F. S.; Lodge, T. P., Polymer Nanogels as Reservoirs To Inhibit Hydrophobic Drug Crystallization. *ACS Nano* **2019**, *13* (2), 1232-1243.
- (199) Zabih, F.; Wieczorek, S.; Dimde, M.; Hedtrich, S.; Borner, H. G.; Haag, R., Intradermal Drug Delivery by Nanogel-Peptide Conjugates; Specific and Efficient Transport of Temoporfin. *J. Control. Release* **2016**, *242*, 35-41.
- (200) Maeda, K.; Mochizuki, S.; Sanada, Y.; Sakurai, K., Naphthalene-Hydrophobized Beta-1,3-Glucan Nanogel for Doxorubicin Delivery to Immunocytes. *Bioorg. Med. Chem. Lett.* **2014**, *24* (8), 1880-1883.
- (201) Kim, J. O.; Oberoi, H. S.; Desale, S.; Kabanov, A. V.; Bronich, T. K., Polypeptide Nanogels with Hydrophobic Moieties in the Cross-Linked Ionic Cores: Synthesis, Characterization and Implications for Anticancer Drug Delivery. *J. Drug. Target.* **2013**, *21* (10), 981-993.
- (202) Chen, D. Q.; Yu, H. Y.; Sun, K. X.; Liu, W. H.; Wang, H. B., Dual Thermoresponsive and PH-Responsive Self-Assembled Micellar Nanogel for Anticancer Drug Delivery. *Drug Deliv.* **2014**, *21* (4), 258-264.
- (203) Bang, T. H.; Van, T. T. T.; Hung, L. X.; Ly, B. M.; Nhut, N. D.; Thuy, T. T. T.; Huy, B. T., Nanogels of Acetylated Ulvan Enhance the Solubility of Hydrophobic Drug Curcumin. *B. Mater. Sci* **2019**, *42* (1).
- (204) Miller, R. D.; Yusoff, R. M.; Swope, W. C.; Rice, J. E.; Carr, A. C.; Parker, A. J.; Sly, J.; Appel, E. A.; Nguyen, T.; Piunova, V., Water Soluble, Biodegradable Amphiphilic Polymeric Nanoparticles and the Molecular Environment of Hydrophobic Encapsulates: Consistency Between Simulation and Experiment. *Polymer* **2015**, *79*, 255-261.
- (205) Picone, P.; Ditta, L. A.; Sabatino, M. A.; Militello, V.; San Biagio, P. L.; Di Giacinto, M. L.; Cristaldi, L.; Nuzzo, D.; Dispenza, C.; Giacomazza, D.; Di Carlo, M., Ionizing Radiation-Engineered Nanogels as Insulin Nanocarriers for the Development of a New Strategy for the Treatment of Alzheimer's Disease. *Biomaterials* **2016**, *80*, 179-194.
- (206) Picone, P.; Sabatino, M. A.; Ditta, L. A.; Amato, A.; San Biagio, P. L.; Mulè, F.; Giacomazza, D.; Dispenza, C.; Di Carlo, M., Nose-to-Brain Delivery of Insulin Enhanced by a Nanogel Carrier. *J. Control. Release* **2018**, *270*, 23-36.
- (207) Xu, D.; Lu, Y. R.; Kou, N.; Hu, M. J.; Wang, Q. S.; Cui, Y. L., Intranasal Delivery of Icariin via a Nanogel-Thermoresponsive Hydrogel Compound System to Improve its Antidepressant-Like Activity. *Int. J. Pharm.* **2020**, *586*, 119580.
- (208) Jahromi, L. P.; Mohammadi-Samani, S.; Heidari, R.; Azadi, A., In Vitro and In Vivo Evaluation of Methotrexate-Loaded Hydrogel Nanoparticles Intended to Treat Primary CNS Lymphoma via Intranasal Administration. *J. Pharm. Pharm. Sci.* **2018**, *21*, 305-317.

- (209) Azegami, T.; Yuki, Y.; Sawada, S.; Mejima, M.; Ishige, K.; Akiyoshi, K.; Itoh, H.; Kiyono, H., Nanogel-Based Nasal Ghrelin Vaccine Prevents Obesity. *Mucosal Immunol.* **2017**, *10* (5), 1351-1360.
- (210) Kong, I. G.; Sato, A.; Yuki, Y.; Nochi, T.; Takahashi, H.; Sawada, S.; Mejima, M.; Kurokawa, S.; Okada, K.; Sato, S.; Briles, D. E.; Kunisawa, J.; Inoue, Y.; Yamamoto, M.; Akiyoshi, K.; Kiyono, H., Nanogel-Based PspA Intranasal Vaccine Prevents Invasive Disease and Nasal Colonization by *Streptococcus Pneumoniae*. *Infect. Immun.* **2013**, *81* (5), 1625-1634.
- (211) Nochi, T.; Yuki, Y.; Takahashi, H.; Sawada, S.; Mejima, M.; Kohda, T.; Harada, N.; Kataoka, N.; Kong, I. G.; Sato, A.; Tokuhara, D.; Kurokawa, S.; Takahashi, Y.; Tsukada, H.; Kozaki, S.; Akiyoshi, K.; Kiyono, H., Nanogel Antigen Delivery System for Adjuvant-Free Intranasal Vaccines. *J. Immunol.* **2010**, *184* (1), 46.16.
- (212) Pervaiz, F.; Ahmad, M.; Hussain, T.; Idrees, A.; Yaqoob, A.; Abbas, K., Development of Olanzapine Loaded PNA Microgels for Depot Drug Delivery in Treatment of Schizophrenia: In Vitro and In Vivo Release Profile. *Acta Pol. Pharm.* **2016**, *73* (1), 175-81.

Chapter 2 : Evaluating the Therapeutic Efficacy and Biological Transport of Hydrophobized Poly(oligoethylene glycol methacrylate)-Based Nanogels for the Delivery of Lurasidone

Madeline J. Simpson^a, Brendan Fera^b, Jonathan Dorogin^a, Ashley Bernardo^b, Fahed Abu-Hijel^b, Niels M.B. Smeets^a, Ram K. Mishra^{b,c} and Todd Hoare^{a,c,*}

^a Department of Chemical Engineering, McMaster University, 1280 Main Street West, Hamilton, ON, L8S 4L7, Canada

^b Department of Psychiatry and Behavioural Neurosciences, McMaster University, 1200 Main Street West, Hamilton, ON, L8N 3Z5, Canada

^c School of Biomedical Engineering, McMaster University, 1280 Main Street West, Hamilton, ON, L8S 4K1, Canada

Keywords: nanogel, stimuli-responsive, intranasal, lurasidone, hydrophobic drug.

2.1 Abstract

Lurasidone is an atypical antipsychotic drug (APD) with distinct pharmacological features that address the positive, negative and cognitive symptoms associated with schizophrenia. However, lurasidone has very limited aqueous solubility, leading to slow dissolution and poor absorption upon oral administration. Herein, we utilize nanogels, a class of soft, deformable nanocarriers, modified with hydrophobic domains via copolymerization of either butyl methacrylate (BMA) or methyl methacrylate (BMA) to promote lurasidone uptake. Up to ~3 wt% lurasidone loading can be achieved in nanogels prepared with 10 mol% BMA while maintaining high cytocompatibility with SH-SY5Y neuronal cells. Intranasal (IN) administration of nanogels loaded with a low dose (0.75 mg/kg) of lurasidone achieve significant behavioural changes in the locomotor activity of a preclinical rodent model of schizophrenia, responses achieved only with a 3 mg/kg dose of lurasidone when delivered intraperitoneally (IP). IN-administered nanogels remain localized to the nasal tissue for at least two days, with minimal accumulation in clearance organs. This hydrophobized nanogel drug delivery system thus has promising clinical potential as a minimally-invasive alternative for the delivery of hydrophobic APDs to the brain.

2.2 Introduction

Antipsychotic drugs (APDs) are typically prescribed as oral tablets for ease of administration because chronic psychotic disorders require continuous drug intervention for effective treatment. However, the implementation of advanced drug discovery methods has led to the identification of new, highly potent therapeutics with increasing likelihood of poor water solubility.¹⁻² Currently, 70% of new drug discovery candidates demonstrate low aqueous solubility and belong to class II and IV of the Biopharmaceutical Classification system³⁻⁵ with 40% of new compounds requiring additional formulation modification to circumvent insolubility.^{2, 5-6} Lurasidone (LUR), a highly hydrophobic ($\log P = 5.6$),⁷ atypical APD, was approved in the last decade for the treatment of schizophrenia, a neurological disease that affects 1% of the global population.⁸ Clinical prescription of oral lurasidone tablets (20-160 mg/day)⁹⁻¹⁰ is accompanied with the direction to consume 350 kcal of food to improve absorption,¹¹ as only 9-19% of administered drug is bioavailable due to poor dissolution and substantial first-pass metabolism.^{9, 12} Despite its limited bioavailability, lurasidone has unique pharmacological features; it is a potent antagonist of dopamine D_2 and serotonin 5-HT_{2A} and 5-HT₇ receptors, a modest antagonist of noradrenergic α_{2A} and α_{2C} receptors, and a partial agonist of 5-HT₁ receptors, which represents a highly favourable clinical profile.¹³ In particular, unlike typical APDs that can cause severe extrapyramidal neurological side effects¹⁴ and other atypical APDs that are known to produce metabolic side effects,¹⁵ this receptor binding

profile enables potent antipsychotic, anti-depressant, and anxiolytic-like effects in addition to providing procognitive benefits with minimal adverse side effects.^{9-10, 13} As such, the development of effective delivery strategies to make lurasidone bioavailable without requiring co-administration with food is critical to unlock its clinical potential, particularly for its target schizophrenic patient population whose symptoms render it challenging for patients to comply with this dietary directive.¹¹⁻¹²

Several strategies have been explored to enhance the oral bioavailability of lurasidone. Crystal modifications,⁷ inclusion complexes with cyclodextrin,¹⁶ nanosuspensions,¹⁷⁻¹⁹ self-micro/nano- emulsifying drug delivery systems²⁰⁻²⁴ and solid lipid nanoparticles²⁵ have all been proposed to improve the *in vivo* performance of lurasidone by enhancing its solubility and thus accelerating its pharmacokinetics. Although improving the dissolution rate enhances the oral absorption of lurasidone and can produce comparable pharmacokinetics in both the fed and fasted states,²³ studies have yet to determine if rapid dissolution leads to greater systemic exposure or receptor occupancy, both of which can lead to toxicity or contribute to the negative side effects of APDs.

Intranasal (IN) drug delivery is an attractive alternative to oral administration of APDs because direct nose-to-brain transport improves drug bioavailability by circumventing both first-pass metabolism and the blood-brain barrier²⁶ in addition to eliminating any

absorption restrictions imposed by food effects. Nanoparticles are commonly used in IN drug delivery of hydrophobic compounds based on their potential to solubilize such drugs while retaining the potential for facile administration (via spray or drops) into the nose. Lipid-based nanocarriers,²⁷ micelles²⁸ and nanoemulsions²⁹ have been investigated for their potential to enable nose-to-brain delivery of lurasidone. Interestingly, all of these nanoparticles explored to-date have shown enhanced release kinetics compared to pure lurasidone, indicating that the benefits of such vehicles are exclusively in terms of enhancing drug solubility rather than enabling controlled release. As such, such studies do not fully demonstrate the enhanced bioavailability enabled by direct nose-to-brain transport achievable using nanoparticle-mediated IN delivery.

Nanogels, solvent-swollen networks of cross-linked polymers, are attractive drug delivery systems for IN delivery due to their potential to increase drug delivery across cellular barriers and respond to environmental stimuli to trigger controlled drug release and particle degradation.³⁰⁻³² Unlike conventional hard nanoparticles, nanogels have the inherent benefit of swelling but retaining their stability in biological fluids due to physical and/or chemical cross-links, resulting in a soft and deformable particle that can traverse cell membranes and enable passage through the nasal mucosal barrier to promote direct nose-to-brain transport.³³

Nanogels have been previously demonstrated as effective drug carriers due to their small and highly controllable sizes and highly hydrophilic interface that suppresses non-specific protein adsorption and thus promotes extended circulation times;³⁴ furthermore, the soft deformable structure of a nanogel has been demonstrated to further prolong circulation times, result in reduced accumulation in the spleen, and enhance the potential for transport across biological barriers.³⁵⁻³⁶ The inherent hydrophilicity of nanogels requires their chemical modification to enable efficient solubilization of hydrophobic drugs, typically via the incorporation of hydrophobic comonomers into the nanogel phase.³⁷ The nanogels designed herein for lurasidone delivery consist of copolymers of oligo(ethylene glycol) methacrylate (OEGMA), acrylic acid (AA) and either butyl methacrylate (BMA) or methyl methacrylate (MMA) fabricated via free radical precipitation polymerization. PEOGMA has been demonstrated by our group and others³⁸⁻³⁹ to be a highly hydrophilic protein-repellent and non-immunogenic polymer that imparts excellent swelling properties and steric stability to the nanogel while the BMA/MMA comonomers enable the creation of hydrophobic nanodomains (via self-assembly) within the nanogel to augment lurasidone loading. Nanogels were demonstrated to be both slowly degradable under physiologically-relevant conditions and cytocompatible to a neuronal cell line, while *in vivo* studies in a rodent model of schizophrenia demonstrated that low doses of nanogel-encapsulated lurasidone induce significant behavioural changes by enhancing drug bioavailability via the nose-to-brain route and facilitating prolonged release.

2.3 Experimental

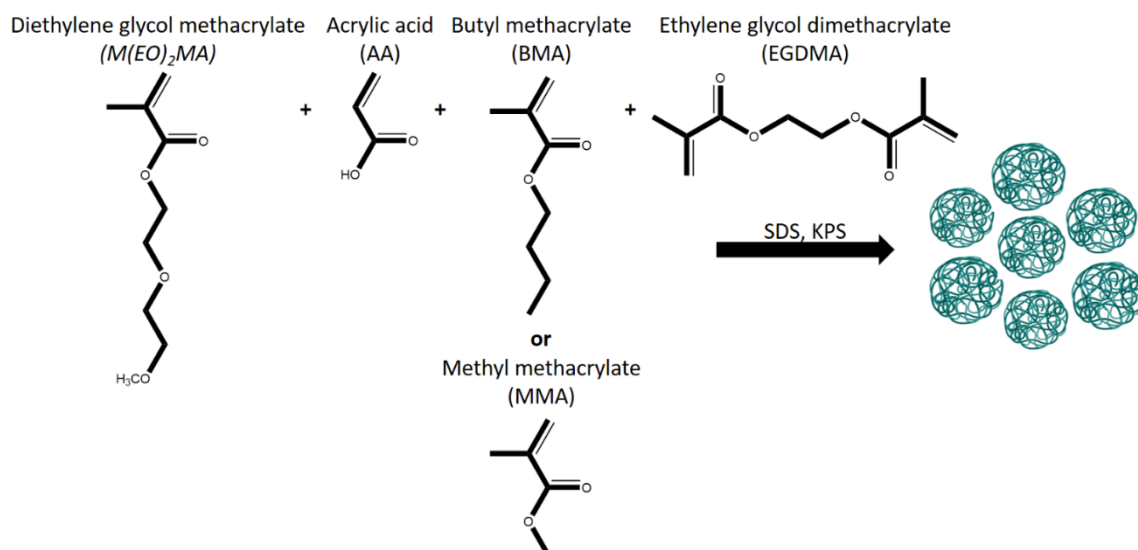
2.3.1 Materials

Anhydrous acrylic acid (AA, 99%), butyl methacrylate (BMA, 99%), 1,3-diaminopropane ($\geq 99\%$), diethylene glycol methyl ether methacrylate (M(EO)₂MA, n=2 ethylene oxide (EO) repeat units, 95%), esterase from porcine liver (68.9 U/mg), ethylene glycol dimethacrylate (EGDMA, 98%), methyl methacrylate (MMA, 99%), *N*-hydroxysuccinimide (NHS, 98%), potassium persulfate (KPS, $\geq 99.0\%$), sodium acetate ($\geq 99\%$) and sodium dodecyl sulfate (SDS, $\geq 99.0\%$) were purchased from Millipore Sigma (Oakville, ON) and used as received. *N*'-ethyl-*N*-(3-dimethylaminopropyl)-carbodiimide (EDC, 99%) was purchased from AK Scientific (Union City, CA). Cyanine5-NHS ester (Cy5) was purchased from Lumiprobe (Hunt Valley, MD). Lurasidone (99%) was purchased from MedKoo Biosciences (Morrisville, NC).

2.3.2 Nanogel synthesis

POEGMA nanogels were synthesized using precipitation polymerization. To synthesize nanogels containing 10 mol% hydrophobic comonomer, M(EO)₂MA (1.51 g, 8 mmol), AA (90 μ L, 1 mmol), EGDMA (90 μ L, 0.5 mmol), SDS (60 mg, 0.2 mmol), BMA (165 μ L, 1 mmol) or MMA (111 μ L, 1 mmol), and 145 mL DIW were added to a 250 mL two-neck round bottom flask. The flask was attached to a condenser and stirred at 350 rpm while the contents were purged with N₂ gas for at least 30 minutes. The flask was submerged in a

90°C oil bath and allowed to heat up for at least 10 minutes. KPS (61.5 mg, 0.2 mmol) was dissolved in 5 mL of DIW and injected into the heated reagents using a syringe to initiate the polymerization (Scheme 2.1). After 4 hours of polymerization, the reaction was terminated by exposing the product to air. The cooled product was transferred to 3.5-5 kDa molecular weight cut off (MWCO) tubing for purification by dialysis against DIW (six cycles of 6+ hours). Purified nanogels were stored in aqueous suspension at 4°C. Gravimetric analysis was used to determine the polymer content of the purified nanogel suspension. A similar process was followed to synthesize nanogels containing different quantities of hydrophobic comonomer (Table 2.1).



Scheme 2.1: Synthesis of hydrophobized POEGMA based-nanogels. Precipitation polymerization of diethylene glycol methacrylate (M(EO)₂MA) with acrylic acid (AA), either butyl methacrylate (BMA) or methyl methacrylate (MMA), and ethylene glycol dimethacrylate (EGDMA) as the cross-linker in the presence of sodium dodecyl sulfate (SDS, surfactant) and potassium persulfate (KPS, initiator) yields small, monodisperse nanogels containing BMA or MMA hydrophobic domains.

Table 2.1: Chemical synthesis of nanogels containing different mol% ratios of BMA and MMA.^a

Hydrophobic Comonomer Content (mol%)	BMA (μ L)	MMA (μ L)
0	0	0
5	78	52
10	165	111
15	261	175

^a All polymerizations were performed at 90°C in 150 mL Milli-Q water. Acrylic acid (90 μ L, 1 mmol), ethylene glycol dimethacrylate (90 μ L), sodium dodecyl sulfate (60 mg, 0.02 mmol) and potassium persulfate (61.5 g, 0.02 mmol) were kept constant in all batches.

2.3.3 Synthesis of cyanine-5 labeled nanogels

Fluorescently-labeled nanogels were prepared for *in vivo* pharmacokinetic studies using a fluorescent labeling protocol adapted from the literature.⁴⁰⁻⁴² First, the carboxylic acid groups from the AA within the nanogel formulation were converted to amino groups by preparing a 50 mL suspension of 10 mg/mL 10% BMA nanogels in 10 mM PBS, pH 7.4, after which a 10-fold molar excess of EDC (140 mg, targeted to functionalize 20% of the AA groups) and 44 mg of NHS (final concentration of 5 mM) were added and mixed using magnetic stirring (350 rpm) at room temperature for 30 minutes. Subsequently, a 10-fold molar excess of 1,3-diaminopropane (48 μ L) was added to the solution and allowed to react for 4 hours. The resulting solution was placed into a 3.5-5 kDa MWCO membrane and dialyzed against DIW (six cycles of 6+ hours). The dialyzed solution was collected and measured to determine the volume; gravimetric analysis was used to determine the polymer content. The purified nanogel solution was then mixed with concentrated PBS to create a 10 mg/mL nanogel solution in 10 mM PBS. Following, a 10 mM solution of Cy5

was prepared in DMF and 355 μL of the dye solution was added to the nanogel solution (targeting 0.5% functionalization (1:200) of the introduced amino groups) and reacted for 4 hours at room temperature under magnetic stirring (350 rpm) in a tin foil-wrapped vessel to protect from light exposure. The resulting Cy5-labeled nanogels were purified by dialysis as described above. The polymer content of the fluorescently-labeled nanogel suspension was quantified by gravimetric analysis, and the final nanogel suspension was stored at 4°C in a tin-foil wrapped container to prevent any photodegradation.

2.3.4 Nanogel characterization

Dynamic light scattering (DLS) using a Brookhaven NanoBrook 90Plus Particle Size Analyser equipped with a 659 nm laser configured at a 90° angle and running BIC Particle solutions software (Version 2.6, Brookhaven Instruments Corporation) was used to measure the effective nanogel diameter. Nanogel solutions ranging from 1-10 mg/mL were prepared to result in a count rate ranging from 500-600 kcps. Phase Analysis Light Scattering (PALS), using the ZetaPlus zeta potential analyzer (Brookhaven Instruments Corporation), was used to measure the electrophoretic mobility of nanogels in 10 mM KCl. Five measurements were recorded for each sample, with results presented as the average \pm one standard deviation. Conductometric base-into-acid titration (ManTech Inc.) was used to measure the acrylic acid content of the nanogels by titrating a 1 mM NaCl solution containing 1 mg/mL nanogel with 0.1 M NaOH.

2.3.5 Determination of lurasidone drug loading capacity and encapsulation efficiency

Lurasidone was dissolved in methanol at a concentration of 1 mg/mL and placed on a shaking vortex for at least 1 hour. A solution of nanogel (25 mg) was centrifuged at 18 000 rpm for 30 minutes using an Allegra 64R benchtop centrifuge (Beckman Coulter Canada, Mississauga, ON). The nanogel pellet was re-dispersed in 2 mL of the lurasidone solution and placed on a shaking vortex for 24 hours. This dispersion was centrifuged (as above), and the supernatant was collected. Lurasidone loading was determined by analyzing the supernatant absorbance at 318 nm using a Cary 100 Bio UV-vis spectrophotometer (Varian Inc.). Triplicate measurements were performed for each nanogel, with the average \pm one standard deviation reported. Drug uptake was quantified by the drug loading capacity (DLC, Equation 2.1) and the encapsulation efficiency (EE, Equation 2.2).

$$\text{Drug Loading Capacity} = \frac{\text{Mass of drug loaded}}{\text{Total nanogel mass}} \times 100\% \quad (2.1)$$

$$\text{Encapsulation Efficiency} = \frac{\text{Mass of drug loaded}}{\text{Mass of total drug added}} \times 100\% \quad (2.2)$$

2.3.6 *In vitro* nanogel degradation and stability

Nanogel responses to different physiological conditions were monitored using DLS as described above. A 1 mg/mL solution of 10% BMA nanogels was prepared in (1) 10 mM phosphate buffered saline (PBS), pH 7.4 (stability test); (2) 20 U/mL esterase, pH 7.4 (enzyme-catalyzed hydrolytic degradation); (3) 100 mM acetate buffer, pH 4.5 (acid-

catalyzed hydrolytic degradation) or (4) 100 mM HCl, pH 1 (accelerated acid-catalyzed hydrolytic degradation). The response was monitored at 37°C to assess nanogel size and count rate as a function of time. The light intensity was maximized prior to the first measurement and maintained constant throughout the full time course of experiments, with measurements conducted for 2 minutes every 15 minutes for a total of 12 h. After 24 hours, the samples were characterized by nanoparticle tracking analysis (NTA) using a Malvern NanoSight LS10 instrument (Version 3.2, NTA software).

2.3.7 *In vitro* cytotoxicity

Nanogel cytocompatibility was evaluated using SH-SY5Y neuronal cells cultured in DMEM-F12 media supplemented with 10% FBS, 1% penicillin/streptomycin and 1% L-glutamine (ThermoFisher Scientific, Burlington, ON). Cells were plated into the wells of a 96-well plate at a cell density of 4×10^4 cells per well and allowed to adhere for 24 hours, after which they were incubated for 48 hours with concentrations over the range of 14-115 mg/mL nanogel or lurasidone-loaded nanogel (LUR-nanogel). Cell metabolic activity was determined by incubating the treated cells with (3-(4,5-dimethylthiazol-2-yl)-2,5-diphenyltetrazolium bromide) (MTT) (ThermoFisher Scientific) for three hours and subsequently measuring the absorbance of each well at 570 nm using a Tecan Infinite M200 Microplate Reader. The average cell viability relative to a non-treated cell-only control is presented ($n=4 \pm$ one standard deviation).

2.3.8 Animal procurement and care

The *in vivo* response to 10% BMA nanogels was evaluated using male Wistar Hans rats weighing 250-300 g upon arrival from Charles River (St. Constant, QC). The rats were housed at the McMaster University Central Animal Facility with *ad libitum* access to food and water in a reverse 12 h light/dark cycle room. Animal testing protocols were approved by the Animal Research Ethics Board of McMaster University (Animal Utilization Protocol 18-06-27) in compliance with the Canadian Council on Animal Care.

2.3.9 Pharmacodynamics of lurasidone-loaded nanogels

Rats were administered IN with 10% BMA nanogels prepared at concentrations corresponding to 0.75 mg/kg lurasidone, with the nanogel mass administered calculated based on the measured DLC. Two negative controls were prepared: (1) IN saline with IP saline; and (2) an equivalent concentration of empty (non-drug loaded) nanogels was administered IN followed by IP saline. Two positive controls were also executed: (1) a MK-801 cohort received IN saline; and (2) a nanogel/MK-801 cohort was dosed IN with empty nanogel. Drug administration occurred 60 minutes prior to behavioural testing. Intranasal administration was conducted on rats (n=6 per group) anesthetized using isoflurane. Two rounds of administration were conducted, with 30 μ L of nanogel suspension first pipetted into each nostril, the rat returned to the anesthetic chamber for 1-2 minutes, and a second round of 30 μ L administrations then dosed to each nostril (120 μ L total volume

administered); rats were maintained under anesthesia for less than 5 minutes in total. To safely recover from the anesthesia, rats were placed in an empty recovery chamber prior to being returned to their home cage. To assess the effect of administration pathway, rats (n=6 per group) alternately received intraperitoneal (IP) doses of LUR-nanogel containing 0.75 mg/kg or 3 mg/kg lurasidone using a single injection with a volume corresponding to 2 mL/kg. To induce the schizophrenia model, rats were dosed with 0.35 mg/kg MK-801 via IP injection immediately before behavioural testing. Locomotion was measured using VersaMax Open Field Activity Monitoring computerized locomotion chambers (AccuScan Instruments Inc., Columbus, OH) equipped with infrared sensors to monitor three-dimensional movement based on photo beam breaks. Prior to testing, rats were habituated to the chambers. Movement tracking began immediately after MK-801 dosing; the total displacement reported occurred 21-180 minutes after tracking began to account for rats to acclimatization to the chambers and the full induction of the MK-801 schizophrenia model.

2.3.10 Pharmacokinetic studies of IN administered Cy5-nanogels

To assess the biodistribution of the IN-administered nanogels, Cy5-labeled nanogels were administered IN to rats as described for the pharmacodynamics study (2 × 30 µL aliquots of a 15 wt% nanogel suspension per nostril, total volume administered = 120 µL). At time points of 3, 24 or 48 hours post-administration, rats (n=4/time point) were heavily

anesthetized using isoflurane and decapitated. The nasal tissue, olfactory bulb (OLB), brain, lungs, liver, kidneys and spleen from each animal were collected, wrapped in plastic wrap, placed in individual wells of a 6-well plate wrapped in tin foil, and frozen at -80°C . To assess the Cy5-nanogel biodistribution in each tissue, samples of each tissue were weighed and homogenized in ice-cold PBS to prepare 15 wt% solutions. Aliquots of each sample (200 μL , $n=4$) were added to the wells of a 96-well plate and analyzed for Cy5 fluorescence (660/680 nm excitation/emission) using a Tecan Infinite M1000 microplate reader (ThermoFisher Scientific).

2.4 Results and Discussion

2.4.1 Nanogel synthesis and characterization

POEGMA nanogels were synthesized using thermally-initiated free radical precipitation polymerization. Co-polymerization with either BMA or MMA introduces hydrophobic domains into the nanogel to improve the affinity of hydrophobic drugs for nanogel uptake. A small quantity (5 mol%) of AA was also copolymerized to impart functional groups to enable post-synthesis fluorescent labeling and enhance the colloidal stability of the hydrophobized nanogels. EGDMA was selected as the cross-linker to facilitate the slow degradation of the nanogels; the ester bond connecting the cross-linker and comonomer side chains to the polymer backbone can be cleaved through hydrolytic (low pH) or enzymatic (esterase) mediated reactions. These formulations yield small (65-87

nm), monodisperse (PD <0.08) and colloiddally stable populations of nanogels (Tables 2.2 and 2.3). Incorporation of 5 mol% increments of the hydrophobic comonomers causes gradual nanogel deswelling leading to smaller particle sizes (Figure 2.1), with the BMA-containing nanogels showing higher deswelling consistent with the longer alkyl side chain of BMA relative to MMA (i.e. four carbons compared to one carbon). Incorporation of hydrophobic co-monomer beyond 15 mol% yielded unstable formulations that were prone to aggregation, indicating a balance must be maintained between the hydrophobic and hydrophilic components of the nanogel to retain colloidal stability. The slightly negative mobility values are consistent with the incorporation of ionized AA groups into the nanogel.

Table 2.2: Effective particle diameter, polydispersity (PD) (from DLS) and electrophoretic mobility (from PALS) of nanogels containing various amounts of BMA comonomer. Average values (n=5) \pm one standard deviation are presented.

BMA Mole %	Diameter (nm)	PD	Mobility (μ /s)/(V/cm)
0	86 \pm 2	0.05 \pm 0.04	-0.78 \pm 0.22
5	80 \pm 1	0.04 \pm 0.01	-1.42 \pm 0.20
10	73 \pm 3	0.08 \pm 0.03	-0.63 \pm 0.16
15	65 \pm 1	0.06 \pm 0.02	-0.33 \pm 0.41

Table 2.3: Effective particle diameter, polydispersity (PD) (from DLS) and electrophoretic mobility (from PALS) of nanogels containing various amounts of MMA comonomer. Average values (n=5) \pm one standard deviation are presented.

MMA Mole %	Diameter (nm)	PD	Mobility (μ /s)/(V/cm)
0	86 \pm 2	0.05 \pm 0.04	-0.78 \pm 0.22
5	87 \pm 1	0.06 \pm 0.02	-0.60 \pm 0.22
10	85 \pm 6	0.07 \pm 0.02	-0.66 \pm 0.30
15	76 \pm 4	0.04 \pm 0.03	-0.51 \pm 0.31

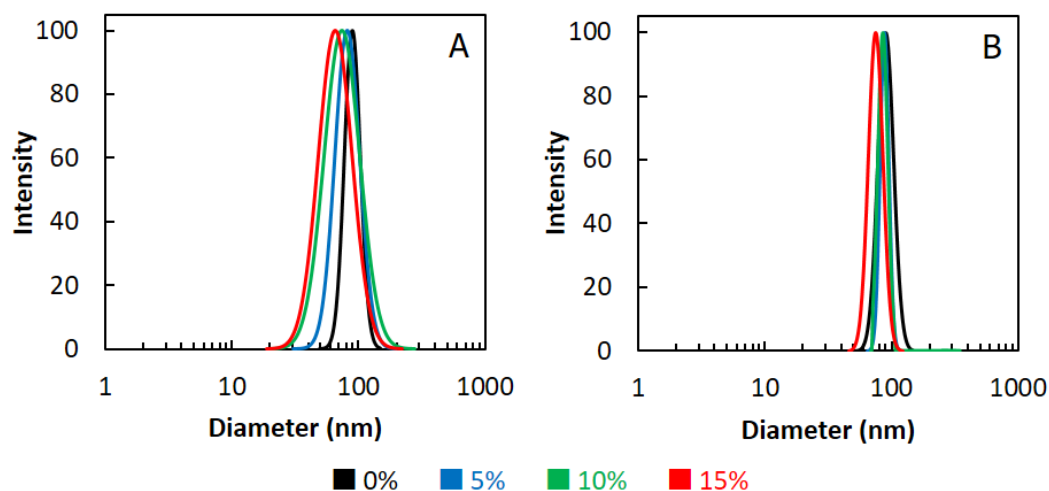


Figure 2.1: Logarithmic intensity-based size distribution from DLS of (A) BMA nanogels or (B) MMA nanogels containing either 0 mol% (black), 5 mol% (blue), 10 mol% (green) or 15 mol% (red) hydrophobic comonomer.

2.4.2 Drug loading capacity and encapsulation efficiency of lurasidone

Lurasidone uptake in the different nanogel formulations was assessed to determine how the incorporation of hydrophobic domains within the nanogel affects drug loading. Passive diffusion was used to carry out drug loading; given the limited solubility of lurasidone in water (8 $\mu\text{g}/\text{mL}$), the drug was dissolved at a concentration of 1 mg/mL in methanol, a solvent which can also re-disperse (and swell) the nanogels. The drug loading capacity (DLC, wt%) and encapsulation efficiency (EE, %) of each formulation are presented in Table 2.4. The BMA nanogels consistently show larger drug loading than the MMA nanogels, consistent with the higher hydrophobicity of the BMA monomer residues providing a more favorable binding site for the binding of lurasidone. Both the BMA and MMA nanogels show improved drug uptake as the hydrophobic comonomer content is

increased up to 10 mol%; however, the 15 mol% nanogels show decreased drug loading, suggesting that lurasidone uptake is governed by a balance between the generation of hydrophobic domains (increased at higher MMA/BMA content) and maintaining sufficient nanogel swelling to allow free drug diffusion into the nanogel (reduced at higher MMA/BMA content). Based on these results, the 10% BMA nanogel that enabled the highest lurasidone encapsulation with among the smallest particle sizes (promoting biological transport) was selected for the subsequent degradation, cytotoxicity, and animal efficacy studies.

Table 2.4: Drug loading capacity (DLC) and encapsulation efficiency (EE) of lurasidone in nanogels prepared with 0-15 mol% BMA or MMA. Average values (n=3) \pm one standard deviation are presented.

Hydrophobic Comonomer Mole %	BMA		MMA	
	DLC (wt%)	EE (%)	DLC (wt%)	EE (%)
0	2.1 \pm 0.1	26 \pm 2	2.1 \pm 0.1	26 \pm 2
5	2.5 \pm 0.1	31 \pm 1	1.7 \pm 0.3	21 \pm 6
10	2.8 \pm 0.1	35 \pm 1	2.5 \pm 0.1	32 \pm 2
15	2.4 \pm 0.1	30 \pm 1	0.9 \pm 0.1	11 \pm 1

2.4.3 *In vitro* nanogel degradability and stability

Nanogels amenable for drug delivery need to remain stable during storage, drug loading and administration but then degrade over time in response to *in vivo* stimuli. The degradation of the EGDMA-cross-linked nanogels herein would primarily be mediated by cleavage of the ester bonds within the EGDMA cross-linker, a process potentially

accelerated by the cleavage of the ester bonds linking the OEGMA side chains to the polymer backbone that would generate carboxylic acid residues on the polymer backbone that can induce nanogel swelling. To assess the performance of the hydrophobized nanogels in this context, nanogel stability in various physiological conditions was monitored over a 12 hour period using DLS and quantified by examining the particle size and count rate relative to the initial ($t=0$ h) nanogel measurements (Figure 2.2). After 1 and 7 days of incubation in the various conditions, NTA was used to measure the particle size distribution (Figure 2.3). The stability of 10 % BMA nanogels in 10 mM PBS, mimicking the most simplistic physiological conditions, does not result in any change in particle size or count rate for the duration of the 12 hour measurement period. Exposure to 20 U/mL esterase at pH 7.4 did not cause a change in nanogel diameter; however, the count rate of the solution did increase upon introduction of the enzyme, which can be attributed to the presence of the 162 kDa molecule causing additional light scattering. The large size of the enzyme sterically limits its ability to penetrate the nanogel, thereby minimizing its capacity for degradation. Moderate degradation occurred upon incubation of the 10% BMA nanogels in the pH 4.5 buffer (mimicking the acidic environment of lysosomes that can uptake nanogels⁴³⁻⁴⁵), as reflected by the slight increase in particle size accompanied by a substantial decrease in particle count rate consistent with cross-link cleavage; further reduction in pH to pH 1 (accelerated degradation conditions) correspondingly showed rapid and substantial increases in nanogel size coupled with the largest decrease in

particle count rate. Analysis of the suspensions using NTA after 24 hours one day (Figure 2.3A) and one week (Figure 2.3B) of incubation in each respective condition provided additional insight into the nanogel response. After 24 hours, the nanogels suspended in 10 mM PBS maintain their unimodal and monodisperse particle size distribution; in contrast, nanogels exposed to degradation conditions have broader and multimodal size distributions consisting of both smaller particle sizes (corresponding to degraded polymer fragments) and larger particle sizes (corresponding to swollen nanogels and/or nanogel aggregates formed as the degradation process alters the colloidal stability of the nanogel), with the acid-degraded samples also exhibiting substantially lower total particle counts consistent with particle degradation. After one week, minimal hydrolytic degradation caused some broadening of the size distribution of nanogels incubated in PBS (Figure 2.3B), although the turbidity of the suspension was not significantly different (see inset photos in Figure 2.3A and 2.3B). In comparison, for the acid degradation samples, significant reductions in the turbidity are observed in conjunction with more broadening in the particle size distribution consistent with continued degradation. As such, the lead nanogel is degradable under physiologically-relevant conditions. Note that complete degradation of the nanogels will produce short chains of poly(ethylene glycol) and poly(methacrylic acid), both of which have been approved by the FDA in independent settings.⁴⁶⁻⁴⁸

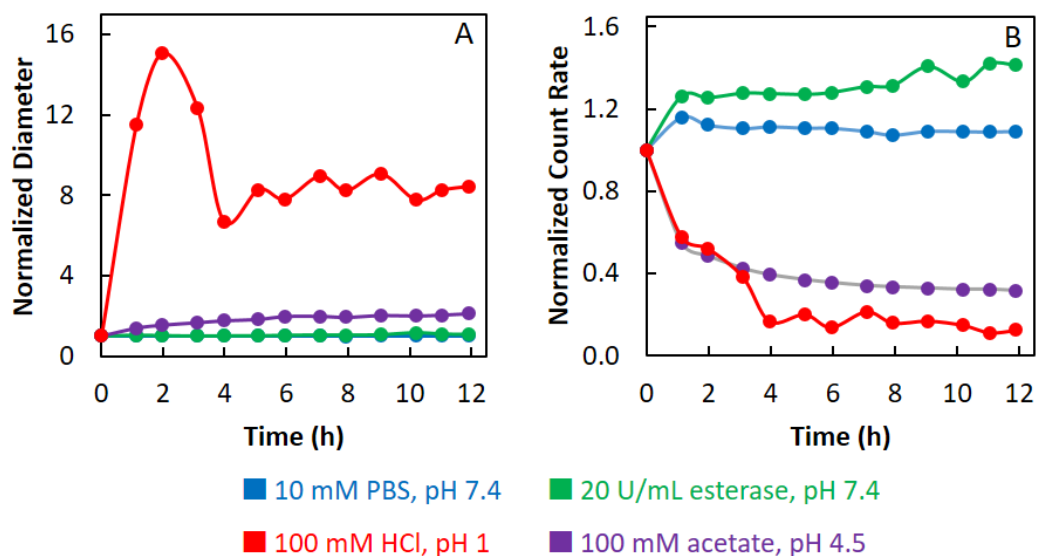


Figure 2.2: Degradation and stability of EGDMA cross-linked 10% BMA nanogels. (A) Normalized effective diameter and (B) normalized count rate (both relative to the $t=0$ h measurement) over 12 hours at 37°C in (1) 10 mM PBS, pH 7.4 (blue); (2) 20 U/mL esterase, pH 7.4 (enzymatic degradation - green); (3) 100 mM acetate, pH 4.5 (hydrolytic degradation-purple) or (4) 100 mM HCl, pH 1 (accelerated hydrolytic degradation-red).

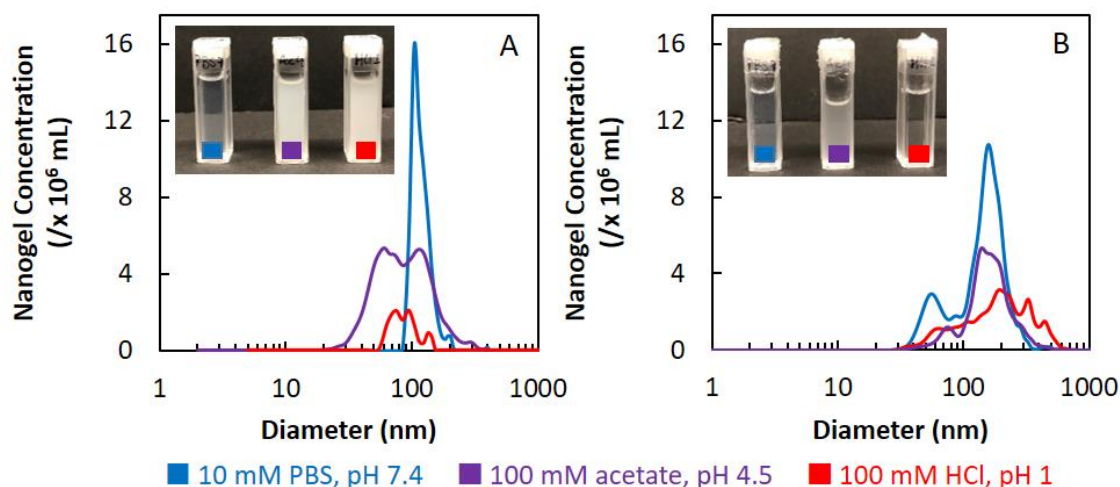


Figure 2.3: Particle size distribution of nanogels incubated in mimics of physiological conditions using nanoparticle tracking analysis (NTA). (A) After 1 day and (B) after 7 days at 37°C in either in (1) 10 mM PBS, pH 7.4 (blue); (2) 100 mM acetate, pH 4.5 (hydrolytic degradation-purple) or (3) 100 mM HCl, pH 1 (accelerated hydrolytic degradation-red).

2.4.4 *In vitro* cell compatibility

Nanogel cytocompatibility of the lead 10% BMA nanogel was assessed by quantifying the metabolic activity of SH-SY5Y cells using an MTT assay. Cells were exposed to different concentrations of nanogels or lurasidone-loaded nanogels (LUR-nanogel) at concentrations corresponding to those required for *in vivo* IN drug administration. The cell viability, relative to a non-treated cell only control, was assessed after 48 hours of exposure to the different nanogel treatments. For all cell treatments, the relative viability of nanogel-exposed cells relative to cell-only controls was >1, indicating good cytocompatibility of the nanogels with cells *in vitro* (Figure 2.4). As POEGMA is known to be

a cytocompatible polymer,^{39, 49} these results reinforce that these nanogels have potential for *in vivo* use without toxic effects.

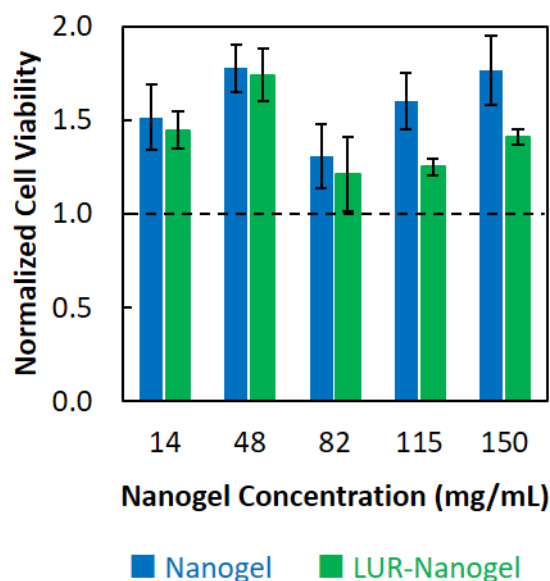


Figure 2.4: SH-SY5Y neuronal cell viability measured via an MTT assay after 48 hours of exposure to empty nanogels (blue) or lurasidone-loaded nanogels (LUR-nanogel, green) at *in vivo*-administered concentrations relative to a non-treated cell control. Error bars represent standard error of n=4 samples.

2.4.5 Locomotor activity

The pharmacodynamics of lurasidone delivered in 10% BMA nanogels was examined in male Sprague-Dawley rats using a MK-801 induced model of hyperlocomotor activity that is broadly used as a preclinical model of the positive symptoms of schizophrenia. Rats were dosed with nanogel IN 60 minutes prior to testing at a concentration corresponding to a lurasidone dose of 0.75 mg/kg as calculated based on the measured DLC (Table 2.3, corresponding to ~80 mg/kg nanogel); after one hour, IP MK-801 injections (0.35 mg/kg)

were subsequently administered immediately before transferring the rats to the chambers to induce the schizophrenic model. Two negative control cohorts of rats received either IN saline followed by IP saline administered in place of MK-801 (Saline), or the same IN dose of (unloaded) 10% BMA nanogel again followed by IP saline (NG). Rat locomotion was then tracked over a total of 160 minutes, with data recorded beginning 20 minutes after placement in the chamber to allow for activation of the MK-801 model and acclimatization of the rats to the chamber. In these rats, the total distance travelled was ~3 500 cm over the tracking period; no significant differences were observed between the two negative control groups ($p > 0.9999$). Two positive control cohort of rats received either IN saline and 0.35 mg/kg MK-801 (MK-801) (model induced but no therapy) or IN nanogel with MK-801 (NG/MK-801) (model induced and only empty nanogel administered). In these rats, locomotion increased to ~50 000 cm over the tracking period, a 14-fold greater distance than the negative control groups ($p < 0.0001$); this result is consistent with MK-801 inducing schizophrenia-like hyperlocomotion. The presence of the empty nanogel has no influence on the locomotion response ($p = 0.9982$ between MK-801 and NG-MK-801 positive control groups) (Figure 2.5), confirming that the nanogel itself does not alter the behavioural response of the rats.

Intranasal administration of nanogel loaded with 0.75 mg/kg lurasidone in MK-801 dosed rats (IN 0.75 LUR/MK-801) significantly reduced locomotion relative to the NG/MK-801

group ($p=0.0015$); furthermore, in comparison to the negative control (NG) study, the locomotion in this group was not significantly different ($p=0.1689$). This confirms that IN administration of a low dose of lurasidone has therapeutic efficacy, as it can attenuate the effects of MK-801 to a degree that the rats exhibit behavior comparable to that observed with healthy animals. To elucidate if this low drug dose is equally efficacious using an alternative route of administration similarly independent of the food effects associated with absorption via the oral route, rats were given an IP dose of nanogel containing 0.75 mg/kg lurasidone (IP 0.75 LUR/MK-801). The total distance travelled in this test group was not significantly lower than the NG/MK-801 treated rats ($p=0.2009$) but (unlike the IN dose applied at the same concentration) significantly higher than that observed for the control rats ($p=0.0089$); instead, IP administration of 3 mg/kg LUR-nanogel (IP 3 LUR/MK-801) was required to achieve both a statistically significant difference from the NG/MK-801 test group ($p<0.0001$) and an insignificant change relative to the negative control cohort ($p=0.584$). As such, the extent of recovery when low dose LUR-nanogel is administered IP is significantly less effective than that achieved following IN delivery, showing the clear advantage of direct nose-to brain transport in enhancing the bioavailability of lurasidone.

In comparison to previous studies examining the impact of emulsion-encapsulated IN lurasidone on locomotor activity²⁹, the nanogel-based drug delivery system achieves

effective behavioral changes in a relevant preclinical model of schizophrenia using 5.4× less drug coupled with prolonged behavioural attenuation over at least 160 minutes consistent with controlled release from the nanogel; in the prior study cited, locomotion was only quantified over a 10 minute period. Interestingly, IP administered nanogels also showed promising intervention, although 4-fold more drug was required to produce comparable effects to the IN administration. As IP-administered formulations must enter systemic circulation and the nanogel and/or the released drug must ultimately permeate the BBB to enable effective behavioral modification, we hypothesize that the 10% BMA nanogels have the desirable small size and soft, deformable mechanical properties to prolong circulation, avoid nonspecific accumulation in larger organs,⁵⁰ and/or promote BBB transport, all of which would increase the probability that lurasidone reaches its target in therapeutically-relevant quantities. However, the direct-to-brain access enabled by the IN pathway further enhances bioavailability and thus enables the use of lower doses of lurasidone (0.75 vs. 3 mg/kg) to produce similar behavioral outcomes. Smaller doses require less nanogel carrier, minimizing the potential for accumulated polymer toxicity upon frequent re-administration on a timescale faster than nanogel degradation.

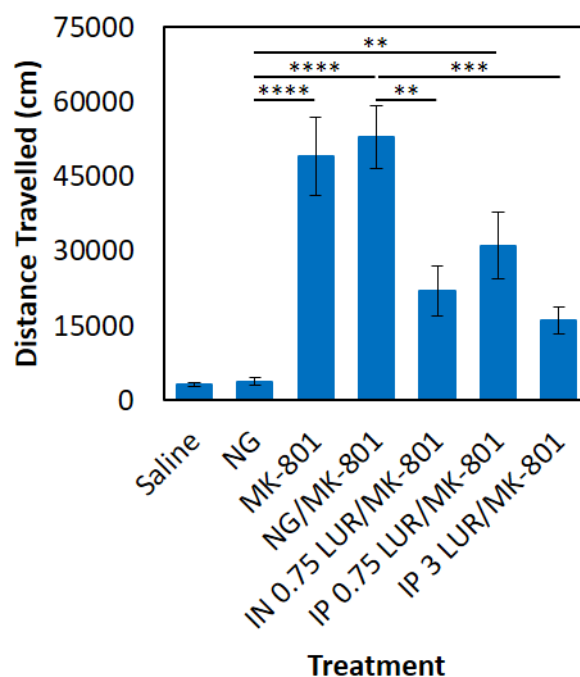


Figure 2.5: Locomotor activity of male Wistar Hans rats dosed 1.33 hr prior to movement tracking. Rats received either saline (negative control), 10% BMA nanogels alone (negative control), MK-801 only (positive control), NG/MK-801 (positive control), 10% BMA nanogels loaded with 0.75 mg/kg lurasidone administered IN or IP followed by MK-801, and 10% BMA nanogels loaded with 3 mg/kg lurasidone administered IP followed by MK-801. Error bars represent standard error with ** $p < 0.01$, *** $p < 0.0001$, and **** $p < 0.0001$ for the indicated pairwise comparison via ANOVA with Tukey post-hoc test.

2.4.6 Biodistribution

To assess the fate and distribution of 10% BMA nanogels in the body after IN administration, nanogels were fluorescently-labeled with cyanine5 (Cy5). The carboxylic acid groups of the AA comonomer incorporated into the nanogel were first converted into amino groups using 1,3-diaminopropane followed by conjugation of those amino groups with Cy5-NHS using EDC-mediated carbodiimide chemistry. Cy5-nanogels were then

administered IN at a concentration of 150 mg/mL; this larger dose was administered based on the apparent non-toxicity of the nanogel in the behavioural study such that the lowest possible detection thresholds for the presence of nanogel in different clearance organs could be achieved. Rats were sacrificed 3, 24 and 48 hours after administration; tissues were subsequently collected, homogenized and analyzed for their fluorescence content to measure the quantity of nanogel in each tissue (Figure 2.6). The nasal tissue showed by far the largest fluorescence intensity at all three time points examined, with little variability up to at least 48 hours and minimal fluorescence observed in any other organ (Figure 2.6). This high degree of nasal retention strongly suggests the formulation is able to overcome mucociliary clearance and mucus layer turnover that occurs approximately every 20 minutes,⁵¹ consistent with the ability of the small and soft nanogels to rapidly permeate the mucus layer. Smaller particles in the nanoscale range are less likely to be entrapped in the mucus mesh,⁵² while a dense surface coating of low molecular weight poly(ethylene glycol) (PEG, the composition of side chains in the nanogels) has been shown to aid in the rapid penetration of highly viscoelastic mucus.^{53,54} The use of a nanogel rather than a more hydrophobic nanoparticle (e.g. solid lipid nanoparticle or emulsion) is also likely beneficial in this context, as hydrophobic interactions with mucous can lead to entrapment and subsequent clearance of nanoparticles.⁵⁴ Given the almost exclusive retention of the nanogels in the nasal tissue, and in particular the lack of fluorescence detected in the olfactory bulbs and the brain,

uptake of the lurasidone-loaded nanogels by nasal epithelial cells (and the subsequent role of those cells as a drug depot to enable prolonged lurasidone delivery via the nose-to-brain pathway) is likely the main driver of drug release in this system rather than nose-to-brain transport of the nanogels themselves; this result is consistent with examples of nanogel uptake by the nasal epithelium after IN administration in prior studies.⁵⁵⁻⁵⁷ This could enable administration of larger doses of drug at less frequent intervals, which can be clinically advantageous as patient compliance to frequent dosing regimens is often ineffectual. The spleen is the only organ to show minor fluorescence, consistent with its role in filtering nanoparticles of size <100 nm that enter systemic circulation;³⁶ however, the transient nature of the small increase in spleen nanoparticle concentration (disappearing by 48 hours without a corresponding decrease in nasal concentration) coupled with the lack of fluorescence detected in the lung, liver and kidneys suggest that these nanogels do not collect in the typical organs, at least on the time scale of the therapeutic utility of the nanogels. As such, IN administration of nanogels can be exploited for direct nose-to-brain transport of hydrophobic therapeutics with the potential for prolonged release behavior.

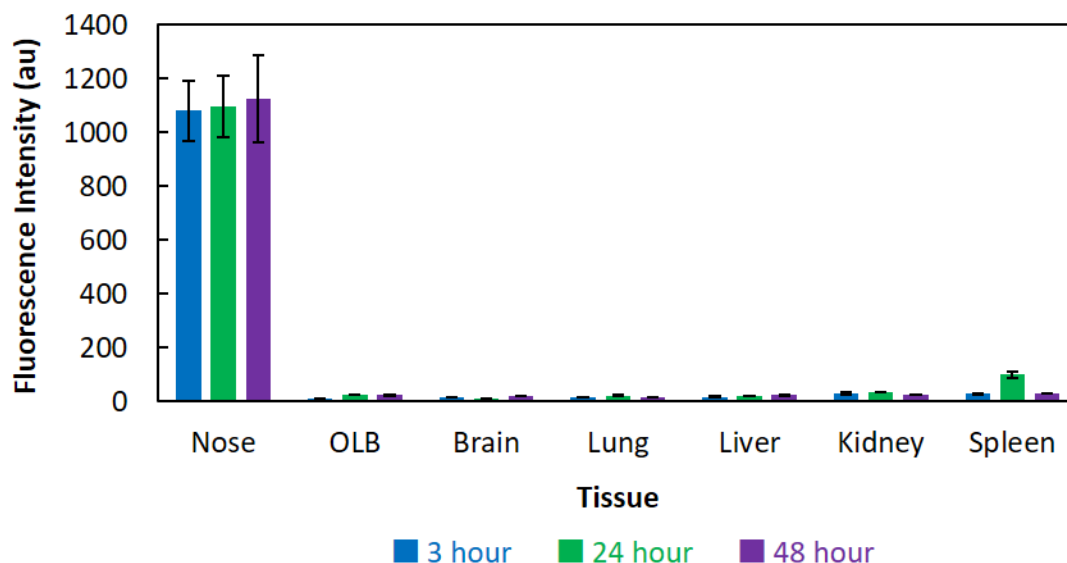


Figure 2.6: Biodistribution of Cy5 fluorescently-labeled 10% BMA nanogels administered intranasally at a concentration of 15 wt%. Tissues and organs were collected after 3 hours (blue), 24 hours (green) and 48 hours (purple) and were analyzed for fluorescence after homogenization.

2.5 Conclusions

POEGMA-based nanogels functionalized with hydrophobic domains based on copolymerization of BMA can effectively deliver the poorly-water soluble APD lurasidone. The small size (<100 nm) of the nanogels enabled effective biological transport, while the incorporation of hydrolytically-labile functional groups in the cross-linker enabled degradation of the nanogels over time. 10% BMA nanogels showed high *in vitro* cytocompatibility with SH-SY5Y neuronal cells, while *in vivo* administration of a low drug dose (0.75 mg/kg) lurasidone-loaded 10% BMA nanogel resulted in significant attenuation of hyperlocomotor activity in a MK-801-induced rodent model of schizophrenia when

administered via the nasal route. Biodistribution studies revealed that the nanogels remain almost exclusively localized to the nasal tissue for at least 48 hours post-IN administration without accumulation in typical clearance organs. Collectively, these results demonstrate the potential of hydrophobized nanogels to deliver therapeutically-relevant doses of hydrophobic APD to the brain.

2.6 Acknowledgements

The Natural Sciences and Engineering Research Council of Canada (NSERC) and the Canadian Institutes of Health Research (CIHR) are acknowledged for funding (Canada Graduate Scholarship to MS, Collaborative Health Research Partnerships Grants CPG-151963 and CHRPJ-508393-2017 to TH and RKM). We are grateful for support from the staff at McMaster's Central Animal Facility, including Marion Corrick for her help coordinating the biodistribution studies and Tamara Kearns for her expertise in tissue collection.

2.7 References

- (1) Porter, C. J. H.; Trevaskis, N. L.; Charman, W. N., Lipids and Lipid-Based Formulations: Optimizing the Oral Delivery of Lipophilic Drugs. *Nat. Rev. Drug Discov.* **2007**, *6* (3), 231-248.
- (2) Williams, H. D.; Trevaskis, N. L.; Charman, S. A.; Shanker, R. M.; Charman, W. N.; Pouton, C. W.; Porter, C. J. H., Strategies to Address Low Drug Solubility in Discovery and Development. *Pharmacol. Rev.* **2013**, *65* (1), 315-499.
- (3) D. Deshpande, R.; D. V, G.; Vegesna, N. S. K. V.; Vaghela, R.; P. K, K., The Effect of Nanonization on Poorly Water Soluble Glibenclamide Using a Liquid Anti-Solvent Precipitation Technique: Aqueous Solubility, In Vitro and In Vivo Study. *RSC Adv.* **2015**, *5* (99), 81728-81738.
- (4) Di, L.; Fish, P. V.; Mano, T., Bridging Solubility Between Drug Discovery and Development. *Drug Discov. Today* **2012**, *17* (9), 486-495.
- (5) Kawabata, Y.; Wada, K.; Nakatani, M.; Yamada, S.; Onoue, S., Formulation Design for Poorly Water-Soluble Drugs Based on Biopharmaceutics Classification System: Basic Approaches and Practical Applications. *Int. J. Pharm.* **2011**, *420* (1), 1-10.
- (6) Ku, M. S.; Dulin, W., A Biopharmaceutical Classification-Based Right-First-Time Formulation Approach to Reduce Human Pharmacokinetic Variability and Project Cycle Time From First-in-Human to Clinical Proof-Of-Concept. *Pharm. Dev. Technol.* **2012**, *17* (3), 285-302.
- (7) Shah, S.; Parmar, B.; Soniwala, M.; Chavda, J., Design, Optimization, and Evaluation of Lurasidone Hydrochloride Nanocrystals. *AAPS PharmSciTech* **2016**, *17* (5), 1150-1158.
- (8) Charlson, F. J.; Ferrari, A. J.; Santomauro, D. F.; Diminic, S.; Stockings, E.; Scott, J. G.; McGrath, J. J.; Whiteford, H. A., Global Epidemiology and Burden of Schizophrenia: Findings from the Global Burden of Disease Study 2016. *Schizophrenia Bull.* **2018**, *44* (6), 1195-1203.
- (9) Samalin, L.; Garnier, M.; Llorca, P. M., Clinical Potential of Lurasidone in the Management of Schizophrenia. *Ther. Clin. Risk Manag.* **2011**, *7*, 239-250.
- (10) Tarazi, F. I.; Riva, M. A., The Preclinical Profile of Lurasidone: Clinical Relevance for the Treatment of Schizophrenia. *Expert. Opin. Drug Dis.* **2013**, *8* (10), 1297-1307.
- (11) Kantrowitz, J. T.; Citrome, L., Lurasidone for Schizophrenia: What's Different? *Expert Rev. Neurother.* **2012**, *12* (3), 265-273.
- (12) Greenberg, W. M.; Citrome, L., Pharmacokinetics and Pharmacodynamics of Lurasidone Hydrochloride, a Second-Generation Antipsychotic: A Systematic Review of the Published Literature. *Clin. Pharmacokinet.* **2017**, *56* (5), 493-503.

- (13) Ishibashi, T.; Horisawa, T.; Tokuda, K.; Ishiyama, T.; Ogasa, M.; Tagashira, R.; Matsumoto, K.; Nishikawa, H.; Ueda, Y.; Toma, S.; Oki, H.; Tanno, N.; Saji, I.; Ito, A.; Ohno, Y.; Nakamura, M., Pharmacological Profile of Lurasidone, a Novel Antipsychotic Agent with Potent 5-Hydroxytryptamine 7 (5-HT7) and 5-HT1A Receptor Activity. *J. Pharmacol. Exp. Ther.* **2010**, *334* (1), 171-181.
- (14) Sykes, D. A.; Moore, H.; Stott, L.; Holliday, N.; Javitch, J. A.; Lane, J. R.; Charlton, S. J., Extrapyramidal Side Effects of Antipsychotics are Linked to Their Association Kinetics at Dopamine D2 Receptors. *Nat. Commun.* **2017**, *8* (1), 763.
- (15) Freyberg, Z.; Aslanoglou, D.; Shah, R.; Ballon, J. S., Intrinsic and Antipsychotic Drug-Induced Metabolic Dysfunction in Schizophrenia. *Front. Neurosci.* **2017**, *11*, 432.
- (16) Londhe, V. Y.; Deshmane, A. B.; Singh, S. R.; Kulkarni, Y. A., Lurasidone- β -Cyclodextrin Complexes: Physicochemical Characterization and Comparison of their Antidepressant, Antipsychotic Activities Against that of Self Microemulsifying Formulation. *J. Mol. Struct.* **2018**, *1157*, 395-400.
- (17) Kumar, R. S.; Ratan, S. S.; Nethravathi, P., Development and Characterization of Oral Disintegrating Tablet Containing Nanosuspension of Lurasidone Hydrochloride Antipsychotic Drug. *Asian J. Pharm.* **2017**, *11* (2), 102-111.
- (18) Lu, S.; Yu, P.P.; He, J.H.; Zhang, S.S.; Xia, Y.L.; Zhang, W.L.; Liu, J.P., Enhanced Dissolution and Oral Bioavailability of Lurasidone Hydrochloride Nanosuspensions Prepared by Antisolvent Precipitation–Ultrasonication Method. *RSC Adv.* **2016**, *6* (54), 49052-49059.
- (19) Yu, P. P.; Lu, S.; Zhang, S. S.; Zhang, W. L.; Li, Y.; Liu, J. P., Enhanced Oral Bioavailability and Diminished Food Effect Of Lurasidone Hydrochloride Nanosuspensions Prepared by Facile Nanoprecipitation Based on Dilution. *Powder Technol.* **2017**, *312*, 11-20.
- (20) Basalious, E. B.; Abdallah Ahmed, M., Phospholipid Based Self-Nanoemulsifying Self-Nanosuspension (P-SNESNS) as a Dual Solubilization Approach for Development of Formulation with Diminished Food Effect: Fast/Fed In Vivo Pharmacokinetics Study in Human. *Eur. J. Pharm. Sci.* **2017**, *109*, 244-252.
- (21) Dondapati, D.; Srimathkandala, M. H.; Sanka, K.; Bakshi, V., Improved Solubility and Dissolution Release Profile of Lurasidone by Solid Self-Nanoemulsifying Drug Delivery System. *Anal. Chem. Lett.* **2016**, *6* (2), 86-97.
- (22) Jangipuria, F.; Londhe, V., Solubility Enhancement of Lurasidone Hydrochloride by Preparing SMEDDS. *Int. J. Pharm.* **2015**, *7* (11), 283-288.
- (23) Miao, Y.; Sun, J.; Chen, G.; Lili, R.; Ouyang, P., Enhanced Oral Bioavailability of Lurasidone by Self-Nanoemulsifying Drug Delivery System in Fasted State. *Drug Dev. Ind. Pharm.* **2016**, *42* (8), 1234-1240.
- (24) Patel, M. H.; Sawant, K. K., Self Microemulsifying Drug Delivery System of Lurasidone Hydrochloride for Enhanced Oral Bioavailability by Lymphatic

- Targeting: In Vitro, Caco-2 Cell Line and In Vivo Evaluation. *Eur. J. Pharm. Sci.* **2019**, *138*, 105027.
- (25) Patel, M. H.; Mundada, V. P.; Sawant, K. K., Fabrication of Solid Lipid Nanoparticles of Lurasidone HCl for Oral Delivery: Optimization, In Vitro Characterization, Cell Line Studies and In Vivo Efficacy in Schizophrenia. *Drug Dev. Ind. Pharm.* **2019**, *45* (8), 1242-1257.
- (26) Lochhead, J. J.; Thorne, R. G., Intranasal Delivery of Biologics to the Central Nervous System. *Adv. Drug Deliver. Rev.* **2012**, *64* (7), 614-628.
- (27) Jazuli, I.; Annu; Nabi, B.; Moolakkadath, T.; Alam, T.; Baboota, S.; Ali, J., Optimization of Nanostructured Lipid Carriers of Lurasidone Hydrochloride Using Box-Behnken Design for Brain Targeting: In Vitro and In Vivo Studies. *J. Pharm. Sci.* **2019**, *108* (9), 3082-3090.
- (28) Pokharkar, V.; Suryawanshi, S.; Dhapte-Pawar, V., Exploring Micellar-Based Polymeric Systems for Effective Nose-To-Brain Drug Delivery as Potential Neurotherapeutics. *Drug Deliv. Transl. Res.* **2020**, *10* (4), 1019-1031.
- (29) Patel, M. R.; Patel, R. B.; Thakore, S. D.; Solanki, A. B., Brain Targeted Delivery of Lurasidone HCl via Nasal Administration of Mucoadhesive Nanoemulsion Formulation for the Potential Management of Schizophrenia. *Pharm. Dev. Technol.* **2020**, *25* (8) 1018-1030.
- (30) Yin, Y. L.; Hu, B.; Yuan, X.; Cai, L.; Gao, H. L.; Yang, Q., Nanogel: A Versatile Nano-Delivery System for Biomedical Applications. *Pharmaceutics* **2020**, *12* (3), 290.
- (31) Zhang, H.; Zhai, Y.; Wang, J.; Zhai, G., New Progress and Prospects: The Application of Nanogel in Drug Delivery. *Mater. Sci. Eng. C* **2016**, *60*, 560-568.
- (32) Bang, T. H.; Van, T. T. T.; Hung, L. X.; Ly, B. M.; Nhut, N. D.; Thuy, T. T. T.; Huy, B. T., Nanogels of Acetylated Ulvan Enhance the Solubility of Hydrophobic Drug Curcumin. *B. Mater. Sci.* **2019**, *42*, 1.
- (33) Picone, P.; Sabatino, M. A.; Ditta, L. A.; Amato, A.; San Biagio, P. L.; Mulè, F.; Giacomazza, D.; Dispenza, C.; Di Carlo, M., Nose-to-Brain Delivery of Insulin Enhanced by a Nanogel Carrier. *J. Control. Release* **2018**, *270*, 23-36.
- (34) Karg, M.; Pich, A.; Hellweg, T.; Hoare, T.; Lyon, L. A.; Crassous, J. J.; Suzuki, D.; Gumerov, R. A.; Schneider, S.; Potemkin, I. I.; Richtering, W., Nanogels and Microgels: From Model Colloids to Applications, Recent Developments, and Future Trends. *Langmuir* **2019**, *35* (19), 6231-6255.
- (35) Merkel, T. J.; Chen, K.; Jones, S. W.; Pandya, A. A.; Tian, S.; Napier, M. E.; Zamboni, W. E.; DeSimone, J. M., The Effect of Particle Size on the Biodistribution of Low-Modulus Hydrogel PRINT Particles. *J. Control. Release* **2012**, *162* (1), 37-44.
- (36) Zhang, L.; Cao, Z.; Li, Y.; Ella-Menye, J.-R.; Bai, T.; Jiang, S., Softer Zwitterionic Nanogels for Longer Circulation and Lower Splenic Accumulation. *ACS Nano* **2012**, *6* (8), 6681-6686.

- (37) Zabihi, F.; Wiecezorek, S.; Dimde, M.; Hedtrich, S.; Börner, H. G.; Haag, R., Intradermal Drug Delivery by Nanogel-Peptide Conjugates; Specific and Efficient Transport of Temoporfin. *J. Control. Release* **2016**, *242*, 35-41.
- (38) Lutz, J. F.; Hoth, A., Preparation of Ideal PEG Analogues with a Tunable Thermosensitivity by Controlled Radical Copolymerization of 2-(2-Methoxyethoxy)Ethyl Methacrylate and Oligo(Ethylene Glycol)Methacrylate. *Macromolecules* **2006**, *39* (2), 893-896.
- (39) Smeets, N. M. B.; Bakaic, E.; Patenaude, M.; Hoare, T., Injectable Poly(Oligoethylene Glycol Methacrylate)-Based Hydrogels with Tunable Phase Transition Behaviours: Physicochemical and Biological Responses. *Acta Biomater.* **2014**, *10* (10), 4143-4155.
- (40) Liu, J.; Zhang, Y.; Yang, T.; Ge, Y.; Zhang, S.; Chen, Z.; Ning, G., Synthesis, Characterization, and Application of Composite Alginate Microspheres with Magnetic and Fluorescent Functionalities. *J. Appl. Polym. Sci.* **2009**, *113*, 4042-4051.
- (41) Hermanson, G. T., Chapter 4 - Zero-Length Crosslinkers. In *Bioconjugate Techniques (Third Edition)*, Hermanson, G. T., Ed. Academic Press: Boston, 2013; pp 259-273.
- (42) Hermanson, G. T., Chapter 10 - Fluorescent Probes. In *Bioconjugate Techniques (Third Edition)*, Hermanson, G. T., Ed. Academic Press: Boston, 2013; pp 395-463.
- (43) Oh, N. M.; Oh, K. T.; Youn, Y. S.; Lee, D.-K.; Cha, K.-H.; Lee, D. H.; Lee, E. S., Poly(L-Aspartic Acid) Nanogels for Lysosome-Selective Antitumor Drug Delivery. *Colloid. Surface. B* **2013**, *101*, 298-306.
- (44) Oishi, M.; Hayashi, H.; Iijima, M.; Nagasaki, Y., Endosomal Release and Intracellular Delivery of Anticancer Drugs Using PH-Sensitive PEGylated Nanogels. *J. Mater. Chem.* **2007**, *17* (35), 3720-3725.
- (45) Zhang, W.; Tung, C. H., Real-Time Visualization of Lysosome Destruction Using a Photosensitive Toluidine Blue Nanogel. *Chem.-Eur. J.* **2018**, *24* (9), 2089-2093.
- (46) Alconcel, S. N. S.; Baas, A. S.; Maynard, H. D., FDA-Approved Poly(Ethylene Glycol)-Protein Conjugate Drugs. *Polym. Chem.* **2011**, *2* (7), 1442-1448.
- (47) Mansour, H. M.; Sohn, M.; Al-Ghananeem, A.; DeLuca, P. P., Materials for Pharmaceutical Dosage Forms: Molecular Pharmaceutics and Controlled Release Drug Delivery Aspects. *Int. J. Mol. Sci.* **2010**, *11* (9), 3298-3322.
- (48) Saade, H.; Guillen, M. D.; Romero, J. C.; Cepeda, J.; Ilyna, A.; Fernandez, S.; Enriquez-Medrano, F. J.; Lopez, R. G., Biocompatible and Biodegradable Ultrafine Nanoparticles of Poly(Methyl Methacrylate-Co-Methacrylic Acid) Prepared via Semicontinuous Heterophase Polymerization: Kinetics and Product Characterization. *Int. J. Polym. Sci.* **2016**, 2016, 7674620.

- (49) Xu, F.; Dodd, M.; Sheardown, H.; Hoare, T., Single-Step Reactive Electrospinning of Cell-Loaded Nanofibrous Scaffolds as Ready-to-Use Tissue Patches. *Biomacromolecules* **2018**, *19* (11), 4182-4192.
- (50) Blanco, E.; Shen, H.; Ferrari, M., Principles of Nanoparticle Design for Overcoming Biological Barriers to Drug Delivery. *Nat. Biotechnol.* **2015**, *33* (9), 941-951.
- (51) Lai, S. K.; Wang, Y. Y.; Hanes, J., Mucus-Penetrating Nanoparticles for Drug and Gene Delivery to Mucosal Tissues. *Adv. Drug Deliver. Rev.* **2009**, *61* (2), 158-171.
- (52) Suk, J. S.; Xu, Q.; Kim, N.; Hanes, J.; Ensign, L. M., PEGylation as a Strategy for Improving Nanoparticle-Based Drug and Gene Delivery. *Adv. Drug Deliver. Rev.* **2016**, *99*, 28-51.
- (53) Tang, B. C.; Dawson, M.; Lai, S. K.; Wang, Y.-Y.; Suk, J. S.; Yang, M.; Zeitlin, P.; Boyle, M. P.; Fu, J.; Hanes, J., Biodegradable Polymer Nanoparticles that Rapidly Penetrate the Human Mucus Barrier. *PNAS* **2009**, *106* (46), 19268-19273.
- (54) Wang, Y.-Y.; Lai, S. K.; Suk, J. S.; Pace, A.; Cone, R.; Hanes, J., Addressing the PEG Mucoadhesivity Paradox to Engineer Nanoparticles that “Slip” Through the Human Mucus Barrier. *Angew. Chem. Int. Ed.* **2008**, *47* (50), 9726-9729.
- (55) Fukuyama, Y.; Yuki, Y.; Katakai, Y.; Harada, N.; Takahashi, H.; Takeda, S.; Mejima, M.; Joo, S.; Kurokawa, S.; Sawada, S.; Shibata, H.; Park, E. J.; Fujihashi, K.; Briles, D. E.; Yasutomi, Y.; Tsukada, H.; Akiyoshi, K.; Kiyono, H., Nanogel-Based Pneumococcal Surface Protein A Nasal Vaccine Induces Microrna-Associated TH17 Cell Responses with Neutralizing Antibodies Against Streptococcus Pneumoniae in Macaques. *Mucosal Immunol.* **2015**, *8* (5), 1144-1153.
- (56) Nochi, T.; Yuki, Y.; Takahashi, H.; Sawada, S.-i.; Mejima, M.; Kohda, T.; Harada, N.; Kong, I. G.; Sato, A.; Kataoka, N.; Tokuhara, D.; Kurokawa, S.; Takahashi, Y.; Tsukada, H.; Kozaki, S.; Akiyoshi, K.; Kiyono, H., Nanogel Antigenic Protein-Delivery System for Adjuvant-Free Intranasal Vaccines. *Nat. Mater.* **2010**, *9* (7), 572-578.
- (57) Kong, I. G.; Sato, A.; Yuki, Y.; Nochi, T.; Takahashi, H.; Sawada, S.; Mejima, M.; Kurokawa, S.; Okada, K.; Sato, S.; Briles, D. E.; Kunisawa, J.; Inoue, Y.; Yamamoto, M.; Akiyoshi, K.; Kiyono, H., Nanogel-based PspA Intranasal Vaccine Prevents Invasive Disease and Nasal Colonization by Streptococcus Pneumoniae. *Infect. Immun.* **2013**, *81* (5), 1625-1634.

Chapter 3 : Degradable, Hydrophobized Poly(oligoethylene glycol methacrylate)-Based Nanogels for Intranasal Delivery of Haloperidol to the Brain

Madeline J. Simpson^a, Ugonwa C. Echendu^a, Ali Babar^b, Niels M. B. Smeets^a, Ram K. Mishra^{b,c} and Todd Hoare^{a,b*}

^a Department of Chemical Engineering, McMaster University, 1280 Main Street West, Hamilton, ON, L8S 4L7, Canada

^b School of Biomedical Engineering, McMaster University, 1280 Main Street West, Hamilton, ON, L8S 4K1, Canada

^c Department of Psychiatry and Behavioural Neurosciences, McMaster University, 1200 Main Street West, Hamilton, ON, L8N 3Z5, Canada

Keywords: nanogel, biodegradable, intranasal, haloperidol, blood-brain barrier.

3.1 Abstract

Delivery of therapeutics to the brain to treat central nervous system (CNS) disorders, including schizophrenia, is challenging due to the highly impenetrable blood-brain barrier (BBB). Nanoparticle-based drug delivery systems administered intranasally can improve the bioavailability and efficacy of therapeutics. Herein, degradable poly(oligoethylene glycol methacrylate) (POEGMA)-based nanogels containing hydrophobic domains of butyl methacrylate (BMA) or methyl methacrylate (MMA) are utilized as non-invasive carriers for the poorly-water soluble antipsychotic drug (APD) haloperidol to treat schizophrenia. The nanogel formulations are tailored to exhibit small particle sizes with narrow size distributions ideal for nose-to-brain delivery through the nasal epithelium while showing capacity to encapsulate up to 15 wt% haloperidol. The inclusion of a biodegradable disulfide cross-linker promotes haloperidol release upon nanogel erosion into low molecular weight polymer fragments that can be cleared *in vivo*. The nanogels show no significant cytotoxicity to SH-SY5Y neuronal cells, while intranasal administration of haloperidol-loaded nanogels effectively induces catalepsy and decreases locomotor activity in male Sprague-Dawley rats using a haloperidol dose one half of that typically administered intraperitoneally to induce similar effects. By decreasing the required APD dose, the associated adverse effects (e.g. extrapyramidal side-effects) of clinically prescribed APDs can be limited to improve patient compliance to their therapeutic regimen.

3.2 Introduction

Schizophrenia is a chronic and debilitating mental disorder that globally affects about 1% of the population (21 million individuals).¹ Patients may suffer from hallucinations or delusions (positive symptoms), social withdrawal or depression (negative symptoms) and/or difficulty with memory, recall and attention span (cognitive deficits).²⁻³ As there is no known cure for schizophrenia, the current standard for medical intervention relies on a class of small molecule compounds known as antipsychotic drugs (APDs).⁴⁻⁵

Haloperidol (HLP), otherwise known as (4-[4-(4-chlorophenyl)-4-hydroxypiperidin-1-yl]-1-(4-fluorophenyl)butan-1-one, is a first-generation, typical APD listed on the World Health Organization's (WHO) list of essential medicines for its role in treating psychotic disorders.⁶⁻⁸ When administered at low doses, haloperidol is a potent dopamine D₂ receptor antagonist and also binds α_1 -adrenergic receptors to modulate positive symptoms; when administered at high doses, haloperidol binds to 5-HT₂ receptors to regulate negative symptoms.⁹ Haloperidol is conventionally administered orally, with the resulting first-pass metabolism limiting the quantity of drug that can be delivered to the brain;¹⁰⁻¹¹ the presence of the blood-brain barrier (BBB) restricts access of the remaining haloperidol dose to the brain.¹² As such, to achieve clinically-relevant concentrations in the brain, haloperidol must be administered in chronically high doses, leading to undesirable neurological side effects (including severe extrapyramidal side effects such as

tardive dyskinesia) that may persist even after treatment is withdrawn.^{9, 13-16} As a result, patient adherence to orally-administered haloperidol regimens is often low, leading to poor treatment outcomes and limiting haloperidol's long-term utility as an APD.¹⁷⁻¹⁸

The relatively high hydrophobicity of haloperidol ($\log P = 3.36$) limits its potential dosage forms, as dissolution requires very low pH or solvents that are not physiologically compatible.^{12, 19} As such, haloperidol is an excellent candidate for encapsulation in a drug delivery vehicle that can improve its bioavailability while reducing the risk of extrapyramidal side effects, ultimately enabling reduced drug dosing due to better APD targeting and localized sustained release. Several different materials and strategies have been employed to enhance the delivery of haloperidol, but all have certain drawbacks. Prodrug approaches in which haloperidol is conjugated to a lipophilic decanoate chain through a degradable ester bond²⁰ or a hydrophilic low molecular weight poly(ethylene glycol) graft (PEG, > 6 kDa) through a non-degradable carbamate linkage²¹ enable prolonged local haloperidol activity but require invasive injections (intramuscular for the decanoate graft and intracranial for the PEG graft) that limit their practical utility. Strategies to create polymer implants, matrixes, films and most recently 3D printed tablets that entrap haloperidol have also been proposed.²²⁻²⁵ However, many of these systems require invasive surgeries or result in the rapid release of haloperidol *in vitro*, limiting clinical utility.

Nanoparticles are attractive drug delivery vehicles for APDs because their physiochemical properties can be specifically tailored to increase drug uptake, targeting and release.²⁶ Nanoparticle compositions can be engineered to enhance drug solubility (enabling different routes of drug administration), protect against premature degradation (improving drug bioavailability) and meter diffusion-based release of the drug (to control drug release kinetics).²⁷⁻²⁸ The most popular polymer drug delivery vehicle for haloperidol encapsulation is based on poly(lactic acid) (PLA), poly (glycolic acid) (PGA) or their copolymer (PLGA). Cheng *et al.* used the emulsification-solvent evaporation technique to create micron scale (0.8-8 μm) PLGA particles with broad size distributions that enabled moderate uptake of haloperidol (5-10 wt%) and prolonged drug release (>55 days) without a substantial initial burst.²⁹ PLGA nanoparticles have also been synthesized using a similar technique followed by sonication to produce nanoscale particles on the order of 200 nm. Increasing the L:G ratio in the constituent PLGA polymers increased the haloperidol loading to 2 wt% by enhancing hydrophobic interactions between the polymer and drug, while optimization of the surface functional groups and particle size enabled relevant reductions in burst release while extending overall release.³⁰⁻³² Despite the substantial optimization efforts, none of the formulations were tested *in vivo* to elucidate their therapeutic effects. Very small (<50 nm) haloperidol-loaded self-assembled micelles based on PEG-*b*-PLA have also been reported by directly conjugating haloperidol to the polymer to create a prodrug and/or encapsulating free haloperidol in

the PLA micelle core. The prodrug formulation has limited drug loading (3.5 wt%) while the polymer alone physically encapsulates up to 20 wt% free drug; however, chronic intraperitoneal (IP) delivery of these micelles was less effective at inhibiting locomotor activity relative to a comparable acute dose of HLP alone, likely due to rapid sequestration of the micelles to non-target organs due to their small size.³³⁻³⁴ Polysorbate nanocapsules have also been investigated for HLP delivery, enabling high encapsulation efficiencies of >95% and comparable inhibition of locomotor activity to free haloperidol when injected IP in chronic dosing studies.³⁵⁻³⁶ However, only acute effects (<2 h) were tested, while effective antipsychotic effects over prolonged periods would be strongly preferred clinically.

Given the penetration challenges associated with any kind of therapeutic (drug or nanovehicle) through the BBB, alternate non-invasive routes of drug administration to the brain are attracting increasing interest.³⁷⁻³⁹ Intranasal (IN) “nose-to-brain” delivery can bypass the BBB via direct or indirect transport pathways that project into the brain, thereby avoiding hepatic first-pass metabolism and enhancing drug bioavailability.⁴⁰⁻⁴² However, there are to-date only a limited number of studies investigating the intranasal delivery of haloperidol-loaded nanocarriers. IN delivery of solid lipid nanoparticles (SLNs) with high drug loading content (25 wt%) enabled the delivery of haloperidol with significantly higher brain/blood ratios and larger/faster maximum drug concentrations

(C_{max}) relative to IP delivery,¹² while haloperidol-loaded miniemulsions showed nearly 2-fold greater haloperidol levels in the brain achieved six times faster with IN administration compared to IV administration.⁴³ In previous work from our group, Piazza *et al.* demonstrated that conjugating PEG-PLGA self-assembled nanoparticles with lectin groups that can specifically bind to nasal epithelial cells increased haloperidol concentrations in the brain up to 3-fold compared to non-functionalized IN-administered particles or IP administration.⁴⁴ Katare *et al.* intranasally administered 15 nm dendrimers that more rapidly produced comparable pharmacodynamic outcomes while using ~6 times less drug than an IP injection of free haloperidol., albeit with significant carrier toxicity concerns at higher dose levels.⁴⁵ Combined, these studies demonstrate the benefits of exploiting the intranasal route to improve the efficacy of nanoparticle-based haloperidol therapeutics. However, the faster transport to the brain enabled by the IN delivery is typically offset by faster clearance, with smaller particles (e.g. dendrimers) clearing particularly quickly while larger “hard” nanoparticles achieve more limited uptake via the IN route and thus require larger overall drug dosages that limit the degree to which side-effects can be avoided.

Herein, we describe a nanogel formulation that is chemically and physically tailored to enhance haloperidol uptake and improve its *in vivo* pharmacodynamics following IN delivery. We have recently used a strategy for hydrophobic nanogel fabrication based on

the precipitation copolymerization of diethylene glycol methacrylate (M(EO)₂MA), acrylic acid (AA) and either butyl methacrylate (BMA) or methyl methacrylate (MMA) to yield small (<100 nm) nanogels with narrow size distributions (polydispersity (PD) <0.1) and hydrophobic domains via BMA or MMA self-association that can significantly enhance the uptake and control the delivery of another APD, lurasidone. Herein, we adapt this strategy to effectively deliver haloperidol via IN delivery. The use of a redox responsive disulfide cross-linker enables stimuli-triggered drug release while also addressing the long-term toxicity concerns associated with the use of conventional precipitation-derived nanogels that are typically not degradable *in vivo*. The nanogels are demonstrated to enable IN delivery of haloperidol while significantly improving its bioavailability in a rodent model at substantially lower drug concentrations than required via IP administration, thus offering potential to reduce the quantity and frequency of dosing, minimize the associated negative side effects, and ultimately improve patient compliance to an APD-based treatments.

3.3 Experimental

3.3.1 Materials

Diethylene glycol methacrylate (M(EO)₂MA, n = 2 ethylene oxide (EO) repeat units, 95%), oligo(ethylene glycol methacrylate) (OEGMA₅₀₀, n = 8-9 EO repeat units), butyl methacrylate (BMA, 99%), methyl methacrylate (MMA, 99%), anhydrous acrylic acid (AA, 99%), acryloyl chloride (97%), esterase from porcine liver (68.9 U/mg), 2-hydroxyethyl disulfide (technical grade), L-glutathione reduced (GSH, ≥98%), potassium persulfate (KPS, ≥99.0%), sodium acetate (≥99%), sodium dodecyl sulfate (SDS, ≥99.0%) and Tween 80 were purchased from Millipore Sigma (Oakville, ON) and used as received. Haloperidol (98.2%, ApexBio) was purchased from Cedarlane (Burlington, ON). Deionized water (Milli-Q H₂O) was purified using the Millipore Simplicity System (Millipore, Bedford, USA) prior to use. All other reagents were analytical grade and used without further purification.

3.3.2 Synthesis of 2-hydroxyethyl disulfide diacrylate cross-linker

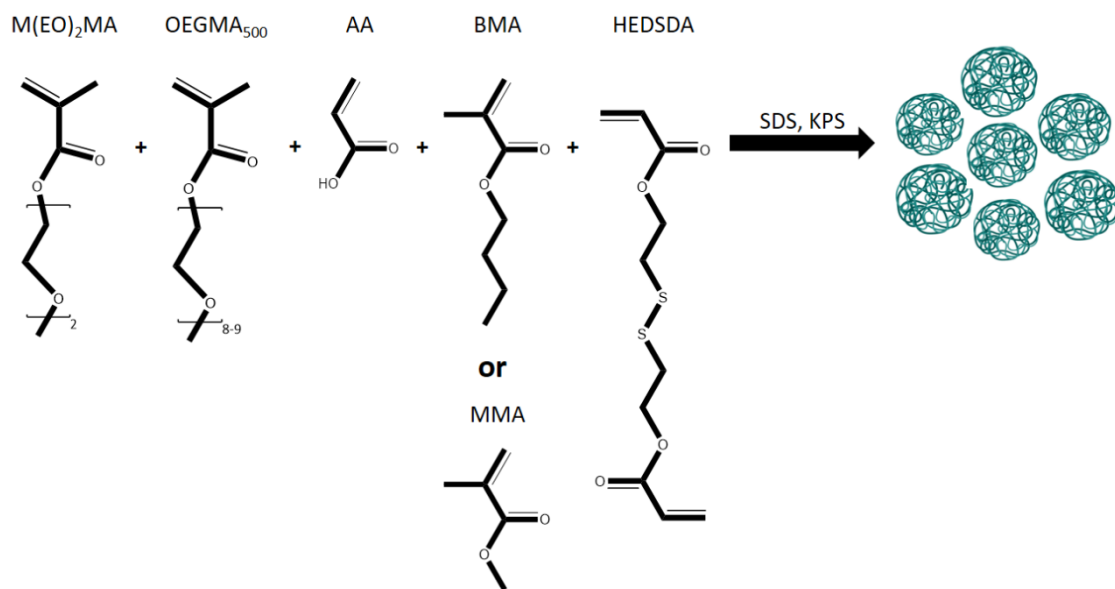
The degradable cross-linker 2-hydroxyethyl disulfide diacrylate (HEDSDA) containing a disulfide bridge was synthesized. Anhydrous DCM (300 mL) and triethylamine (36 g, 0.36 mol) were added to a 500 mL two-neck flask and subsequently placed under nitrogen into an ice bath. Subsequently, 2-hydroxyethyl disulfide (25 g, 0.16 mol) was added, followed by the dropwise addition of acryloyl chloride (32 g, 0.36 mol). The reaction proceeded under magnetic stirring at 350 rpm for 8 h. The crude product was then filtered, rotary

evaporated to remove the solvent, and washed three times with 1 M NaHSO₄, twice with 0.1 M Na₂CO₃, and once with brine. The final HEDSDA product was dried using MgSO₄, placed under vacuum overnight, and stored at 4°C.

3.3.3 Nanogel synthesis

Free radical precipitation polymerization was used to synthesize hydrophobized POEGMA nanogels. Nanogels were prepared by varying the ratio of M(EO)₂MA and OEGMA₅₀₀ as well as the quantity of hydrophobic comonomer (BMA or MMA). For a nanogel composition containing only short chain POEGMA and 10 mol% hydrophobic comonomer, 1.5 g of M(EO)₂MA (8 mmol) was mixed with acrylic acid (0.09 g, 1 mmol) and either BMA (0.15 g, 1 mmol) or MMA (0.1 g, 1 mmol) were added to a two-neck round bottom flask along with HEDSDA (90 µL), SDS (60 mg, 0.2 mmol) and 145 mL of Milli-Q H₂O. The flask was attached to a condenser and stirred continuously with a magnetic stir bar at 350 rpm while the solution was purged under nitrogen for 30 minutes. The flask was then placed into an oil bath heated to 90°C and allowed to warm up for 10 minutes. A KPS solution (61.5 mg, 0.2 mmol) in 5 mL of Milli-Q H₂O was prepared in a syringe and injected into the pre-heated reagents to initiate the polymerization (Scheme 3.1). After four hours, the reaction was quenched by removing the flask from the heated oil bath and exposing the contents of the flask to air. The cooled solution was then transferred to dialysis tubing (molecular weight cut off 3.5-5 kDa) and dialysed against Milli-Q H₂O for a total of six (6+

h) cycles. The nanogels were stored in solution at 4°C. A similar procedure was followed to synthesize nanogels also containing OEGMA₅₀₀ or different quantities of hydrophobic comonomer (Tables S3.1 and S3.2). Nanogels were labeled based on the code “x% <hydrophobic comonomer> y:z”, where x is the mole % of the hydrophobic comonomer used (MMA or BMA) and y:z represents the molar ratio of M(EO)₂MA:OEGMA₅₀₀ used to synthesize the nanogel. The polymer content of the nanogel solutions was determined using gravimetric analysis.



Scheme 3.1: Synthesis of hydrophobized nanogels containing disulfide cross-linker.

POEGMA-based nanogels, containing varying ratios of diethylene glycol methacrylate (M(EO)₂MA) and oligo(ethylene glycol methacrylate) (OEGMA₅₀₀), are copolymerized with acrylic acid (AA) and either butyl methacrylate (BMA) or methyl methacrylate (MMA) in the presence of the disulfide-containing cross-linker 2-hydroxyethyl disulfide diacrylate (HEDSDA) with sodium dodecyl sulfide (SDS, surfactant) and potassium persulfate (KPS, initiator) to produce hydrophobized nanogels.

3.3.4 Nanogel characterization

The effective nanogel diameter was measured via dynamic light scattering (DLS) using a Brookhaven NanoBrook 90Plus instrument running BIC Particle Solutions software (Version 2.6, Brookhaven Instruments Corporation). Scattering was detected using a 659 nm laser configured at a 90° angle. Nanogel solutions were prepared at concentrations of 1-10 mg/mL in 10 mM PBS, conforming to a count rate of 500-600 kcps. Electrophoretic mobility measurements were carried out using the phase analysis light scattering (PALS) mode of the ZetaPlus zeta potential analyzer (Brookhaven Instruments Corporation). Conductometric base-into-acid titration (ManTech Inc.) was carried out to determine the degree of acrylic acid functionalization of the nanogels, titrating a 1 mM NaCl solution containing 1 mg/mL nanogel with 0.1 M NaOH.

3.3.5 *In vitro* degradation of nanogels

Nanogel degradation was measured in three different degradation buffers to assess the extent of degradation and characterize the degradation products. A 1 mg/mL solution of 10% BMA 100:0 nanogels was prepared in (1) 10 mM GSH, pH 7.4 (reductive degradation); (2) 20 U/mL esterase, pH 7.4 (enzyme-catalyzed hydrolytic degradation); or (3) 100 mM acetate buffer, pH 4.5 (acid-catalyzed hydrolytic degradation). The degradation was monitored at 37°C using DLS (same configuration as above) to assess nanogel size and count rate as a function of time. The light intensity was maximized prior to the first

measurement and maintained constant throughout the full time course of experiments, with measurements conducted for 2 minutes every 15 minutes for a total of 12 h. After 24 h, the samples were measured via nanoparticle tracking analysis (NTA) using a NanoSight LS10 instrument (Malvern NTA 3.2 software). The samples were then lyophilized and resuspended in DMF. To determine the molecular weight of the degradation products, a Polymer Laboratories PL-50 Integrated GPC System equipped with a Phenomenex Phenogel Linear LC column (300 × 4.6 mm, 5 µm) was operated at room temperature with 50 mM LiBr in DMF as the eluent. The GPC system was calibrated using PEG standards from Polymer Laboratories. The samples were injected into the GPC through a 0.2 µm PTFE filter.

3.3.6 Determination of haloperidol loading

An aliquot of solution containing 25 mg of nanogel was centrifuged at 18 000 rpm (Beckman Coulter) for 20 minutes. The collected nanogel pellet was re-dispersed in 2 mL anhydrous ethanol containing 2 mg/mL haloperidol. The nanogel/haloperidol solution was placed on a shaker for 24 h to allow the drug to freely diffuse into the nanogels. Following equilibration, the dispersion was centrifuged, the supernatant was collected, and the supernatant was filtered through a 0.2 µm PTFE syringe filter. To determine the quantity of haloperidol loaded into the nanogels, an HPLC-UV procedure was adapted from Igarashi et al. using a Waters Alliance 2695 Separation Module with a Nova-Pak C18

column (4 μm particle size, 3.9 \times 150 mm). The mobile phase had a solvent composition of 10 mM ammonium acetate: glacial acetic acid: methanol: acetonitrile (57.2:0.8:22:40) and was run in isocratic mode using a 1 mL/min flow rate at 25°C.⁷ Injections (10 μL each) were carried out in triplicate. Drug was detected by UV/vis spectrophotometry at 254 nm using a Waters W2489 UV-VIS detection system. Drug loading was quantified by the drug loading capacity (DLC, Equation 3.1) and the encapsulation efficiency (EE, Equation 3.2).

$$\text{Drug Loading Capacity} = \frac{\text{Mass of drug loaded}}{\text{Total nanogel mass}} \times 100\% \quad (3.1)$$

$$\text{Encapsulation Efficiency} = \frac{\text{Mass of drug loaded}}{\text{Mass of total drug added}} \times 100\% \quad (3.2)$$

3.3.7 *In vitro* haloperidol release:

Haloperidol release from 10% BMA 100:0 nanogels was assessed under five different aqueous conditions to determine how different physiological conditions impact drug release kinetics. Drug loading was carried out as described above, after which the drug-loaded nanogels were re-suspended at a concentration of 1 mg/mL in (1) 10 mM phosphate buffered saline (PBS), pH 7.4; (2) 0.5 wt% Tween 80 in PBS, pH 7.4; (3) 10 mM GSH in PBS, pH 7.4; (4) 0.5 wt% Tween 80/10 mM GSH in PBS, pH 7.4; or (5) 100 mM acetate buffer, pH 4.5. All samples were placed in a shaking incubator (100 rpm) at 37°C. At specified time points (1, 2, 4, 8, 16, and 24 hour), samples (n=3) were collected and centrifuged at 18 000 rpm for 15 min. The supernatant was collected and analyzed using the HPLC protocol described above to assess haloperidol release.

3.3.8 *In vitro* cytotoxicity

Nanogel cytocompatibility was evaluated using SH-SY5Y cells derived from a bone marrow biopsy of a patient with neuroblastoma. SH-SY5Y cells were cultured in DMEM-F12 media supplemented with 10% FBS, 1% penicillin/streptomycin and 1% L-glutamine (ThermoFisher Scientific, Burlington ON). Cells were plated into the wells of a 96-well plate at a cell density of 2×10^4 cells per well and allowed to adhere for 24 h, after which they were incubated for 24 h with the nanogel formulations of interest. Cell metabolic activity was determined by incubating the treated cells with (3-(4,5-dimethylthiazol-2-yl)-5-(3-carboxymethoxyphenyl)-2-(4-sulfophenyl)-2H-tetrazolium) (MTS) (Abcam, Toronto, ON) for four hours and subsequently measuring the absorbance of each well at 490 nm using a Tecan Infinite M200 Microplate Reader.

3.3.9 Pharmacological evaluation of haloperidol-loaded nanogels

The *in vivo* behavioral response of haloperidol-loaded nanogels was evaluated using male Sprague-Dawley (SD) rats (Charles River, St. Constant, Quebec) weighing 250-300 g. The rats were housed at the McMaster University Central Animal Facility in a reverse 12 h light/dark cycle and were provided *ad libitum* access to food and water. All the protocols were approved by the Animal Research Ethics Board of McMaster University (Animal Utilization Protocol 18-06-27) in compliance with the Canadian Council on Animal Care.

The rats were divided into different test groups (n=6 per group) based on the nanogel formulation being administered: (1) 10% BMA 100:0; (2) 10% MMA 100:0; or (3) 10% BMA 90:10. To administer the formulations intranasally, the rats were lightly anesthetized using isoflurane. Using a 200 μL pipette tip, a 30 μL aliquot of nanogel dispersion was then administered to each nostril. The rat was placed back in the anesthetic chamber for 2 minutes after which the nasal administration was repeated, for a total of four (two per nostril) 30 μL applications (120 μL total volume). The total time rats were maintained under anesthesia was less than five minutes. Rats were placed in a recovery chamber to safely recuperate from the anesthesia before being returned to their home cage.

Prior to locomotion assessment, rats were habituated to the chambers. To assess locomotion inhibition, the rats were intranasally administered a dose of 0.3 mg haloperidol/kg, adjusting the nanogel concentration as required based on the measured drug uptake to achieve the required dose within the 120 μL total injection volume. One hour post-administration, the rats were transferred to individual computerized locomotion chambers (AccuScan Instruments, USA) equipped with infrared sensors that monitor three dimensional movement based on photobeam breaks. Locomotion was monitored for 2.5 hour, with analysis omitting the first 20 minutes to account for an acclimatization period in which rats are typically more mobile due to curiosity.

The evaluation of the cataleptic response was conducted at specified time points (0.5, 1, 3, 6 and 24 h) post-administration using a dose of 1 mg haloperidol/kg, calculated as described above for the locomotion study. The front paws of the rats were placed on a 10 cm high horizontally mounted metal bar. The amount of time over which the rat maintained this unnatural position was measured until the rat retracted both its front paws. Each individual animal was tested in triplicate, with a 30 s rest time between each repetition; the maximum intensity of the cataleptic response was recorded in seconds. Rats were given a rated score (1–6) based upon time spent on the bar (0 = <10 s, 1 = 11–20 s, 2 = 21–30 s, 3 = 31–40, 4=41–50 s and 6= >50 s). To be considered cataleptic, a score of at least 3 (>20 s) must be achieved.⁴⁶ A minimum of three days was maintained between each round of experimentation to ensure complete washout of the previously administered formulation.

3.4 Results and Discussion

3.4.1 Nanogel characterization

Free radical precipitation polymerization was used to synthesize monodisperse POEGMA nanogels following procedures adapted for this application.⁴⁷⁻⁴⁸ To introduce hydrophobic domains into the nanogel structure to improve nanogel affinity for haloperidol, BMA or MMA were copolymerized at mole fractions between 5-25 mol%; acrylic acid was also copolymerized at a low (5 mol%) concentration to promote improved colloidal stability in

the context of the enhanced hydrophobicity of the nanogels. The disulfide containing cross-linker, 2-hydroxyethyl disulfide diacrylate (HEDSDA), was incorporated to enable stimuli-responsive degradation in the presence of biologically-relevant molecules such as glutathione (redox-mediated disulfide cleavage) and esterase (enzymatic cleavage of ester linkage to carbon backbone) to enable *in vivo* clearance. Table 3.1 and Table 3.2 show the size, polydispersity and electrophoretic mobility of all nanogel formulations. Nanogels are consistently small (85-200 nm) with monodisperse (PD <0.1) particle size distributions and slight negative surface charges attributable to the ionization of the acrylic acid at physiological pH and the use of the persulfate initiator. As the quantity of BMA and MMA in the nanogels was increased up to 10 mol%, the nanogel diameter decreased consistent with the expulsion of water from within the increasingly hydrophobic core of the nanogel. BMA nanogels have smaller diameters than their MMA counterparts at equal comonomer contents, consistent with the longer hydrophobe in BMA that results in more nanogel dewatering. However, at MMA or BMA loadings of >10 mol%, significant increases were observed in the particle size and, at high enough hydrophobic comonomer loadings, the polydispersity (e.g. 25 mol% BMA). This result indicates that the incorporation of too much hydrophobic comonomer reduces nanogel stability, suggesting the use of 10 mol% hydrophobically-functionalized nanogels may be optimal for preserving high colloidal stability.

To further examine the net effect of hydrophobic and hydrophilic interactions on nanogel swelling, the ratio of M(EO)₂MA and OEGMA₅₀₀ monomers in the nanogel formulations was varied in 10 mol% increments; a constant 10% mole fraction of BMA (noted in Table 3.1 to result in the smallest but still colloidally stable nanogels) was used in each formulation. Increasing the quantity of OEGMA₅₀₀ results in a significant increase in nanogel hydrodynamic diameter (Table 3.3) and polydispersity (Figure 3.1). Nanogels containing 90 mol% M(EO)₂MA and 10% OEGMA₅₀₀ retain sizes of ~100 nm appropriate for improving transport across biological barriers and minimizing interactions with the mononuclear phagocytotic system;⁴⁹ however, increasing the fraction of OEGMA₅₀₀ to ≥ 20 mol% significantly increases both diameter and (particularly for the 10% BMA 70:30 nanogel) polydispersity, undesirable for optimizing brain delivery.

Table 3.1: Effective diameter (from DLS) and electrophoretic mobility (from PALS) of 100:0 POEGMA nanogels prepared with various amounts of BMA comonomer (10 mM PBS, pH 7.4, n=5 ± one standard deviation).

BMA Content (mol %)	Diameter (nm)	Polydispersity	Mobility (μ/s)/(V/cm)
0	190 ± 3	0.03 ± 0.02	-0.8 ± 0.4
5	115 ± 1	0.04 ± 0.02	-1.1 ± 0.2
10	87 ± 2	0.05 ± 0.02	-0.7 ± 0.4
15	100 ± 1	0.04 ± 0.03	-0.2 ± 0.4
20	119 ± 2	0.06 ± 0.03	-1.5 ± 0.1
25	140 ± 2	0.21 ± 0.02	-1.3 ± 0.1

Table 3.2: Effective diameter (from DLS) and electrophoretic mobility (from PALS) of 100:0 POEGMA nanogels prepared with various amounts of MMA comonomer (10 mM PBS, pH 7.4, n=5 ± one standard deviation).

MMA Content (mol %)	Diameter (nm)	Polydispersity	Mobility (μ/s)/(V/cm)
0	190 ± 3	0.03 ± 0.02	-0.8 ± 0.4
5	106 ± 1	0.02 ± 0.02	-0.6 ± 0.3
10	92 ± 1	0.04 ± 0.02	-0.9 ± 0.1
15	108 ± 1	0.03 ± 0.02	-0.7 ± 0.1
20	113 ± 1	0.04 ± 0.02	-0.7 ± 0.2
25	104 ± 1	0.06 ± 0.02	0 ± 0.9

Table 3.3 Effective diameter (from DLS) and electrophoretic mobility (from PALS) of 10% BMA nanogels prepared with varying POEGMA monomer ratios (M(EO)₂MA:OEGMA₅₀₀) (10 mM PBS, pH 7.4; n=5 ± one standard deviation).

Nanogel Formulation	Diameter (nm)	Polydispersity	Mobility (μ/s)/(V/cm)
10% BMA 100:0	87 ± 2	0.05 ± 0.02	-0.7 ± 0.4
10% BMA 90:10	117 ± 2	0.03 ± 0.03	-1.0 ± 0.2
10% BMA 80:20	366 ± 6	0.11 ± 0.06	-1.4 ± 0.2
10% BMA 70:30	1161 ± 77	0.35 ± 0.02	-0.7 ± 0.1

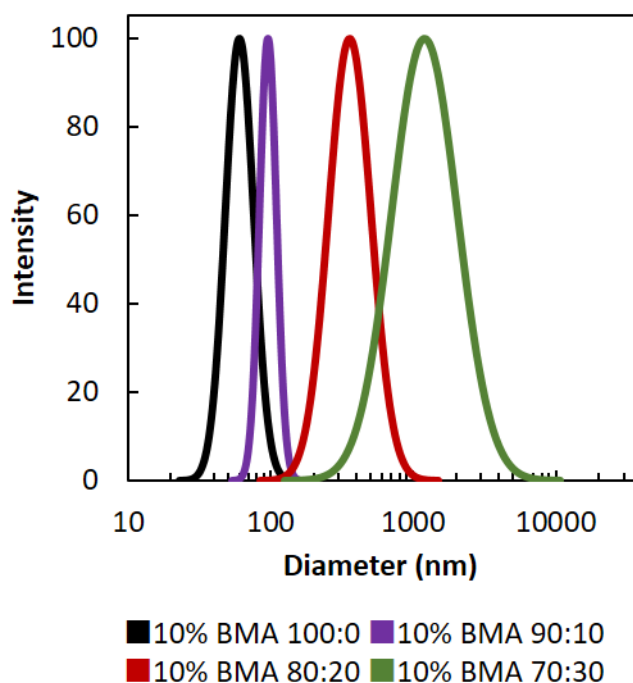


Figure 3.1: Logarithmic intensity-based particle size distribution (from DLS) of 10% BMA nanogels fabricated using varying ratios of M(EO)₂MA:OEGMA₅₀₀.

To characterize the morphology of the nanogels, transmission electron microscopy (TEM) was used to image dehydrated nanogels using uranyl acetate as a negative stain to enhance contrast. Figure 3.2 shows 10% BMA 100:0 nanogels that are discrete, spherical and appear highly monodisperse, consistent with the DLS results. Note that the smaller apparent diameter observed by TEM relative to the DLS result is attributable to the drying of the nanogels on the grid.

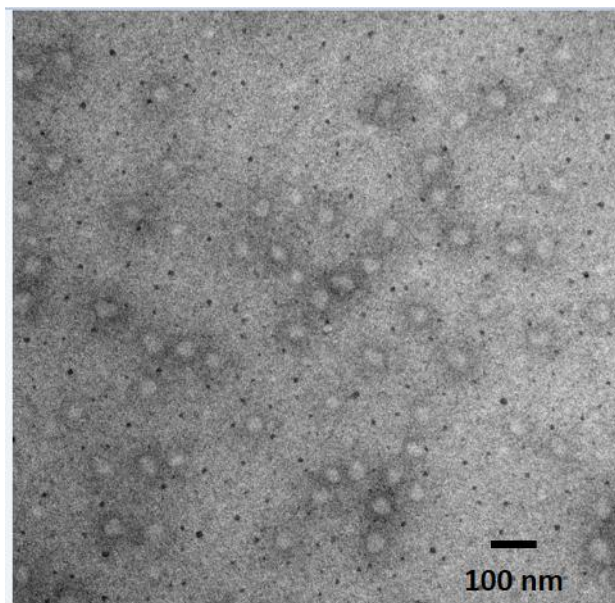


Figure 3.2: Transmission electron microscopy image (magnification 100 000×) of 0.1 wt% 10% BMA 100:0 nanogel stained with 1% uranyl acetate.

3.4.2 Nanogel degradation

To explicitly assess the potential of the nanogel to degrade into byproducts that will not accumulate in the liver/kidneys, nanogels were incubated in different degradation media simulating different *in vivo* degradation promoters: 10 mM glutathione (GSH, an endogenous reducing agent present at low concentrations in the extracellular space and at the chosen concentration intracellularly that can reductively degrade the cross-linker^{48,50}, pH 4.5 100 mM acetate buffer (promoting acid-catalyzed degradation of ester groups in the cross-linker and/or connecting the PEG side chain to the backbone⁵¹⁻⁵², and 20 U/mL esterase (promoting enzymatic degradation of the same ester groups). Degradation was monitored using DLS (Figure 3.3), while the degradation products were

characterized using NTA (Figure 3.4A) and GPC (Figure 3.4B). Upon exposure to 10 mM GSH, nanogels rapidly undergo an almost 5-fold increase in hydrodynamic diameter (Figure 3.3A) and a decrease in the count rate (Figure 3.3D), consistent with rapid cleavage of the disulfide bonds in the cross-linker; at the conclusion of the 12 hour incubation time, the cuvette had collected precipitate on the bottom, indicating the formation of large aggregates consistent with colloidal destabilization (i.e. partially degraded) nanogels. This process of nanogel swelling followed by destabilization is also supported by the NTA data (Figure 3.4G), which shows significantly larger nanoparticles present at the 24 hour time point. Degradation under acidic conditions using the 100 mM acetate buffer showed comparable outcomes to the GSH-mediated degradation but with much slower kinetics, with significant nanogel swelling not observed until 6 h of exposure to the low pH conditions (Figure 3.3B,E,H). Esterase-mediated degradation is much slower (Figure 3.3C,F,I) given that its large size (168 kDa) makes its diffusion into the hydrophobized nanogels limited; the moderate change in hydrodynamic diameter is likely due to ester cleavage on or close to the surface of the nanogel that results in minimal overall nanogel swelling (Figure 3.3C and Figure 3.3I). In comparison, in PBS (10 mM, pH 7.4) or 2 μ M GSH (mimicking the reductive conditions of the extracellular space), only very minimal changes in nanogel size were observed over the same period (Figure S3.1). As such, the degradability of the nanogels is significantly accelerated by specific

intracellular stimuli, suggesting potential for nanogels to facilitate site-specific drug delivery.

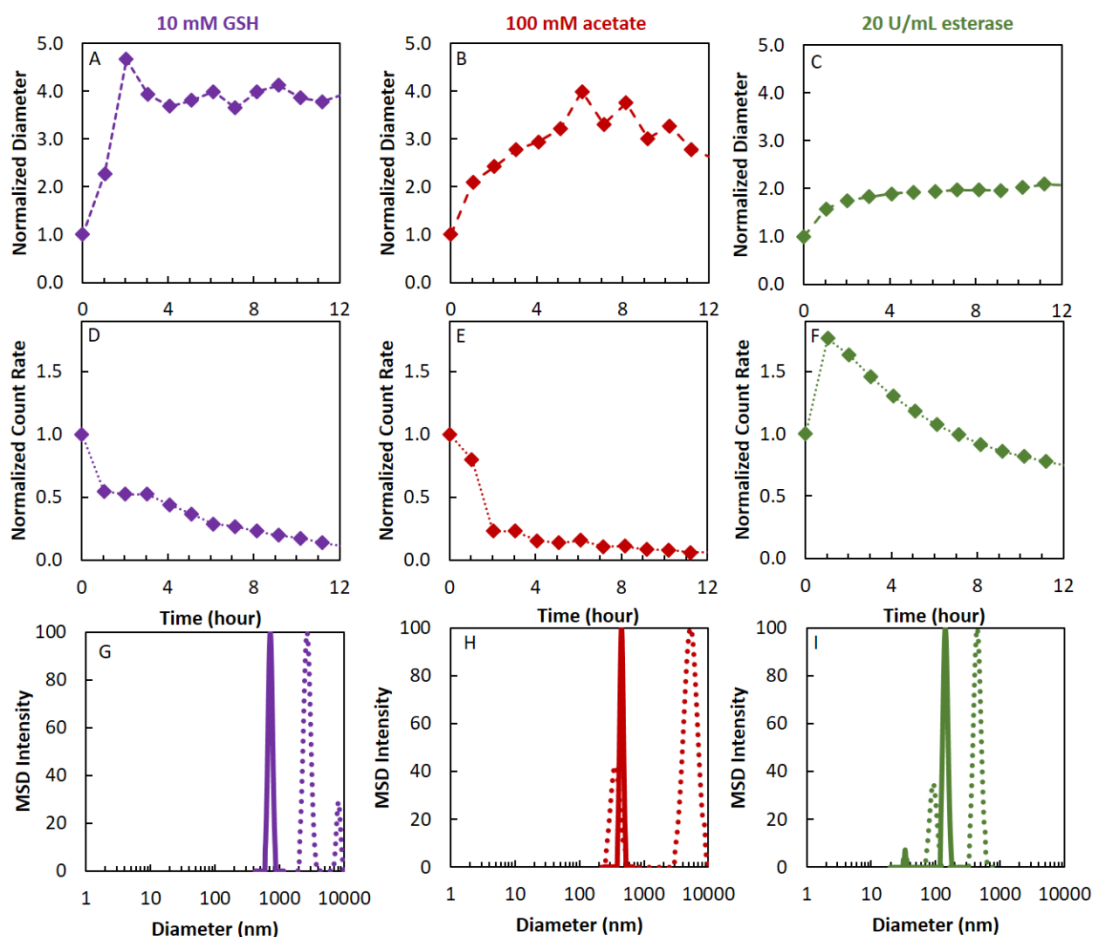


Figure 3.3: Degradation of 10% BMA 100:0 nanogels at 37°C over 12 h in 10 mM GSH, pH 7.4 (A,D,G), 100 mM acetate buffer, pH 4.5 (B,E,H) or 20 U/mL esterase (C,F,I). (A-C) Normalized effective hydrodynamic diameter (from DLS); (D-F) Normalized rate (from DLS); and (G-I): Multimodal intensity-based size distributions at t=0 hour (solid line) and t=12 hour (dashed line).

To assess the nature of the degradation products of the nanogels following incubation in the degradation-promoting environments, further characterization of the degraded nanogels was carried out using NTA (Figure 3.4A). The degraded suspensions are very

polydisperse, consistently showing multimodal size distributions that confirm the presence of both smaller (degraded) polymer fragments and larger (colloidally destabilized) aggregates as the nanogels degrade; in comparison, the fresh nanogels all show unimodal and narrow particle size distributions. Analysis of the molecular weight of the degradation products (after 24 hour of degradation) using GPC (Figure 3.4B) confirms that the majority of the degraded nanogels have chain lengths significantly below the molecular weight of the original nanogels, with the majority of the degradation products exhibiting molecular weights well below the 50 kDa cut-off for renal clearance; in particular, >95% of the residual polymer following degradation in 10 mM GSH has a molecular weight below this threshold after only 24 hour of degradation.⁵³ The GPC result is consistent with the expected degradation of POEGMA-based nanogels into primarily poly(ethylene glycol) (PEG) and short-chain poly(methacrylic acid), both of which are FDA-approved in various contexts.⁵⁴⁻⁵⁶

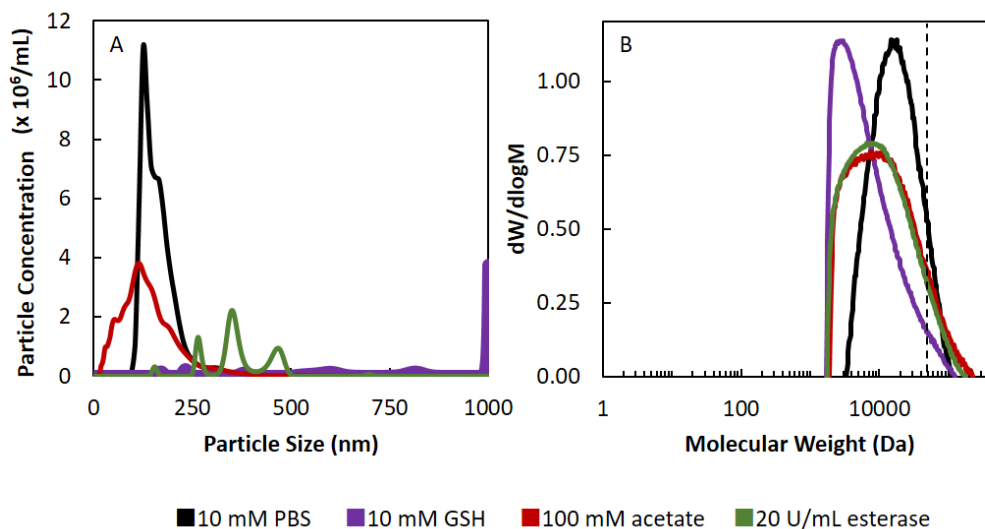


Figure 3.4: Characterization of nanogels after 24 hour exposure to various mimics of physiological conditions using (A) nanoparticle tracking analysis (NTA) and (B) gel permeation chromatography (GPC).

3.4.3 Haloperidol uptake and release

The suitability of these nanogels as therapeutically-relevant drug delivery vehicles for haloperidol was assessed by loading HLP into the nanogel via passive diffusion in ethanol to determine the drug loading capacity (DLC) and encapsulation efficiency (EE). As shown in Table 3.4, both BMA and MMA-functionalized nanogels show similar trends with respect to drug loading, with 10 mol% BMA or MMA facilitating the greatest haloperidol uptake. This result is hypothesized to relate to achieving an optimal balance between maximizing the availability of hydrophobic domains for promoting nanogel-drug interactions and minimizing deswelling that may block drug access into the nanogel structure. When less hydrophobic comonomer is used, the nanogel is insufficiently

hydrophobic to support high drug uptakes; when more BMA or MMA is incorporated, the nanogel collapses to limit drug in-diffusion. This trend mirrors that observed in optimizing the L:G ratio in PLGA nanoparticles; increasing the quantity of more hydrophobic lactic acid enhances drug loading and prolongs release.³¹⁻³² The EE and DLC results are similar, if not higher, than achieved with other reported nanoparticle systems^{12, 44} minimizing the amount of polymer required to deliver a relevant dose of haloperidol to the nose.

Table 3.4: Drug loading capacity (DLC) and encapsulation efficiency (EE) of haloperidol in BMA and MMA nanogels as a function of their hydrophobic comonomer content (n=3 ± one standard deviation).

Nanogel Formulation	BMA		MMA	
	DLC (wt%)	EE (%)	DLC (wt%)	EE (%)
0% 100:0	13.0 ± 0.1	81 ± 1	13.0 ± 0.1	81 ± 1
5% 100:0	13.3 ± 0.2	83 ± 1	13.3 ± 0.6	83 ± 3
10% 100:0	14.4 ± 0.1	90 ± 1	14.8 ± 0.5	93 ± 3
15% 100:0	12.5 ± 0.1	78 ± 1	12.8 ± 0.1	80 ± 1
20% 100:0	0.8 ± 0.4	20 ± 3	1.5 ± 0.6	38 ± 5
25% 100:0	0.5 ± 0.8	13 ± 6	0.8 ± 0.5	20 ± 4

Haloperidol was also loaded into the formulations containing the more hydrophilic OEGMA₅₀₀ comonomer, the results of which are shown in Table 3.5. Increasing the OEGMA₅₀₀ content does not significantly affect the quantity of haloperidol loading, confirming that it is the presence of the hydrophobic domains within the nanogel that imparts affinity for drug loading.

Table 3.5: Drug loading capacity (DLC) and encapsulation efficiency (EE) of haloperidol in 10% BMA nanogels as a function of their OEGMA500 contents (n=3 ± one standard deviation).

Nanogel Formulation	DLC (wt%)	EE (%)
10% BMA 100:0	14.4 ± 0.1	90 ± 1
10% BMA 90:10	15.2 ± 1.1	93 ± 4
10% BMA 80:20	15.4 ± 2.0	91 ± 1
10% BMA 70:30	15.3 ± 1.0	93 ± 3

The 10% BMA 100:0 nanogel was selected to assess *in vitro* haloperidol release given that it has the smallest size (Table 3.1) and among the highest encapsulation efficiencies (Table 3.4) and thus is particularly suitable for *in vivo* use. Drug release was assessed *in vitro* using five different release media that simulate different aspects of extracellular or intracellular fluids. As haloperidol is highly insoluble in aqueous media at typical physiological conditions, phosphate buffered saline (PBS, 10 mM pH 7.4) was supplemented with a surfactant (Tween 80, whose micelle formation mimics cell membranes *in vivo*),^{12, 35-36, 43-44} a reducing agent (GSH, as previously explained), and/or an acidic buffer (100 mM acetate pH 4.5, corresponding to lysosomal pH); the former provides a sink for the release of hydrophobic haloperidol while the latter two promote degradation of the cross-linker. Figure 3.5 shows the cumulative haloperidol release after incubation at 37°C for 24 hour in these different media or combinations thereof. Minimal haloperidol release (~4%) was observed in PBS due to the low aqueous solubility of haloperidol at neutral pH, while the addition of Tween 80 more than triples the drug release (~13%) consistent with the presence of a lipophilic domain enhancing haloperidol

solubility. Conversely, inducing nanogel degradation by chemically reducing the disulfide cross-linker significantly enhances drug release (~45% in 24 h); including both GSH and Tween 80 in the release media further enhances drug release (~62% in 24 h). Acidic conditions induce similar effects, enabling ~50% haloperidol release within 24 h. These results suggest that endogenous molecules at intracellular concentrations will trigger degradation of the labile bonds within the nanogel formulation to promote haloperidol release *in vivo* while maintaining extended overall release times (>24 h) relevant to at minimum daily rather than multiple times daily dosing.

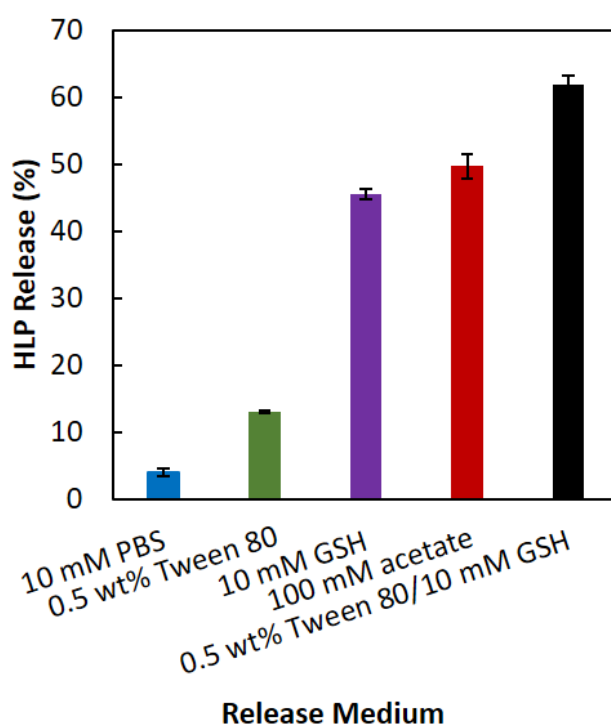


Figure 3.5: Cumulative *in vitro* release of haloperidol from 10% BMA 100:0 nanogels after 24 h of incubation at 37°C into 10 mM PBS, pH 7.4, 0.5 wt% Tween 80, 10 mM GSH, 100 mM ammonium acetate, pH 4.5 or 0.5 wt% Tween 80/10 mM GSH. Error bars represent the standard deviation of n=3 samples.

3.4.4 *In vitro* cytocompatibility

To assess the potential of these nanogels for *in vivo* applications, a MTS assay was used to examine the metabolic activity of SH-SY5Y human neuronal cells after 24 hour of exposure to various formulations and concentrations of nanogels (Figure 3.6). POEGMA is known to be a cytocompatible polymer, which is confirmed by the high viability of cells observed following treatment with the 0% 100:0 formulation lacking hydrophobic comonomer.⁵⁷⁻⁵⁸ The 100:0 nanogels containing 10% BMA or MMA and the 10% BMA 90:10 nanogels (all of which exhibit the small sizes/high drug loadings targeted for *in vivo* use) also maintained cell viabilities of >85% up to concentrations of at least 1 mg/mL, confirming the high cytocompatibility of these materials.

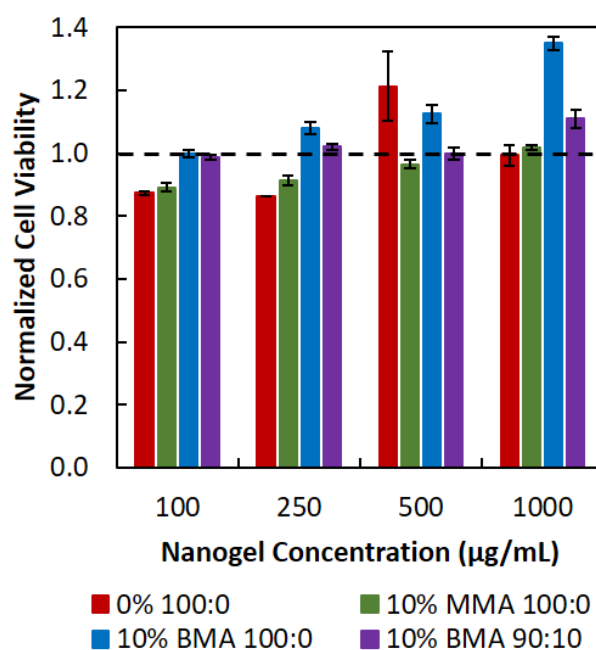


Figure 3.6: Nanogel cytotoxicity to SH-SY5Y neuronal cells, measured via the MTS assay, after 24 hour of treatment relative to cell-only (no treatment) control. Error bars represent one standard deviation of n=3 samples.

3.4.5 *In vivo* pharmacological efficacy

To examine the pharmacodynamics of the haloperidol-loaded nanogels *in vivo*, two behavioural experiments (locomotion inhibition and cataleptic response) were conducted in male Sprague-Dawley rats.

Locomotion test

Positive symptoms of schizophrenia include hallucinations and agitation; haloperidol treats such symptoms since it has a locomotor depressant effect due to its interactions

with dopamine receptors within the mesolimbic system.⁵⁹ A baseline measure of locomotion was first collected by administering saline solution without any nanogel or drug to quantify the behavior of a “normal” rat prior to haloperidol-loaded nanogel therapy. Interestingly, both the 10% BMA 100:0 and the 10% MMA 100:0 nanogels produced a statistically significant ($p < 0.05$) attenuation of rodent locomotion over the period studied even without haloperidol loading, with the 10% BMA 100:0 nanogel showing the largest decrease in motor activity (Figure 3.7). As locomotor activity is not only driven by neurological cues but also sensory (sniffing) factors, we hypothesize that the presence of polymer within the nasal cavity partly impedes olfactory orientation, resulting in decreased movement.⁶⁰⁻⁶¹ All three 0.3 mg/kg haloperidol-loaded nanogel formulations further reduced rat locomotion compared to the baseline in a statistically significant manner, although only the two BMA-containing nanogels produced a statistically significant locomotion suppression relative to their individual nanogel formulations. Although these nanogels delivered the same low dose of haloperidol previously employed to induce motor suppression using PAMAM dendrimers,⁴⁵ the same locomotion suppression effects were observed even with the significantly larger nanogel particles (90 -120 nm) compared to dendrimers (15 nm); this result is attributed to the soft and deformable structure of the nanogel enabling the effective permeation of the nasal mucosa, thereby enhancing the delivery of nanogel encapsulated APDs to the brain.

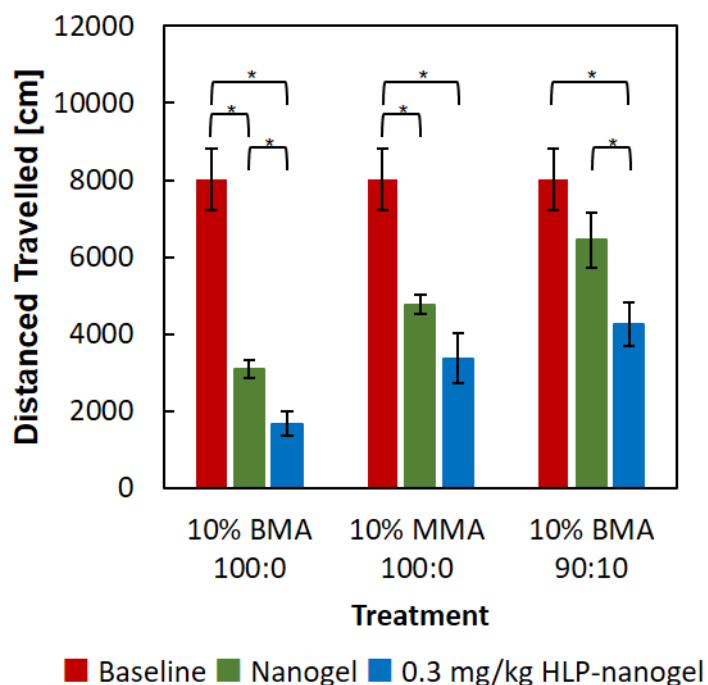


Figure 3.7: Locomotor activity of rats over a 2.5 hour period beginning 1 hour post-intranasal administration of saline, nanogel or 0.3 mg/kg haloperidol in nanogel. Error bars represent standard error of n=6 samples with *= p<0.05 from pairwise analysis.

Catalepsy test

Catalepsy is considered a Parkinson-like extrapyramidal side effect of typical APDs like haloperidol⁶² and is characterized by muscular rigidity and failure to correct an externally imposed posture, resulting in an observable and quantifiable behavioural change that is directly correlated with the concentration of haloperidol in the brain.⁶³ Rats were given a higher intranasal dose of nanogel corresponding to 1 mg haloperidol per kg to induce the cataleptic side-effect. Across all time points, the empty (unloaded) nanogels did not induce catalepsy (Figure 8), suggesting that the nanogels are not neurotoxic even at a ~3-

fold higher dose than administered in the locomotion assay. However, significant cataleptic effects were apparent 30 minutes after administration for haloperidol-loaded 10% BMA 100:0-HLP and 10% MMA 100:0-HLP nanogels and maintained across all acute time points tested (up to 6 hour post-administration), suggesting both rapid transport of haloperidol to the brain as well as subsequent controlled release of the haloperidol once there to maintain the effects over extended periods. The haloperidol-loaded 10% BMA 90:10-HLP nanogels also induced catalepsy but not until 1 hour post-administration, reflective of slower drug transport to the brain using this somewhat larger and more hydrophilic formulation; however, catalepsy then persisted over the remainder of the 6 hour acute assessment period. Interestingly, when catalepsy was again checked 24 hour post-IN administration, rats administered with 10% BMA 100:0-HLP nanogels still maintained a cataleptic response, indicative of high residual drug concentrations in the brain; all cataleptic responses subsided by 48 hour post-administration, confirming this result was not associated with any kind of toxicity response. In comparison, previous reports of IN-induced cataleptic behaviour by administering 2 mg haloperidol/kg loaded in lectin-functionalized PLGA nanoparticles or 0.3 mg haloperidol/kg loaded in PAMAM dendrimers achieved catalepsy for only one hour post-administration.⁴⁴⁻⁴⁵

The significantly longer antipsychotic activity maintained by haloperidol-loaded nanogels can be attributed to the specific characteristics of the nanogel-based drug delivery

vehicle; specifically, the small particle size and high deformity of nanogels relative to other delivery vehicles enable enhanced transport across the nasal epithelium while the hydrophobic domains imparted by BMA/MMA enable higher drug encapsulation and sustained drug release. In particular, the 10% BMA 100:0 nanogel that exhibits both the smallest particle size and highest interfacial hydrophobicity of all the nanogels tested provides both the fastest onset of catalepsy as well as the longest-term sustained therapeutic benefit when administered intranasally. By comparison, the 10% BMA 90:10 formulation, which shows the slowest onset cataleptic response, has a larger size and a more hydrophilic interface due to the presence of long-brush OEGMA at the surface. While particle size and drug-nanogel interactions are thought to be the dominant driver of these effects, an appropriate hydrophilic/hydrophobic balance is also known to be critical for regulating mucosal transport,⁶⁴⁻⁶⁵ with higher hydrophilicity minimizing mucosal entrapment and higher hydrophobicity promoting stronger affinity for epithelial cells and more efficient embedding of the nanoparticles within the bilayers of the cell membrane.⁶⁶ Furthermore, linear PEG coatings have been shown to help nanoparticles rapidly diffuse through the dense mesh of mucus and thus reach the epithelial nasal tissue more effectively, prolonging nanoparticle residence time within the nasal cavity and making the nanoparticles more likely to travel to the brain.⁶⁷⁻⁷⁰ While there is currently no clear understanding of the role of brush-PEG structures on mucosal penetration, POEGMA-based nanogels may induce a similar effect.

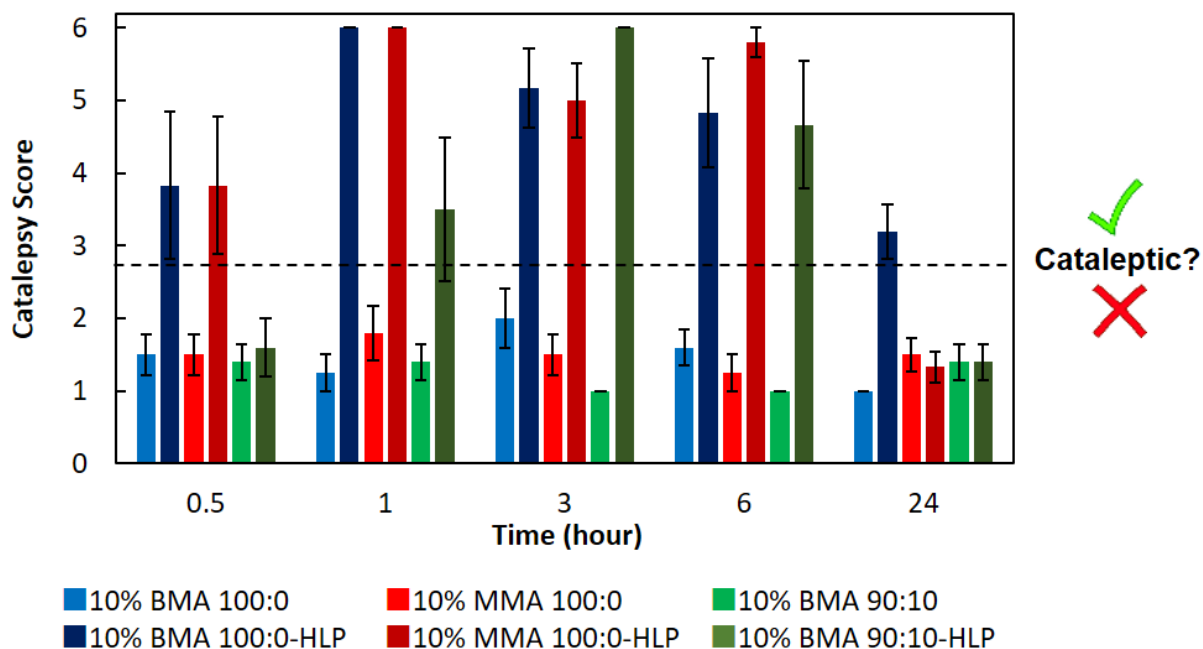


Figure 3.8 Cataleptic response following intranasal administration of empty (unloaded) nanogels and 1 mg/kg haloperidol-loaded nanogels (nanogel-HLP). Error bars represent the standard error of n=6 samples.

3.5 Conclusions

The incorporation of hydrophobic domains (via butyl methacrylate or methyl methacrylate copolymerization) into degradable poly(oligoethylene glycol methacrylate) nanogels creates nanocarriers with chemical and physical properties ideal for delivering antipsychotic drugs to the brain. The deformable gel network coupled with the incorporation of hydrophobic domains to enhance haloperidol loading affinity enables high drug encapsulation efficiencies and sustained haloperidol release suitable for the delivery of therapeutically-relevant doses of APD while maintaining high colloidal

stability. The stimuli-responsive labile bonds incorporated within the nanogel structure trigger enhanced haloperidol release and nanogel degradation in the intracellular environment to prevent toxic polymer accumulation *in vivo*. The nanogels show high cytocompatibility at concentrations comparable to those used for IN delivery, while *in vivo* studies demonstrate that intranasal delivery can facilitate nose-to-brain delivery of therapeutically-effective doses of APD that elicit behavioural changes in rats that can be rapidly induced but also sustained over extended periods of up to 1 day post-IN administration (significantly longer than other reported nanoscale formulations). Overall, hydrophobized POEGMA nanogels represent a minimally-invasive and effective therapeutic option that can lower required APD doses and re-administration frequencies, both essential to reduce neurological side effects and improve patient compliance with APD treatment regimens.

3.6 Acknowledgements

The Natural Sciences and Engineering Research Council of Canada (NSERC) and the Canadian Institutes of Health Research (CIHR) are acknowledged for funding (Canada Graduate Scholarship to MS, Collaborative Health Research Partnerships Grants CPG-151963 and CHRPJ-508393-2017 to TH and RKM). We gratefully acknowledge Ashley Bernardo, Brendan Fera and Fahed Abu-Hijleh for providing training and assistance with the animal studies and Judy Tran for her assistance with cell culture.

3.7 References

- (1) Charlson, F. J.; Ferrari, A. J.; Santomauro, D. F.; Diminic, S.; Stockings, E.; Scott, J. G.; McGrath, J. J.; Whiteford, H. A., Global Epidemiology and Burden of Schizophrenia: Findings from the Global Burden of Disease Study 2016. *Schizophrenia Bull.* **2018**, *44* (6), 1195-1203.
- (2) van Os, J.; Kapur, S., Schizophrenia. *Lancet* **2009**, *374* (9690), 635-645.
- (3) Seeman, M. V.; Seeman, P., Is Schizophrenia a Dopamine Supersensitivity Psychotic Reaction? *Prog. Neuropsychopharmacol. Biol. Psychiatry* **2014**, *48*, 155-160.
- (4) Seah, C.; Brennard, K. J., If There Is Not One Cure For Schizophrenia, There May Be Many. *npj Schizophr.* **2020**, *6* (1), 11.
- (5) Rossler, W.; Salize, H. J.; van Os, J.; Riecher-Rossler, A., Size of Burden of Schizophrenia and Psychotic Disorders. *Eur. Neuropsychopharmacol.* **2005**, *15* (4), 399-409.
- (6) Granger, B.; Albu, S., The Haloperidol Story. *Ann. Clin. Psychiatry* **2005**, *17* (3), 137-140.
- (7) Igarashi, K.; Kasuya, F.; Fukui, M.; Usuki, E.; Castagnoli, N., Studies on the Metabolism of Haloperidol (HP): The Role of CYP3A in the Production of the Neurotoxic Pyridinium Metabolite HPP+ Found in Rat Brain Following IP Administration of HP. *Life Sci.* **1995**, *57* (26), 2439-2446.
- (8) World Health Organization. World Health Organization Model List of Essential Medicines, 21st List, 2019. World Health Organization: Geneva, 2019.
- (9) Schotte, A.; Janssen, P. F. M.; Megens, A.; Leysen, J. E., Occupancy of Central Neurotransmitter Receptors by Risperidone, Clozapine and Haloperidol, Measured Ex Vivo by Quantitative Autoradiography. *Brain Res.* **1993**, *631* (2), 191-202.
- (10) Forsman, A. O., Individual Variability in Response to Haloperidol. *P. Roy. Soc. Med.* **1976**, *69*, 9-12.
- (11) Vella-Brincat, J.; Macleod, A. D., Haloperidol in Palliative Care. *Palliative Med.* **2004**, *18* (3), 195-201.
- (12) Yasir, M.; Sara, U. V. S., Solid Lipid Nanoparticles for Nose to Brain Delivery of Haloperidol: In Vitro Drug Release and Pharmacokinetics Evaluation. *Acta Pharm. Sinic.* **2014**, *4* (6), 454-463.
- (13) Davis, J. M.; Chen, N., Dose Response and Dose Equivalence of Antipsychotics. *J. Clin. Psychopharm.* **2004**, *24* (2), 192-208.
- (14) Gerlach, J.; Casey, D. E., Tardive Dyskinesia. *Acta Psychiat. Scand.* **1988**, *77* (4), 369-378.

- (15) Hou, Y.; Yang, J. Y.; Wu, C. F.; Huang, M., Effects of Clozapine, Olanzapine and Haloperidol on Ethanol-Induced Ascorbic Acid Release in Mouse Striatum. *Prog. Neuropsychopharmacol. Biol. Psychiatry* **2005**, *29* (1), 83-89.
- (16) Oosthuizen, P. P.; Emsley, R. A.; Maritz, J. S.; Turner, J. A.; Keyter, N., Incidence of Tardive Dyskinesia in First-Episode Psychosis Patients Treated with Low-Dose Haloperidol. *J. Clin. Psychiat.* **2003**, *64* (9), 1075-1080.
- (17) Corriss, D. J.; Smith, T. E.; Hull, J. W.; Lim, R. W.; Pratt, S. I.; Romanelli, S., Interactive Risk Factors for Treatment Adherence in a Chronic Psychotic Disorders Population. *Psychiat. Res.* **1999**, *89* (3), 269-274.
- (18) Leucht, S.; Burkard, T.; Henderson, J.; Maj, M.; Sartorius, N., Physical Illness and Schizophrenia: A Review of the Literature. *Acta Psychiat. Scand.* **2007**, *116* (5), 317-333.
- (19) Subrahmanyam, C. V. S.; Suresh, S., Solubility Behaviour of Haloperidol in Individual Solvents Determination of Partial Solubility Parameters. *Eur. J. Pharm. Biopharm.* **1999**, *47* (3), 289-294.
- (20) Park, E. J.; Amatya, S.; Kim, M. S.; Park, J. H.; Seol, E.; Lee, H.; Shin, Y. H.; Na, D. H., Long-Acting Injectable Formulations of Antipsychotic Drugs for the Treatment Of Schizophrenia. *Arch. Pharm. Res.* **2013**, *36* (6), 651-659.
- (21) Heath, F.; Newman, A.; Clementi, C.; Pasut, G.; Lin, H.; Stephens, G. J.; Whalley, B. J.; Osborn, H. M. I.; Greco, F., A Novel PEG-Haloperidol Conjugate with a Non-Degradable Linker Shows the Feasibility of Using Polymer-Drug conjugates in a Non-Prodrug Fashion. *Polym. Chem.* **2016**, *7* (47), 7204-7210.
- (22) Kohler, U.; Schroder, U.; Augustin, W.; Sabel, B. A., A New Animal-Model of Dopamine Supersensitivity using SC Implantation of Haloperidol Releasing Polymers. *Neurosci. Lett.* **1994**, *170* (1), 99-102.
- (23) Siegel, S. J.; Winey, K. I.; Gur, R. E.; Lenox, R. H.; Bilker, W. B.; Ikeda, D.; Gandhi, N.; Zhang, W. X., Surgically Implantable Long-Term Antipsychotic Delivery Systems for the Treatment Of Schizophrenia. *Neuropsychopharmacol.* **2002**, *26* (6), 817-823.
- (24) Samanta, M. K.; Dube, R.; Suresh, B., Transdermal Drug Delivery System of Haloperidol to Overcome Self-Induced Extrapyrmidal Syndrome. *Drug Dev. Ind. Pharm.* **2003**, *29* (4), 405-415.
- (25) Solanki, N. G.; Tahsin, M.; Shah, A. V.; Serajuddin, A. M., Formulation of 3D Printed Tablet for Rapid Drug Release by Fused Deposition Modeling: Screening Polymers for Drug Release, Drug-Polymer Miscibility and Printability. *J. Pharm. Sci.* **2018**, *107* (1), 390-401.
- (26) Haque, S.; Md, S.; Alam, M. I.; Sahni, J. K.; Ali, J.; Baboota, S., Nanostructure-Based Drug Delivery Systems for Brain Targeting. *Drug Dev. Ind. Pharm.* **2012**, *38* (4), 387-411.

- (27) Garcia-Garcia, E.; Andrieux, K.; Gil, S.; Couvreur, P., Colloidal Carriers and Blood–Brain Barrier (Bbb) Translocation: A Way to Deliver Drugs to The Brain? *Int. J. Pharm.* **2005**, *298* (2), 274-292.
- (28) Wohlfart, S.; Gelperina, S.; Kreuter, J., Transport of Drugs Across The Blood-Brain Barrier by Nanoparticles. *J. Control. Release* **2012**, *161* (2), 264-73.
- (29) Cheng, Y. H.; Illum, L.; Davis, S. S., A Poly(D,L-Lactide-Co-Glycolide) Microsphere Depot System for Delivery of Haloperidol. *J. Control. Release* **1998**, *55* (2-3), 203-212.
- (30) Budhian, A.; Siegel, S. J.; Winey, K. I., Production of Haloperidol-Loaded PLGA Nanoparticles for Extended Controlled Drug Release of Haloperidol. *J. Microencapsul.* **2005**, *22* (7), 773-785.
- (31) Budhian, A.; Siegel, S. J.; Winey, K. I., Haloperidol-Loaded PLGA Nanoparticles: Systematic Study of Particle Size and Drug Content. *Int. J. Pharm.* **2007**, *336* (2), 367-375.
- (32) Budhian, A.; Siegel, S. J.; Winey, K. I., Controlling the In Vitro Release Profiles for a System of Haloperidol-Loaded PLGA Nanoparticles. *Int. J. Pharm.* **2008**, *346* (1-2), 151-159.
- (33) Hans, M.; Shimoni, K.; Danino, D.; Siegel, S. J.; Lowman, A., Synthesis and Characterization of mPEG-PLA Prodrug Micelles. *Biomacromolecules* **2005**, *6* (5), 2708-2717.
- (34) Hans, M. L.; Maxwell, C.; Ehrlichman, R. S.; Metzger, K.; Liang, Y.; Siegel, S. J.; Lowman, A. M., Evaluation of In Vitro Release and In Vivo Efficacy of mPEG-PLA-Haloperidol Conjugate Micelle-Like Structures. *J. Biomed. Mater. Res. B.* **2007**, *83* (2), 422-430.
- (35) Benvegnú, D. M.; Barcelos, R. C. S.; Boufleur, N.; Pase, C. S.; Reckziegel, P.; Flores, F. C.; Ourique, A. F.; Nora, M. D.; Silva, C. B.; Beck, R. C. R.; Bürger, M. E., Haloperidol-Loaded Polysorbate-Coated Polymeric Nanocapsules Decrease its Adverse Motor Side Effects and Oxidative Stress Markers in Rats. *Neurochem. Int.* **2012**, *61* (5), 623-631.
- (36) Benvegnú, D. M.; Barcelos, R. C. S.; Boufleur, N.; Reckziegel, P.; Pase, C. S.; Ourique, A. F.; Beck, R. C. R.; Bürger, M. E., Haloperidol-Loaded Polysorbate-Coated Polymeric Nanocapsules Increase its Efficacy in the Antipsychotic Treatment in Rats. *Eur. J. Pharm. Biopharm.* **2011**, *77* (2), 332-336.
- (37) Hwang, S. R.; Kim, K., Nano-Enabled Delivery Systems Across the Blood-Brain Barrier. *Arch. Pharm. Res.* **2014**, *37* (1), 24-30.
- (38) Jacob, A.; Alexander, J. J., Complement and Blood-Brain Barrier Integrity. *Mol. Immunol.* **2014**, *61* (2), 149-152.
- (39) Illum, L., Is Nose-To-Brain Transport of Drugs in Man a Reality? *J. Pharm. Pharmacol.* **2004**, *56* (1), 3-17.

- (40) Katare, Y. K.; Piazza, J. E.; Bhandari, J.; Daya, R. P.; Akilan, K.; Simpson, M. J.; Hoare, T.; Mishra, R. K., Intranasal Delivery of Antipsychotic Drugs. *Schizophr. Res.* **2017**, *184*, 2-13.
- (41) Illum, L., Transport of Drugs from the Nasal Cavity to The Central Nervous System. *Eur. J. Pharm. Sci.* **2000**, *11* (1), 1-18.
- (42) Mathison, S.; Nagilla, R.; Kompella, U. B., Nasal Route for Direct Delivery of Solutes to the Central Nervous System: Fact or Fiction? *J. Drug Target.* **1998**, *5* (6), 415-441.
- (43) El-Setouhy, D. A.; Ibrahim, A. B.; Amin, M. M.; Khowessah, O. M.; Elzanfaly, E. S., Intranasal Haloperidol-Loaded Miniemulsions for Brain Targeting: Evaluation of Locomotor Suppression and In Vivo Biodistribution. *Eur. J. Pharm. Sci.* **2016**, *92*, 244-254.
- (44) Piazza, J.; Hoare, T.; Molinaro, L.; Terpstra, K.; Bhandari, J.; Selvaganapathy, P. R.; Gupta, B.; Mishra, R. K., Haloperidol-Loaded Intranasally Administered Lectin Functionalized Poly(Ethylene Glycol)-Block-Poly(D,L)-Lactic-Co-Glycolic Acid (PEG-PLGA) Nanoparticles for the Treatment of Schizophrenia. *Eur. J. Pharm. Biopharm.* **2014**, *87* (1), 30-39.
- (45) Katare, Y. K.; Daya, R. P.; Gray, C. S.; Luckham, R. E.; Bhandari, J.; Chauhan, A. S.; Mishra, R. K., Brain Targeting of a Water Insoluble Antipsychotic Drug Haloperidol via the Intranasal Route Using PAMAM Dendrimer. *Mol. Pharm.* **2015**, *12* (9), 3380-3388.
- (46) Costain, W. J.; Buckley, A. T.; Evans, M. C.; Mishra, R. K.; Johnson, R. L., Modulatory Effects of PLG and its Peptidomimetics on Haloperidol-Induced Catalepsy in Rats. *Peptides* **1999**, *20* (6), 761-767.
- (47) Boularas, M.; Gombart, E.; Tranchant, J. F.; Billon, L.; Save, M., Design of Smart Oligo(Ethylene Glycol)-Based Biocompatible Hybrid Microgels loaded with Magnetic Nanoparticles. *Macromol. Rapid Commun.* **2015**, *36* (1), 79-83.
- (48) Tian, Y.; Bian, S.; Yang, W., A Redox-Labile Poly(Oligo(Ethylene Glycol)Methacrylate)-Based Nanogel with Tunable Thermosensitivity for Drug Delivery. *Polym. Chem.* **2016**, *7* (10), 1913-1921.
- (49) Blanco, E.; Shen, H.; Ferrari, M., Principles of Nanoparticle Design for Overcoming Biological Barriers to Drug Delivery. *Nat. Biotechnol.* **2015**, *33* (9), 941-951.
- (50) Zhang, X.; Malhotra, S.; Molina, M.; Haag, R., Micro- and Nanogels with Labile Crosslinks – from Synthesis to Biomedical Applications. *Chem. Soc. Rev.* **2015**, *44* (7), 1948-1973.
- (51) Li, S.; Wong, S.; Sethia, S.; Almoazen, H.; Joshi, Y. M.; Serajuddin, A. T., Investigation of Solubility and Dissolution of a Free Base and Two Different Salt Forms as a Function of pH. *Pharm. Res.* **2005**, *22* (4), 628-635.

- (52) Oh, J. K.; Bencherif, S. A.; Matyjaszewski, K., Atom Transfer Radical Polymerization in Inverse Miniemulsion: A Versatile Route Toward Preparation and Functionalization of Microgels/Nanogels for Targeted Drug Delivery Applications. *Polymer* **2009**, *50* (19), 4407-4423.
- (53) Fox, M. E.; Szoka, F. C.; Fréchet, J. M. J., Soluble Polymer Carriers for the Treatment Of Cancer: the Importance of Molecular Architecture. *Accounts Chem. Res.* **2009**, *42* (8), 1141-1151.
- (54) Alconcel, S. N. S.; Baas, A. S.; Maynard, H. D., FDA-Approved Poly(Ethylene Glycol)-Protein Conjugate Drugs. *Polym. Chem.* **2011**, *2* (7), 1442-1448.
- (55) Mansour, H. M.; Sohn, M.; Al-Ghananeem, A.; DeLuca, P. P., Materials for Pharmaceutical Dosage Forms: Molecular Pharmaceutics and Controlled Release Drug Delivery Aspects *Int. J. Mol. Sci.* **2010**, *11* (9), 3298-3322.
- (56) Saade, H.; Guillen, M. D.; Romero, J. C.; Cepeda, J.; Ilyna, A.; Fernandez, S.; Enriquez-Medrano, F. J.; Lopez, R. G., Biocompatible and Biodegradable Ultrafine Nanoparticles of Poly(Methyl Methacrylate-Co-Methacrylic Acid) Prepared Via Semicontinuous Heterophase Polymerization: Kinetics and Product Characterization. *Int. J. Polym. Sci.* **2016**, *8*.
- (57) Smeets, N. M. B.; Bakaic, E.; Patenaude, M.; Hoare, T., Injectable Poly(Oligoethylene Glycol Methacrylate)-Based Hydrogels with Tunable Phase Transition Behaviours: Physicochemical and Biological Responses. *Acta Biomater.* **2014**, *10* (10), 4143-4155.
- (58) Smeets, N. M. B.; Bakaic, E.; Patenaude, M.; Hoare, T., Injectable and Tunable Poly(Ethylene Glycol) Analogue Hydrogels Based on Poly(Oligoethylene Glycol Methacrylate). *Chem. Commun.* **2014**, *50* (25), 3306-3309.
- (59) Bardo, M. T.; Bowling, S. L.; Pierce, R. C., Changes in Locomotion and Dopamine Neurotransmission Following Amphetamine, Haloperidol, and Exposure to Novel Environmental Stimuli. *Psychopharmacology* **1990**, *101* (3), 338-343.
- (60) Graham, D. L.; Meyer, J. S.; Stanwood, G. D., Chapter 25 - Behavioral Phenotyping in Developmental Neurotoxicology-Simple approaches Using Unconditioned Behaviors in Rodents. In *Handbook of Developmental Neurotoxicology (Second Edition)*, Slikker, W.; Paule, M. G.; Wang, C., Eds. Academic Press: 2018; 287-308.
- (61) Thompson, S. M.; Berkowitz, L. E.; Clark, B. J., Behavioral and Neural Subsystems of Rodent Exploration. *Learn. Motiv.* **2018**, *61*, 3-15.
- (62) Honma, T.; Fukushima, H., Correlation between Catalepsy and Dopamine Decrease in the Rat Striatum Induced by Neuroleptics. *Neuropharmacology* **1976**, *15* (10), 601-607.
- (63) Sanberg, P. R.; Bunsey, M. D.; Giordano, M.; Norman, A. B., The Catalepsy Test: Its Ups and Downs. *Behav. Neurosci.* **1988**, *102* (5), 748-759.

- (64) Wu, L.; Liu, M.; Shan, W.; Cui, Y.; Zhang, Z.; Huang, Y., Lipid Nanovehicles with Adjustable Surface Properties for Overcoming Multiple Barriers Simultaneously in Oral Administration. *Int. J. Pharm.* **2017**, *520* (1-2), 216-227.
- (65) Witten, J.; Samad, T.; Ribbeck, K., Selective Permeability of Mucus Barriers. *Curr. Opin. Biotechnol.* **2018**, *52*, 124-133.
- (66) Curtis, E. M.; Bahrami, A. H.; Weikl, T. R.; Hall, C. K., Modeling Nanoparticle Wrapping or Translocation in Bilayer Membranes. *Nanoscale* **2015**, *7* (34), 14505-14514.
- (67) Tang, B. C.; Dawson, M.; Lai, S. K.; Wang, Y.-Y.; Suk, J. S.; Yang, M.; Zeitlin, P.; Boyle, M. P.; Fu, J.; Hanes, J., Biodegradable Polymer Nanoparticles that Rapidly Penetrate the Human Mucus Barrier. *P. Natl. A. Sci.* **2009**, *106* (46), 19268-19273.
- (68) Wang, Y.-Y.; Lai, S. K.; Suk, J. S.; Pace, A.; Cone, R.; Hanes, J., Addressing the PEG Mucoadhesivity Paradox to Engineer Nanoparticles that “Slip” Through The Human Mucus Barrier. *Angew. Chem. Int. Ed.* **2008**, *47* (50), 9726-9729.
- (69) Yang, M.; Lai, S. K.; Wang, Y.-Y.; Zhong, W.; Happe, C.; Zhang, M.; Fu, J.; Hanes, J., Biodegradable Nanoparticles Composed Entirely of Safe Materials that Rapidly Penetrate Human Mucus. *Angew. Chem. Int. Ed.* **2011**, *50* (11), 2597-2600.
- (70) Suk, J. S.; Xu, Q.; Kim, N.; Hanes, J.; Ensign, L. M., PEGylation as a Strategy for Improving Nanoparticle-Based Drug and Gene Delivery. *Adv. Drug Deliver. Rev.* **2016**, *99*, 28-51.

S3.1 Supporting Information

Table S3.1: Chemical synthesis of BMA nanogels.^a

	M(EO)₂MA (g)	OEGMA₅₀₀ (g)	BMA (μL)
0% 100:0	1.5	-	-
5% BMA 100:0	1.5	-	78
10% BMA 100:0	1.5	-	165
15% BMA 100:0	1.5	-	261
20% BMA 100:0	1.5	-	370
25% BMA 100:0	1.5	-	494
10% BMA 90:10	1.4	0.4	165
10% BMA 80:20	1.2	0.8	165
10% BMA 70:30	1.1	1.2	165

^a All polymerizations were performed at 90°C in 150 mL Milli-Q water. Acrylic acid (90 μ L, 1 mmol), 2-hydroxyethyl disulfide (90 μ L), sodium dodecyl sulfate (60 mg, 0.02 mmol) and potassium persulfate (61.5 g, 0.02 mmol) were kept constant in all batches. Nanogels were labeled based on the code “x% <hydrophobic comonomer> y:z”, where x is the mole % of the hydrophobic comonomer used (BMA) and y:z represents the molar ratio of M(EO)₂MA:OEGMA₅₀₀ used to synthesize the nanogel.

Table S3.2: Chemical synthesis of MMA nanogels.^a

	M(EO)₂MA (g)	OEGMA₅₀₀ (g)	MMA (μL)
5% MMA 100:0	1.5	-	52
10% MMA 100:0	1.5	-	111
15% MMA 100:0	1.5	-	175
20% MMA 100:0	1.5	-	249
25% MMA 100:0	1.5	-	332

^a All polymerizations performed at 90°C in 150 mL Milli-Q water. Acrylic acid (90 μ L, 1 mmol), 2-hydroxyethyl disulfide (90 μ L), sodium dodecyl sulfate (60 mg, 0.02 mmol) and potassium persulfate (61.5 g, 0.02 mmol) were kept constant in all batches. Nanogels were labeled based on the code “x% <hydrophobic comonomer> y:z”, where x is the mole % of the hydrophobic comonomer used (MMA) and y:z represents the molar ratio of M(EO)₂MA:OEGMA₅₀₀ used to synthesize the nanogel.

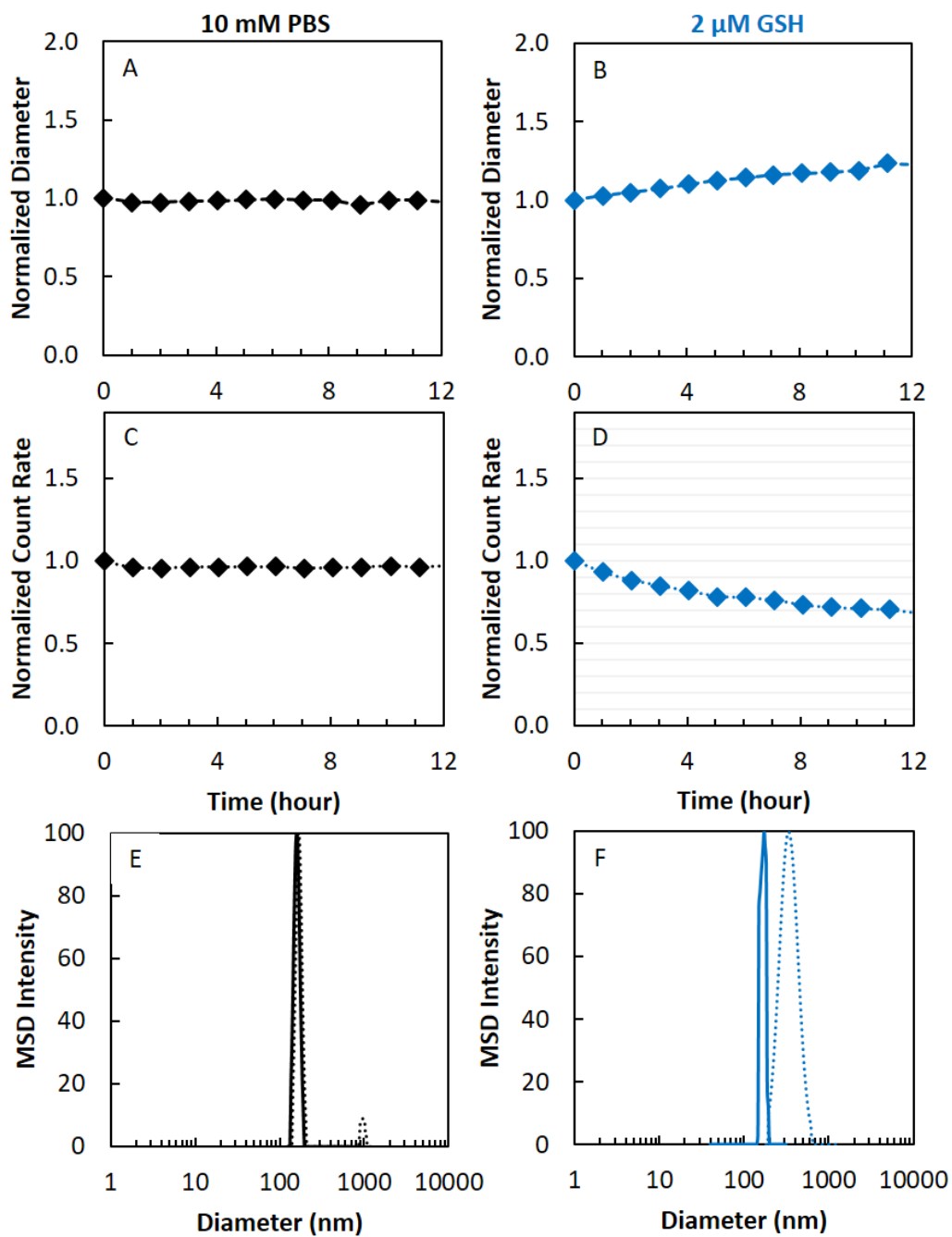


Figure S3.1: Stability of 10% BMA 100:0 nanogels measured by DLS at 37°C over 12 h. (A-B) Normalized effective hydrodynamic diameter; (C-D) normalized count rate; and (E-F): multimodal intensity-based size distribution at t=0 h (solid line) and t=12 h (dashed line) in 10 mM PBS, pH 7.4 (A,C,E) or 2 μ M GSH, pH 7.4 (B,D,F).

Chapter 4 : Narrowly Dispersed, Degradable, and Scalable Poly(oligoethylene glycol methacrylate)-Based Nanogels via Thermal Self-Assembly

Madeline J. Simpson, Brandon Corbett, Ana Arezina and Todd Hoare

Department of Chemical Engineering, McMaster University, 1280 Main Street West, Hamilton, Ontario, Canada L8S 4L7

Reprinted with permission from *Ind. Eng. Chem. Res.* **2018**, 57, 7495 - 7506.
Copyright 2018 American Chemical Society.

Keywords: self-assembly, nanogel, degradable, hydrazone bond, tunable.

4.1 Abstract

Covalently cross-linked and hydrolytically degradable poly(oligoethylene glycol methacrylate) (POEGMA)-based nanogels are fabricated using an all-aqueous self-assembly approach. The nanogels are composed of hydrazide- (POH) and aldehyde-functionalized (POA) POEGMA precursor polymers that exhibit lower critical solution temperature (LCST) behavior in aqueous media and form a covalent, yet degradable, hydrazone linkage upon mixing. By systematically changing the chemistry of the core and cross-linking precursor polymers, the concentration of the core precursor polymer, the ratio of core to cross-linking precursor polymer, and the temperature at which the assembly is conducted, a library of nanogels was produced with significant differences in size, polydispersity, and colloidal stability. Multivariate statistics indicates the presence of significant non-linear responses within the process variables as well as correlations between the output variables, reflective of the complex balance of aggregation and stabilization mechanisms at play to produce a stable, monodisperse nanogel population. Furthermore, formulations that yield more polydisperse nanogels on a small scale result in macroscopic aggregate formation when scaled up while formulations that yield more monodisperse nanogels can be scaled to yield nanogels with matched properties. We anticipate these results can be applied to strategically synthesize stable, covalently cross-linked degradable nanogels with targeted sizes at scalable quantities for a range of biomedical and biosensing applications.

4.2 Introduction

Nanogels, solvent-swollen networks of cross-linked polymers, have been utilized as catalytic nanoreactors,¹⁻² sensors,³⁻⁶ drug delivery vehicles,⁷ tissue engineering scaffolds,⁸⁻⁹ biomedical imaging agents,¹⁰⁻¹¹ enzyme immobilization supports,¹² and antifouling agents¹³⁻¹⁵, among other applications. The tunable chemical composition and physical morphology of nanogels makes them attractive materials for such a wide variety of applications,¹⁶ aided by the demonstrated capacity to tune nanogel properties such as size, shape, water content, and cross-link density (and thus porosity) based on judicious selection of nanogel building blocks and reaction conditions.¹⁷⁻²⁰

Stimuli-responsive polymers that dynamically change in response to external stimuli such as temperature,²¹ pH,²² light,²³⁻²⁴ or the presence of a small molecule⁶ are often used to form nanogels, as the “smart” properties of such polymers are retained upon cross-linking of the polymers into nanogels.^{19, 25} Temperature is among the most widely investigated and technologically-relevant stimuli owing to the utility of temperature both a sensing stimulus (e.g. detecting intracellular temperature changes due to biological processes²⁶) and a triggering stimulus, either via direct heating or via remote-controlled induction heating (e.g. superparamagnetic nanoparticles in the presence of an oscillating magnetic field²⁷⁻²⁸ or anisotropic plasmonic nanoparticles in the presence of near-infrared irradiation²⁹). Most reported nanogels are fabricated based on thermoresponsive

polymers that exhibit a lower critical solution temperature (LCST),³⁰⁻³³ although there are some examples of upper critical solution temperature (UCST) nanogels³⁴. In particular, the LCST polymers poly(N-isopropylacrylamide) (PNIPAM)³⁵ and, more recently, poly(oligoethylene glycol methacrylate) (POEGMA)³⁶ have been used to generate thermoresponsive nanogels that exhibit a volume phase transition temperature (VPTT) due to their potential to undergo temperature-induced swelling and shrinking (and thus changes in porosity) in aqueous media^{12, 19, 34}.

Thermoresponsive nanogels have traditionally been prepared from either precipitation polymerization³⁷ or inverse emulsion-templated free radical polymerization³⁸ from monomers, although newer methods like inverse nanoprecipitation and polymerization-induced self-assembly (PISA) coupled with controlled living radical polymerization have also been developed by exploiting the solubility change of the polymer in the reaction media during the polymerization to drive nanoparticle formation^{20, 34}. However, all these methods have drawbacks. The conventional precipitation polymerization can be performed in water, is scalable, and can result in highly monodisperse nanogels over a range of tunable sizes between 80 to >1000 nm³⁹. However, the simultaneous *in situ* polymerization and cross-linking can be problematic for degradation *in vivo* due to the molecular weight of the carbon-carbon backbone exceeding the renal clearance limit, creating long-term clearance challenges even if degradable cross-linkers like ethylene

glycol dimethacrylate (enzymatically/ hydrolytically degradable)⁴⁰ or those containing disulfides (reducible)⁴¹⁻⁴², acetals (hydrolytically degradable at lower pH)⁴³ or polyvinylalkoxysiloxanes (hydrolytically degradable at higher pH)⁴⁴ are used. Furthermore, the kinetically-controlled polymerization process typically produces nanogels with highly heterogeneous internal structures.⁴⁵ Nanogel preparation using water in-oil emulsions is also scalable but typically results in highly polydisperse nanogel sizes and poses challenges around the removal of residual monomer, organic solvent, and surfactant.¹⁸ Inverse nanoprecipitation, a surfactant-free process whereby nanogels are prepared by mixing a polymer solution in a water-miscible solvent with a large volume of water to induce phase separation into 100-1000 nm clusters,⁴⁶ similarly poses challenges around solvent removal in addition to being highly mixing-dependent and thus challenging to scale, although it has been successfully used on the lab scale to create ~150 nm diameter nanogels with a size well-suited to prolonged circulation *in vivo*⁴⁷. PISA-based controlled radical polymerization techniques such as atom-transfer radical polymerization (ATRP) and reversible addition-fragmentation chain transfer (RAFT) in which chain growth and cross-linking is conducted simultaneously to create nanogels⁴⁸ offer the benefits of creating more uniform and homogeneously cross-linked networks⁴⁹ with the option of introducing more complex morphologies like vesicles and worms⁵⁰ but at a cost of synthetic complexity and scalability. As such, developing an adaptable and

scalable method for fabricating monodisperse and degradable thermoresponsive nanogels remains desirable.

Recently, we have reported a rapid, one-pot, thermally-driven method to produce stable, covalently cross-linked, and monodisperse populations of poly(N-isopropylacrylamide) (PNIPAM) nanogels in aqueous media.⁵¹ PNIPAM oligomers with molecular weights below the renal clearance limit are functionalized with hydrazide or aldehyde groups and are mixed together above their LCST to form nanoaggregates that are cross-linked *in situ* through hydrazone bond formation. The resulting thermally self-assembled PNIPAM nanogels have a homogeneous internal cross-link structure⁵² and, due to the lability of the hydrazone bond (weeks at acidic conditions, months at neutral conditions),⁵³ can be hydrolytically degraded back to their initial precursor polymers over time.⁵¹ However, from a biomedical translational perspective in terms of bringing such nanogels to practical use as nanotherapeutics, the use of PNIPAM remains challenging. Although most cytocompatibility and tissue compatibility studies involving PNIPAM-based materials have yielded promising results,^{51, 54-55} the highly toxic nature of the NIPAM monomer and the lack of a clear degradation pathway for PNIPAM *in vivo* has complicated the regulatory approval of PNIPAM for biomedical use.

In this context, the application of a similar methodology to create monodisperse and degradable nanogels based on poly(oligo ethylene glycol methacrylate) (POEGMA) instead of PNIPAM offers clear benefits. While POEGMA itself has not to our knowledge yet been approved by regulatory agencies for human use, the degradation products of POEGMA are short-chain poly(ethylene glycol) and poly(methacrylic acid), both of which have been approved for many biomedical uses⁵⁶⁻⁵⁸. In addition, POEGMA offers similar low cytotoxicity and as good or better protein repellency and non-inflammatory properties *in vivo* relative to PNIPAM⁵⁹; indeed, POEGMA-based materials have been demonstrated to suppress protein adsorption (key to promoting long-term nanoparticle circulation and/or low inflammatory responses) on par with or better than poly(ethylene glycol), the current gold standard.⁵⁹ However, POEGMA and PNIPAM undergo mechanistically different types of LCST transitions,⁶⁰ making the direct application of our thermally-driven self-assembly approach (which relies on the initial formation of a compact, well-defined nanoaggregate of one of the two functional precursor polymers in aqueous solution) challenging. Indeed, initial efforts to directly replicate the assembly conditions found to create highly monodisperse microgels using PNIPAM resulted in the formation of large and highly polydisperse POEGMA-based nanogels and/or bulk aggregates. As such, to effectively apply the self-assembly method to create degradable, monodisperse, and size-controlled POEGMA nanogels, an improved understanding of the process conditions leading to small, monodisperse nanogels is required.

Herein, we address this challenge by investigating how altering the different self-assembly parameters such as the chemistry of the core and cross-linking polymer, the assembly temperature, and the ratio of core and cross-linking polymer affects the size and polydispersity of the self-assembled POEGMA nanogels. We analyze the results in the frameworks of both the fundamentals of smart polymers as well as multivariate statistical analysis aiming to identify correlations both between and within process conditions and nanogel properties. We are particularly interested in identifying synthetic conditions that lead to the formation of small (50-150 nm) and monodisperse POEGMA-based nanogels, which have attractive potential applications as long-term circulating nanoparticles for drug delivery⁶¹⁻⁶² and biosensing²⁶; however, developing a broader understanding of the structure-property correlation framework would also enable the generation of narrowly dispersed nanogel populations of different sizes that may be relevant to producing nanogels for a broader range of applications. Finally, we demonstrate how the identification of such conditions can enabling the scaling of the self-assembly method to higher volume nanogel production, key to the use of such nanogels in practical applications.

4.3 Experimental

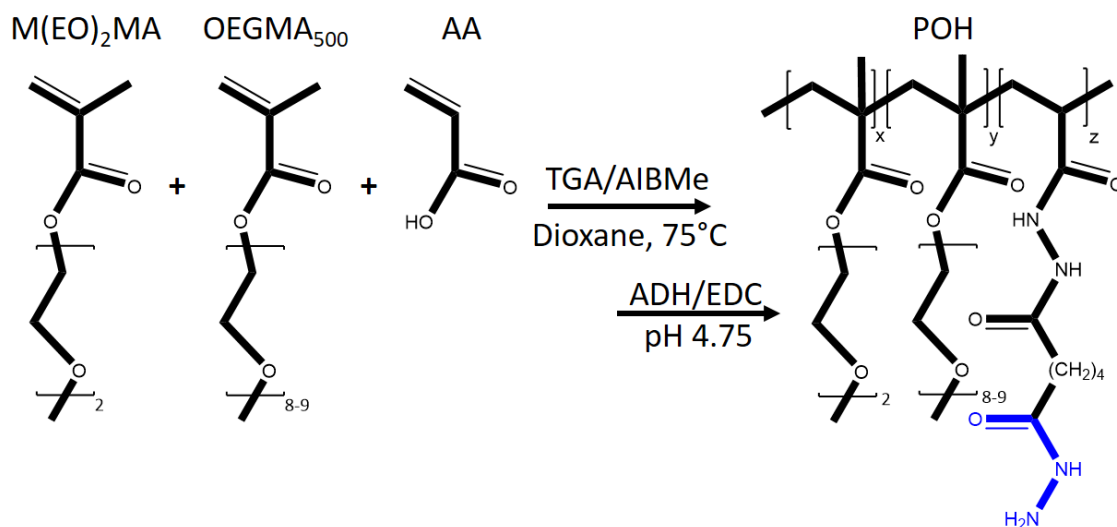
4.3.1 Materials

Diethylene glycol methacrylate (M(EO)₂MA, EO repeats=2) and oligo(ethylene glycol) methacrylate (OEGMA₄₇₅, EO repeats=8-9) were purchased from Millipore Sigma and purified by running the monomer through a column of aluminum oxide (Millipore Sigma) to remove the inhibitors. 2,2-azobisisobutyric acid dimethyl ester (AIBMe, Wako Chemicals), acrylic acid (AA, Millipore Sigma), thioglycolic acid (TGA, Millipore Sigma), sodium chloride (NaCl, Millipore Sigma), adipic acid dihydrazide (ADH, Alfa Aesar), *N*'-ethyl-*N*-(3-dimethylaminopropyl)-carbodiimide (EDC, Carbosynth), hydrochloric acid (HCl, LabChem Inc.), sodium hydroxide (NaOH, Lab Chem Inc.), and dioxane (Caledon Laboratory Chemicals) were all used as received. The acetal-containing monomer *N*-(2,2-dimethoxyethyl)methacrylamide (DMEMAm) was synthesized according to our previous reports⁵⁹. Milli-Q grade distilled deionized water (DIW, 18.2 MΩ cm resistivity) was used in all experiments.

4.3.2 Synthesis of hydrazide-functionalized POEGMA (POH)

POH synthesis was carried out according to the protocol described by Smeets *et al*⁵⁹. Briefly, M(EO)₂MA (3.5 g, 18.6 mmol), OEGMA₄₇₅ (0.5 g, 1.1 mmol), and AA (0.6 g, 8.3 mmol) were mixed with TGA (7 μL, 0.12 mmol) and AIBMe (37 mg, 0.14 mmol) in 20 mL of dioxane in a 100 mL round bottom flask. The solution was purged with nitrogen for 30

minutes and then lowered into an oil bath at 75°C, after which the reaction was allowed proceed for 4 hours under magnetic stirring. The solvent was removed by evaporation, and the isolated polymer was dissolved in 150 mL of Milli-Q H₂O. To convert the carboxylic acid groups of the acrylic acid to hydrazide groups, a carbodiimide-mediated conjugation was carried out by mixing the prepolymer with a five-fold excess of ADH (3.6 g, 20.5 mmol) and adjusting the pH to 4.75. EDC (1.6 g, 10.2 mmol) was then added, and the pH was continuously adjusted through the addition of 0.1 M HCl to facilitate the conjugation of ADH to the acrylic acid groups (Scheme 4.1). The solution was dialyzed using 3.5-5 kDa molecular weight cut-off membranes for a minimum of six hours over six cycles, lyophilized, and stored as a 20 wt% solution in water at 4°C. The degree of functionalization was determined using base-into acid titration (ManTech Inc.) by analyzing 50 mg of polymer dissolved in 50 mL of 1 mM NaCl using 0.1 M NaOH as the titrant. For ¹H-NMR, polymers were dissolved in deuterated chloroform and analyzed using a Bruker AVANCE 600 MHz spectrometer. Gel permeation chromatography (GPC) was carried out using a Polymer Laboratories PL-50 GPC equipped with three Phenomenex Phenogel™ columns (300 × 4.6 mm, 5 μm; pore sizes: 100, 500, 10⁴ Å) at room temperature; DMF with 50mM LiBr was used as the eluent, and calibrated using PEG narrow standards obtained from Polymer Laboratories. All samples were filtered using a 0.2 μm nylon filter.

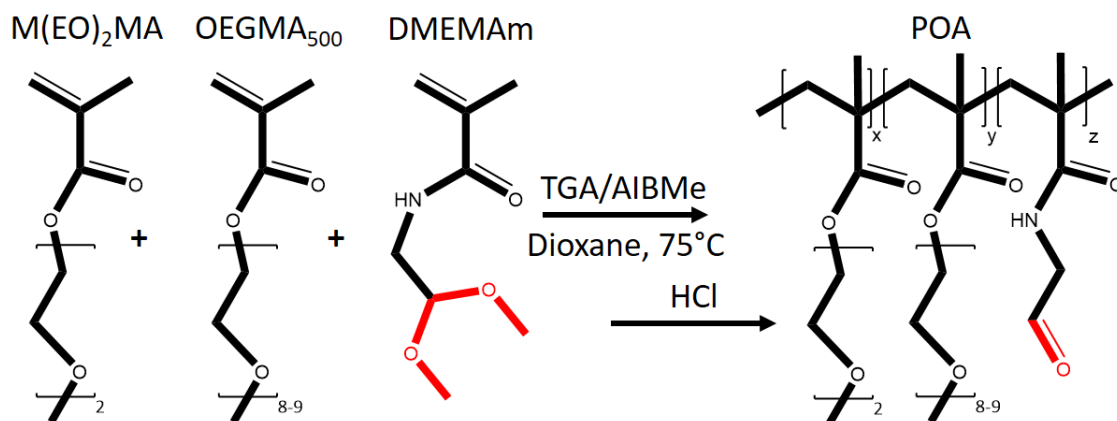


Scheme 4.1: Synthesis of hydrazide-functionalized POEGMA (POH). Free radical polymerization of $M(\text{EO})_2\text{MA}$, OEGMA_{500} and AA, followed by post-synthesis conversion of the AA carboxylic acid groups to hydrazides with ADH using EDC-mediated chemistry produces the final POH polymer.

4.3.3 Synthesis of aldehyde-functionalized POEGMA (POA)

POA was synthesized using protocols extensively described elsewhere.⁵⁹ Briefly, $M(\text{EO})_2\text{MA}$ (3.1 g, 16.5 mmol), OEGMA_{475} (0.9 g, 1.9 mmol) and DMEAMAm (1.3 g, 7.5 mmol) were mixed with TGA (7 μL , 0.12 mmol) and AIBMe (32 mg, 0.14 mmol) in 20 mL of dioxane in a 100 mL round bottom flask. The solution was magnetically stirred and purged with nitrogen for 30 minutes, after which it was lowered into a 75°C oil bath to polymerize for four hours. The dioxane was removed using rotary evaporation, after which the polymer was dissolved in 100 mL of 0.5 M HCl and left to stir for 24 hours to convert the acetal groups to aldehydes (Scheme 4.2). The polymer was purified by six cycles of dialysis against Milli-Q H_2O , lyophilized, and finally stored at 4°C as a 20 wt%

solution in water. $^1\text{H-NMR}$ and GPC characterization of polymer chemistry and molecular weight respectively was performed using the same techniques described above for POH.



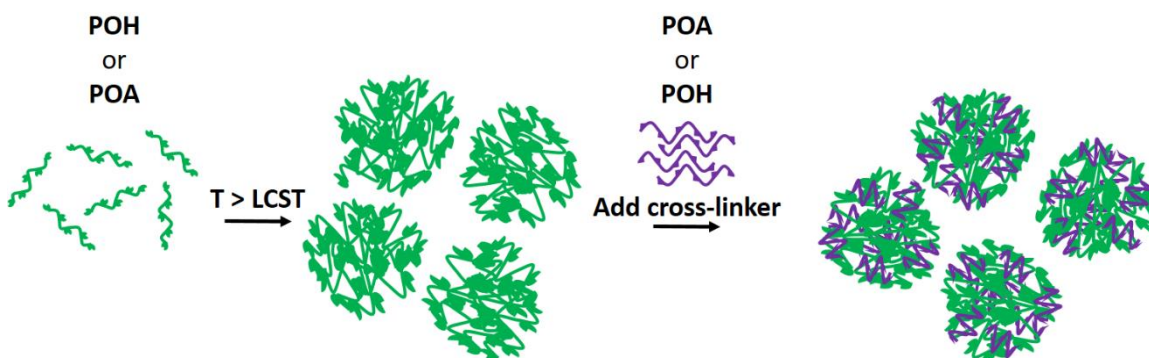
Scheme 4.2: Synthesis of aldehyde-functionalized POEGMA (POA). Free radical polymerization of M(EO)₂MA, OEGMA₅₀₀ and DMEMAm, followed by post-synthesis acid-catalyzed hydrolysis of the DMEMAm acetal groups to aldehydes yields the final POA polymer.

4.3.4 Determination of polymer LCST

The LCST of the precursor polymers was determined using a Variant Cary 100 UV-visible spectrophotometer. The polymers were dissolved at a concentration of 10 mg/mL in water and placed in a two-sided clear polystyrene cuvette. The absorbance was measured at 500 nm over a temperature range of 10-80°C and recorded at 0.5°C intervals during a temperature ramp performed at a rate of 1°C/minute. The absorbance measurements were converted to transmittance values, with the (onset) LCST identified as the temperature at which the sample transmittance fell below 95%.

4.3.5 Nanogel self-assembly

Nanogel self-assembly was performed as per the sequential addition process illustrated in Scheme 4.3. Either 0.5 wt% or 1 wt% stock solutions of POH and POA were first prepared. A 5 mL aliquot of the core polymer solution (POH or POA) was loaded into a 20 mL glass vial and heated in an oil bath to a pre-determined temperature for five minutes under magnetic stirring at 350 rpm. The complementary cross-linker solution (POA or POH) was then diluted to the targeted concentration and slowly added dropwise (~30 s) to core polymer solutions, with the mixtures stirred for 15 minutes. The resulting nanogel suspensions were removed from the oil bath and cooled overnight at room temperature. Different assemblies were conducted by switching the identity of the core and cross-linking polymers, changing the core solution concentrations, and altering the mass ratio between the core and cross-linking polymers.



Scheme 4.3: Schematic of self-assembly method. The core polymer (POH or POA) is heated above its LCST to form nanoaggregates in solution. The complementary cross-linking polymer (POA or POH) is then added to the solution, leading to the spontaneous formation of covalent hydrazone bonds to form stable, cross-linked nanogels.

4.3.7 Multivariate analysis

Regression analysis was used to identify relationships between self-assembly properties and nanogel properties. For this analysis, projection to latent structures (PLS) regression was applied using ProSensus' ProMV software package. X-space variables were associated with the various self-assembly reaction conditions, i.e. the identity of core and cross-linking polymer, the concentration of the core prepolymer solution, the ratio of core:cross-linking polymer, and the difference in the temperature at which the self-assembly process was run relative to core polymer LCST. Y-space variables included the key properties of the resulting nanogels, i.e. hydrodynamic diameter, polydispersity and multimodal number-based diameter distributions.

4.3.6 Nanogel particle size measurements

Dynamic light scattering measurements were carried out at 25°C using a Brookhaven NanoBrook 90Plus particle analyzer running BIC Particle Solutions software (Brookhaven Instruments Corporation). A 659 nm laser was used with a detector aligned at a 90° angle. Nanogel solutions were diluted to produce a count rate of ~500 kcps. Five two-minute measurements were carried out per sample, with the reported values representing the cumulant averages from the intensity-weighted particle size distributions plus or minus one standard deviation.

4.3.8 Self-assembly scale up

To demonstrate the feasibility of scaling up the self-assembly technique, three synthetic conditions producing nanogels with varying sizes and polydispersities were selected for scale up to a 50 mL volume. A core pre-polymer solution (38.5 mL total volume) was prepared in a 100 mL round-bottom flask, while a cross-linking pre-polymer solution (11.5 mL total volume) was loaded into a syringe. The core pre-polymer solution was heated to a temperature above the LCST of the core pre-polymer and allowed to form the nanoaggregate under 350 rpm magnetic stirring for 10 minutes, a longer time relative to that used for the small volume assemblies to compensate for heat transfer kinetics. Subsequently, a syringe pump was used to add the cross-linking pre-polymer solution at a flow rate of 3 mL/min for 3.85 min (compared to 30 s for the 6.5 mL scale). The final mixture was stirred for 15 minutes, removed from the oil bath to cool, and then characterized by DLS in the same manner as the smaller scale samples.

4.4 Results and Discussion

4.4.1 Polymer synthesis and characterization

Thermosensitive linear precursor polymers were synthesized using chain transfer agent-mediated free radical polymerization of short ($M(\text{EO})_2\text{MA}$, EO repeat units, $n=2$) and long (OEGMA_{475} , $n=8-9$) POEGMA monomers. The monomer ratio of 90 mol% $M(\text{EO})_2\text{MA}$ and 10 mol% OEGMA_{475} was selected to produce a polymer with an LCST similar to that of

PNIPAM (~32°C), ensuring that the LCSTs of the more polar hydrazide and aldehyde-functionalized pre-polymers were still accessible in aqueous solution. Hydrazide-functionalized POEGMA (POH) polymers were synthesized by copolymerizing acrylic acid with the two POEGMA monomers followed by a post-polymerization carbodiimide-mediated modification with an excess of ADH (Scheme 4.1); aldehyde-functionalized POEGMA (POA) polymers were prepared by copolymerizing POEGMA monomers with the acetal monomer DMEMAm, which was subsequently converted to an aldehyde by an acid-catalyzed hydrolysis reaction post-polymerization (Scheme 4.2). The total functional group content of each functional pre-polymer was measured to be ~20% (Table 4.1), consistent with essentially stoichiometric functionalization of the polymers relative to the recipes used. Similarly, the molecular weights of both POH and POA polymers were 15-20 kDa (Table 4.1), well below the renal clearance limit of 30-50 kDa to ensure efficient biological clearance upon degradation.⁶³ The introduction of the hydrophilic hydrazide and aldehyde functional groups increases the LCST of the 90:10 POEGMA polymer from 39°C to 66°C and 54°C for POH and POA, respectively (Table 4.1 and Figure 4.1). This change in LCST value is similar to those measured for the PNIPAM-based pre-polymers previously used for the self-assembly process, whereby functionalization increases the LCST of pNIPAM from 32°C to 44°C for NIPAM-Ald and 58°C for NIPAM-Hzd.⁵⁹ The temperature range over which the phase transition occurs is significantly smaller for both POH and POA compared to hydrazide- and aldehyde-functionalized PNIPAM precursor

polymers (Figure 4.1). This result suggests that the assembly temperature may be a significantly more sensitive variable for POEGMA nanogel assembly relative to PNIPAM nanogel assembly.

Table 4.1: Chemical characterization of linear polymer precursors.

	M(EO ₂)MA (mol %) ^a	OEGMA ₄₇₅ (mol %) ^a	M _n (x10 ³ g/mol) ^b	Đ ^b	Functional group	Functional content (mol %)	LCST (°C) ^d
POH	70.5	7.8	20.1	1.8	NH ₂	21.7 ^c	66
POA	72.8	7.3	15.1	1.9	COH	19.9 ^a	54

^a Determined by ¹H NMR.

^b Determined using DMF GPC.

^c Determined using conductometric titration

^d Determined at 95% transmittance in DIW.

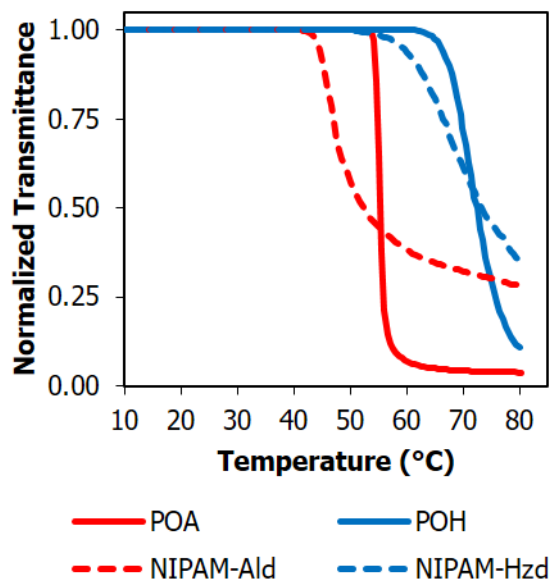


Figure 4.1: Lower critical solution temperature behavior of 1 wt% POA, POH, NIPAM-Ald and NIPAM-Hzd polymer solutions in DIW.

4.4.2 Nanogel self-assembly and characterization

Scheme 4.3 shows the steps of the self-assembly process. To form the initial nanoaggregate, the core solution was heated above the LCST and subsequently cross-linked by the addition of the second polymer with complementary functionality to stabilize the aggregate into a nanogel by the formation of the hydrazone bond. By changing the temperature of the assembly (expressed as the difference between the assembly temperature and the LCST of the core pre-polymer), the mass concentration of the core pre-polymer in the initial solution, and the mass ratio of the core to cross-linking polymer, a broad range of nanogel diameters and polydispersities ranging from small (~50 nm) to large (~700 nm) and from monodisperse (PD ~0.1) to highly polydisperse (PD >0.3) were achieved (refer to Supporting Information Tables S4.1-S4.6 for raw data for the complete nanogel library). Relative to PNIPAM nanogel assemblies previously performed over a similar range of input variables in which all tested formulations yielded particle sizes over a narrow range (219-252 nm) but consistently low polydispersities (~0.1 or less)⁵¹, POEGMA assemblies can access both significantly higher and (of particular interest) significantly lower particle sizes but result in less consistently low polydispersities. However, aside from two formulations that resulted in bulk aggregation (Table S4.2), all POEGMA nanogels showed monomodal particle size distributions (Supporting Information, Tables S4.3-S4.6, Figure S4.2), confirming the general efficacy of the assembly strategy to produce definable POEGMA nanogel populations. To understand

how to control the size and polydispersity of POEGMA nanogels, we systematically investigated the effects of the different assembly conditions on POEGMA nanogel properties in the following sections.

4.4.3 Effect of core prepolymer identity on nanogel diameter

The choice of the core pre-polymer has a large impact on the fabricated nanogel properties (Figure 4.2). POH-core nanogels are consistently much larger than POA-core nanogels irrespective of the assembly temperature and the core:cross-linker pre-polymer mass ratio used for nanogel fabrication. Several nanogels produced using POA as the core polymer showed particle sizes <100 nm and as low as ~50 nm (albeit with only moderate to higher polydispersities, Tables S4.2 and S4.4), while most nanogels produced using a POH core showed hydrodynamic diameters >200 nm and as high as 450 nm. We attribute this variation to the different hydrophobicity of the hydrazide and aldehyde-functionalized polymers, as evidenced by both the lower LCST and the significant sharper transition of POA compared to POH (Figure 4.1). The polymer that forms the initial nanoaggregate dominates the nanogel composition since it is always in at least 5-fold excess of the quantity of cross-linking polymer; as such, the majority of free functional groups within each nanogel can be attributed to the core polymer. Furthermore, the lower polarity of POA compared to POH means that the POA nanoaggregates above their LCST will be more tightly condensed than those formed by POH above its LCST. Thus, using

POH as the core polymer would lead to larger nanoaggregates and a more hydrophilic gel phase following nanogel fabrication, accounting for the higher sizes observed. Similarly, the higher polarity of POH compared to POA would more strongly colloidally stabilize the nanoaggregate above the LCST, accounting for the lower general polydispersity values observed for POH core nanogels. However, the capacity to fabricate ~50 nm nanogels with at least average polydispersities of ~0.2 (achievable using the more condensed POA as the core polymer) does offers a significant advantage relative to the conventional precipitation-based synthesis technique, in which sizes <100 nm are rarely achievable.

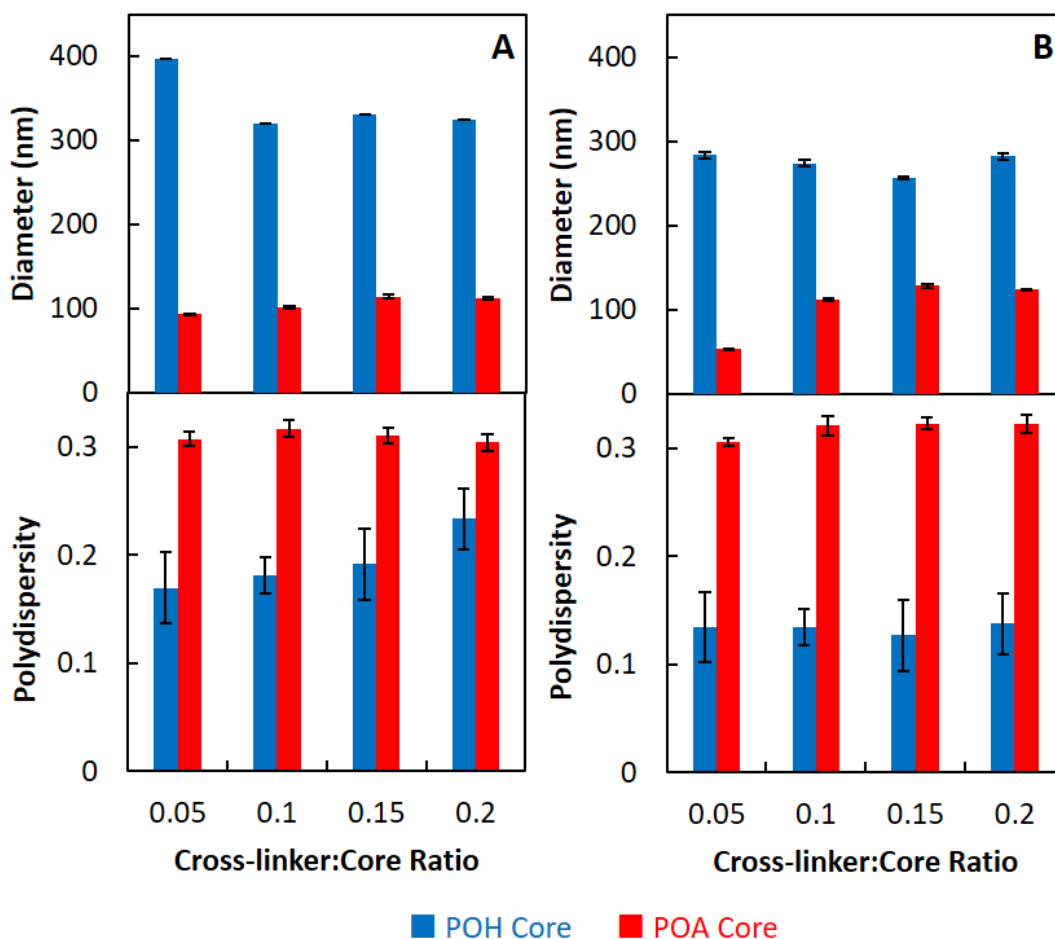


Figure 4.2: Effect of POH polymer content on nanogel diameter and polydispersity (1 wt% core pre-polymer solution concentration). (A) Nanogels assembled at 5°C above the core polymer LCST; (B) nanogels assembled at 10°C above the core polymer LCST.

4.4.4 Impact of reaction temperature

While no direct correlation between absolute assembly temperature and size was observed between the POH and POA core results, a clear correlation was observed when the absolute difference between the assembly temperature and the LCST of the core

polymer was considered. This temperature difference dictates the degree to which the core pre-polymer nanoaggregates collapse prior to the addition of the cross-linking polymer as well as both the degree and rate at which the cross-linking pre-polymer (originally at room temperature) undergoes an LCST transition following addition to the pre-heated core pre-polymer solution.

Assemblies conducted below the LCST of the core POH pre-polymer result in larger and more polydisperse nanogels (Table 4.1). In this case, no defined POH nanoaggregate is formed prior to cross-linking pre-polymer (POA) addition; furthermore, an assembly temperature 5°C below the LCST of POH is still above the LCST of POA (Figure 4.1), leading to the formation of poorly defined POA aggregates over time and thus poorly controlled nanogel/microgel formation from solution. Assemblies performed at the LCST of the core pre-polymer maintained these higher polydispersities when POA was used as the core pre-polymer (i.e. the nanoaggregate itself was less stable, Table S4.2) and/or lower core POH pre-polymer concentrations were used (i.e. fewer and/or smaller and thus colloiddally less stable nanoaggregates were formed, Table S4.1).

Assemblies conducted above the LCST of the core pre-polymer showed different trends depending on the chemistry of the core polymer. For POH core materials (Figure 4.3A and Tables S4.1, S4.3 and S4.5), assemblies performed at 5°C above the LCST resulted in the

formation of nanogels with higher particle sizes but lower polydispersities, with highly monodisperse nanogels formed when the more dilute (0.5 wt%) core pre-polymer solution was used. We attribute both these results to the formation of better-defined nanoaggregates above the LCST, which can subsequently template the formation of more uniform nanogels. Performing assembly at a temperature 10°C above the POH core pre-polymer LCST results in the formation of smaller nanogels at higher POH concentrations. This result is consistent with the continuing collapse but maintained stability of the nanoaggregate upon further heating, aided by the relatively broad thermal transition of POH (Figure 4.1). However, at the lower 0.5 wt% core polymer concentration, higher particle sizes and polydispersities were observed at the +10°C assembly temperature, with bulk aggregation visually observed at intermediate POA:POH ratios. This result is consistent with the occurrence of gradually increasing bulk thermoaggregation between the (initially smaller) nanoaggregates as the nanoaggregates further collapse upon heating above their LCST (Figure 4.1). Collectively, these observations suggest the importance of balancing nanoaggregate formation with nanoaggregate stability during the assembly process in order to achieve stable and narrowly disperse nanogel populations.

In contrast, for POA core materials (Figure 4.3B and Table S4.2), increasing the reaction temperature relative to the LCST generally results in an increase in the hydrodynamic

diameter of the nanogel. This result is consistent with the increased compaction and hydrophobicity of the POA nanoaggregate as the temperature increases, resulting in the formation of larger pre-polymer aggregates and thus ultimately larger nanogels. Furthermore, the increased degree of collapse of the initial nanoaggregates results in fewer aldehyde groups being sterically available to react with the added POH cross-linking pre-polymer; in addition, all POA assembly temperatures tested lie below the LCST of POH, meaning that the POH cross-linking pre-polymer is less likely to mix with the hydrophobic POA nanoaggregate. As a result, fewer (less hydrophilic) hydrazone bonds and greater (more hydrophilic) excess hydrazide/aldehyde groups will be present in the final nanogel, resulting in increased nanogel swelling upon cooling and thus larger measured particle sizes. This interpretation is further supported by the large increase in nanogel particle size observed when the core POA pre-polymer solution was heated 15°C higher than its LCST (Table S4.2), a temperature that is also above the LCST of the cross-linking POH pre-polymer (Figure 4.1). The resulting nanoaggregation of both pre-polymers reduces the probability of POH cross-linking the highly condensed POA nanoaggregate while increasing the potential for POH and POA nanoaggregates to peripherally cross-link, ultimately leading to larger, less stable, and more polydisperse nanogel populations.

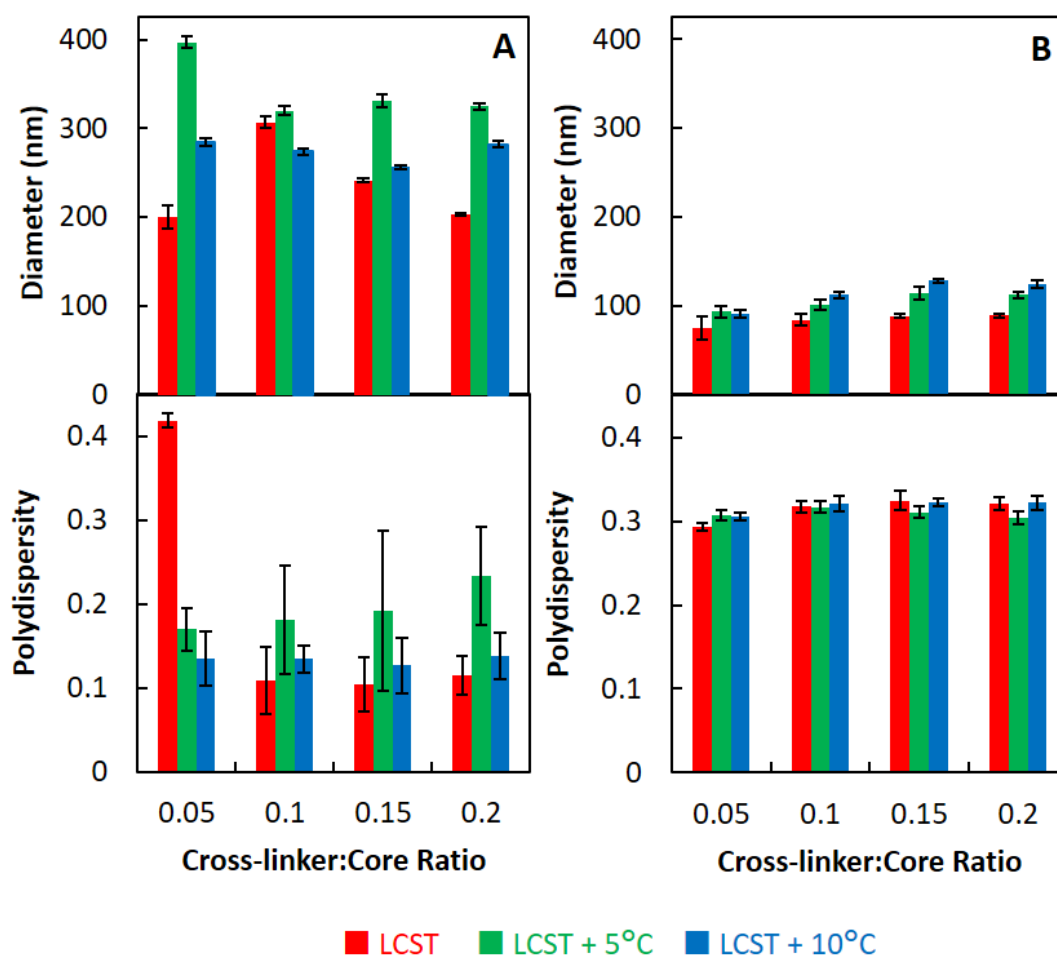


Figure 4.3: Effect of self-assembly temperature (at the core pre-polymer LCST, 5°C above the core pre-polymer LCST, and 10°C above the core pre-polymer LCST) on nanogel diameter and polydispersity (1 wt% core pre-polymer solution concentration). (A) POH core; (B) POA core.

4.4.5 Effect of core prepolymer concentration

In general, increasing the core pre-polymer solution concentration from 0.5 to 1 wt% for either POH- (Tables S4.3 and S4.5) or POA-core (Tables S4.4 and S4.6) nanogel formulations results in the formation of larger nanogels, consistent with the increased

collision frequency of core pre-polymers at higher pre-polymer concentrations (Figure 4.4). For example, nanogels assembled at or just above (+5°C) the LCST were consistently smaller when the lower 0.5 wt% core pre-polymer concentration was used regardless whether POH or POA was used as the core pre-polymer (Tables S4.1 and S4.2). However, the smaller nanoaggregates formed at lower core pre-polymer concentrations are also less stable as they are further heated and the nanoaggregates become more hydrophobic, leading to the observation of large-scale aggregation in some samples at higher temperatures (Table S4.1). Less obvious trends are apparent in comparing the polydispersities achieved at different core pre-polymer concentrations, although certain assembly temperatures can induce significantly different polydispersities as a function of core pre-polymer composition. For example, with POH core nanogel assemblies (Table S4.1 and Figure 4.4), the more dilute 0.5 wt% core pre-polymer concentration resulted in nanogels with substantially higher polydispersities when assembly was conducted at the LCST while the trend was reversed when assembly was conducted 5°C above the LCST. The balance between forming a well-defined nanoaggregate (requiring $T > \text{LCST}$) versus inducing larger-scale aggregation (accelerated as the temperature is further raised above the LCST) results in certain assembly conditions giving substantially more monodisperse products, albeit at less systematically predictable recipes than observed with the other variables.

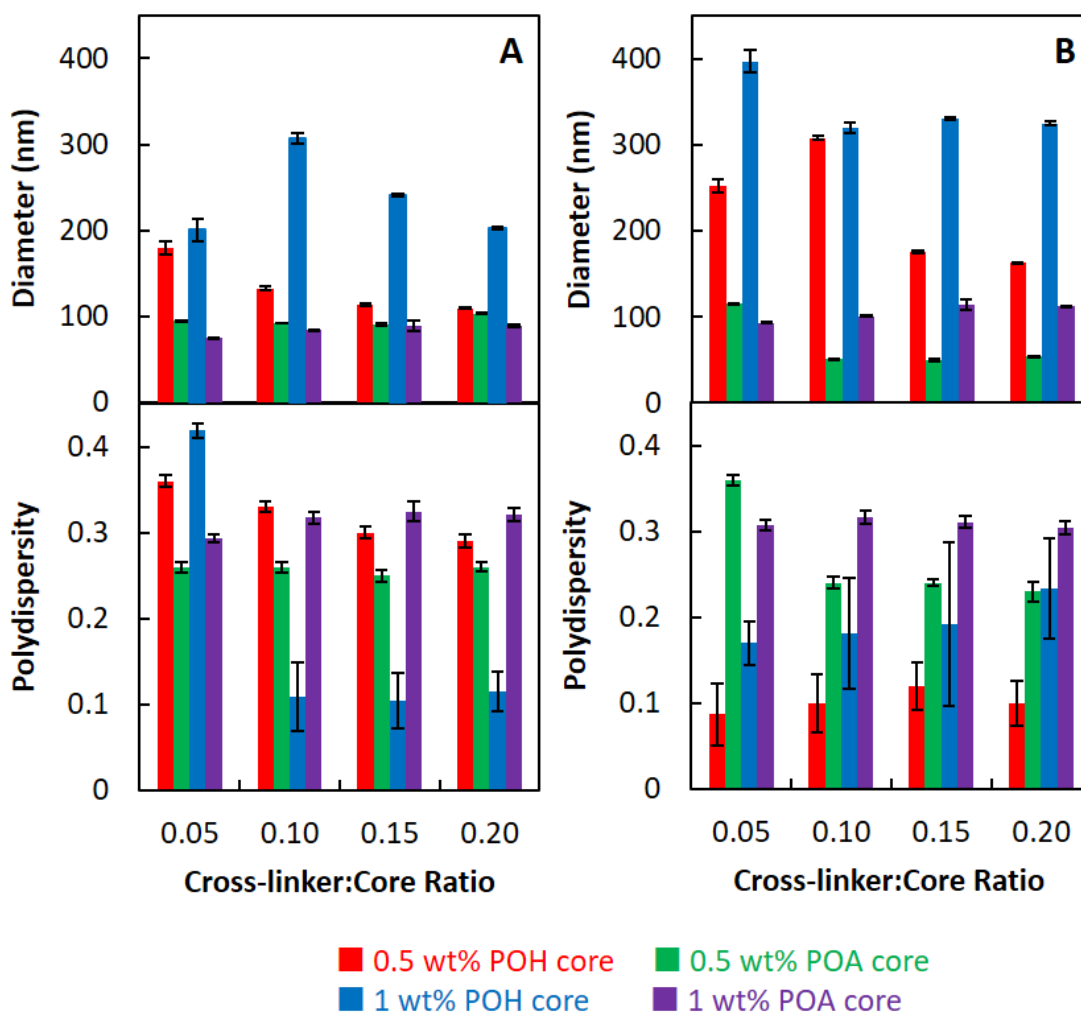


Figure 4.4. Effect of core solution concentration (0.5 or 1 wt%, POH or POA core) on nanogel diameter and polydispersity. (A) Assemblies conducted at the core polymer LCST and (B) assemblies conducted at LCST + 5°C.

4.4.6 Effect of cross-linker ratio

Increasing the ratio of cross-linking to core pre-polymer used for nanogel fabrication is expected to increase the cross-linking density within the final nanogel and thus reduce the nanogel size, a trend we observed in our previous work on fabricating PNIPAM-based

nanogels.^{51, 64} However, this trend is largely not observed with POEGMA nanogel self-assembly. Indeed, with POA-core nanogels (Table S4.2), a small but significant *increase* in particle size was observed as the relative amount of cross-linking polymer added was increased at assembly temperatures below the LCST of the cross-linking POH polymer. In this case, even if added cross-linking polymer results in a higher cross-link density (increasing the elastic resistance to swelling), the introduction of more highly polar hydrazide groups upon POH addition (increasing the mixing driving force for swelling) more than offsets the cross-linking effect. For POH core nanogels, the most common result is that the cross-link:core pre-polymer ratio has no significant effect on either the size or the polydispersity of the nanogels formed (for example, see Figure 5A), a result consistent with the lower hydrophilicity of the POA cross-linking polymer that reduces the mixing contributions to swelling. There are also several cases of the lowest cross-linker:core pre-polymer ratio of 0.05 yielding nanogels either significantly larger or significantly smaller than the other nanogels within the same group (Tables S4.1 and S4.2), suggesting that low amounts of cross-linker cannot in some cases provide sufficient stabilization of the nanoaggregate to create well-defined nanogels. Overall though, the cross-linker:core ratio has substantially less impact on the final nanogel properties than the other parameters studied.

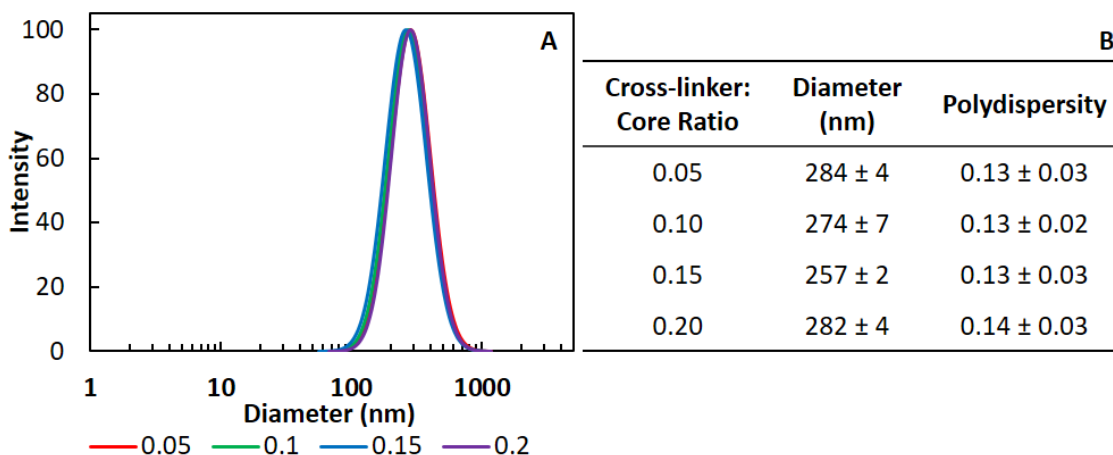


Figure 4.5: Representative example of the effect of the cross-linker:core ratio on the diameter of 1 wt% POH core nanogels assembled at 10°C above the LCST of the core POH polymer. (A) Intensity versus diameter particle size distributions from DLS; (B) tabulated average diameters and polydispersities from DLS. See Supplementary Tables S4.3-S4.6 for full data.

4.4.7 Multivariate analysis of nanogel diameter and polydispersity

To clarify our understanding of the relative effects of different process parameters on nanogel diameter and polydispersity, statistical analysis techniques were applied. First, principal component analysis was carried out on the response (Y-space) observations of the particle size, the standard deviation of the particle size (based on $n=4$ repeat measurements at each assembly condition tested), and the nanogel polydispersity. Figure 4.6 shows the first component weightings arising from a PCA model constructed using two latent variables, which collectively describe 90.0% of the variance in the response variables. Note that the average diameter and standard deviation of the average diameter weightings are similar, indicating that these two variables are correlated and cannot be

set independently in product optimization. This correlation matches our observations that larger nanogels tend to exhibit higher absolute standard deviations in average diameter based on the higher aggregative driving forces leading to nanogel formation in such cases. However, the lack of correlation observed between the average diameter and the polydispersity suggest promise for independently tuning particle size using the self-assembly technique without compromising polydispersity.

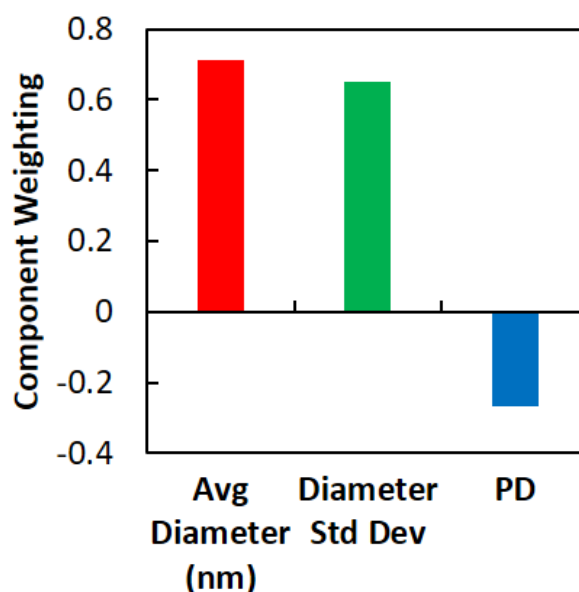


Figure 4.6. Component weightings of average diameter (red), standard deviation of average diameter (green), and polydispersity (blue) from Principle Component Analysis of the response variables.

To account for this correlation within the key performance variables, partial least squares multivariate statistical analysis was attempted. Figure 4.7 shows the relative contributions of the key process variables (i.e. the difference between the self-assembly

temperature and the core pre-polymer LCST, the concentration of the core pre-polymer solution, and the amount of POH added relative to the total pre-polymer concentration, a variable directly correlated to the core:cross-linker pre-polymer ratio) on the diameter of the fabricated nanogels. The analysis indicates that the concentration of the core pre-polymer solution has no effect on nanogel diameter, while increasing the self-assembly process temperature difference with the core pre-polymer LCST and the POH:total polymer ratio both have positive but very weak correlations with nanogel diameter. These results contradict our more qualitative analysis of the data, which suggested the only variable that latent variable methods identify as statistically significant (the core:cross-linker polymer ratio) was the least effective at tuning nanogel size (Figure 4.5). The inconsistency between the conclusions drawn between the statistical and qualitative methods clearly shows the lack of linearity in the response of nanogel size to changes in process conditions, with the subtle balance between nanoaggregate formation and nanoaggregate stabilization resulting in an intermediate “sweet spot” of compositions that is poorly predicted by linear models. Indeed, the $R^2 = 0.22$ value of the model reflects this inherent complexity in correlating self-assembly conditions with nanogel properties, although such model quality can still be useful for identifying useful directions to explore for analyzing the data. On this basis, we proceeded to invert the latent variable model to predict a set of assembly conditions that could minimize particle size, polydispersity, and/or both (equally weighting the importance of both variables); see Supporting

Information, Table S4.7 for the identified recipes. However, the majority of the predicted conditions resulted in bulk aggregation, with only the low polydispersity prediction yielding a colloidally stable but still reasonably polydisperse (PD = 0.26) nanogel (albeit with a well-predicted nanogel size; see Supporting Information, Table S4.8). As such, while multivariate statistics can give insight into the correlations between the output variables and how process conditions affect particle properties, the high non-linearity of the response variables made it only minimally useful to predict optimal assembly conditions.

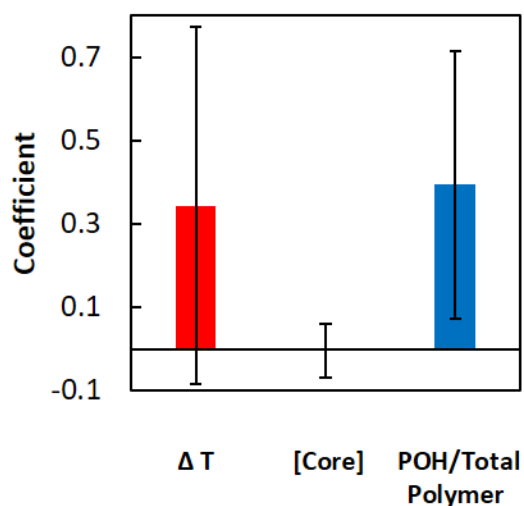


Figure 4.7: Contribution of different reaction composition and condition parameters on the diameter of self-assembled nanogels. The self-assembly process temperature relative to the core polymer LCST (red), the concentration of the core pre-polymer solution (green), and the mass of POH relative to the total mass of polymer (correlated with the core:cross-linker polymer ratio) (blue).

4.4.8 Scale up of nanogel self-assembly

The simplicity, speed (<20 minutes), and relative insensitivity to mixing of this thermal self-assembly technique make the method promising for scaling to larger volumes. To demonstrate the role of the selection of assembly conditions to produce larger batches of narrowly dispersed nanogels, we selected synthetic conditions that produced (1) <300 nm nanogels with a low polydispersity (1 wt% POH core, 0.2 wt% POA cross-linker, LCST + 10°C); (2) <100 nm nanogels with PD ~0.2 (0.5 wt% POA core, 0.1 wt% POH cross-linker, LCST + 10 °C); and (3) the low polydispersity nanogels predicted by the latent variable model (0.43 wt% POH core, 0.011 wt% POA core, LCST + 15°C, PD = 0.26 at the screening scale). The self-assembly volume was scaled from 6.5 mL to 50 mL (~7.5× scale up), mandating a change in the assembly vessel from a 20 mL vial to a 100 mL round-bottom flask. This scale was chosen as it represents a significant volume increase from the screening assembly volume (relevant to at least lab-scale particle production) and requires significant changes in equipment that, if successful, would suggest that further scaling is possible; however, it does not consume an excessive amount of the pre-polymers. While we sought to keep as many process parameters as possible constant between the two scales, the aggregation time was increased to ensure sufficient time for heat transfer and the cross-linker addition time was adjusted proportionate to the increase in the reactor volume to ensure uniform mixing of the cross-linking pre-polymer during addition. Figure 4.8 shows pictures of the resulting nanogel suspensions, while

Table 4.2 shows a comparison of the nanogel properties between the case (1) nanogels produced at both smaller and larger scales. Scale-up of nanogels exhibiting broader polydispersities at smaller scales results in bulk aggregation upon larger scale assembly (Figure 4.8C); however, scaling of the nanogels exhibiting low polydispersities at smaller scale is highly successful (Figure 4.8A and 9), with statistically indistinguishable particle sizes and polydispersities measured following self-assembly at each scale ($p > 0.05$ in each pair-wise comparison, Table 4.2 and Figure 4.9). These results demonstrate the potential for this technique to be scaled up and utilized to produce larger batches of nanogels with comparable properties to the small volumes prepared at the lab scale.

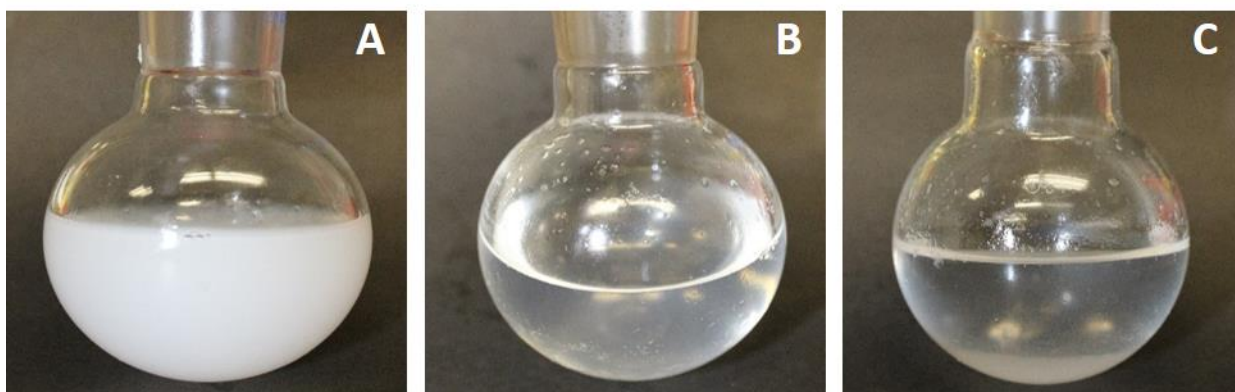
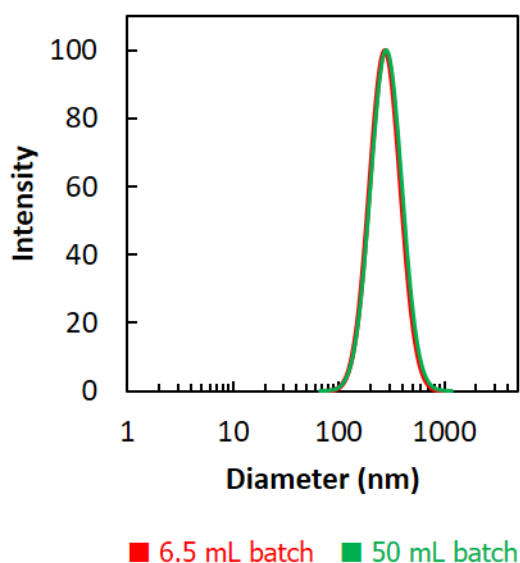


Figure 4.8: Suspensions produced by scaling up of three different synthetic conditions. (A) Case 1 – 1 wt% POH core, 0.2 wt% POA cross-linker, LCST + 10°C; (B) Case 2 – 0.5 wt% POA core, 0.1 wt% POH cross-linker, LCST + 10°C; (C) Case 3 – 0.43 wt% POH core, 0.011 wt% POA core, LCST + 15°C.

Table 4.2: Comparison of nanogel diameter and polydispersity achieved via small scale (6.5 mL) and large scale (50 mL) self-assembly conditions for recipe (1).

Sample Scale	Diameter (nm)	Polydispersity
6.5 mL	282 ± 4	0.14 ± 0.03
50 mL	278 ± 1	0.12 ± 0.05

**Figure 4.9: Logarithmic intensity-based nanogel size distribution of small (6.5 mL - red) and large (50 mL - green) batches of self-assembled 1 wt% POH core and 0.2 wt% POA cross-linked nanogels produced at 10°C above the core polymer LCST.**

4.5 Conclusions

While we have successfully identified scalable conditions in which monodisperse and size-controlled POEGMA-based nanogels can be fabricated, the differences between the self-assembly behavior of POEGMA and PNIPAM (the latter as described in our previous work^{51, 64}) are notable. Overall, it is significantly easier to produce monodisperse nanogels using PNIPAM; in addition, finer control over particle size via, for example, tuning the

cross-linker:core polymer ratio was routinely possible for PNIPAM nanogels. In comparison, with POEGMA, monodisperse nanogels are formed only under very specific conditions, with the most monodisperse nanogels formed at temperatures just above the LCST of the core pre-polymer and at core pre-polymer concentrations leading to the formation of discrete but not highly compacted/hydrophobic nanoaggregates. We hypothesize that this difference is related to the less abrupt LCST behavior of functionalized PNIPAM pre-polymers relative to POEGMA pre-polymers (Figure 1), resulting in a broader range of thermal self-assembly conditions in which a nanoaggregate can be formed but also remains sufficiently hydrophilic to retain colloidal stability. However, aside from the effect of the cross-linker:core pre-polymer ratio (which showed only subtle but still systematic effects on nanogel size with PNIPAM materials), the other general trends observed are similar between POEGMA and PNIPAM self-assemblies (i.e. hydrazide-functionalized pre-polymers perform better as core pre-polymers and decreasing the core pre-polymer concentration reduces nanogel size); this result suggests that similar fabrication mechanisms are at play. In addition, the capacity of the POEGMA self-assembly process to produce very small nanogels (~50 nm) with acceptable polydispersities (~0.2) is a unique feature of the POEGMA self-assembly process that has significant potential benefits for fabricating nanogels for enhancing biological penetration and/or bioimaging applications.

The size and polydispersity of POEGMA nanogels is primarily controlled by the physiochemical characteristics of the core pre-polymer. The cross-linking pre-polymer ratio showed no significant impact on the nanogel size or polydispersity provided that unusually low (i.e. an initial nanoaggregate is not formed) or high (i.e. both pre-polymers are highly aggregated) self-assembly temperatures were not used; we attribute this result to the balance between the elastic-induced deswelling effects of increasing the cross-link density and the mixing-induced swelling effects of adding residual (unreacted) aldehyde or, in particular, hydrazide groups during the cross-linking process. This attribute offers advantages in the design of nanogels with defined sizes but different cross-link densities, as the cross-link density (and thus the mechanics and internal porosity) of the nanogels can be altered without significantly impacting the targeted particle size.

The capacity to fabricate low dispersity and hydrolytically degradable POEGMA nanogels on the 50-150 nm size range offers several potential applications. Specifically, the highly protein-repellent properties of POEGMA,⁵⁹ the capacity to easily surface functionalize the nanogels post-fabrication based on click chemistry reactions with residual hydrazide and/or aldehyde groups⁶⁵, the high water content and thus tissue-mimetic internal morphology of nanogels,⁶⁶⁻⁶⁷ and the intermediate accessible particle size (i.e. too large for routine clearance from the blood via simple diffusion but too large for rapid macrophage-mediated clearance⁶⁸) all suggest the potential of self-assembled POEGMA

nanogels as long-circulating targeted drug delivery vehicles and/or bioimaging aids. Relative to existing available methods for fabricating POEGMA nanogels, this method is unique in terms of enabling the production of monodisperse, small, and degradable nanogels based on an easily scalable process.

4.6 Acknowledgements

Funding from the Natural Sciences and Engineering Research Council of Canada (NSERC, Discovery Grant Program and Canada Graduate Scholarship to M.J.S.), Mitacs (Accelerate Post-Doctoral Fellowship to B.C.), and ProSensus Inc. is gratefully acknowledged.

4.7 References

- (1) Zhang, J.; Xu, S.; Kumacheva, E., Polymer Microgels: Reactors for Semiconductor, Metal, and Magnetic Nanoparticles. *J. Am. Chem. Soc.* **2004**, *126* (25), 7908-7914.
- (2) Lu, A.; Moatsou, D.; Longbottom, D. A.; O'Reilly, R. K., Tuning the Catalytic Activity of L-Proline Functionalized Hydrophobic Nanogel Particles in Water. *Chem. Sci.* **2013**, *4* (3), 965-969.
- (3) Qiao, J.; Chen, C.; Qi, L.; Liu, M.; Dong, P.; Jiang, Q.; Yang, X.; Mu, X.; Mao, L., Intracellular Temperature Sensing by a Ratiometric Fluorescent Polymer Thermometer. *J. Mater. Chem. B* **2014**, *2* (43), 7544-7550.
- (4) Wu, W.; Mitra, N.; Yan, E. C. Y.; Zhou, S., Multifunctional Hybrid Nanogel for Integration of Optical Glucose Sensing and Self-Regulated Insulin Release at Physiological PH. *ACS Nano* **2010**, *4* (8), 4831-4839.
- (5) Zhou, X.; Nie, J.; Du, B., 4-(2-Pyridylazo)-Resorcinol Functionalized Thermosensitive Ionic Microgels for Optical Detection of Heavy Metal Ions at Nanomolar Level. *ACS Appl. Mater. Inter.* **2015**, *7* (39), 21966-21974.
- (6) Hoare, T.; Pelton, R., Engineering Glucose Swelling Responses in Poly(N-Isopropylacrylamide)-Based Microgels. *Macromolecules* **2007**, *40* (3), 670-678.
- (7) Molina, M.; Asadian-Birjand, M.; Balach, J.; Bergueiro, J.; Miceli, E.; Calderon, M., Stimuli-Responsive Nanogel Composites and their Application in Nanomedicine. *Chem. Soc. Rev.* **2015**, *44* (17), 6161-6186.
- (8) Fujioka-Kobayashi, M.; Ota, M. S.; Shimoda, A.; Nakahama, K.-i.; Akiyoshi, K.; Miyamoto, Y.; Iseki, S., Cholesteryl Group- and Acryloyl Group-Bearing Pullulan Nanogel to Deliver BMP2 and FGF18 for Bone Tissue Engineering. *Biomaterials* **2012**, *33* (30), 7613-7620.
- (9) Steinhilber, D.; Rossow, T.; Wedepohl, S.; Paulus, F.; Seiffert, S.; Haag, R., A Microgel Construction Kit for Bioorthogonal Encapsulation and pH-Controlled Release of Living Cells. *Angew. Chem. Int. Ed.* **2013**, *52* (51), 13538-13543.
- (10) Sun, W.; Yang, J.; Zhu, J.; Zhou, Y.; Li, J.; Zhu, X.; Shen, M.; Zhang, G.; Shi, X., Immobilization of Iron Oxide Nanoparticles Within Alginate Nanogels for Enhanced MR Imaging Applications. *Biomater. Sci.* **2016**, *4* (10), 1422-1430.
- (11) Xing, T.; Mao, C.; Lai, B.; Yan, L., Synthesis of Disulfide-Cross-Linked Polypeptide Nanogel Conjugated with a Near-Infrared Fluorescence Probe for Direct Imaging of Reduction-Induced Drug Release. *ACS Appl. Mater. Inter.* **2012**, *4* (10), 5662-5672.
- (12) Tehrani, S. M.; Lu, Y.; Winnik, M. A., PEGMA-Based Microgels: A Thermoresponsive Support for Enzyme Reactions. *Macromolecules* **2016**, *49* (22), 8711-8721.

- (13) Zhao, C.; Chen, Q.; Patel, K.; Li, L.; Li, X.; Wang, Q.; Zhang, G.; Zheng, J., Synthesis and Characterization of PH-Sensitive Poly(N-2-Hydroxyethyl acrylamide)-Acrylic Acid (Poly(HEAA/AA)) Nanogels with Antifouling Protection for Controlled Release. *Soft Matter* **2012**, *8* (30), 7848-7857.
- (14) Bridges, A. W.; Singh, N.; Burns, K. L.; Babensee, J. E.; Andrew Lyon, L.; García, A. J., Reduced Acute Inflammatory Responses to Microgel Conformal Coatings. *Biomaterials* **2008**, *29* (35), 4605-4615.
- (15) Shen, W.; Chang, Y.; Liu, G.; Wang, H.; Cao, A.; An, Z., Biocompatible, Antifouling, and Thermosensitive Core–Shell Nanogels Synthesized by RAFT Aqueous Dispersion Polymerization. *Macromolecules* **2011**, *44* (8), 2524-2530.
- (16) Hoare, T.; Pelton, R., Impact of Microgel Morphology on Functionalized Microgel–Drug Interactions. *Langmuir* **2008**, *24* (3), 1005-1012.
- (17) Menne, D.; Pitsch, F.; Wong, J. E.; Pich, A.; Wessling, M., Temperature-Modulated Water Filtration Using Microgel-Functionalized Hollow-Fiber Membranes. *Angew. Chem. Int. Ed.* **2014**, *53* (22), 5706-5710.
- (18) Ekkelenkamp, A. E.; Elzes, M. R.; Engbersen, J. F. J.; Paulusse, J. M. J., Responsive Crosslinked Polymer Nanogels for Imaging and Therapeutics Delivery. *J. Mater. Chem. B* **2018**, *6* (2), 210-235.
- (19) Plamper, F. A.; Richtering, W., Functional Microgels and Microgel Systems. *Accounts Chem. Res.* **2017**, *50* (2), 131-140.
- (20) Zhang, X.; Malhotra, S.; Molina, M.; Haag, R., Micro- and Nanogels with Labile Crosslinks – From Synthesis to Biomedical Applications. *Chem. Soc. Rev.* **2015**, *44* (7), 1948-1973.
- (21) Lutz, J.-F.; Hoth, A., Preparation of Ideal PEG Analogues with a Tunable Thermosensitivity by Controlled Radical Copolymerization of 2-(2-Methoxyethoxy)Ethyl Methacrylate and Oligo(Ethylene glycol) Methacrylate. *Macromolecules* **2006**, *39* (2), 893-896.
- (22) Hoare, T.; Pelton, R., Highly pH and Temperature Responsive Microgels Functionalized with Vinylacetic Acid. *Macromolecules* **2004**, *37* (7), 2544-2550.
- (23) Jochum, F. D.; Theato, P., Temperature- and Light-responsive Smart Polymer Materials. *Chem. Soc. Rev.* **2013**, *42* (17), 7468-7483.
- (24) Dübner, M.; Spencer, N. D.; Padeste, C., Light-Responsive Polymer Surfaces via Postpolymerization Modification of Grafted Polymer-Brush Structures. *Langmuir* **2014**, *30* (49), 14971-14981.
- (25) Wei, M.; Gao, Y.; Li, X.; Serpe, M. J., Stimuli-Responsive Polymers and Their Applications. *Polym. Chem.* **2017**, *8* (1), 127-143.
- (26) Gota, C.; Okabe, K.; Funatsu, T.; Harada, Y.; Uchiyama, S., Hydrophilic Fluorescent Nanogel Thermometer for Intracellular Thermometry. *J. Am. Chem. Soc.* **2009**, *131* (8), 2766-2767.

- (27) Campbell, S.; Maitland, D.; Hoare, T., Enhanced Pulsatile Drug Release from Injectable Magnetic Hydrogels with Embedded Thermosensitive Microgels. *ACS Macro Lett.* **2015**, *4* (3), 312-316.
- (28) Campbell, S. B.; Patenaude, M.; Hoare, T., Injectable Superparamagnets: Highly Elastic and Degradable Poly(N-isopropylacrylamide)–Superparamagnetic Iron Oxide Nanoparticle (SPION) Composite Hydrogels. *Biomacromolecules* **2013**, *14* (3), 644-653.
- (29) Lee, S. W.; Lee, K. S.; Ahn, J.; Lee, J. J.; Kim, M. G.; Shin, Y. B., Highly Sensitive Biosensing Using Arrays of Plasmonic Au Nanodisks Realized by Nanoimprint Lithography. *ACS Nano* **2011**, *5* (2), 897-904.
- (30) Škvarla, J.; Raya, R. K.; Uchman, M.; Zedník, J.; Procházka, K.; Garamus, V. M.; Meristoudi, A.; Pispas, S.; Štěpánek, M., Thermoresponsive Behavior of Poly(N-Isopropylacrylamide)s with Dodecyl and Carboxyl Terminal Groups in Aqueous Solution: PH-dependent Cloud Point Temperature. *Colloid Poly. Sci.* **2017**, *295* (8), 1343-1349.
- (31) Jiang, Y.; Colazo, M. G.; Serpe, M. J., Poly(N-isopropylacrylamide) microgel-based sensor for progesterone in aqueous samples. *Colloid Poly. Sci.* **2016**, *294* (11), 1733-1741.
- (32) Welsch, N.; Lyon, L. A., Oligo(Ethylene Glycol)-Sidechain Microgels Prepared in Absence of Cross-Linking Agent: Polymerization, Characterization and Variation of Particle Deformability. *PLOS ONE* **2017**, *12* (7), e0181369.
- (33) Hou, L.; Wu, P., Microgels with Linear Thermosensitivity in a Wide Temperature Range. *Macromolecules* **2016**, *49* (16), 6095-6100.
- (34) Fu, W.; Luo, C.; Morin, E. A.; He, W.; Li, Z.; Zhao, B., UCST-Type Thermosensitive Hairy Nanogels Synthesized by RAFT Polymerization-Induced Self-Assembly. *ACS Macro Lett.* **2017**, *6* (2), 127-133.
- (35) Hoare, T.; Pelton, R., Calorimetric Analysis of Thermal Phase Transitions in Functionalized Microgels. *J. Phys. Chem. B* **2007**, *111* (6), 1334-1342.
- (36) Tian, Y. F.; Bian, S. S.; Yang, W. L., A Redox-Labile Poly(Oligo(Ethylene Glycol)Methacrylate)-Based Nanogel with Tunable Thermosensitivity for Drug Delivery. *Polym. Chem.* **2016**, *7* (10), 1913-1921.
- (37) Pelton, R. H.; Chibante, P., Preparation of Aqueous Lattices with N-Isopropylacrylamide. *Colloid. Surface.* **1986**, *20* (3), 247-256.
- (38) Kriwet, B.; Walter, E.; Kissel, T., Synthesis of Bioadhesive Poly(Acrylic Acid) Nano- and Microparticles Using an Inverse Emulsion Polymerization Method for the Entrapment of Hydrophilic Drug Candidates. *J. Control. Release* **1998**, *56* (1-3), 149-158.
- (39) Pelton, R., Temperature-Sensitive Aqueous Microgels. *Adv. Colloid Interface Sci.* **2000**, *85* (1), 1-33.

- (40) Sun, X. D.; Chiu, Y. Y.; Lee, L. J., Microgel Formation in the Free Radical Cross-Linking Copolymerization of Methyl Methacrylate (MMA) and Ethylene Glycol Dimethacrylate (EGDMA). *Ind. Eng. Chem. Res.* **1997**, *36* (4), 1343-1351.
- (41) Wang, Y.; Nie, J. S.; Chang, B. S.; Sun, Y. F.; Yang, W. L., Poly(Vinylcaprolactam)-Based Biodegradable Multiresponsive Microgels for Drug Delivery. *Biomacromolecules* **2013**, *14* (9), 3034-3046.
- (42) Ulasan, M.; Yavuz, E.; Bagriacik, E. U.; Cengeloglu, Y.; Yavuz, M. S., Biocompatible Thermoresponsive PEGMA Nanoparticles Crosslinked with Cleavable Disulfide Based Crosslinker for Dual Drug Release. *Abstr. Pap. Am. Chem. S.* **2014**, *103*(1), 243-251.
- (43) Binauld, S.; Stenzel, M. H., Acid-Degradable Polymers for Drug Delivery: A Decade of Innovation. *Chem. Commun.* **2013**, *49* (21), 2082-2102.
- (44) Zhang, Y.; Aigner, A.; Agarwal, S., Degradable and Biocompatible Poly(N,N-dimethylaminoethyl Methacrylate-co-caprolactone)s as DNA Transfection Agents. *Macromol. Biosci.* **2013**, *13* (9), 1267-1275.
- (45) Hoare, T.; McLean, D., Kinetic Prediction of Functional Group Distributions in Thermosensitive Microgels. *J. Phys. Chem. B* **2006**, *110* (41), 20327-20336.
- (46) Beck-Broichsitter, M.; Nicolas, J.; Couvreur, P., Solvent Selection Causes Remarkable Shifts of the "Ouzo region" for Poly(Lactide-Co-Glycolide) Nanoparticles Prepared by Nanoprecipitation. *Nanoscale* **2015**, *7* (20), 9215-9221.
- (47) Zhang, X.; Achazi, K.; Steinhilber, D.; Kratz, F.; Dervede, J.; Haag, R., A Facile Approach for Dual-Responsive Prodrug Nanogels Based on Dendritic Polyglycerols with Minimal Leaching. *J. Control. Release* **2014**, *174*, 209-216.
- (48) Gao, H. F.; Matyjaszewski, K., Synthesis of Functional Polymers with Controlled Architecture by CRP of Monomers in the Presence of Cross-linkers: From Stars to Gels. *Prog. Polym. Sci.* **2009**, *34* (4), 317-350.
- (49) Gao, Y.; Newland, B.; Zhou, D.; Matyjaszewski, K.; Wang, W., Controlled Polymerization of Multivinyl Monomers: Formation of Cyclized/Knotted Single-Chain Polymer Architectures. *Angew. Chem. Int. Ed.* **2017**, *56* (2), 450-460.
- (50) Tan, J.; Bai, Y.; Zhang, X.; Huang, C.; Liu, D.; Zhang, L., Low-Temperature Synthesis of Thermoresponsive Diblock Copolymer Nano-Objects via Aqueous Photoinitiated Polymerization-Induced Self-Assembly (Photo-PISA) using Thermoresponsive Macro-RAFT Agents. *Macromol. Rapid Comm.* **2016**, *37* (17), 1434-1440.
- (51) Sivakumaran, D.; Mueller, E.; Hoare, T., Temperature-Induced Assembly of Monodisperse, Covalently Cross-Linked, and Degradable Poly(N-isopropylacrylamide) Microgels Based on Oligomeric Precursors. *Langmuir* **2015**, *31* (21), 5767-5778.

- (52) Mueller, E.; Alsop, R. J.; Scotti, A.; Bleuel, M.; Rheinstadter, M. C.; Richtering, W.; Hoare, T., Dynamically Cross-Linked Self-Assembled Thermoresponsive Microgels with Homogeneous Internal Structures. *Langmuir* **2018**, *34* (4), 1601-1612.
- (53) Prabakaran, M.; Grailer, J. J.; Pilla, S.; Steeber, D. A.; Gong, S. Q., Amphiphilic Multi-Arm-Block Copolymer Conjugated with Doxorubicin via PH-Sensitive Hydrazone Bond for Tumor-Targeted Drug Delivery. *Biomaterials* **2009**, *30* (29), 5757-5766.
- (54) Patenaude, M.; Hoare, T., Injectable, Degradable Thermoresponsive Poly(N-isopropylacrylamide) Hydrogels. *ACS Macro Lett.* **2012**, *1* (3), 409-413.
- (55) Prospero-Porta, G.; Muirhead, B.; Sheardown, H., Tunable Release of Ophthalmic Therapeutics from Injectable, Resorbable, Thermoresponsive Copolymer Scaffolds. *J. Biomed. Mater. Res. Part B* **2017**, *105* (1), 53-62.
- (56) Alconcel, S. N. S.; Baas, A. S.; Maynard, H. D., FDA-Approved Poly(Ethylene Glycol)-Protein Conjugate Drugs. *Polym. Chem.* **2011**, *2* (7), 1442-1448.
- (57) Mansour, H. M.; Sohn, M.; Al-Ghananeem, A.; DeLuca, P. P., Materials for Pharmaceutical Dosage Forms: Molecular Pharmaceutics and Controlled Release Drug Delivery Aspects. *Int. J. Mol. Sci.* **2010**, *11* (9), 3298-3322.
- (58) Saade, H.; Guillen, M. D.; Romero, J. C.; Cepeda, J.; Ilyna, A.; Fernandez, S.; Enriquez-Medrano, F. J.; Lopez, R. G., Biocompatible and Biodegradable Ultrafine Nanoparticles of Poly(Methyl Methacrylate-Co-Methacrylic Acid) Prepared via Semicontinuous Heterophase Polymerization: Kinetics and Product Characterization. *Int. J. Polym. Sci.* **2016**, *8*.
- (59) Smeets, N. M. B.; Bakaic, E.; Patenaude, M.; Hoare, T., Injectable Poly(Oligoethylene Glycol Methacrylate)-Based Hydrogels with Tunable Phase Transition Behaviours: Physicochemical and Biological Responses. *Acta Biomater.* **2014**, *10* (10), 4143-4155.
- (60) Lutz, J.-F.; Akdemir, Ö.; Hoth, A., Point by Point Comparison of Two Thermosensitive Polymers Exhibiting a Similar LCST: Is the Age of Poly(NIPAM) Over? *J. Am. Chem. Soc.* **2006**, *128* (40), 13046-13047.
- (61) Oh, J. K.; Siegwart, D. J.; Lee, H. I.; Sherwood, G.; Peteanu, L.; Hollinger, J. O.; Kataoka, K.; Matyjaszewski, K., Biodegradable Nanogels Prepared by Atom Transfer Radical Polymerization as Potential Drug Delivery Carriers: Synthesis, Biodegradation, In Vitro Release, and Bioconjugation. *J. Am. Chem. Soc.* **2007**, *129* (18), 5939-5945.
- (62) Vinogradov, S. V.; Bronich, T. K.; Kabanov, A. V., Nanosized Cationic Hydrogels for Drug Delivery: Preparation, Properties and Interactions with Cells. *Adv. Drug Deliv. Rev.* **2002**, *54* (1), 135-147.
- (63) Duncan, R., The Dawning Era Of Polymer Therapeutics. *Nat. Rev. Drug Discov.* **2003**, *2*, 347-360.

- (64) Mueller, E.; Alsop, R. J.; Scotti, A.; Bleuel, M.; Rheinstadter, M. C.; Richtering, W.; Hoare, T., Dynamically-Crosslinked Self-Assembled Thermoresponsive Microgels with Homogeneous Internal Structures. *Langmuir* **2018**, *34* (4), 1601-1612.
- (65) Gilbert, T.; Smeets, N. M. B.; Hoare, T., Injectable Interpenetrating Network Hydrogels via Kinetically Orthogonal Reactive Mixing of Functionalized Polymeric Precursors. *ACS Macro Lett.* **2015**, *4* (10), 1104-1109.
- (66) Hashimoto, Y.; Mukai, S.; Sawada, S.; Sasaki, Y.; Akiyoshi, K., Nanogel Tectonic Porous Gel Loading Biologics, Nanocarriers, and Cells for Advanced Scaffold. *Biomaterials* **2015**, *37*, 107-115.
- (67) Bencherif, S. A.; Washburn, N. R.; Matyjaszewski, K., Synthesis by AGET ATRP of Degradable Nanogel Precursors for In Situ Formation of Nanostructured Hyaluronic Acid Hydrogel. *Biomacromolecules* **2009**, *10* (9), 2499-2507.
- (68) Alexis, F.; Pridgen, E.; Molnar, L. K.; Farokhzad, O. C., Factors Affecting the Clearance and Biodistribution of Polymeric Nanoparticles. *Mol. Pharm.* **2008**, *5* (4), 505-515.

S4.1 Supporting Information

Table S4.1: Diameter and polydispersity of self-assembled nanogels comprised of a POH core and cross-linked by POA as a function of the self-assembly temperature (set relative to the LCST of the POH core pre-polymer), the ratio of cross-linker:core pre-polymers added, and the core pre-polymer concentration.

Core polymer LCST + ΔT	Cross-linker Ratio	0.5 wt% core		1 wt% core	
		Diameter (nm)	Polydispersity	Diameter (nm)	Polydispersity
10	0.05	309 ± 3	0.16	284 ± 4	0.13 ± 0.03
	0.10	Bulk Aggregation		274 ± 7	0.13 ± 0.02
	0.15			257 ± 2	0.13 ± 0.03
	0.20	445 ± 5	0.18	282 ± 4	0.14 ± 0.03
5	0.05	252 ± 3	0.09 ± 0.04	397 ± 6	0.17 ± 0.03
	0.10	308 ± 5	0.10 ± 0.03	320 ± 5	0.18 ± 0.06
	0.15	175 ± 2	0.12 ± 0.03	331 ± 7	0.19 ± 0.09
	0.20	163 ± 2	0.10 ± 0.03	325 ± 4	0.23 ± 0.06
0	0.05	179 ± 7	0.36 ± 0.007	200 ± 13	0.42 ± 0.008
	0.10	132 ± 3	0.33 ± 0.006	307 ± 6	0.11 ± 0.04
	0.15	113 ± 2	0.30 ± 0.006	241 ± 2	0.10 ± 0.03
	0.20	109 ± 1	0.29 ± 0.007	203 ± 2	0.12 ± 0.02
-5	0.05	441 ± 10	0.35 ± 0.02	352 ± 7	0.32 ± 0.02
	0.10	407 ± 9	0.29 ± 0.01	208 ± 6	0.32 ± 0.01
	0.15	440 ± 7	0.26 ± 0.02	182 ± 12	0.31 ± 0.01
	0.20	761 ± 24	0.39 ± 0.03	190 ± 6	0.33 ± 0.007

Table S4.2: Diameter and polydispersity of self-assembled nanogels comprised of a POA core and cross-linked by POH as a function of the self-assembly temperature (set relative to the LCST of the POH core pre-polymer), the ratio of cross-linker:core pre-polymers added, and the core pre-polymer concentration.

Core polymer LCST + ΔT	0.5 wt% core		1 wt% core		
	Cross-linker Ratio	Diameter (nm)	Polydispersity	Diameter (nm)	Polydispersity
15	0.05	192 ± 5	0.38 ± 0.007	321 ± 5	0.24 ± 0.01
	0.10	139 ± 5	0.36 ± 0.009	366 ± 5	0.25 ± 0.02
	0.15	128 ± 1	0.33 ± 0.007	402 ± 7	0.28 ± 0.02
	0.20	132 ± 2	0.32 ± 0.007	356 ± 11	0.29 ± 0.02
10	0.05	53 ± 1	0.21 ± 0.008	91 ± 1	0.31 ± 0.004
	0.10	57 ± 1	0.20 ± 0.007	112 ± 2	0.32 ± 0.009
	0.15	59 ± 1	0.23 ± 0.01	129 ± 2	0.32 ± 0.05
	0.20	68 ± 1	0.26 ± 0.006	124 ± 1	0.32 ± 0.008
5	0.05	115 ± 2	0.36 ± 0.006	93 ± 1	0.31 ± 0.006
	0.10	51 ± 1	0.24 ± 0.007	101 ± 1	0.32 ± 0.008
	0.15	50 ± 1	0.24 ± 0.004	114 ± 2	0.31 ± 0.007
	0.20	54 ± 1	0.23 ± 0.01	112 ± 2	0.30 ± 0.008
0	0.05	95 ± 1	0.26 ± 0.006	75 ± 1	0.29 ± 0.005
	0.10	92 ± 1	0.26 ± 0.006	84 ± 1	0.32 ± 0.06
	0.15	90 ± 2	0.25 ± 0.007	89 ± 7	0.32 ± 0.01
	0.20	103 ± 1	0.26 ± 0.005	89 ± 1	0.32 ± 0.008

Table S4.3: Hydrodynamic diameters and size distributions of 0.5 wt% POH core nanogels. Size distributions are shown as a function of core:cross-linker pre-polymer ratio - 0.05 (red), 0.10 (green), 0.15 (blue), and 0.20 (purple).

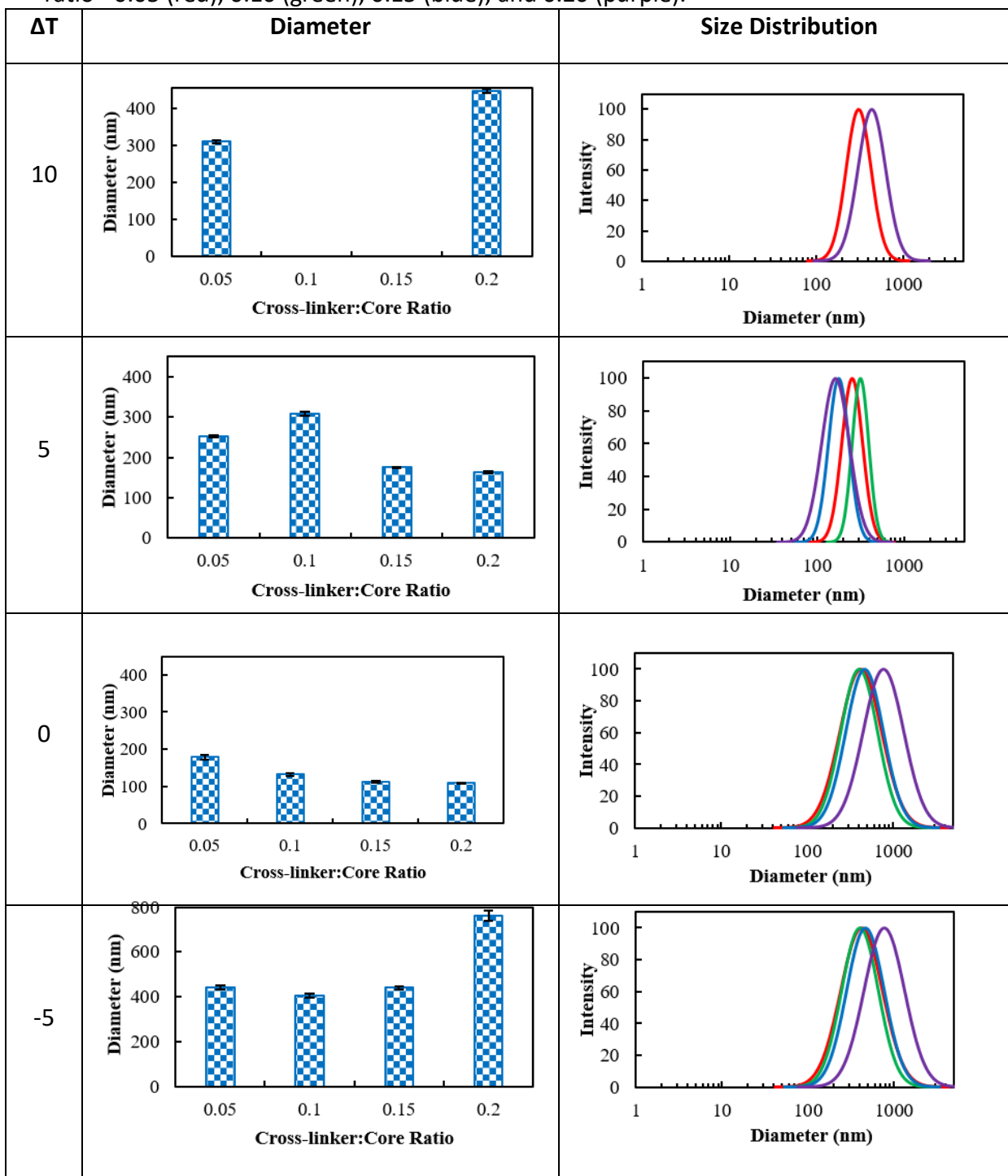


Table S4.4: Hydrodynamic diameters and size distributions of 0.5 wt% POA core nanogels. Size distributions are shown as a function of core:cross-linker pre-polymer ratio - 0.05 (red), 0.10 (green), 0.15 (blue), and 0.20 (purple).

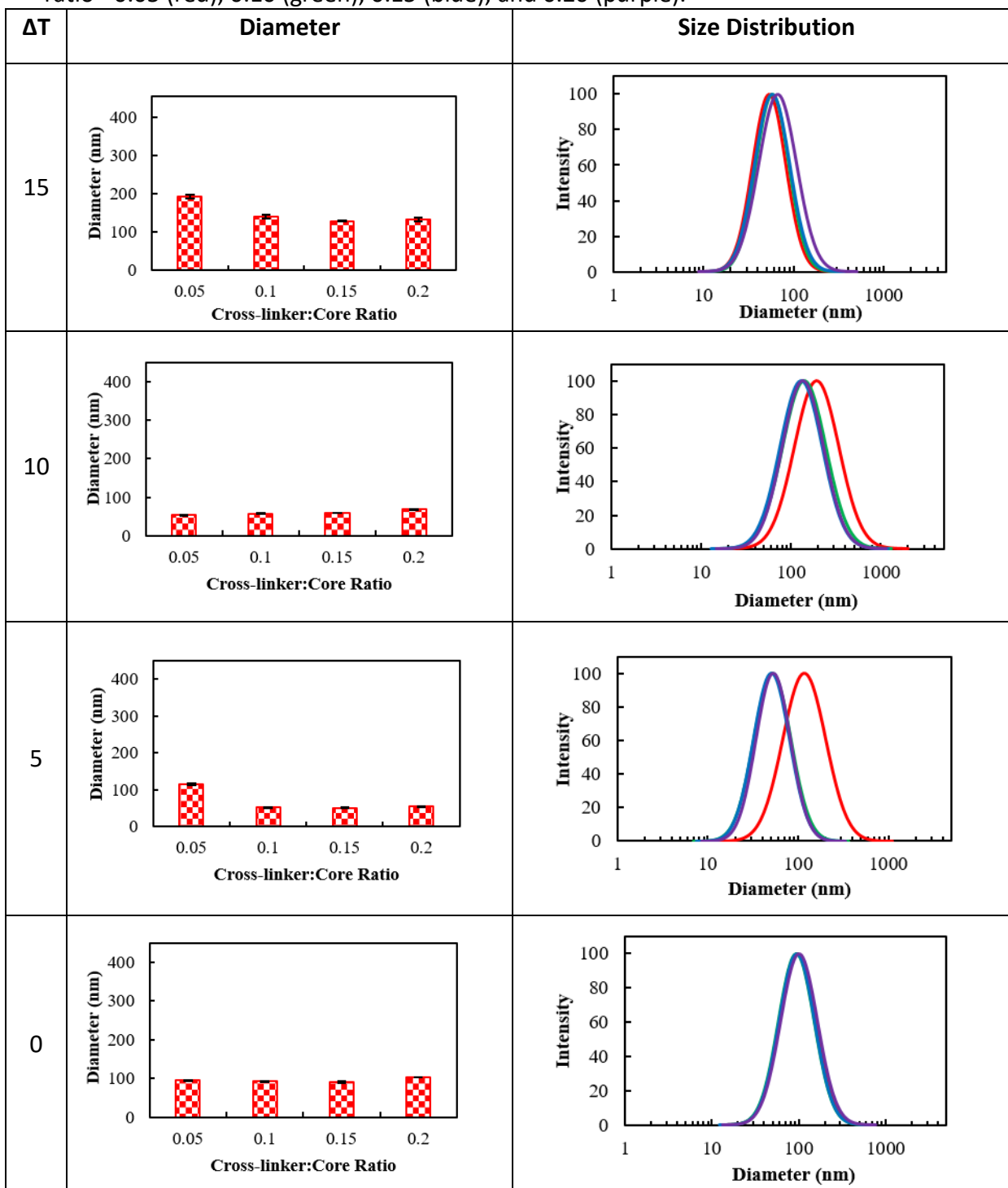


Table S4.5: Hydrodynamic diameters and size distributions of 1.0 wt% POH core nanogels. Size distributions are shown as a function of core:cross-linker pre-polymer ratio - 0.05 (red), 0.10 (green), 0.15 (blue), and 0.20 (purple).

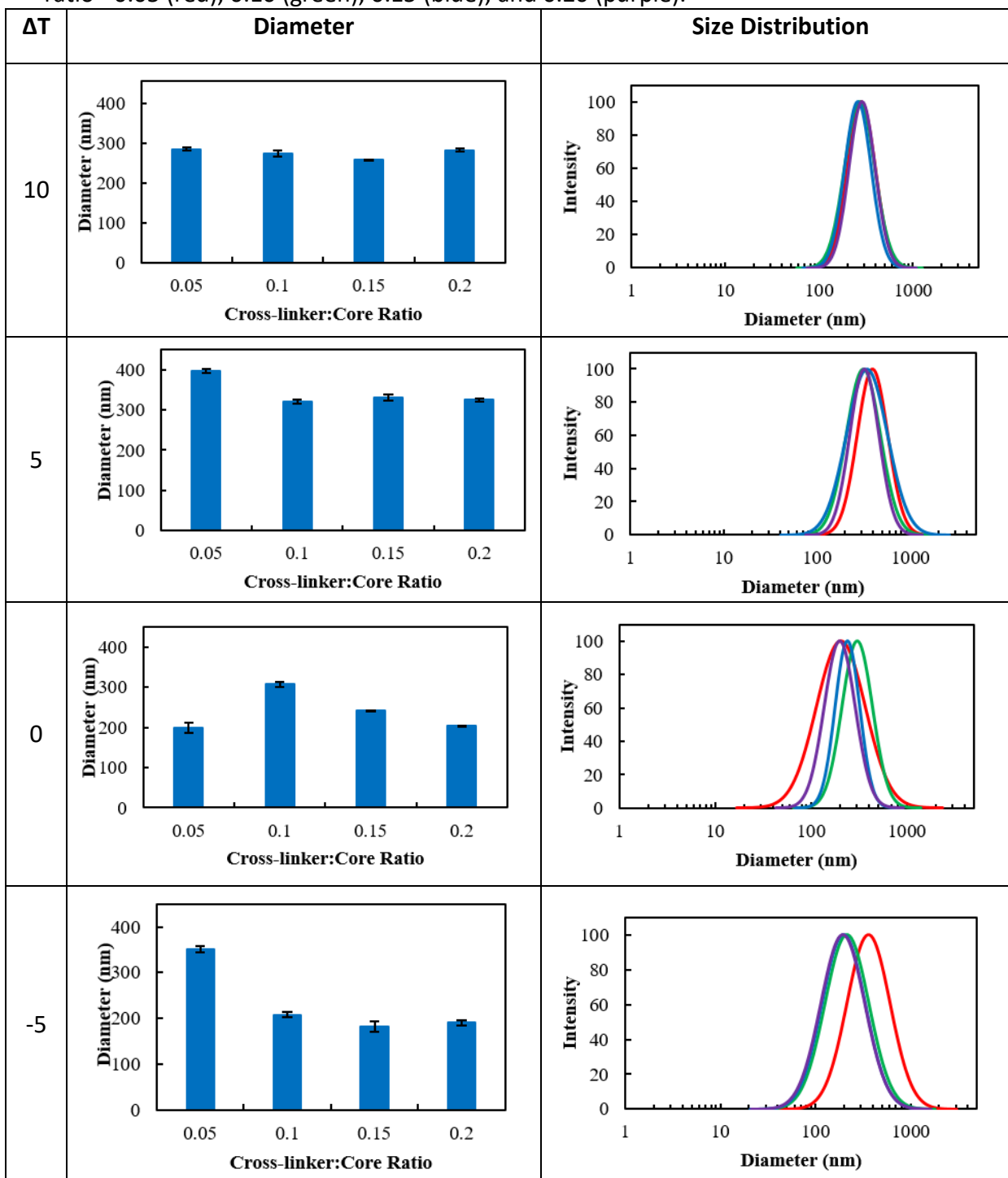
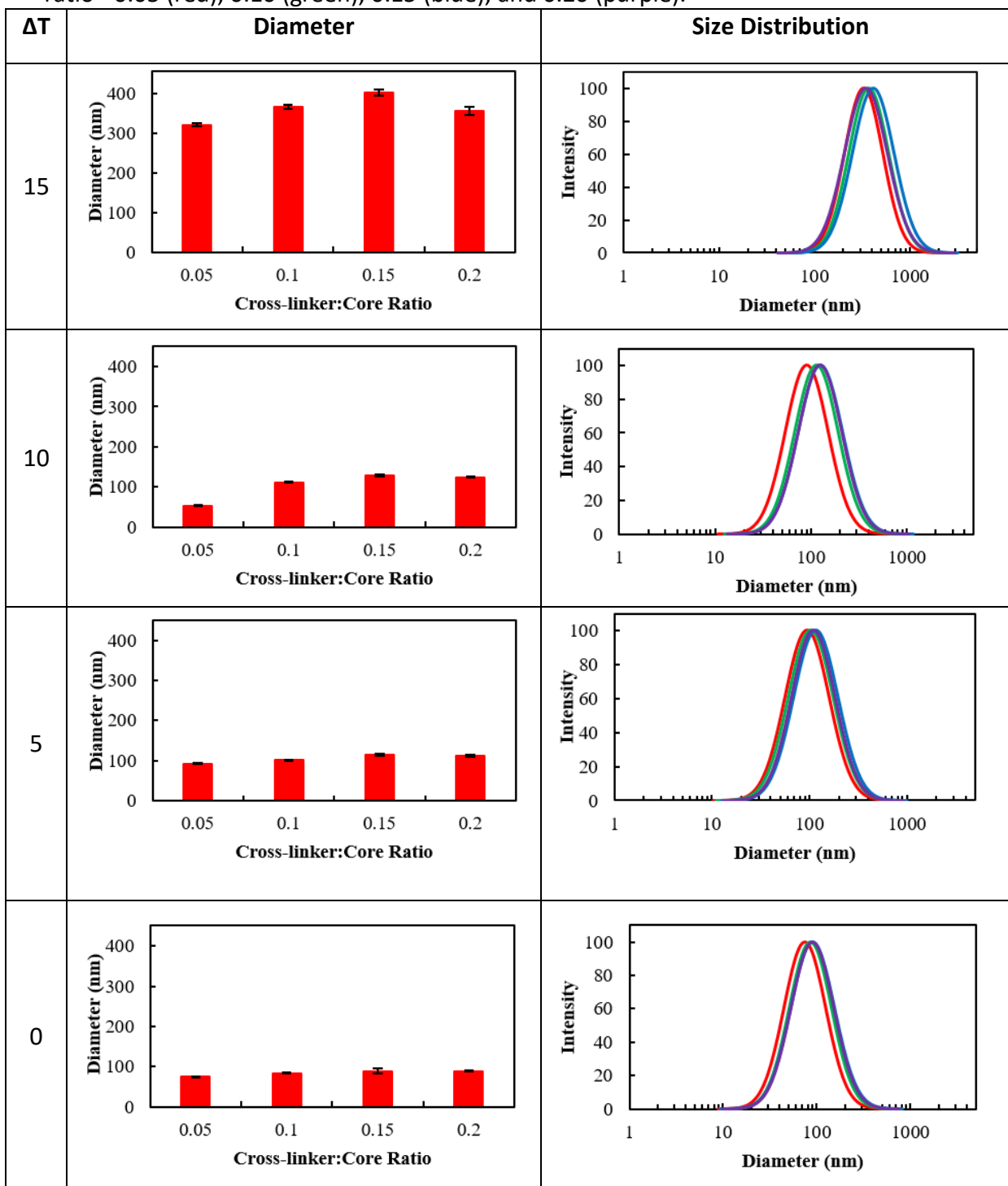


Table S4.6: Hydrodynamic diameters and size distributions of 1.0 wt% POA core nanogels. Size distributions are shown as a function of core:cross-linker pre-polymer ratio - 0.05 (red), 0.10 (green), 0.15 (blue), and 0.20 (purple).



S4.1.1 Optimization Using Multivariate Statistics

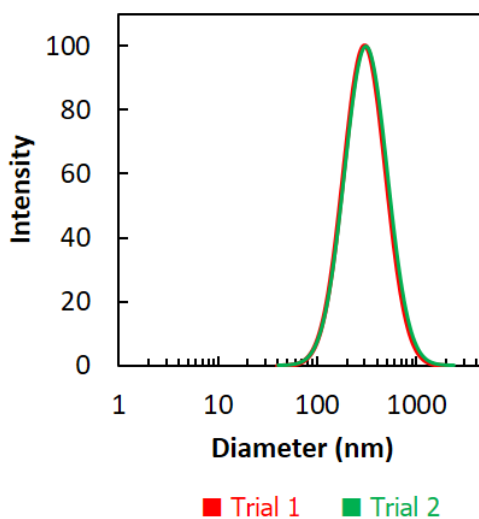
The key potential advantage of using latent variable models is the ability to optimize the input variables to reach a desired product quality. To apply this concept to our data, three new assembly conditions were identified by optimizing the model with three different objective functions: (1) minimize particle size (with a 1% weight on polydispersity control); (2) minimize polydispersity (with a 1% weight on particle size control); and (3) an optimal combination showing both low polydispersity and low particle sizes (with both variables equally weighted in the optimization protocol). Table S4.7 shows the optimal input levels determined by this procedure. Note that all these recipes include parameters that lie significantly outside the initially studied model space, particularly with regards to the core pre-polymer concentrations. Table S4.8 compares the predicted to actual nanogel diameter/polydispersity achieved with each recipe. Only the minimal polydispersity recipe yielded a colloidally stable nanogel, although reasonable correspondence in both polydispersity and particularly diameter was achieved between the model predicted and experimental diameter. Furthermore, the same properties can be achieved upon repeated assemblies (Figure S4.1). As such, while the strongly non-linear correlations within the data (as evidenced by the relative low $R^2 = 0.22$ of the latent variable model) limit the utility of model inversion to identify optimal assembly conditions, the model still has some degree of predictive value for identifying recipes that will yield targeted nanogel properties provided that the recipe leads to a colloidally stable nanogel.

Table S4.7: Optimized synthetic conditions to produce nanogel populations with desired size and population distributions.

Case	ΔT	Core Pre-Polymer Concentration (mg/mL)	POH:Total Polymer Ratio
Balanced	0.42	3.57	0.040
Minimize diameter	-5.0	9.11	0.055
Minimal polydispersity	15.0	4.31	0.979

Table S4.8: Comparison of predicted versus actual particle sizes and polydispersities of nanogels assembled using model-predicted optimal recipes for each optimization case studied.

	Predicted		Actual	
	Diameter (nm)	Polydispersity	Diameter (nm)	Polydispersity
Balanced	134 ± 2	0.29	Bulk Aggregation	
Minimize diameter	107 ± 1	0.30		
Minimize polydispersity	331 ± 9	0.21	306 ± 5	0.26 ± 0.03

**Figure S4.1: Logarithmic intensity-based size distributions of self-assembled nanogels prepared using the latent variable model-predicted synthetic conditions to minimize the overall polydispersity. Trial 1 is shown in red and trial 2 is shown in green.**

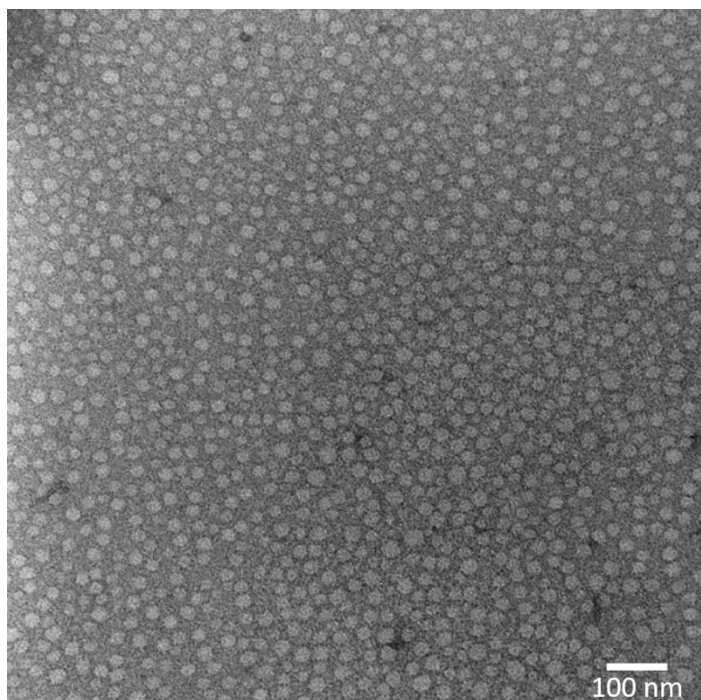


Figure S4.2: Transmission electron microscopy image (120 000 \times magnification) of self-assembled 1 wt% POH core/0.2 wt% POA cross-linked nanogels produced at 10 $^{\circ}$ C above the core polymer LCST. Nanogels are stained with 1% uranyl acetate. Note that the size of the nanogels via TEM is substantially smaller than the DLS values given the dehydration of the nanogels upon the preparation of the TEM samples. However, the nanogels appear highly spherical and relatively monodisperse, consistent with DLS data.

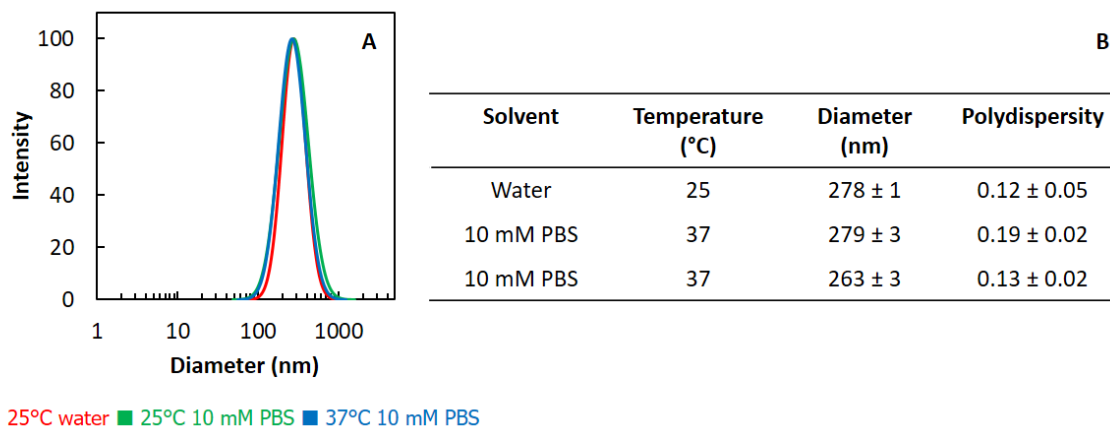


Figure S4.3: Nanogel particle size distributions measured using DLS (1 wt% POH core/0.2 wt% POA cross-linked nanogels produced at 10°C above the core polymer LCST): (A) Comparison of size distributions for nanogels measured at 25°C in water, 25°C in 10 mM PBS, and 37°C in 10 mM PBS; (B) Comparison of diameter and polydispersity under the same conditions. PBS = pH 7.4, 10 mM phosphate buffer, 0.15 M total ionic strength to mimic *in vivo* conditions.

Chapter 5 : Thermally Self-Assembled Poly(oligoethylene glycol methacrylate)-co-Poly(oligolactic acid methacrylate) Nanogels for the Intranasal Delivery of Olanzapine to the Brain

Madeline J. Simpson^a, Ana Arezina^a, Judy Tran^b, Ram K. Mishra^{b,c} and Todd Hoare^{a,c,*}

^a Department of Chemical Engineering, McMaster University, 1280 Main Street West, Hamilton, ON, L8S 4L7, Canada

^b Department of Psychiatry and Behavioural Neurosciences, McMaster University, 1200 Main Street West, Hamilton, ON, L8N 3Z5, Canada

^c School of Biomedical Engineering, McMaster University, 1280 Main Street West, Hamilton, ON, L8S 4K1, Canada

Keywords: self-assembly, nanogel, degradable, controlled release, olanzapine.

5.1 Abstract

The soft mechanics, chemically tunability, and low interfacial tension of nanogels offer promise for drug delivery; however, degradability and drug uptake remain key limitations to the delivery of hydrophobic drugs. Herein, hydrazone-cross-linked poly(oligoethylene glycol methacrylate) (POEGMA)-based nanogels containing hydrophobic domains derived from an oligo(lactic acid methacrylate) (OLAMA) comonomer are fabricated via the self-assembly of hydrazide and aldehyde-functionalized oligomers. The OLAMA domains act as a sink for the uptake of olanzapine (OLZ), a poorly-water soluble antipsychotic drug used to treat schizophrenia. Nanogel degradation in acidic conditions produces small polymer fragments that can be easily cleared in vivo, and both the nanogels and the degradation products show no significant toxicity to SH-SY5Y neuronal cells. The nanogel formulations load up to 10 wt% olanzapine and can be administered intranasally (IN), with a low dose of drug (2 mg OLZ/kg) showing prolonged (up to 48 hr) maintenance of pre-pulse inhibition in a rodent-model of schizophrenia. By administering a well-defined degradable nanogel with sustained olanzapine release kinetics, the frequency of therapeutic intervention and the associated metabolic side effects can both be significantly decreased, thus potentially improving patient compliance to this clinically-prescribed APD.

5.2 Introduction

Nanogels, three-dimensional networks of solvent-swollen cross-linked polymer, have the unique ability to rapidly swell in response to external stimuli.¹ The ability to tune the physiochemical properties of nanogels, including their composition, size, and cross-link density, can leverage their distinct properties to promote drug uptake and control release kinetics to design drug delivery systems.² However, due to the conventional synthetic routes employed, the majority of reported nanogels for drug delivery are limited in terms of their *in vivo* use given their lack of predictable degradability into well-defined degradation products over controllable degradation times.³ Novel approaches to promote degradability and enhance drug release have been proposed to exploit the stimuli-responsive nature of nanogels, primarily by incorporating labile moieties within the polymer matrix; for example, redox-responsive bonds such as disulfides can be cleaved by endogenous glutathione⁴⁻⁷ while acid-labile groups such as acetals,⁸ ketals,⁹⁻¹⁰ and esters¹¹ enable pH-dependent hydrolysis. Enzymatic degradation can also be facilitated *in vivo* by the use of peptide cross-linkers incorporating specific recognition sequences for proteolytic enzymes such as aspartic proteases (e.g. pepsin¹²), serine proteases (e.g. collagenase,¹³⁻¹⁴ elastase,¹⁵⁻¹⁶ trypsin,¹⁷ chymotrypsin^{15-16, 18} and plasmin¹⁹), or aminoproteases (e.g. thermolysin¹⁵⁻¹⁶), and/or utilizing biodegradable polymer backbones such as hyaluronic acid, which degrades in the presence of hyaluronidase²⁰⁻²¹. However, the use of many of these degradation approaches limits the

type of chemistry that can be used to fabricate the nanogel; furthermore, except in the case in which the backbone polymer is physiologically degradable, the degradation products of such nanogels are not well-defined, problematic for clinical translation.

In addition to this limitation regarding degradation, the high water content of nanogels limits their capacity to encapsulate hydrophobic molecules. To improve nanogel affinity for poorly-water soluble molecules, hydrophobic domains are typically introduced by copolymerization with specific monomers. Domains or grafts of poly(lactic acid)²², poly(lactic-co-glycolic acid) (PLGA),²³ and aromatic materials such as poly(valerolactone),²⁴ ulvan,²⁵ and 2-vinylanthraquinone²⁶ have all been used to facilitate the encapsulation of poorly-water soluble compounds. However, the low incorporation efficiency of these groups within the polymer chains leads to weak physical interactions, rendering it difficult to produce nanogels with controlled sizes. In addition, the lack of clear degradation/clearance pathways for the grafted hydrophobic moieties may cause accumulation and toxicity concerns *in vivo*. Alternately, exploitation of the thermoresponsive nature of poly(N-isopropylacrylamide) (PNIPAM)²⁷⁻²⁸ or oligo(ethylene glycol) derivatives²⁹⁻³⁰ that form more hydrophobic internal structures above their lower critical solution temperature can improve hydrophobic drug loading, although often at the cost of nanogel swellability and/or colloidal stability.³¹⁻³²

Developing an effective strategy for creating nanogels enabling good hydrophobic drug loading/release is particularly critical to the use of nanogels for the delivery of antipsychotic drugs (APDs), the majority of which are identified as class II drugs by the Biopharmaceutical Class System due to their low aqueous solubility.³³ Olanzapine (OLZ, 2-methyl-4-(4-methyl-1-piperazinyl)-10H-thieno[2,3-b][1,5]benzodiazepine) is a second generation atypical APD commonly prescribed to treat schizophrenia, a chronic and debilitating mental disorder that affects 1% of the global population.³⁴ Olanzapine has a unique pharmacological profile that offers relief from both positive and negative symptoms of schizophrenia³⁵ with minimal extrapyramidal side effects often experienced with first generation APDs.³⁶ However, olanzapine has dose-dependent negative metabolic effects, specifically weight gain, that can lead to elevated plasma glucose levels, hyperlipidemia, and insulin resistance causing type II diabetes,³⁷⁻³⁸ in particular, chronic oral dosing of olanzapine treatment produces inflammatory cytokine reactions in peripheral tissues that induce metabolic symptoms.³⁹⁻⁴² As such, administering olanzapine in a manner that avoids systemic circulation would be advantageous for preventing the non-specific interactions with off-target tissues causing negative side effects.

The intranasal (IN) route of delivery is able to provide direct nose-to brain transport by allowing drugs and/or nanomaterials to travel through the nasal epithelium and along the

olfactory or trigeminal nerves or extracellular pathways into the brain.⁴³⁻⁴⁴ IN administration has the advantage of rapid drug absorption and higher bioavailability due to the avoidance of hepatic first-pass metabolism and the highly selective blood-brain barrier, leading to faster onset of therapeutic action.⁴⁵ Strategies to exploit IN delivery of olanzapine have been explored using different nanomaterials such as Pluronic micelles,⁴⁶ PLGA nanoparticles,⁴⁷ lipid-based transfersomal vesicles,⁴⁸ mucoadhesive nanoemulsions,⁴⁹ chitosan nanoparticles,^{46, 50} and poly(ϵ -caprolactone) nanocapsules⁵¹. However, rapid *in vitro* drug release,⁵¹ dose-dependent toxicity towards nasal epithelial cells,⁵⁰ inflammation in the nasal cavity,⁴⁸ and a lack of long-term pharmacodynamics data⁴⁶⁻⁵¹ represent key limitations of existing nanoparticle delivery technologies for IN olanzapine delivery.

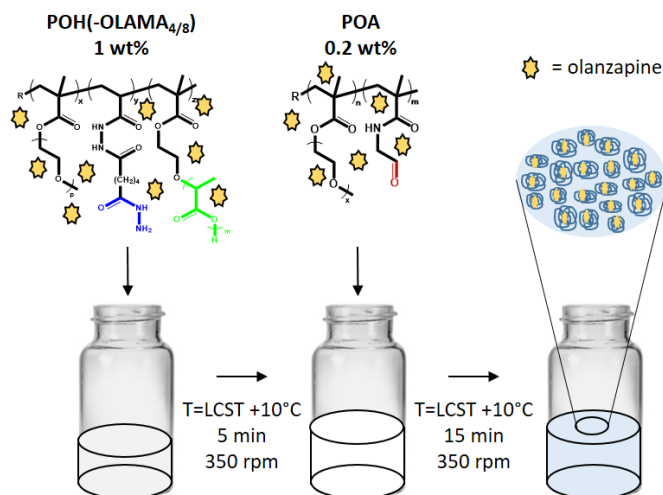
Our group has extensively studied the use of degradable hydrazone cross-linking within hydrogel systems more broadly to address the challenge of degradability. Well-defined polymers of PNIPAM⁵² or poly(oligo ethylene glycol methacrylate) (POEGMA)⁵³ functionalized with either aldehyde or hydrazide groups will spontaneously produce covalent hydrazone bonds upon mixing, creating hydrogels that remain stable for periods ranging from days to months depending on the storage conditions.⁵⁴ The cross-linking hydrazone bonds are hydrolytically labile and, upon degradation, will release the oligomeric polymer precursors,^{52, 55} which are designed to be below the renal molecular

weight cut-off (MWCO) limit⁵⁶ to ensure their clearance from the body. This approach reduces the variability in the degradation products observed from nanogels produced via standard free radical precipitation polymerization that can result in at least a fraction of non-clearable polymer product. By exploiting the unique thermoresponsive properties of both PNIPAM and POEGMA, we have more recently implemented this chemistry to fabricate nanogels using a rapid, scalable, thermally-driven self-assembly method to synthesize well-defined hydrazone-cross-linked nanogels (Scheme 5.1).⁵⁷⁻⁵⁹ We have demonstrated how varying the composition and conditions of the self-assembly method can affect both particle size and polydispersity, enabling the tunable design of nanogels suitable for drug-delivery.⁵⁹ However, as with most reported nanogels which typically have high water contents, the capacity of such self-assembled nanogels to deliver class II hydrophobic drugs such as olanzapine is inherently limited, requiring re-engineering of the nanogel composition (and, by extension, the precursor polymer composition) to enable improved hydrophobic drug uptake.

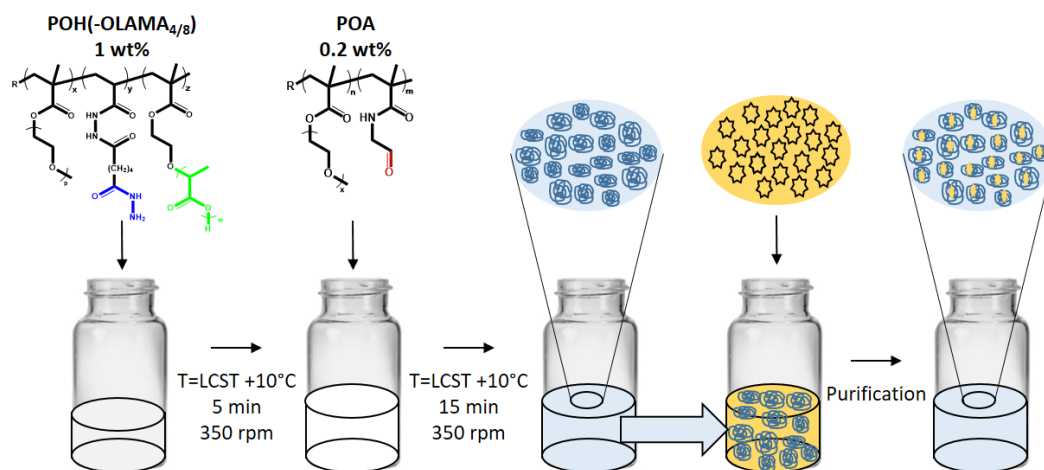
To address the poor nanogel affinity for poorly-water soluble therapeutics, herein we present a strategy to synthesize self-assembled POEGMA nanogels with hydrophobic domains based on the preparation of oligomeric precursor materials containing oligo(lactic acid) methacrylate (OLAMA). Copolymerization of OLAMA with different side chain lengths of oligo(lactic acid) into the POEGMA-based precursor polymers enables the

introduction of degradable hydrophobic self-assembly sites into the nanogel, resulting in colloidally stable nanogels that are chemically cross-linked through hydrazone bonds in addition to the physical interactions between the hydrophobic OLAMA side chains. The self-assembled OLAMA side chains create hydrophobic domains to promote hydrophobic drug uptake/release, while degradation is enabled over time due to hydrazone bond hydrolysis in the covalent cross-links as well as hydrolysis of the polymer side chains via both oligo(lactic acid) hydrolysis and ester group hydrolysis between the backbone and the oligo(ethylene glycol) side chains. We demonstrate that this approach leads to hydrophobized nanogels that retain the advantageous attributes of nanogels (swelling and deformation) while still facilitating the encapsulation of therapeutically-relevant quantities of olanzapine. The self-assembled nanogels can degrade under acidic conditions, while the nanogels and the precursor polymer/degradation products are not cytotoxic to SH-SY5Y neuronal cells. Finally, IN delivery of olanzapine-loaded nanogels provides prolonged therapeutic efficacy in a rodent model of schizophrenia, indicating the potential to enhance bioavailability, lower the dose and frequency of olanzapine administration, and ultimately lessen the metabolic side effects of this drug while improving patient compliance with this therapeutic regimen.

A. Direct Loading



B. Passive Diffusion



Scheme 5.1: Schematic of the self-assembly process and olanzapine loading strategies used to produce OLZ-loaded PEOGMA-POLAMA nanogels. (A) In the direct drug loading method, hydrazide-functionalized polymer (POH-OLAMA_{4/8}) is prepared in an olanzapine solution and heated to a temperature 10°C greater than the polymer LCST, followed by dropwise addition of the cross-linking aldehyde-functionalized polymer (POA) in an olanzapine solution to simultaneously form the nanogels via self-assembly and load drug in the formed hydrophobic domains. (B) In the passive diffusion loading method, self-assembly of the polymers occurs in DIW to first form the nanogels followed by an additional olanzapine loading step carried out by re-suspending the self-assembled nanogels in an olanzapine solution in ethanol. Both drug-loaded nanogels are then purified by centrifugation to create a drug-loaded degradable nanogel suspension.

5.3 Experimental

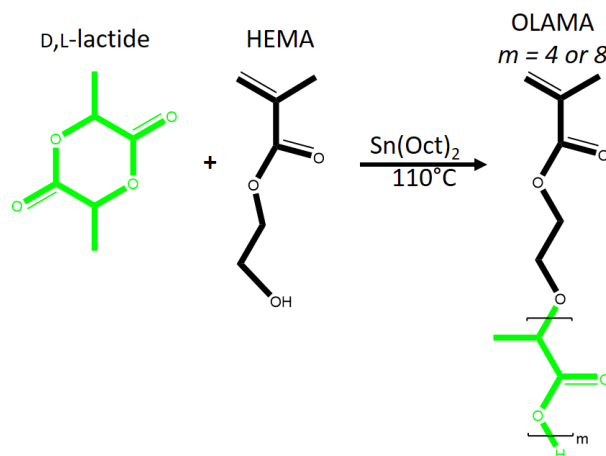
5.3.1 Materials

Diethylene glycol methacrylate (M(EO)₂MA, 2 EO repeats, 95%) and oligo(ethylene glycol) methyl ether methacrylate (OEGMA₄₇₅, 8-9 EO repeats) were purchased from Millipore Sigma (Oakville, ON, Canada) and purified to remove inhibitors using an aluminum oxide column. Acetonitrile (HPLC grade, Caledon Laboratory Chemicals, Georgetown, ON, Canada), acrylic acid (AA, 99%, Millipore Sigma), adipic acid dihydrazide (ADH, 97%, Alfa Aesar, Ottawa, ON, Canada), ammonium acetate (HPLC grade, Millipore Sigma) 2,2-azobisisobutyric acid dimethyl ester (AIBMe, Pure Chemistry Scientific Inc., Watertown, MA, USA), deuterated chloroform (CDCl₃, 99.9% atom D, Millipore Sigma), 3,6-dimethyl-1,4-dioxane-2,5-dione (D,L-lactide, 99%, Millipore Sigma), dizocilpine hydrogen maleate (MK-801, Millipore Sigma), ethanol (anhydrous, Greenfield Global, Brampton, ON, Canada), *N'*-ethyl-*N*-(3-dimethylaminopropyl)-carbodiimide (EDC, 99% AK Scientific, Union City, CA, USA), glacial acetic acid (Caledon Laboratory Chemical), 2-hydroxyethylmethacrylate (HEMA, ≥99%, Millipore Sigma), methanol (HPLC grade, Caledon Laboratory Chemicals), thioglycolic acid (TGA, ≥98%, Millipore Sigma), tin (II) 2-ethylhexanoate (Sn(Oct)₂, Millipore Sigma) and Tween 80 (Millipore Sigma) were all used as received. Olanzapine (OLZ, 99.16%, ApexBio), was purchased from Cedarlane (Burlington, ON, Canada). N-(2,2-dimethoxyethyl)methacrylamide (DMEMAm) was synthesized according to previous reports.⁵³ Deionized water (DIW) (18.2 MΩ cm

resistivity) purified using the Millipore Simplicity System (Millipore, Bedford, USA) was used in all experiments. All other reagents used were analytical grade and were not purified before use.

5.3.2 Synthesis of oligo(lactic acid methacrylate)

Oligo(lactic acid methacrylate) macromonomers with $m=4$ and 8 lactic acid repeat units were synthesized according to the procedure developed by Ishimoto *et al.*⁶⁰ Briefly, a 100 mL round bottom flask containing a stir bar was flamed dried under vacuum and then purged with nitrogen. This cycle was repeated three times. D,L-lactide ($m=4$, 5 g or $m=8$, 10 g) was placed in the flask and dried under vacuum for one hour. HEMA (2.1 mL) and Sn(Oct)₂ (32 μ L) were added to the flask and purged with nitrogen gas for 30 minutes. Following, the flask was heated to 110°C, and the reaction was allowed to proceed for 3 hours (Scheme 5.2). The flask was then removed from the oil bath and allowed to cool, after which the product was dissolved in 50 mL chloroform and added to a separation funnel together with 50 mL of 1 M HCl to extract the impurities from the product. The bottom organic phase was collected, while the aqueous phase was extracted twice more with chloroform (collecting the bottom organic layer each time). The organic phase was further rinsed once with brine solution, after which MgSO₄ was added to remove any residual water. Excess chloroform was removed using rotary evaporation, and the final product was vacuum dried overnight and stored at 4°C.

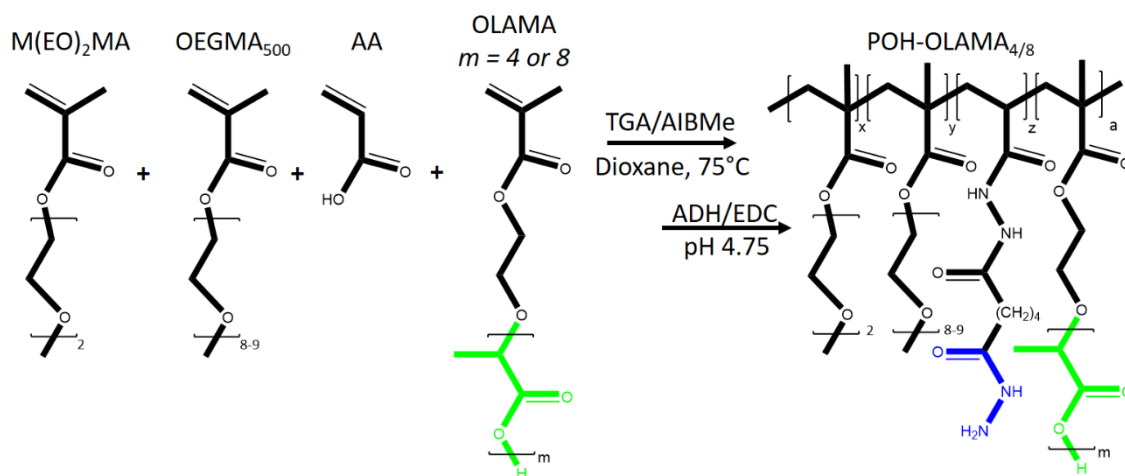


Scheme 5.2: Synthesis of oligo(lactic acid methacrylate) (OLAMA) via ring opening polymerization of D,L-lactide catalyzed by tin (II) ethylhexanoate in the presence of 2-hydroxyethyl methacrylate (HEMA).

5.3.3 Synthesis of hydrazide-functionalized POEGMA (POH)

POH was synthesized according to the protocol developed by our group.⁵⁵ AIBMe (39 mg), M(EO)₂MA (1.9 g), OEGMA₄₇₅ (2.1 g), acrylic acid (560 μL) and 10% TGA in dioxane (75 μL) were dissolved in 20 mL of dioxane and placed into a 100 mL single neck round bottom flask. The flask was purged with nitrogen (minimum 30 minutes) and heated to 75°C under magnetic stirring (350 rpm). Following the four hour polymerization reaction, the dioxane was removed using rotary evaporation and the intermediate polymer product was re-dissolved in 100 mL of DIW. Carboxylic acid groups were subsequently converted to hydrazide groups by conjugating a 5 \times molar excess of adipic acid dihydrazide (4.9 g) using carbodiimide chemistry (EDC, 1.9 g) while maintaining the pH of the reaction at 4.75 with 1 M HCl (Scheme 5.3). The polymer solution was then placed in 3.5-5 kDa MW cut-off

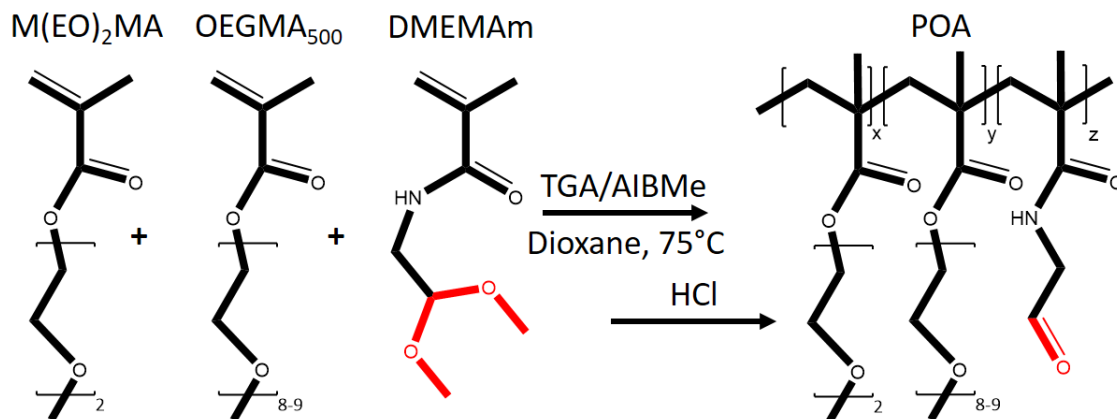
(MWCO) membranes for dialysis against DIW (six cycles of six hours each) to produce the final purified product. The product was lyophilized and then dissolved in DIW using magnetic stirring to create a 20 wt% solution. The polymer solution was finally filtered using a 0.2 μm syringe filter and stored at 4°C. The final polymer concentration in the solution was determined using gravimetric analysis. To confirm the conversion of carboxylic acid groups to hydrazide groups, the intermediate (carboxylated) product and the final product were both analyzed via conductometric titration using 0.1 M NaOH as the titrant. A similar protocol was followed to synthesize hydrazide-functionalized POEGMA incorporating a theoretical 20 mol% of OLAMA ($m=4$, 2.4 g or $m=8$, 4 g, with all other masses kept constant) (Table S5.1).⁶¹



Scheme 5.3: Free radical polymerization of POH-OLAMA_{4/8}. Polymerization of M(EO)₂MA, OEGMA₅₀₀, AA, and OLAMA₄ or OLAMA₈, and subsequent functionalization with ADH using EDC-mediated chemistry post-synthesis produces POH-OLAMA_{4/8}.

5.3.4 Synthesis of aldehyde-functionalized POEGMA (POA)

A detailed synthetic protocol for the synthesis of aldehyde-functional POEGMA has been previously reported by our group.⁵⁵ Briefly, AIBMe (50 mg), M(EO)₂MA (3.1 g), OEGMA₄₇₅ (0.9 g), DMEMAm (1.3 g) and 75 μ L of a 10% solution of TGA in dioxane were dissolved in 20 mL of dioxane and added to a 100 mL single-neck round bottom flask. The contents of the flask were stirred at 350 rpm and purged with nitrogen for a minimum of 30 minutes while an oil bath was heated to 75°C. The stirred flask was placed into the heated oil bath and maintained under nitrogen for the duration of the four hour reaction. The dioxane was subsequently removed using rotary evaporation. The isolated product was then dissolved in 100 mL of 0.25 M HCl and stirred for 24 hours to convert the acetal groups to aldehydes (Scheme 5.4). The polymer was purified using dialysis as described above and then similarly lyophilized, re-dissolved in DIW, filtered and stored at 4°C. ¹H NMR was performed using Bruker AV700 in CDCl₃ to confirm the degree of functionalization. The final polymer concentration was determined using gravimetric analysis.



Scheme 5.4: Free radical polymerization of POA. Polymerization of M(EO)₂MA, OEGMA₅₀₀, DMEMAm, and subsequent acidic hydrolysis post-synthesis produces POA.

5.3.5 Polymer characterization

To determine the composition of the final products, the polymers were dissolved in CDCl₃ and analyzed using ¹H NMR (Bruker AVANCE 600 MHz spectrometer). Molecular weight was assessed via gel permeation chromatography (GPC) using a Polymer Laboratories PL-50 Integrated GPC System equipped with a Phenomenex Phenogel Linear LC column (300 × 4.6 mm, 5 μm) operating at room temperature and using 50 mM LiBr in DMF as the eluent. The GPC system was calibrated using PEG standards from Polymer Laboratories. The samples were injected into the GPC through a 0.2 μm PTFE filter. To determine the lower critical solution temperature (LCST) of the polymers, 1 wt% solutions were prepared in DIW and placed in two-sided clear quartz cuvettes. Using a Varian Cary 100 UV-Visible spectrophotometer equipped with a circulating temperature bath, the absorbance was measured at 500 nm by ramping the temperature at 1°C/min and recording data at 0.5°C

intervals from 20-85°C. The absorbance measurements were subsequently converted to transmittance values, and the onset LCST was identified as the temperature at which the transmittance of the polymer samples fell below 95%.

5.3.6 Nanogel self-assembly

Nanogel self-assembly was carried out according to the optimized method previously described by our group and shown in Scheme 5.1.⁵⁹ Briefly, a 1 wt% solution of the hydrazide (POH or POH-OLAMA_{4/8}) core polymer was prepared in DIW and aliquoted in 5 mL volumes into 20 mL glass vials containing a stir bar. An oil bath was pre-heated to a temperature 10°C greater than the pre-determined LCST of the core polymer, after which the glass vials containing the hydrazide polymer were placed in the oil bath and incubated for 5 min under magnetic stirring at 350 rpm. The complementary cross-linking POA polymer was prepared at a concentration of 0.2 wt% in DIW, and 1.5 mL aliquots were added dropwise (~30 s) to each vial containing the pre-heated core polymer. The solutions were stirred for an additional 15 min and then removed from the oil bath. The nanogel suspensions (POH core=P0 nanogel, POH-OLAMA₄ core=P4 nanogel or POH-OLAMA₈ core=P8 nanogel) were allowed to cool to room temperature and then stored at 4°C.

5.3.7 Nanogel characterization

Dynamic light scattering (DLS) measurements were carried out using a Brookhaven NanoBrook 90Plus particle analyzer operating BIC Particle Solutions Software (Version 2.6, Brookhaven Instruments Corporation). Scattering was detected using a 659 nm laser at a 90° angle. Nanogel suspensions were diluted to 1 mg/mL in 10 mM phosphate buffered saline (PBS), producing a count rate of ~500-600 kcps at 25°C. Each sample was measured 5 times for 2 min; the average effective hydrodynamic diameter from the intensity-weighted particle size distribution plus/minus one standard deviation is reported. Electrophoretic mobility measurements were carried out using the phase analysis light scattering (PALS) mode of the ZetaPlus zeta potential analyzer.

5.3.8 *In vitro* degradation of nanogels

Nanogel degradation was monitored under acidic conditions to characterize the extent of degradation and the degradation products. A 1 mg/mL solution of nanogel (P0, P4 or P8) was prepared in either 100 mM HCl (pH 1) or 100 mM acetate buffer (pH 4.5). Nanogel diameter and count rate was monitored as function of time using DLS (configured as above). Prior to the first measurement, the laser intensity was maximized and maintained constant throughout the entire experiment; measurements were taken for 2 minutes every 15 minutes for a total of 12 hours. After 24 h, each sample was measured using nanoparticle tracking analysis (NTA) with a Malvern NanoSight LS10 instrument (Version

3.2, NTA software). These samples were then lyophilised and re-suspended in DMF for GPC analysis using the system described above.

5.3.9 Determination of olanzapine loading

Olanzapine uptake was evaluated using two methods; (1) direct loading during the self-assembly process (Scheme 5.1A) and (2) passive diffusion in an additional step post-nanogel synthesis (Scheme 5.1B). In the case of direct loading, olanzapine was first dissolved in DIW at a concentration of 94 µg/mL (aqueous solubility limit) and placed on a shaker for 1 hour. The POH(-OLAMA_{4/8}) core solution and POA cross-linking solutions were prepared by diluting the stock polymers with the OLZ solution to 1 wt% and 0.2 wt% respectively. The self-assembly process was carried out as described above, and the nanogel suspensions were cooled to room temperature (~1 hour). Triplicate 1 mL aliquots were taken from each sample and centrifuged at 20°C for 10 min at 18 000 rpm in an Allegra 64R centrifuge (Beckman Coulter). The supernatant from each sample was collected, filtered through a 0.2 µm PTFE syringe filter, and analyzed using HPLC (described below) to detect the total amount of unloaded (residual) drug; the remainder of the drug was determined to be encapsulated.

For olanzapine loading using passive diffusion, nanogels were first synthesized in DIW as described above, with triplicate 1 mL aliquots taken from each sample and centrifuged as

above. Olanzapine was dissolved in anhydrous ethanol at a concentration of 2 mg/mL, after which the nanogel pellets following centrifugation were re-suspended in 1 mL of the OLZ/ethanol solution and placed on a shaker for 24 hours. The nanogels were then centrifuged and the supernatant was collected and filtered as above for HPLC analysis of unloaded residual drug.

A Waters HPLC system equipped with a Waters 2695 separation model (Model SM4), a Waters 2489 ultraviolet detector (Model 246) operating at 254 nm and a Phenomenex C18 column (150 × 4 mm, 5 µm) was used for the detection of olanzapine. The mobile phase, consisting of 10 mM ammonium acetate:methanol:acetonitrile:acetic acid (57.2:22:20:0.8), was run at a flow rate of 1 mL/min with a sample injection volume of 10 µL. Drug loading was quantified by the drug loading capacity (DLC, Equation 5.1) and the encapsulation efficiency (EE, Equation 5.2):

$$\text{Drug Loading Capacity} = \frac{\text{Mass of drug loaded}}{\text{Total nanogel mass}} \times 100\% \quad (5.1)$$

$$\text{Encapsulation Efficiency} = \frac{\text{Mass of drug loaded}}{\text{Mass of total drug added}} \times 100\% \quad (5.2)$$

5.3.10 *In vitro* release of olanzapine

Olanzapine release from each nanogel formulation (P0, P4, P8) was assessed using two different aqueous conditions to examine drug release kinetics under different physiologically-relevant conditions. Olanzapine loading was carried out using passive

diffusion as described above, after which a 1 mL aliquot of nanogel was diluted to contain 325 µg olanzapine and placed in the membrane of a 20 kDa MWCO Spectra-Por Float-A-Lyzer G2 dialysis system. The membrane was then submerged in 5 mL of either: (1) 10 mM phosphate buffered saline (PBS), pH 7.4; or (2) 100 mM acetate buffer, pH 4.5 (simulating lysosomal pH). The samples were placed in a shaking incubator (100 rpm) at 37°C. At specific time points (1, 2, 4, 12 and 24 hours, followed by daily sampling over the next 13 days), 3 mL of the release solution was collected and replaced with fresh solution. The collected solution was filtered through 0.2 µm PTFE syringe filters and analyzed using HPLC. Release of free olanzapine (no nanogel) was also monitored under the same conditions.

5.3.11 *In vitro* cytotoxicity

SH-SY5Y neuronal cells were cultured using Dulbecco's Modified Eagle Medium/Nutrient Mix F-12 (DMEM F-12, Invitrogen Canada) supplemented with 10% fetal bovine serum (FBS, Gibco), 1% L-glutamine (Gibco) and 1% penicillin/streptomycin (Gibco) to create proliferation media. The cytocompatibility of SH-SY5Y cells with precursor polymers/degradation products, nanogels, and OLZ-loaded nanogels was assessed using a thiazolyl blue tetrazolium bromide (MTT) assay. SH-SY5Y cells were seeded in proliferation media at a concentration of 4×10^4 cells/well in 96-well polystyrene plates for 24 hr. Cells were subsequently treated with polymer formulations ranging in

concentration from 0.1 to 1 mg/mL for an additional 24 hr. MTT reagent was then applied and incubated with the cells for 3 hr. The concentration of solubilized formazan product was measured using a wavelength of 570 nm using a Synergy 4 BioTek plate reader. Cell viability was calculated by the ratio of the measured absorbance of the polymer samples to the measured absorbance of the cell-only control.

5.3.12 *In vivo* behavioural evaluation of pre-pulse inhibition

Animal procurement and care was conducted in compliance with the Canadian Council on Animal Care, and all housing/testing procedures were approved by McMaster University's Animal Research Ethics Board (Animal Utilization Protocol 18-06-27). Eighteen male Sprague-Dawley rats weighing between 250-300 g were procured from Charles River. The rats were housed in pairs with *ad libitum* access to food and water and were maintained on a reverse 12/12 light/dark cycle.

Prior to testing, animals were randomly divided into three groups (n=6/group) corresponding to the nanogel formulation each rat received: (1) P0; (2) P4; or (3) P8. Rats were dosed with 2 mg/kg olanzapine intranasally, adjusting the nanogel concentration as required (based on the DLC of each nanogel) to achieve the desired dose; control studies were conducted using saline and/or non-drug loaded nanogels at concentrations equivalent to the amount required to administer 2 mg OLZ/kg. Intranasal administration

was performed on rats lightly anesthetized with isoflurane. The first dose was administered by applying 30 μ L of solution to each nostril. The rat was then returned to anesthetic chamber for ~1 minute, after which a second dose of 30 μ L per nostril was then applied (resulting in a total of 120 μ L of solution being administered to the nose). Rats were maintained under anesthesia for <5 minutes in each case, after which they were placed in an empty chamber to safely recover before being returned to their home cage.

The therapeutic efficacy of the olanzapine-loaded nanogels was evaluated by assessing rodent startle response using a pre-pulse inhibition (PPI) test. Startle response was measured using the SR-Lab Startle Response System from San Diego Instruments. All rats were habituated to the testing chambers prior to any dosing. Prior to PPI testing, 0.35 mg/kg MK-801 was dosed using an intraperitoneal (IP) injection (saline was used for control studies) to induce schizophrenia-like behavior. After a 15 minute period to allow for MK-801 model induction, PPI testing was started using a five minute acclimatization period with 65 dB background noise. Next, five startle pulses (120 dB) were presented to all groups. Subsequently, 65 random trials of either (1) no pulse (0 dB), (2) startle pulse (120 dB); (3) a pre-pulse (68, 71 or 77 dB) 100 ms prior to a 120 dB startle pulse or, (4) one of the three pre-pulse stimuli only (no startle pulse) were presented, with the time between the trials ranging from 10-20 s. The testing concluded with five 120 dB startle pulses. Startle response was measured every 1 ms for 100 ms after the stimulus. PPI (%)

is calculated using Equation 5.3, where P is the average response for the pre-pulse/startle pulse trials and S is the average response magnitude to the startle-only trials:

$$PPI(\%) = \left[1 - \left(\frac{P}{S} \right) \right] \times 100 \% \quad (5.3)$$

PPI tests were conducted at 1, 3, 6, 24 and 48 hr post-IN olanzapine administration to assess the long-term efficacy of nanogel-mediated OLZ delivery on reversing schizophrenia symptoms.

5.4 Results and Discussion

5.4.1 Synthesis and physiochemical characterization of POEGMA polymers

The synthesis of methacrylated oligo(D,L-lactide) monomers (OLAMA_m) was carried out by performing a HEMA-initiated Sn-catalyzed ring-opening polymerization of D,L-lactide. The number of lactic acid units per monomer (m) was controlled by the ratio of D,L-lactide to HEMA.⁶⁰ Two macromonomers with different chain lengths of D,L-lactide were synthesized: OLAMA₄ (average of 4 repeat units of D,L-lactide) and OLAMA₈ (average of 8 repeat units of D,L-lactide).

Free radical copolymerization of one OLAMA monomer with oligo(ethylene glycol methacrylate) monomers with varying ethylene glycol side chain lengths (M(EO)₂MA $n=2$ or OEGMA₄₇₅ $n=8-9$) and one additional functional monomer to enable hydrazide (AA) or

aldehyde (DMEMAm) functionalization was employed to synthesize thermoresponsive POEGMA precursor polymers. The short:long side chain ratio of each POEGMA polymer was selected to ensure that all polymers exhibited a detectable lower critical solution temperature (LCST) greater than room temperature, as this is a crucial characteristic to carry out the self-assembly reaction. Lutz previously demonstrated how increasing the mole fraction of the long-chain OEGMA₄₇₅ increases the LCST of POEGMA polymers from 28°C (all M(EO)₂MA) to 90°C (all OEGMA₄₇₅);⁶² subsequent work from our group has demonstrated how copolymerizing OEGMA monomers with AA and subsequently modifying the carboxylic acid group to a hydrazide significantly increases the measured LCST by ~25-30°C, with the all OEGMA₄₇₅ hydrazide polymer showing no detectable LCST in water.⁵⁵ Incorporating up to 30 mol% OLAMA_{4/8} in PO₁₀₀H₃₀ polymers did not display a LCST up to 80°C,⁶¹ requiring the use of a M(EO)₂MA/OEGMA₄₇₅ copolymer to enable nanogel self-assembly. Synthesis of PO₃₀H₃₀ (POH, 30 mol% OEGMA₄₇₅ and 70 mol% M(EO)₂MA) yielded a polymer with a LCST of 81°C; incorporation of 20 mol% of either OLAMA₄ or OLAMA₈, a mole fraction hypothesized to introduce significant hydrophobicity into the nanogel while maintaining the water solubility of the precursor polymer, lowered the LCST to 69°C (POH-OLAMA₄) or 65°C (POH-OLAMA₈) respectively (Figure 5.1), enabling nanogel self-assembly at temperatures <80°C in water.

The aldehyde-functionalized POEGMA polymer was synthesized by copolymerizing OEGMA monomers with an acetal containing monomer (DMEMAm) that is converted to an aldehyde post-synthesis via acid-catalyzed hydrolysis. A ratio of 90:10 M(EO)₂MA:OEGMA₄₇₅ with 30 mol% aldehyde (POA) was selected for this polymer to ensure the LCST (54°C) is much lower than the hydrazide polymers, which is important for the self-assembly reaction (Figure 5.1). All precursor polymers have a number-average molecular weight <25 kDa, which is sufficiently lower than the renal clearance limit of 50 kDa to enable polymer clearance upon degradation *in vivo* (Table 5.1).⁵⁶

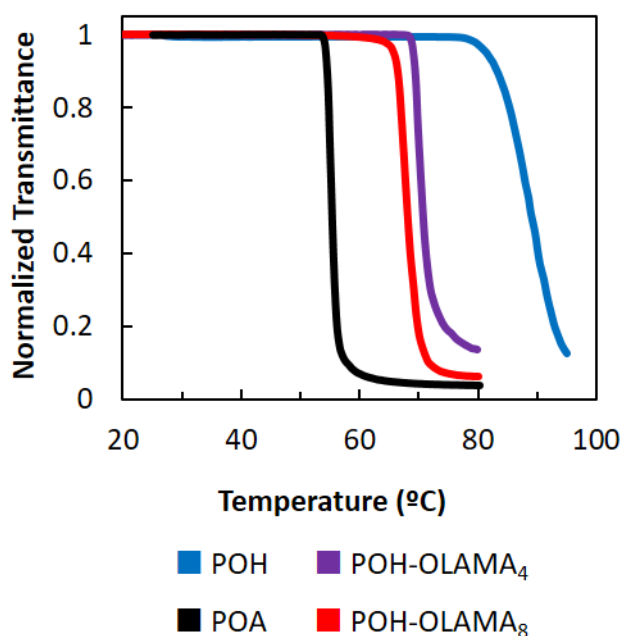


Figure 5.1: Lower critical solution behaviour of nanogel precursor polymers. 1 wt% POA (aldehyde-functionalized POEGMA) (black), POH (hydrazide-functionalized POEGMA) (blue), POH-OLAMA₄ (hydrazide functionalized POEGMA with 20 mol% OLAMA₄) (purple), and POH-OLAMA₈ (hydrazide functionalized POEGMA with 20 mol% OLAMA₈) (red) polymer solutions in DIW.

Table 5.1: Physiochemical properties of linear POEGMA polymers.

Polymer	M(EO) ₂ MA: OEGMA ₅₀₀	Functional group mol %	OLAMA m	M _n (kDa) ^a	Đ ^a	LCST (°C) ^b
POH	70:30	NH ₂ 30%	-	22	2.6	81
POH-OLAMA ₄	70:30	NH ₂ 30%	4	14	2.6	69
POH-OLAMA ₈	70:30	NH ₂ 30%	8	18	2.5	65
POA	90:10	CHO 30%	-	23	2.4	54

^a Determined from DMF GPC calibrated with PEG standards.

^b Measured using UV-vis spectrophotometry at 500 nm in DIW.

5.4.2 Nanogel self-assembly and characterization

Nanogel self-assembly was carried out using the step-wise process previously described and shown in Scheme 5.1.⁵⁸⁻⁵⁹ A precursor POH solution was stirred and heated at a temperature 10°C higher than the polymer LCST; this ensures complete collapse of the polymer chain to form the core nanoaggregate (Figure 5.1). The nanogel was then cross-linked via hydrazone bonds upon the addition of the aldehyde-containing polymer (POA). The selection of the POH polymer as the core polymer and POA as the cross-linker is based on previous studies that indicated the higher polarity of the POH polymers (improving the colloidal stability of the nanoaggregate) coupled with the lower LCST of POA (ensuring rapid deposition of POA on the POH nanoaggregates) aids in producing monodisperse nanogel populations.⁵⁹ In addition, the core POH polymer is present at 5× excess to the cross-linking POA polymer, ensuring the consumption of the vast majority of aldehyde

groups that can interact with proteins and cellular membrane components to induce inflammation.⁶³⁻⁶⁴

Three self-assembled nanogel formulations were developed and characterized: P0 nanogel (POH core); P4 nanogel (POH-OLAMA₄ core) and P8 nanogel (POH-OLAMA₈ core) (Figure 5.2). Table 5.2 shows the effective diameter, polydispersity and electrophoretic mobility of all nanogel formulations measured in 10 mM PBS. The P0 nanogels have the largest diameter (~250 nm), consistent with the high hydrophilicity of the brush PEG side chains; introducing OLAMA into the hydrazide-functionalized polymer results in smaller nanogels consistent with the formation of hydrophobic domains inside the nanogel due to physical cross-linking between the hydrophobic OLAMA side-chains, leading to higher compaction of the initial nanoaggregate. Increasing the chain length of the OLAMA (from 4 to 8) further decreases the nanogel diameter due to the stronger hydrophobic interactions between the longer OLAMA side-chains. The particle size distribution shown in Figure 5.2 is relatively narrow (consistent with the relatively low polydispersities observed, $0.07 < PD < 0.16$), while the electrophoretic mobility of all nanogels is near-neutral, as expected given that there are no charged groups incorporated into the nanogels.

Table 5.2: Dynamic light scattering (hydrodynamic diameter/polydispersity) and phase analysis light scattering (electrophoretic mobility) measurements of self-assembled nanogels. Nanogels were prepared with different core polymers and measured in 10 mM PBS, pH 7.4 ($n=5 \pm$ one standard deviation).

Nanogel	Core Polymer	Effective Diameter (nm)	Polydispersity	Mobility (μ/s)/(V/cm)
P0	POH	254 ± 6^a	0.07 ± 0.04	-0.18 ± 0.42
P4	POH-OLAMA ₄	$211 \pm 4^{a,b}$	0.16 ± 0.04	-0.38 ± 0.39
P8	POH-OLAMA ₈	$196 \pm 5^{a,b}$	0.15 ± 0.03	-0.47 ± 0.25

^a $p < 0.0001$ from one-way ANOVA with Tukey post-hoc test

^b $p < 0.001$ from one-way ANOVA with Tukey post-hoc test

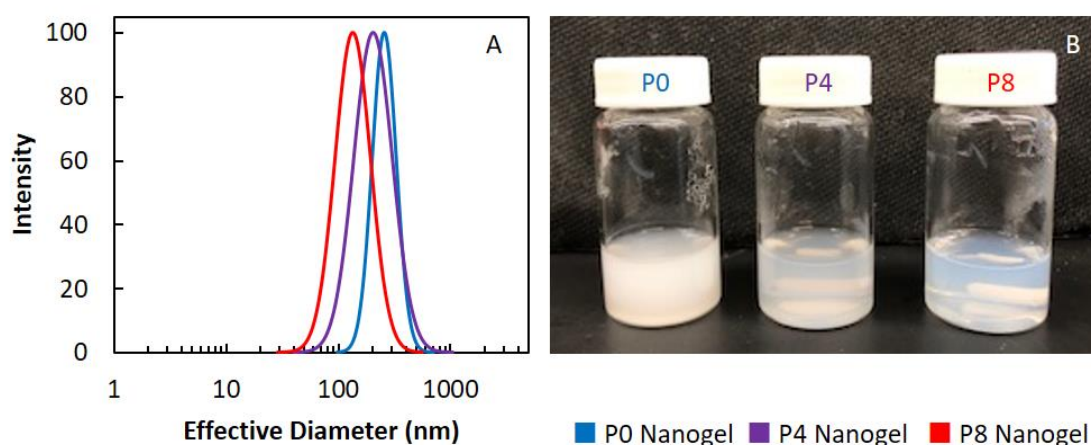


Figure 5.2: Physicochemical properties of self-assembled nanogels. (A) Logarithmic intensity-based size distribution (from DLS) of self-assembled nanogels prepared with different core hydrazide polymers, and (B) image of self-assembled nanogel solutions post-synthesis at room temperature. POH core=P0 nanogel, POH-OLAMA₄ core=P4 nanogel and POH-OLAMA₈ core=P8 nanogel.

5.4.3 Nanogel degradation

The self-assembled nanogels fabricated in this study can degrade in multiple ways: (1) hydrolytic cleavage of the cross-linking hydrazone bond to regenerate the initial PEOGMA

precursor polymers (whose molecular weight is maintained below the MWCO limit for renal clearance, Table 5.1); or (2) hydrolytic cleavage of the brush side chains of PEG and lactic acid via hydrolysis of the linking ester bonds.⁶⁵⁻⁶⁶ To assess nanogel degradation using accelerated conditions, nanogels were suspended in 100 mM HCl (pH 1) and the diameter and count rate was monitored using DLS (Figure 5.3); the degradation products were subsequently characterized using NTA (Figure 5.4) and GPC (Figure 5.5 and Table 5.3). When exposed to the acid, the P0 nanogels retained their size for the first three hours, followed by a decrease in nanogel size (Figure 5.3A); however, the count rate immediately decreased (Figure 5.3B), suggesting that mass loss from the nanogels is occurring but the resulting swelling of the remaining, less cross-linked nanogels maintains the nanogel size over at least the initial observation period. In contrast, the P4 and P8 nanogels have similar degradation profiles in which both the nanogel diameter (Figure 5.3A) and count rate (Figure 5.3B) immediately decreased down to a stable plateau, suggesting fast degradation. Intensity-based multimodal size distributions for P0 (Figure S5.2C), P4 (Figure S5.2F) and P8 (Figure S5.2I) show the occurrence of more polydisperse nanogel populations after 12 hours of incubation compared to the initial time point (t=0). We hypothesize that the physical interactions between the hydrophobic OLAMA domains within the P4 and P8 nanogels introduce steric limitations to the formation of some of the hydrazone bonds, resulting in fewer chemical cross-links that (upon acidic cleavage) enable more rapid degradation of the nanogel structure. Following further incubation in

the degradation media (over a total of 24 hours), nanogels were characterized using NTA (Figure 5.4). The non-degraded nanogel suspensions have a single, narrow peak while the degraded nanogel suspensions have multimodal size distributions. P0 shows significantly lower particle sizes, while P4 and P8 show both smaller particle size peaks (corresponding to degraded polymer fragments) and larger particle size peaks (corresponding to the formation of aggregates as the hydrophobically-modified nanogel fragments become colloidally unstable). Characterization of the molecular weight of the degradation products using GPC confirms that the degraded nanogels have similar molecular weight distributions to the precursor polymers used to fabricate the nanogel (Figure 5.5), with the number average molecular weight of the degraded nanogel (Table 5.3) being well below the renal clearance cut-off limit (~50 kDa). Of note, the potential further degradation of the POEGMA-co-OLAMA polymers would result in release of poly(ethylene glycol) (PEG), oligomeric poly(methacrylic acid), and lactic acid, all of which are either natural products (lactic acid) or have been independently FDA-approved for various applications.^{60, 67-69}

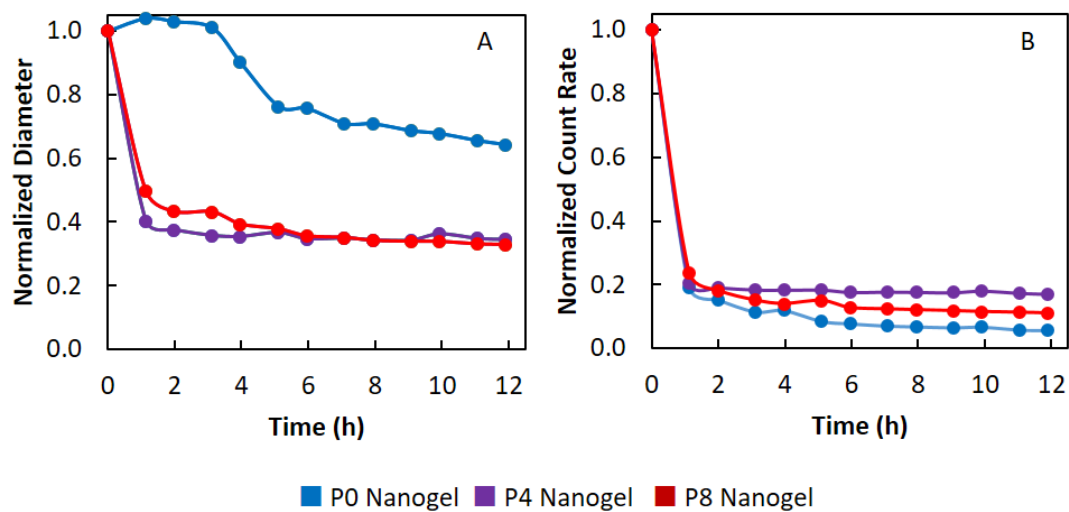


Figure 5.3: Accelerated degradation of self-assembled nanogels. Degradation was measured by DLS at 25°C over 12 h in 100 mM HCl, pH 1. (A) Normalized effective hydrodynamic diameter (from DLS) and (B) Normalized count rate (from DLS).

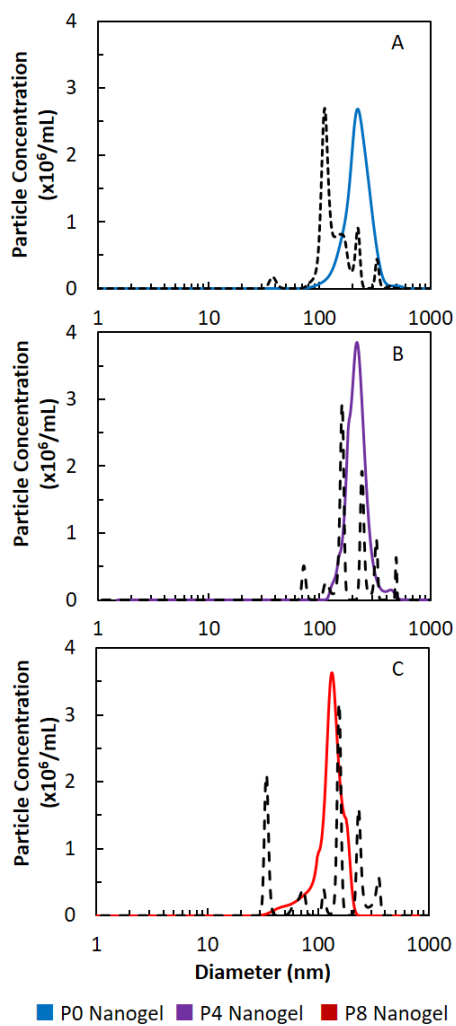


Figure 5.4: Characterization of intact nanogel and degraded nanogels using nanoparticle tracking analysis (NTA). Size distribution of non-degraded nanogels (solid line) and degraded nanogels after 24 hours of exposure to 100 mM HCl (dashed line) for (A) P0 nanogels; (B) P4 nanogels and (C) P8 nanogels.

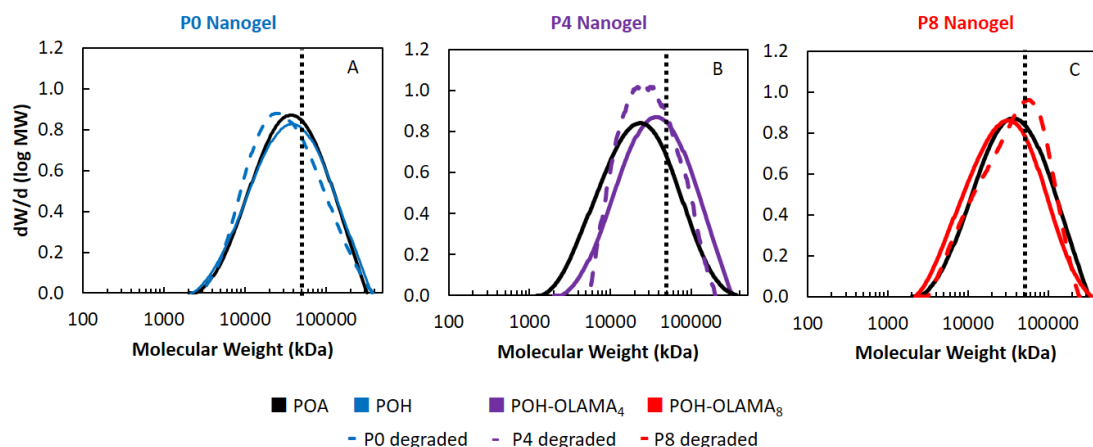


Figure 5.5: Comparison of molecular weights of nanogel precursor polymers and degradation products. Characterization of initial precursor polymers (solid lines) and self-assembled nanogel degradation products after 24 hr of exposure to 100 mM HCl (dashed line) using gel permeation chromatography (GPC): (A) P0 nanogels; (B) P4 nanogels; and (C) P8 nanogels.

Table 5.3: GPC characterization of molecular weight (number average M_n) and dispersity (\mathcal{D}) of untreated precursor polymers and nanogel degradation products after 24 hours of treatment with 100 mM HCl.

	Formulation	M_n (kDa)	\mathcal{D}
Precursor Polymers	POH	22	2.6
	POH-OLAMA ₄	14	2.6
	POH-OLAMA ₈	18	2.5
	POA	23	2.4
Degradation Products	P0	20	2.4
	P4	22	1.8
	P8	24	2.2

To track degradation in more physiologically-relevant conditions, nanogels were similarly incubated in 100 mM acetate buffer (pH 4.5-lysosomal conditions) and monitored using DLS. The diameter of all nanogel formulations remained relatively stable over the initial 12 hour observation time (Figure S5.1A); however, there was a gradual, small increase in

count rate for the P4 (1.5× greater) and P8 (1.2× greater) nanogels (Figure S5.1C). The multimodal size distributions at t=0 and t=12 hours suggest that degradation is occurring in this period, with the P0 formulation showing the presence of a small amount of larger aggregate (Figure S5.2A) while the P4 and P8 nanogels show distinctly more polydisperse particle size distributions (Figure S5.2D and G) with peaks at larger particle sizes (P4 and P8, corresponding to aggregated degradation products) and/or lower particle sizes (P8). These results suggest that a degree of hydrazone bond cleavage occurs in this period, particularly for the P4 and P8 nanogels in which the presence of OLAMA domains inhibits the formation of some hydrazone bonds; in this context, the increased count rates observed can be attributed to increased conformational mobility of the hydrophobic OLAMA side chains upon hydrazone degradation, creating denser nanodomains inside the nanogels that scatter light more light while the particle size remains similar as covalent hydrazone cross-links are supplemented by physical hydrophobic cross-links. The degradation products were further characterized by NTA after 14 days of incubation in the 100 mM acetate buffer, pH 4.5 (Figure 5.6). The P0 nanogels have a broad size distribution with two moderate shoulders towards large particle sizes, indicating nanogel swelling. Comparatively, the P4 and P8 nanogels, both of which have a 10-fold reduction in particle concentration compared to the P0 nanogels, have very distinct multimodal size distributions consistent with substantial degradation as described previously. As such, the hydrophobized POEGMA-POLAMA nanogels are degradable under intracellular pH

conditions. In comparison, assessment of nanogel stability in 10 mM PBS indicated no significant changes in particle size (Figure S5.1B), count rate (Figure S5.1D) or size distribution (Figure S5.2B,E,H) for any of the nanogels over the 12 hr time course of the study.

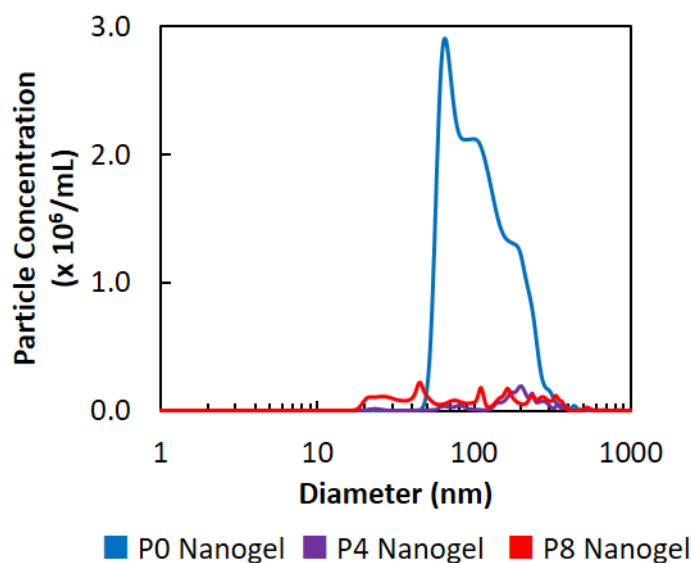


Figure 5.6: Characterization of degraded nanogels at intracellular pH using nanoparticle tracking analysis (NTA). Size distribution of P0 nanogels, P4 nanogels and P8 nanogels after 14 days of exposure to 100 mM acetate buffer, pH 4.5.

5.4.4 Olanzapine loading and release

Olanzapine loading was carried out using two different methods: (1) direct loading by dissolving the drug in the precursor solutions for the self-assembly reaction; and (2) passive diffusion into pre-fabricated nanogels. Direct loading is an attractive benefit of the self-assembly technique because it enables drug loading and synthesis in one step, thereby eliminating the need for multiple purification and isolation steps. However, given

that olanzapine is a highly hydrophobic drug ($\log P=3.6$), the low aqueous solubility of the drug in water ($94 \mu\text{g/mL}$) is a limitation of self-assembly based loading. Table 5.4 summarizes the drug loading capacity (DLC) and encapsulation efficiency (EE) of olanzapine using both loading methods. The direct approach to olanzapine loading shows consistent olanzapine uptake across all three nanogel formulations; while the encapsulation efficiency is moderate, the DLC is low, thus requiring a very high amount of nanogel to deliver a therapeutic dose of olanzapine. Conversely, passive diffusion-based loading in ethanol (in which olanzapine can be dissolved at a concentration of 2 mg/mL , $>20\times$ higher than that achievable in water) enables much higher drug loading to a degree depending on the nanogel composition. P0 nanogels load the least amount of olanzapine (6 wt%), consistent with the relatively high hydrophilicity of this nanogel; introducing the hydrophobic domains via the incorporation of OLAMA significantly improves olanzapine loading, with P4 nanogels showing a DLC of 8 wt% OLZ while P8 nanogels showing the largest DLC of 10 wt% OLZ. While the DLC values are lower than reported for some conventional hard nanoparticles,⁵⁰ the up to 10 wt% drug loading in hydrophobized PEOGMA nanogels is much higher than the 2 wt% olanzapine loading reported for PNIPAM nanogels⁷⁰ (the closest comparable drug delivery system reported for OLZ) and enables clinically-relevant IN doses to be delivered via a practical IN nanoparticle dose.

Table 5.4: Drug loading capacity (DLC) and encapsulation efficiency (EE) of olanzapine in P0, P4 and P8 nanogels. Comparison of direct loading during the self-assembly process or passive diffusion into a pre-fabricated nanogel ($n=3 \pm$ one standard deviation).

Nanogel	Direct Loading		Passive Diffusion	
	DLC (wt%)	EE (%)	DLC (wt%)	EE (%)
P0-OLZ	0.33 ± 0.02	42 ± 3	6 ± 2	$29 \pm 10^{a,b}$
P4-OLZ	0.34 ± 0.02	43 ± 3	8 ± 2	41 ± 10^a
P8-OLZ	0.36 ± 0.01	46 ± 1	10 ± 1	50 ± 2^b

^a $p < 0.001$ or ^b $p < 0.0001$ from pair-wise one-way ANOVA with Tukey post-hoc test.

Compared to the initial nanogel (P0, P4 and P8), nanogels loaded with OLZ via passive diffusion (P0-OLZ, P4-OLZ and P8-OLZ) exhibited larger particle size increases following drug loading, albeit maintaining relatively low polydispersities (Figure 5.7A). For the passively-loaded nanogels (Figure 5.7A), the P0-OLZ nanogel showed a 13% increase in diameter ($p < 0.0001$); the P4-OLZ showed a smaller, but still significant ($p < 0.001$), increases in size of 6%, while the P8-OLZ increased by 4% ($p = 0.707$). The nanogel swelling upon drug loading can likely be attributed the transient nature of the hydrazone cross-links; reinforcement of the hydrophobic interactions by the loaded hydrophobic drug introduces further steric barriers to the dynamic re-formation of hydrazone bonds in water, resulting in increased nanogel swelling. This re-arrangement of polymer chains upon drug-loading is less pronounced in the P4-OLZ and P8-OLZ nanogels because the formation of hydrophobic OLAMA domains during the initial nanogel synthesis already impacted the cross-linking structure of the nanogel.

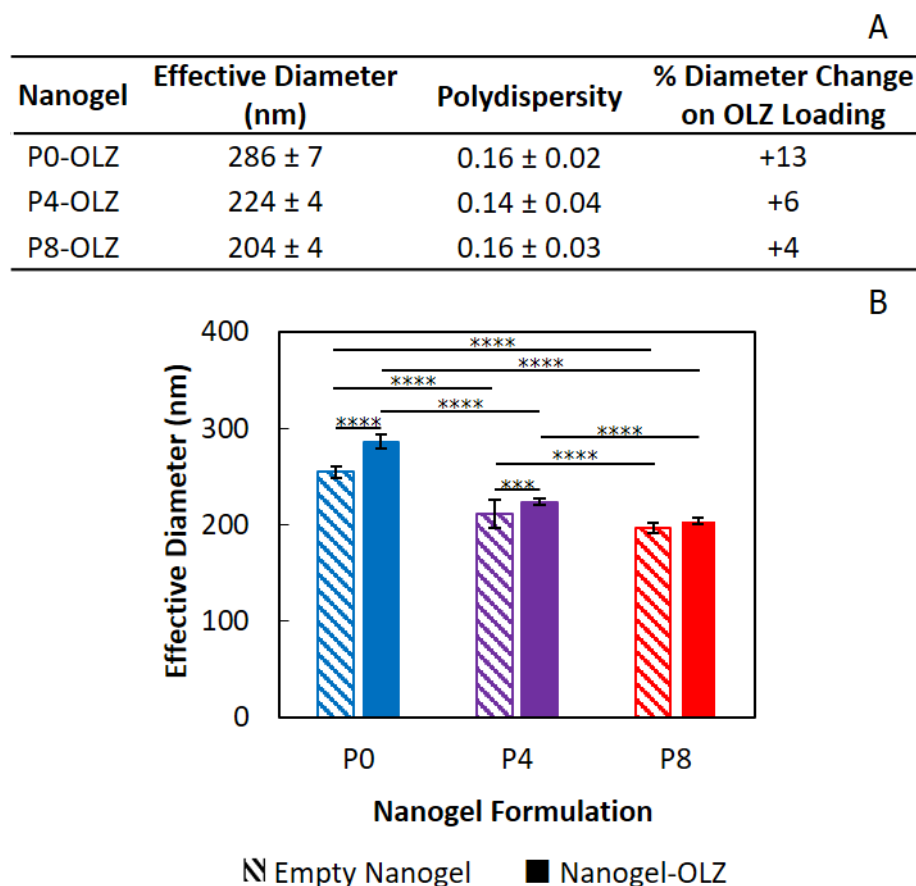


Figure 5.7: Comparison of nanogel diameter (from DLS) before (empty nanogel: P0, P4 and P8) and after olanzapine loading (P0-OLZ, P4-OLZ, P8-OLZ). (A) Effective hydrodynamic diameter and polydispersity (from DLS) of olanzapine-loaded (passive diffusion) self-assembled nanogels. Nanogels fabricated with different core polymers are measured in 10 mM PBS, pH 7.4. (B) Effective hydrodynamic diameter before and after olanzapine loading. Presented error is one standard deviation of n=5 repeats and statistical analysis was conducted using ANOVA with Tukey post-hoc test. *** p < 0.001 and **** p < 0.0001 for pair-wise comparison.

Olanzapine release was studied in two different mimics of physiological conditions: 10 mM PBS, pH 7.4 (physiological pH) and 100 mM acetate buffer, pH 4.5 (mimicking acidic intracellular lysosomal conditions that can both improve olanzapine solubility⁷¹ and

promote gradual nanogel erosion (Figure S5.1 and S5.2). Figure 5.8 presents cumulative olanzapine release over a 2-week period using 20 kDa MWCO Float-A-Lyzer membranes. Free olanzapine showed the expected burst release through the membrane in both release media, albeit with a substantial amount of drug retained inside the membrane (due to adsorption or irreversible precipitation) leading to a maximum cumulative release of 34% under the acidic conditions after two weeks (i.e. the condition at which OLZ is the most water-soluble). In contrast, the nanogel formulations avoided this burst release, with drug release proceeding with zero-order release kinetics for all formulations in each of the release conditions. Release in PBS results in the smallest cumulative release for all formulations (21% for free OLZ, 9% from P0, 14% from P4 and 11% from P8 after 2 weeks). While a small increase in OLZ release from the P0 nanogel was observed under acidic conditions (13% cumulative release after 2 weeks), release from the hydrophobically-modified nanogels that provide more favorable hydrophobic domains for drug binding is not significantly enhanced under acidic conditions (cumulative release of 14% for P4 and 13% for P8). While the membrane partitioning effects do influence the absolute release rates and kinetic profiles observed, the results shown in Figure 5.8 still clearly show that the nanogels can facilitate prolonged and controlled olanzapine release that avoids the burst release of drug that is implicated in inducing more severe metabolic side-effects.

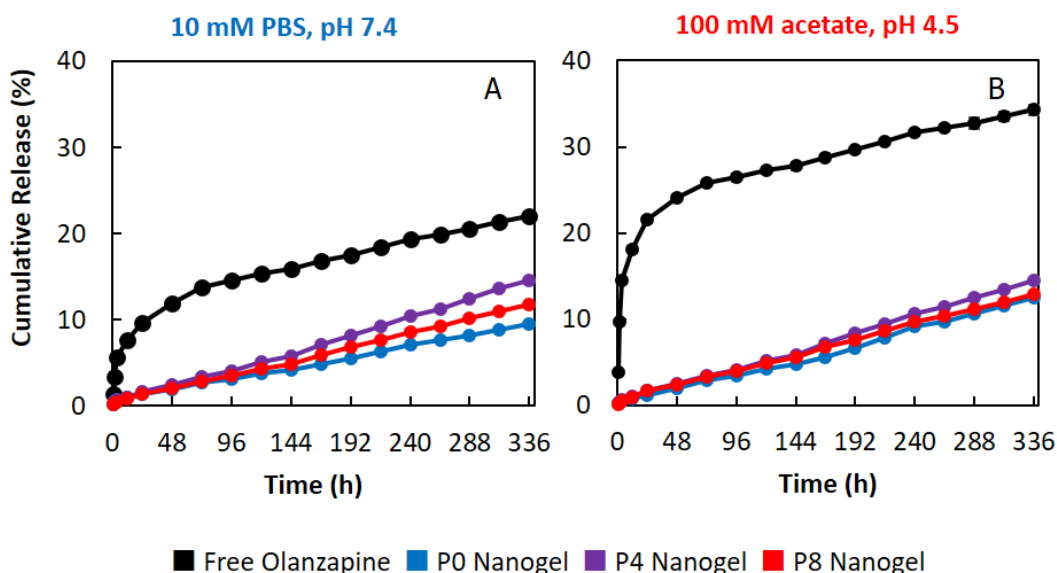


Figure 5.8: Cumulative *in vitro* release of olanzapine in different physiologically-relevant conditions. (A) 10 mM PBS, pH 7.4 and (B) 100 mM ammonium acetate, pH 4.5 for free OLZ, P0-OLZ, P4-OLZ and P8-OLZ incubated at 37°C under 100 rpm shaking. Error bars represent the standard deviation of n=3 samples.

5.4.5 Polymer and nanogel cytotoxicity

The cytocompatibility of the precursor polymers/degradation products (POA, POH, POH-OLAMA₄ and POH-OLAMA₈), nanogels (P0, P4 and P8) and olanzapine-loaded nanogels (P0-OLZ, P4-OLZ, P8-OLZ) was examined using a MTT assay using human SH-SY5Y neuronal cells. Figure 5.9 shows the relative cell viability (to a non-treated cell-only control) of the SH-SY5Y cells after 24 hours of polymer and nanogel exposure at a range of concentrations representing nanogel concentrations that could potentially be administered *in vivo* (and the relevant precursor polymer concentrations to those nanogel concentrations, taking into account that the POA cross-linker is only incorporated at 20

wt% relative to the POH (-OLAMA_{4/8}) mass). All nanogels and precursor polymers exhibited high cytocompatibility with relative cell viabilities are >80%, indicating potential to be used *in vivo* without inducing problematic toxicity.

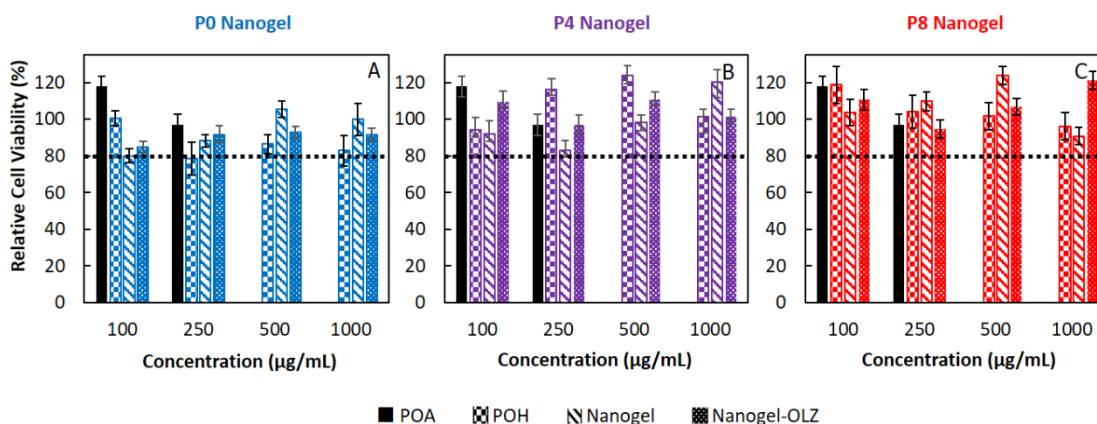


Figure 5.9: Cytotoxicity of precursor polymers and nanogels to SH-SY5Y neuronal cells. Relative cell viability (to a cell-only control) as measured via the MTT assay after 24 hours of exposure to precursor polymers/degradation products (POA, POH, POH-OLAMA₄ and POH-OLAMA₈), nanogels (P0, P4 and P8) and olanzapine-loaded nanogels (P0-OLZ, P4-OLZ, P8-OLZ): (A) P0 formulations; (B) P4 formulations; (C) P8 formulations. Error bars represent standard deviation of n=4 samples. No statistically significant differences were determined from ANOVA.

5.4.6 *In vivo* pharmacological efficacy of OLZ-loaded nanogels

A rodent model of schizophrenia was used to evaluate the pharmacodynamics of the olanzapine-loaded nanogels *in vivo*. Pre-pulse inhibition (PPI) was selected as the behavioural test given that it provides an operational measure of sensorimotor gating, a phenomena that is observed across species related to the filtering of information from one's surroundings.^{72 73-75} In a healthy individual, a weak acoustic stimulus provided prior to a larger startle stimulus will attenuate the startle response; in an individual with

schizophrenia, a reduced startle response is not observed as the pre-pulse information is not processed as effectively.⁷⁶⁻⁷⁷ To induce a rodent model of schizophrenia, male Sprague-Dawley rats received 0.35 mg/kg IP injections of MK-801, a highly selective non-competitive *N*-methyl-D-aspartate (NMDA) glutamate receptor antagonist that produces a complex behavioural syndrome including dose-dependent changes (upon acute exposure) in representative symptoms of schizophrenia including hyperlocomotion, deficits in PPI and social interaction, stereotypy, and ataxia.⁷⁸⁻⁷⁹ Previous studies have shown that disruption in PPI induced by MK-801 can be alleviated by olanzapine treatment due to its preferential action in the mesolimbic area and high affinity for serotonin receptors.⁷⁴⁻⁷⁵

Initially, a negative control measure of PPI was collected by dosing with saline IN 60 minutes and IP 15 minutes prior to PPI testing (Baseline); high levels of PPI (65%) were observed. Rats given IN doses of P0, P4 or P8 nanogel similarly did not exhibit any PPI reductions compared to the baseline; administration of olanzapine-loaded nanogels (P0-OLZ, P4-OLZ and P8-OLZ) similarly retained the same level of PPI as the baseline and empty nanogel trials (not significant (ns), $p > 0.999$). As such, the nanogels themselves do not induce any significant behavioral change due to unexpected receptor interactions or toxicity.

Following, to induce schizophrenia-like symptoms, each animal was anesthetized and dosed with IN saline; an IP injection of MK-801 was then administered 15 minutes prior to PPI testing (MK-801 - positive control). Administration of MK-801 produced a significant ($p < 0.0001$ relative to Baseline) decrease in PPI to only 18%, showing the expected schizophrenia-like responses. When rats were dosed with MK-801 in addition to empty nanogel (P0/MK-801, P4/MK-801, P8/MK-801), PPI again decreased by a substantial amount ($p < 0.0001$ for P0, $p < 0.001$ for P4, and $p < 0.05$ for P8), comparable to that observed in the MK-801 alone trial. No significant differences were observed between any formulations receiving MK-801 without drug (ns, $p > 0.999$). Therapeutic intervention with P0-OLZ, P4-OLZ or P8-OLZ (2 mg/kg OLZ administered per rat) was subsequently monitored 1, 3, 6, 24 and 48 hours after IN administration, with MK-801 dosing 15 min prior to PPI testing at each time point. PPI testing one hour post-IN administration showed substantial deficits were retained for all OLZ-loaded nanogels tested ($p < 0.001$ for P0 and P8, $p < 0.01$ for P4, relative to the relevant no-MK-801 nanogel control). At the 3 hour time point, the PPI of the P0-OLZ ($p < 0.01$) and P4-OLZ ($p < 0.05$) nanogels remained significantly lower than their respective no-MK-801 control; however, while the P8 nanogel PPI values also remained lower than its no-MK-801 control, the difference was no longer statistically significant ($p = 0.06$), suggesting nanogel-facilitated transport of OLZ into the brain. PPI response continued to improve at the 6 hr time point (ns, P0 $p = 0.076$; P4 $p = 0.690$; P8 $p = 0.600$) and was fully recovered 24 hr post-IN

administration for all nanogels tested (ns, P0 $p > 0.999$; P4 and P8 $p = 0.989$), showing that prolonged therapeutic intervention and rescue of PPI deficits can be enabled by all nanogel formulations. At 48 hours post-IN administration, the 2 mg/kg nanogel-OLZ no longer retained its therapeutic benefits in the P0 and P8 systems, with PPI once again decreasing to the positive control baseline ($p < 0.001$ for P0 and P8 relative to their respective no-MK-801 nanogel control). However, the P4 nanogel retained therapeutic efficacy relative to its no-MK-801 nanogel control ($p = 0.053$). To our knowledge, this data represents the first demonstrated prolonged therapeutic intervention enabled by a single, acute low dose of IN OLZ. Previous studies using 5× more drug (10 mg/kg IP) failed to demonstrate similar complete restoration of PPI following 0.1 mg/kg SC MK-801,⁸⁰ 3 mg/kg phencyclidine SC⁸¹ or brain lesion-induced deficits in PPI,⁸² while other studies using a slightly smaller dose of MK-801 than used herein (0.3 mg/kg) have shown PPI reversal only one hour post-SC injection of 2.5 mg/kg free OLZ⁸³ or using 3 mg/kg OLZ SC in isolation-reared rodents.⁸⁴

The persistent maintenance of PPI from 6 hours up to 48 hours post-IN administration of a low (2 mg/kg) dose of OLZ in rats suggests that the combination of the IN route of delivery and the nanogel transport/controlled release properties collectively enable transport of the drug to the brain and prolonged drug release to enable longer-term PPI recovery than observed in previous studies. The half-life of OLZ in rats (2.5-3 hr)⁸⁵⁻⁸⁶ is substantially shorter than the half-life in humans (29-55 hr)⁸⁷ due to metabolic differences, while the frequency of adverse side effects appears to be dose-related as plasma levels of olanzapine increase linearly with daily oral doses.⁸⁸⁻⁸⁹ Supplying low doses of olanzapine encapsulated in nanogels will retain the drug in its active form while providing sustained release of the drug within its therapeutic range; concurrently, the IN delivery strategy enhances the probability of the nanogel penetrating into the brain. Both these factors increase OLZ bioavailability, thus minimizing the non-target drug concentration that contributes to the negative side effects of the APD. The sustained therapeutic effects demonstrated by this self-assembled nanogel system can be attributed to the unique characteristics of the nanocarrier. Nanogels are able to improve therapeutic delivery to the brain due to their enhanced mechanical deformability (enabling improved intracellular drug delivery across cell membranes⁹⁰) and improved cell targeting,⁹¹⁻⁹² thereby facilitating uptake by the nasal epithelium and thus transport via the direct nose-to-brain pathway that bypasses the BBB.⁹³⁻⁹⁴ Soft nanogels are also particularly efficiently transported to lysosomes, which have the ideal acidic conditions to

trigger nanogel degradation and olanzapine release, because their deformability facilitates membrane wrapping and engulfment in vesicles.⁹⁵ Nanogel deformability also enables larger particle sizes that encapsulate higher drug payloads, thus reducing the quantity of polymer required to deliver a therapeutic drug dose.⁹⁶ These self-assembled nanogels are larger (~200-250 nm) than many of the PLGA⁴⁷ and SLN⁴⁹ carriers previously proposed for IN olanzapine delivery as well as most intravenous nanoparticles used given the restricted transport of nanoparticles of size >100 nm through the BBB;⁹⁷ the hydrophilic/hydrophobic balance required to maintain nanogel swelling yet enhance olanzapine uptake also contributes to enhancing mucopenetration and epithelial cell uptake.⁹⁸⁻⁹⁹ On this basis, the P4 nanogels are likely the most suitable candidate for practical application as these nanogels have high DLC values (8 wt%), intermediate swelling responses, and the most prolonged therapeutic benefit in terms of PPI attenuation. Despite the increased internal hydrophobicity imparted by the OLAMA comonomer, the self-assembled nanogels retain their interfacial hydrophilic properties due to the PEG side chains in the brush copolymer preventing particle aggregation while enhancing particle diffusivity through mucus to enable access to the epithelium of the nasal cavity.¹⁰⁰⁻¹⁰¹ Thus, these nanogels have desirable physiochemical properties to provide sustained release of olanzapine using IN delivery to enhance drug bioavailability.

5.5 Conclusions

Nanogels were prepared based on hydrazide and aldehyde-functionalized POEGMA-co-POLAMA precursor polymers using a rapid, thermally-driven, self-assembly method. The resulting covalently cross-linked nanogels contain hydrophobic domains of physically interacting OLAMA side-chains to promote olanzapine uptake; nanogel degradation and drug release was facilitated through hydrolytic degradation of the hydrazone cross-links and/or the lactic acid-based side chains which regenerated the polymer building blocks of the nanogels. The nanogels and their precursor polymers/degradation products were both highly cytocompatible to neuronal cells at concentrations comparable to those used for IN drug delivery, while pharmacodynamic studies confirmed that IN administered drug-loaded nanogels enabled delivery of therapeutic doses of olanzapine that reversed MK-801-induced deficits of pre-pulse inhibition for at least 24 hr following a single nanogel administration, a sustained effect not previously shown by other IN-delivered nanoformulations. IN administration of self-assembled nanogels thus provides a suitable delivery mechanism for low doses of olanzapine that can decrease both the total dose and the dosing frequency required for therapeutic intervention, thus minimizing the adverse metabolic side effects and advancing the efficacy of this clinically prescribed APD.

5.6 Acknowledgements

The Natural Sciences and Engineering Research Council of Canada (NSERC) and the Canadian Institutes of Health Research (CIHR) are acknowledged for funding (Canada Graduate Scholarship to MS, Collaborative Health Research Partnerships Grants CPG-151963 and CHRPJ-508393-2017 to TH and RKM). We gratefully acknowledge Judy Tran for her assistance with cell culture experiments, Ashley Bernardo for providing training on the startle response system and Andrew Lofts for his assistance with animal handling during the behavioural studies.

5.7 References

- (1) Hoare, T.; Pelton, R., Characterizing Charge and Crosslinker Distributions in Polyelectrolyte Microgels. *Curr. Opin. Colloid Interface Sci.* **2008**, *13* (6), 413-428.
- (2) Agrawal, G.; Agrawal, R., Functional Microgels: Recent Advances in Their Biomedical Applications. *Small* **2018**, *14* (39), 1801724.
- (3) Smeets, N. M. B.; Hoare, T., Designing Responsive Microgels for Drug Delivery Applications. *J. Polym. Sci. A Polym. Chem.* **2013**, *51* (14), 3027-3043.
- (4) Hsiao, L.-W.; Lai, Y.-D.; Lai, J.-T.; Hsu, C.-C.; Wang, N.-Y.; Wang, S. S. S.; Jan, J.-S., Cross-linked Polypeptide-Based Gel Particles by Emulsion for Efficient Protein Encapsulation. *Polymer* **2017**, *115*, 261-272.
- (5) Mahmoodzadeh, F.; Ghorbani, M.; Jannat, B., Glutathione and PH-Responsive Chitosan-Based Nanogel as an Efficient Nanoplatfrom for Controlled Delivery of Doxorubicin. *J. Drug. Deliv. Sci. Technol.* **2019**, *54*, 101315.
- (6) Chen, J.; Wu, M.; Veroniaina, H.; Mukhopadhyay, S.; Li, J.; Wu, Z.; Wu, Z.; Qi, X., Poly(N-isopropylacrylamide) Derived Nanogels Demonstrated Thermosensitive Self-Assembly and GSH-Triggered Drug Release for Efficient Tumor Therapy. *Polym. Chem.* **2019**, *10* (29), 4031-4041.
- (7) Zhang, W.; Ai, S.; Ji, P.; Liu, J.; Li, Y.; Zhang, Y.; He, P., Photothermally Enhanced Chemotherapy Delivered by Graphene Oxide-Based Multiresponsive Nanogels. *ACS Appl. Bio Mater.* **2019**, *2* (1), 330-338.
- (8) Murthy, N.; Thng, Y. X.; Schuck, S.; Xu, M. C.; Fréchet, J. M., A Novel Strategy for Encapsulation and Release of Proteins: Hydrogels and Microgels with Acid-Labile Acetal Cross-Linkers. *J. Am. Chem. Soc.* **2002**, *124* (42), 12398-12399.
- (9) Shi, L.; Khondee, S.; Linz, T. H.; Berkland, C., Poly(N-vinylformamide) Nanogels Capable of pH-Sensitive Protein Release. *Macromolecules* **2008**, *41* (17), 6546-6554.
- (10) Nuhn, L.; Vanparijs, N.; De Beuckelaer, A.; Lybaert, L.; Verstraete, G.; Deswarte, K.; Lienenklaus, S.; Shukla, N. M.; Salyer, A. C. D.; Lambrecht, B. N.; Grooten, J.; David, S. A.; De Koker, S.; De Geest, B. G., PH-Degradable Imidazoquinoline-Ligated Nanogels for Lymph Node-Focused Immune Activation. *PNAS* **2016**, *113* (29), 8098-8103.
- (11) Sahiner, N.; Sagbas, S.; Aktas, N., Preparation of Macro-, Micro-, and Nano-Sized Poly(Tannic Acid) Particles With Controllable Degradability and Multiple Biomedical Uses. *Polym. Degrad.* **2016**, *129*, 96-105.
- (12) Koetting, M. C.; Guido, J. F.; Gupta, M.; Zhang, A.; Peppas, N. A., PH-Responsive and Enzymatically-Responsive Hydrogel Microparticles for the Oral Delivery of Therapeutic Proteins: Effects of Protein Size, Crosslinking Density, and Hydrogel Degradation on Protein Delivery. *J. Control. Release* **2016**, *221*, 18-25.

- (13) Schultz, K. M.; Anseth, K. S., Monitoring Degradation of Matrix Metalloproteinases-Cleavable PEG Hydrogels via Multiple Particle Tracking Microrheology. *Soft Matter* **2013**, *9* (5), 1570-1579.
- (14) Foster, G. A.; Headen, D. M.; González-García, C.; Salmerón-Sánchez, M.; Shirwan, H.; García, A. J., Protease-Degradable Microgels for Protein Delivery for Vascularization. *Biomaterials* **2017**, *113*, 170-175.
- (15) Thornton, P. D.; Mart, R. J.; Ulijn, R. V., Enzyme-Responsive Polymer Hydrogel Particles for Controlled Release. *Adv. Mater.* **2007**, *19* (9), 1252-1256.
- (16) Thornton, P. D.; Mart, R. J.; Webb, S. J.; Ulijn, R. V., Enzyme-Responsive Hydrogel Particles for the Controlled Release of Proteins: Designing Peptide Actuators to Match Payload. *Soft Matter* **2008**, *4* (4), 821-827.
- (17) Szilágyi, B. Á.; Némethy, Á.; Magyar, A.; Szabó, I.; Bősze, S.; Gyarmati, B.; Szilágyi, A., Amino Acid Based Polymer Hydrogel with Enzymatically Degradable Cross-Links. *React. Funct. Polym.* **2018**, *133*, 21-28.
- (18) Fairbanks, B. D.; Schwartz, M. P.; Halevi, A. E.; Nuttelman, C. R.; Bowman, C. N.; Anseth, K. S., A Versatile Synthetic Extracellular Matrix Mimic via Thiol-Norbornene Photopolymerization. *Adv. Mater.* **2009**, *21* (48), 5005-5010.
- (19) Raeber, G. P.; Lutolf, M. P.; Hubbell, J. A., Molecularly Engineered PEG Hydrogels: A Novel Model System for Proteolytically Mediated Cell Migration. *Biophys. J.* **2005**, *89* (2), 1374-1388.
- (20) Lee, H.; Mok, H.; Lee, S.; Oh, Y. K.; Park, T. G., Target-Specific Intracellular Delivery of siRNA Using Degradable Hyaluronic Acid Nanogels. *J. Control. Release* **2007**, *119* (2), 245-252.
- (21) Hang, C.; Zou, Y.; Zhong, Y.; Zhong, Z.; Meng, F., NIR and UV-Responsive Degradable Hyaluronic Acid Nanogels for CD44-targeted and Remotely Triggered Intracellular Doxorubicin Delivery. *Colloid. Surface. B* **2017**, *158*, 547-555.
- (22) Lee, W.-C.; Li, Y.-C.; Chu, I. M., Amphiphilic Poly(D,L-lactic acid)/Poly(ethylene glycol)/Poly(D,L-lactic acid) Nanogels for Controlled Release of Hydrophobic Drugs. *Macromol. Biosci.* **2006**, *6* (10), 846-854.
- (23) Osorno, L. L.; Maldonado, D. E.; Whitener, R. J.; Brandley, A. N.; Yiantsos, A.; Medina, J. D. R.; Byrne, M. E., Amphiphilic PLGA-PEG-PLGA Triblock Copolymer Nanogels Varying in Gelation Temperature and Modulus For The Extended and Controlled Release Of Hyaluronic Acid. *J. Appl. Polym. Sci.* **2020**, *137* (25), 48678.
- (24) Wei, G.; Prabhu, V. M.; Piunova, V. A.; Carr, A. C.; Swope, W. C.; Miller, R. D., Spatial Distribution of Hydrophobic Drugs in Model Nanogel-Core Star Polymers. *Macromolecules* **2017**, *50* (24), 9702-9712.
- (25) Bang, T. H.; Van, T. T. T.; Hung, L. X.; Ly, B. M.; Nhut, N. D.; Thuy, T. T. T.; Huy, B. T., Nanogels of Acetylated Ulvan Enhance the Solubility of Hydrophobic Drug Curcumin. *Bull. Mater. Sci.* **2019**, *42* (1), 1.

- (26) Zhu, Z.; Fu, H.; Dong, S.; Ji, W.; Du, B.; Nie, J., Multiresponsive Microgels with Phase-Separated Nanodomains and Self-Regulating Properties via Incorporation of Anthraquinone Moieties. *Langmuir* **2020**, *36* (9), 2427-2438.
- (27) Li, Z.; Van Zee, N. J.; Bates, F. S.; Lodge, T. P., Polymer Nanogels as Reservoirs to Inhibit Hydrophobic Drug Crystallization. *ACS Nano* **2019**, *13* (2), 1232-1243.
- (28) Yang, H.; Wang, Q.; Li, Z.; Li, F.; Wu, D.; Fan, M.; Zheng, A.; Huang, B.; Gan, L.; Zhao, Y.; Yang, X., Hydrophobicity-Adaptive Nanogels for Programmed Anticancer Drug Delivery. *Nano Lett.* **2018**, *18* (12), 7909-7918.
- (29) Fernandes Stefanello, T.; Szarpak-Jankowska, A.; Appaix, F.; Louage, B.; Hamard, L.; De Geest, B. G.; van der Sanden, B.; Nakamura, C. V.; Auzély-Velty, R., Thermoresponsive Hyaluronic Acid Nanogels as Hydrophobic Drug Carrier to Macrophages. *Acta Biomater.* **2014**, *10* (11), 4750-4758.
- (30) Qiao, Z.-Y.; Zhang, R.; Du, F.-S.; Liang, D.-H.; Li, Z.-C., Multi-Responsive Nanogels Containing Motifs of Ortho Ester, Oligo(Ethylene Glycol) and Disulfide Linkage as Carriers of Hydrophobic Anti-Cancer Drugs. *J. Control. Release* **2011**, *152* (1), 57-66.
- (31) Nagahama, K.; Hashizume, M.; Yamamoto, H.; Ouchi, T.; Ohya, Y., Hydrophobically Modified Biodegradable Poly(Ethylene Glycol) Copolymers that Form Temperature-Responsive Nanogels. *Langmuir* **2009**, *25* (17), 9734-9740.
- (32) Cao, H.; Guo, F.; Chen, Z.; Kong, X. Z., Preparation of Thermoresponsive Polymer Nanogels of Oligo(Ethylene Glycol) Diacrylate-Methacrylic Acid and Their Property Characterization. *Nanoscale Res. Lett.* **2018**, *13* (1), 209.
- (33) Golfar, Y.; Shayanfar, A., Prediction of Biopharmaceutical Drug Disposition Classification System (BDDCS) by Structural Parameters. *J. Pharm. Pharm. Sci.* **2019**, *22* (1), 247-269.
- (34) Charlson, F. J.; Ferrari, A. J.; Santomauro, D. F.; Diminic, S.; Stockings, E.; Scott, J. G.; McGrath, J. J.; Whiteford, H. A., Global Epidemiology and Burden of Schizophrenia: Findings From the Global Burden of Disease Study 2016. *Schizophr. Bull.* **2018**, *44* (6), 1195-1203.
- (35) Meltzer, H. Y., The Role of Serotonin in Antipsychotic Drug Action. *Neuropsychopharmacol.* **1999**, *21* (1), 106-115.
- (36) Littrell, K. H.; Littrell, S. H., Therapeutic Efficacy of Olanzapine. *J. Am. Psychiatr. Nurses Assoc.* **1997**, *3* (1), S8-S13.
- (37) Lord, C. C.; Wyler, S. C.; Wan, R.; Castorena, C. M.; Ahmed, N.; Mathew, D.; Lee, S.; Liu, C.; Elmquist, J. K., The Atypical Antipsychotic Olanzapine Causes Weight Gain by Targeting Serotonin Receptor 2C. *J. Clin. Invest.* **2017**, *127* (9), 3402-3406.
- (38) Joseph, E.; Reddi, S.; Rinwa, V.; Balwani, G.; Saha, R., Design and In Vivo Evaluation of Solid Lipid Nanoparticulate Systems of Olanzapine for Acute Phase

- Schizophrenia Treatment: Investigations on Antipsychotic Potential and Adverse Effects. *Eur. J. Pharm. Sci.* **2017**, *104*, 315-325.
- (39) Harrison, P. J., Weight Gain with Antipsychotic Drugs: The Role of the 5-HT_{2C} Receptor (HTR_{2C}) and Other Genes. *Pharmacogenet. Genomics* **2005**, *15* (4), 193-194.
- (40) Reynolds, G. P.; Hill, M. J.; Kirk, S. L., The 5-HT_{2C} Receptor and Antipsychotic-induced Weight Gain - Mechanisms and Genetics. *J. Psychopharmacol. (Oxford)* **2006**, *20* (4), 15-18.
- (41) Wallace, T. J.; Zai, C. C.; Brandl, E. J.; Müller, D. J., Role of 5-HT_{2C} Receptor Gene Variants in Antipsychotic-Induced Weight Gain. *Pharmgenomics Pers. Med.* **2011**, *4*, 83-93.
- (42) Li, H.; Peng, S.; Li, S.; Liu, S.; Lv, Y.; Yang, N.; Yu, L.; Deng, Y.-H.; Zhang, Z.; Fang, M.; Huo, Y.; Chen, Y.; Sun, T.; Li, W., Chronic Olanzapine Administration Causes Metabolic Syndrome Through Inflammatory Cytokines in Rodent Models of Insulin Resistance. *Sci. Rep.* **2019**, *9* (1), 1582.
- (43) Hanson, L. R.; Frey, W. H., Intranasal Delivery Bypasses the Blood-Brain Barrier to Target Therapeutic Agents to the Central Nervous System and Treat Neurodegenerative Disease. *BMC Neurosci.* **2008**, *9* (3), 1-4.
- (44) Illum, L., Is Nose-to-Brain Transport of Drugs in Man a Reality? *J. Pharm. Pharmacol.* **2004**, *56* (1), 3-17.
- (45) Patel, M. M.; Patel, B. M., Crossing the Blood-Brain Barrier: Recent Advances in Drug Delivery to the Brain. *CNS Drugs* **2017**, *31* (2), 109-133.
- (46) Baltzley, S.; Mohammad, A.; Malkawi, A. H.; Al-Ghananeem, A. M., Intranasal Drug Delivery of Olanzapine-Loaded Chitosan Nanoparticles. *AAPS PharmSciTech.* **2014**, *15* (6), 1598-1602.
- (47) Seju, U.; Kumar, A.; Sawant, K. K., Development and Evaluation of Olanzapine-Loaded PLGA Nanoparticles for Nose-to-Brain Delivery: In Vitro and In Vivo Studies. *Acta Biomater.* **2011**, *7* (12), 4169-4176.
- (48) Salama, H. A.; Mahmoud, A. A.; Kamel, A. O.; Abdel Hady, M.; Awad, G. A. S., Brain Delivery of Olanzapine by Intranasal Administration of Transfersomal Vesicles. *J. Liposome Res.* **2012**, *22* (4), 336-345.
- (49) Kumar, M.; Misra, A.; Mishra, A. K.; Mishra, P.; Pathak, K., Mucoadhesive Nanoemulsion-Based Intranasal Drug Delivery System of Olanzapine for Brain Targeting. *J. Drug Target.* **2008**, *16* (10), 806-814.
- (50) Ruby, J. J.; Pandey, V. P., Formulation and Evaluation of Olanzapine Loaded Chitosan Nanoparticles for Nose to Brain Targeting an In Vitro and Ex Vivo Toxicity Study. *J. App. Pharm. Sci.* **2016**, *6* (9), 34-40.
- (51) Fonseca, F. N.; Betti, A. H.; Carvalho, F. C.; Gremiao, M. P.; Dimer, F. A.; Guterres, S. S.; Tebaldi, M. L.; Rates, S. M.; Pohlmann, A. R., Mucoadhesive Amphiphilic Methacrylic Copolymer-Functionalized Poly(Epsilon-Caprolactone) Nanocapsules

- for Nose-to-Brain Delivery of Olanzapine. *J. Biomed. Nanotechnol.* **2015**, *11* (8), 1472-1481.
- (52) Patenaude, M.; Hoare, T., Injectable, Degradable Thermoresponsive Poly(N-isopropylacrylamide) Hydrogels. *ACS Macro Letters* **2012**, *1* (3), 409-413.
- (53) Smeets, N. M. B.; Bakaic, E.; Patenaude, M.; Hoare, T., Injectable And Tunable Poly(Ethylene Glycol) Analogue Hydrogels Based on Poly(Oligoethylene Glycol Methacrylate). *Chem. Commun.* **2014**, *50* (25), 3306-3309.
- (54) Patenaude, M.; Hoare, T., Injectable, Mixed Natural-Synthetic Polymer Hydrogels with Modular Properties. *Biomacromolecules* **2012**, *13* (2), 369-378.
- (55) Smeets, N. M. B.; Bakaic, E.; Patenaude, M.; Hoare, T., Injectable Poly(Oligoethylene Glycol Methacrylate)-Based Hydrogels with Tunable Phase Transition Behaviours: Physicochemical and Biological Responses. *Acta Biomater.* **2014**, *10* (10), 4143-4155.
- (56) Fox, M. E.; Szoka, F. C.; Fréchet, J. M. J., Soluble Polymer Carriers for the Treatment Of Cancer: The Importance of Molecular Architecture. *Acc. Chem. Res.* **2009**, *42* (8), 1141-1151.
- (57) Mueller, E.; Alsop, R. J.; Scotti, A.; Bleuel, M.; Rheinstadter, M. C.; Richtering, W.; Hoare, T., Dynamically Cross-Linked Self-Assembled Thermoresponsive Microgels with Homogeneous Internal Structures. *Langmuir* **2018**, *34* (4), 1601-1612.
- (58) Sivakumaran, D.; Mueller, E.; Hoare, T., Temperature-Induced Assembly of Monodisperse, Covalently Cross-Linked, and Degradable Poly(N-isopropylacrylamide) Microgels Based on Oligomeric Precursors. *Langmuir* **2015**, *31* (21), 5767-5778.
- (59) Simpson, M. J.; Corbett, B.; Arezina, A.; Hoare, T., Narrowly Dispersed, Degradable, and Scalable Poly(Oligoethylene Glycol Methacrylate)-Based Nanogels via Thermal Self-Assembly. *Ind. Eng. Chem. Res.* **2018**, *57* (22), 7495-7506.
- (60) Ishimoto, K.; Arimoto, M.; Okuda, T.; Yamaguchi, S.; Aso, Y.; Ohara, H.; Kobayashi, S.; Ishii, M.; Morita, K.; Yamashita, H.; Yabuuchi, N., Biobased Polymers: Synthesis of Graft Copolymers and Comb Polymers Using Lactic Acid Macromonomer and Properties of the Product Polymers. *Biomacromolecules* **2012**, *13* (11), 3757-3768.
- (61) Smeets, N. M. B.; Patenaude, M.; Kinio, D.; Yavitt, F. M.; Bakaic, E.; Yang, F.-C.; Rheinstadter, M.; Hoare, T., Injectable Hydrogels with In Situ-Forming Hydrophobic Domains: Oligo(D,L-Lactide) Modified Poly(Oligoethylene Glycol Methacrylate) Hydrogels. *Polym. Chem.* **2014**, *5* (23), 6811-6823.
- (62) Lutz, J. F.; Hoth, A., Preparation of Ideal PEG analogues with A Tunable Thermosensitivity by Controlled Radical Copolymerization of 2-(2-Methoxyethoxy)Ethyl Methacrylate and Oligo(Ethylene Glycol) Methacrylate. *Macromolecules* **2006**, *39* (2), 893-896.

- (63) Ahmed Laskar, A.; Younus, H., Aldehyde Toxicity and Metabolism: The Role of Aldehyde Dehydrogenases in Detoxification, Drug Resistance and Carcinogenesis. *Drug Metab. Rev.* **2019**, *51* (1), 42-64.
- (64) LoPachin, R. M.; Gavin, T., Molecular Mechanisms of Aldehyde Toxicity: A Chemical Perspective. *Chem. Res. Toxicol.* **2014**, *27* (7), 1081-1091.
- (65) Li, S.; Wong, S.; Sethia, S.; Almoazen, H.; Joshi, Y. M.; Serajuddin, A. T., Investigation of Solubility and Dissolution of a Free Base and Two Different Salt Forms as a Function of PH. *Pharm. Res.* **2005**, *22* (4), 628-635.
- (66) Oh, J. K.; Bencherif, S. A.; Matyjaszewski, K., Atom Transfer Radical Polymerization in Inverse Miniemulsion: A Versatile Route Toward Preparation and Functionalization of Microgels/Nanogels for Targeted Drug Delivery Applications. *Polymer* **2009**, *50* (19), 4407-4423.
- (67) Alconcel, S. N. S.; Baas, A. S.; Maynard, H. D., FDA-Approved Poly(Ethylene Glycol)-Protein Conjugate Drugs. *Polym. Chem.* **2011**, *2* (7), 1442-1448.
- (68) Mansour, H. M.; Sohn, M.; Al-Ghananeem, A.; DeLuca, P. P., Materials for Pharmaceutical Dosage Forms: Molecular Pharmaceutics and Controlled Release Drug Delivery Aspects. *Int. J. Mol. Sci.* **2010**, *11* (9), 3298-3322.
- (69) Saade, H.; Guillen, M. D.; Romero, J. C.; Cepeda, J.; Ilyna, A.; Fernandez, S.; Enriquez-Medrano, F. J.; Lopez, R. G., Biocompatible and Biodegradable Ultrafine Nanoparticles of Poly(Methyl Methacrylate-Co-Methacrylic Acid) Prepared via Semicontinuous Heterophase Polymerization: Kinetics and Product Characterization. *Int. J. Polym. Sci.* **2016**, *8*, 7674620.
- (70) Pervaiz, F.; Ahmad, M.; Hussain, T.; Idrees, A.; Yaqoob, A.; Abbas, K., Development of Olanzapine Loaded PNA Microgels for Depot Drug Delivery in Treatment of Schizophrenia: In Vitro and In Vivo Release Profile. *Acta Pol. Pharm.* **2016**, *73* (1), 175-181.
- (71) Akula, P.; P.K., L., Effect of PH on Weakly Acidic and Basic Model Drugs and Determination of Their Ex Vivo Transdermal Permeation Routes. *Braz. J. Pharm. Sci.* **2018**, *54* (2), 1-8.
- (72) Geyer, M. A., Prepulse Inhibition as a Cross-Species Model of Sensorimotor Gating Deficits in Schizophrenia. In *Contemporary Issues in Modeling Psychopathology*, Myslobodsky, M. S.; Weiner, I., Eds. Springer US: Boston, MA, 2000; pp 103-112.
- (73) Braff, D. L.; Geyer, M. A., Sensorimotor Gating and Schizophrenia. Human and Animal Model Studies. *Arch. Gen. Psychiatry* **1990**, *47* (2), 181-188.
- (74) Geyer, M. A.; Ellenbroek, B., Animal Behavior Models of the Mechanisms Underlying Antipsychotic Atypicality. *Prog. Neuropsychopharmacol. Biol. Psychiatry* **2003**, *27* (7), 1071-1079.

- (75) Geyer, M. A.; Krebs-Thomson, K.; Braff, D. L.; Swerdlow, N. R., Pharmacological Studies of Prepulse Inhibition Models of Sensorimotor Gating Deficits in Schizophrenia: A Decade in Review. *Psychopharmacol.* **2001**, *156* (2-3), 117-154.
- (76) Murphy, C. A.; Di Iorio, L.; Feldon, J., Effects of Psychostimulant Withdrawal on Latent Inhibition of Conditioned Active Avoidance and Prepulse Inhibition of the Acoustic Startle Response. *Psychopharmacology* **2001**, *156* (2), 155-164.
- (77) Graham, F. K., The More or Less Startling Effects of Weak Prestimulation. *Psychophysiology* **1975**, *12* (3), 238-248.
- (78) Ninan, I.; Kulkarni, S. K., Preferential Inhibition of Dizocilpine-Induced Hyperlocomotion by Olanzapine. *Eur. J. Pharmacol.* **1999**, *368* (1), 1-7.
- (79) Daya, R. P.; Bhandari, J. K.; Hui, P. A.; Tian, Y.; Farncombe, T.; Mishra, R. K., Effects of MK-801 Treatment Across Several Preclinical Analyses Including a Novel Assessment of Brain Metabolic Function utilizing PET and CT fused Imaging In Live Rats. *Neuropharmacology* **2014**, *77*, 325-333.
- (80) Martin, R. S.; Secchi, R. L.; Sung, E.; Lemaire, M.; Bonhaus, D. W.; Hedley, L. R.; Lowe, D. A., Effects of Cannabinoid Receptor Ligands on Psychosis-Relevant Behavior Models in the Rat. *Psychopharmacology* **2003**, *165* (2), 128-135.
- (81) Wiley, J. L.; Kennedy, K. L., Evaluation of the Efficacy of Antipsychotic Attenuation of Phencyclidine-Disrupted Prepulse Inhibition in Rats. *J. Neural Transm.* **2002**, *109* (4), 523-535.
- (82) Le Pen, G.; Moreau, J.-L., Disruption of Prepulse Inhibition of Startle Reflex in a Neurodevelopmental Model of Schizophrenia: Reversal by Clozapine, Olanzapine and Risperidone but not by Haloperidol. *Neuropsychopharmacology* **2002**, *27* (1), 1-11.
- (83) Bubenikova, V.; Votava, M.; Horacek, J.; Palenicek, T.; Dockery, C., The Effect of Zotepine, Risperidone, Clozapine and Olanzapine on MK-801-Disrupted Sensorimotor Gating. *Pharmacol. Biochem. Behav.* **2005**, *80* (4), 591-596.
- (84) Cilia, J.; Reavill, C.; Hagan, J. J.; Jones, D. N. C., Long-Term Evaluation of Isolation-Rearing Induced Prepulse Inhibition Deficits in Rats. *Psychopharmacology* **2001**, *156* (2-3), 327-337.
- (85) Aravagiri, M.; Teper, Y.; Marder, S. R., Pharmacokinetics and Tissue Distribution of Olanzapine in Rats. *Biopharm. Drug Dispos.* **1999**, *20* (8), 369-377.
- (86) Skrede, S.; Martins, L.; Berge, R. K.; Steen, V. M.; López, M.; Fernø, J., Olanzapine Depot Formulation in Rat: A Step Forward in Modelling Antipsychotic-Induced Metabolic Adverse Effects. *Int. J. Neuropsychopharmacol.* **2014**, *17* (1), 91-104.
- (87) SamsDodd, F., Effect of Novel Antipsychotic Drugs on phencyclidine-Induced Stereotyped Behaviour and Social Isolation in the Rat Social Interaction Test. *Behav. Pharmacol.* **1997**, *8* (2-3), 196-215.
- (88) Aravagiri, M.; Ames, D.; Wirshing, W. C.; Marder, S. R., Plasma Level Monitoring of Olanzapine in Patients with Schizophrenia: Determination by High-

- Performance Liquid Chromatography with Electrochemical Detection. *Ther. Drug Monit.* **1997**, *19* (3), 307-313.
- (89) Vishal Gupta, N.; Gowda, D.; Balamuralidhara, V.; Mohammed Khan, S., Formulation and Evaluation of Olanzapine Matrix Pellets for Controlled Release. *DARU* **2011**, *19* (4), 249-256.
- (90) Mauri, E.; Perale, G.; Rossi, F., Nanogel Functionalization: A Versatile Approach To Meet the Challenges of Drug and Gene Delivery. *ACS Appl. Nano Mater.* **2018**, *1* (12), 6525-6541.
- (91) Anselmo, A. C.; Mitragotri, S., Impact of Particle Elasticity on Particle-Based Drug Delivery Systems. *Adv. Drug. Deliv. Rev.* **2017**, *108*, 51-67.
- (92) Anselmo, A. C.; Zhang, M.; Kumar, S.; Vogus, D. R.; Menegatti, S.; Helgeson, M. E.; Mitragotri, S., Elasticity of Nanoparticles Influences Their Blood Circulation, Phagocytosis, Endocytosis, And Targeting. *ACS Nano* **2015**, *9* (3), 3169-3177.
- (93) Mathison, S.; Nagilla, R.; Kompella, U. B., Nasal Route for Direct Delivery of Solutes to the Central Nervous System: Fact or Fiction? *J. Drug Target.* **1998**, *5* (6), 415-441.
- (94) Lochhead, J. J.; Thorne, R. G., Intranasal Delivery of Biologics to the Central Nervous System. *Adv. Drug Deliv. Rev.* **2012**, *64* (7), 614-628.
- (95) Hartmann, R.; Weidenbach, M.; Neubauer, M.; Fery, A.; Parak, W. J., Stiffness-Dependent In Vitro Uptake and Lysosomal Acidification of Colloidal Particles. *Angew. Chem. Int. Ed.* **2015**, *54* (4), 1365-1368.
- (96) Myerson, J. W.; Braender, B.; McPherson, O.; Glassman, P. M.; Kiseleva, R. Y.; Shuvaev, V. V.; Marcos-Contreras, O.; Grady, M. E.; Lee, H. S.; Greineder, C. F.; Stan, R. V.; Composto, R. J.; Eckmann, D. M.; Muzykantov, V. R., Flexible Nanoparticles Reach Sterically Obscured Endothelial Targets Inaccessible to Rigid Nanoparticles. *Adv. Mater.* **2018**, *30* (32), e1802373.
- (97) Saraiva, C.; Praça, C.; Ferreira, R.; Santos, T.; Ferreira, L.; Bernardino, L., Nanoparticle-Mediated Brain Drug Delivery: Overcoming Blood-Brain Barrier to Treat Neurodegenerative Diseases. *J. Control. Release* **2016**, *235*, 34-47.
- (98) Zhu, X.; Wu, J.; Shan, W.; Zhou, Z.; Liu, M.; Huang, Y., Sub-50 nm Nanoparticles with Biomimetic Surfaces to Sequentially Overcome the Mucosal Diffusion Barrier and the Epithelial Absorption Barrier. *Adv. Funct. Mater.* **2016**, *26* (16), 2728-2738.
- (99) Cui, Y.; Shan, W.; Liu, M.; Wu, L.; Huang, Y., A Strategy for Developing Effective Orally-Delivered Nanoparticles Through Modulation of the Surface “Hydrophilicity/Hydrophobicity Balance”. *J. Mater. Chem. B* **2017**, *5* (6), 1302-1314.
- (100) Vila, A.; Gill, H.; McCallion, O.; Alonso, M. a. J., Transport of PLA-PEG Particles Across the Nasal Mucosa: Effect of Particle Size and PEG Coating Density. *J. Control. Release* **2004**, *98* (2), 231-244.

- (101) Yu, M.; Xu, L.; Tian, F.; Su, Q.; Zheng, N.; Yang, Y.; Wang, J.; Wang, A.; Zhu, C.; Guo, S.; Zhang, X.; Gan, Y.; Shi, X.; Gao, H., Rapid Transport of Deformation-Tuned Nanoparticles Across Biological Hydrogels and Cellular Barriers. *Nat. Commun.* **2018**, *9* (1), 2607.

S5. Supporting Information**Table S5.1: Recipes of POH-OLAMA polymers containing 20 mol% OLAMA.**

	POH-OLAMA₄	POH-OLAMA₈
M(EO) ₂ MA	1.9 g	1.9 g
OEGMA ₅₀₀	2.1 g	2.1 g
OLAMA	2.35 g (m=4)	4.0 g (m=8)
AA	560 µL	560 µL
TGA ^a	75 µL	75 µL
AIBME	39 mg	39 mg
Dioxane	20 mL	20 mL

^a 10% in dioxane

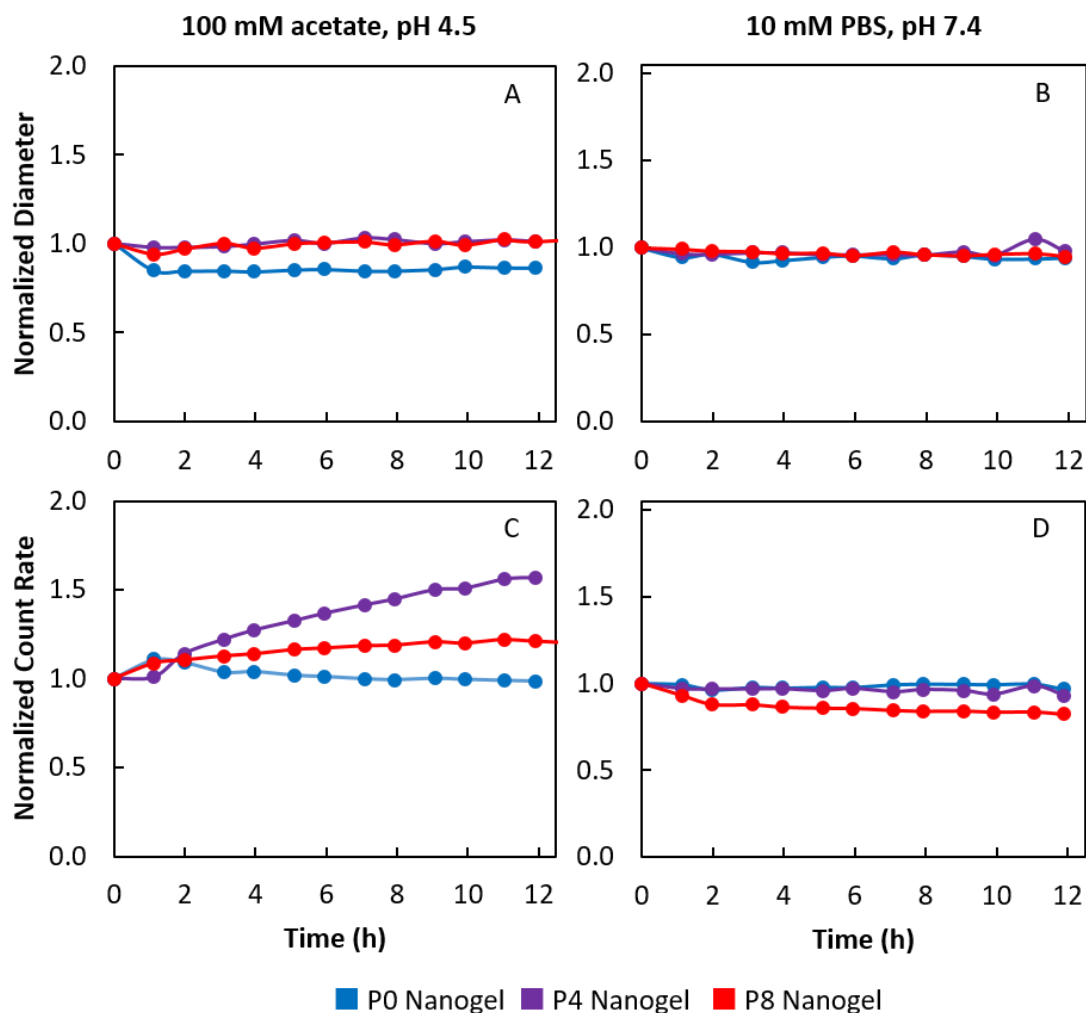


Figure S5.11: Nanogel degradation and stability. Incubation of self-assembled P0 (blue line), P4 (purple line) and P8 (red line) nanogels in (A,C) 100 mM acetate buffer, pH 4.5 and (B,D) 10 mM PBS, pH 7.4 at 37°C: (A-B) Normalized effective hydrodynamic diameter (from DLS); (C-D) Normalized count rate (from DLS).

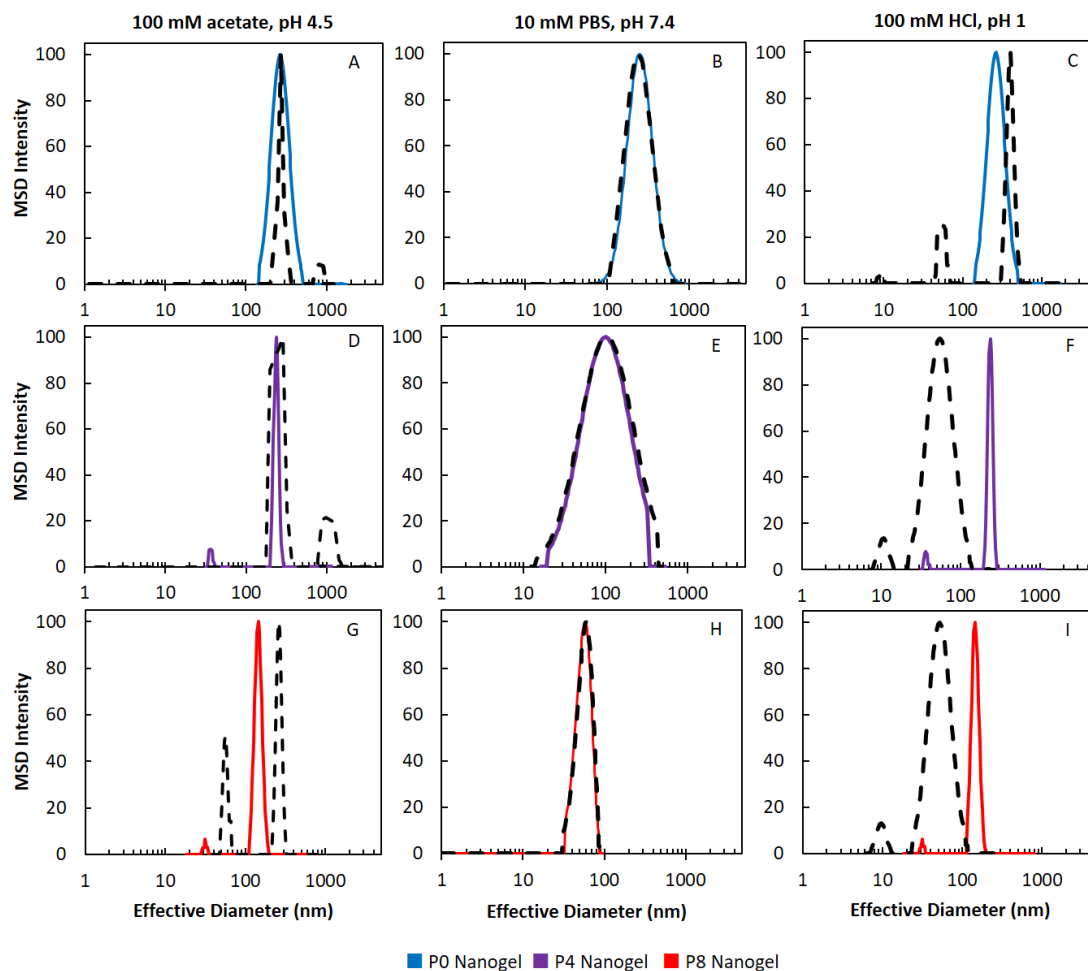


Figure S5.12: Multimodal intensity-based size distributions at t=0 h (solid line) and t=12 h (dashed line) (from DLS) of self-assembled PO (blue line, A-C), P4 (purple line, D-F) and P8 (red line, G-I) nanogels incubated in (A,C,G) 100 mM acetate buffer, pH 4.5; (B,E,H) 10 mM PBS, pH 7.4 and, (C,F,I) 100 mM HCl, pH 1 at 37°C.

Chapter 6 : Conclusions and Future Work

6.1 Summary and Conclusions

The overall goal of this Ph.D. thesis is to develop nanogels with tunable compositions and physiologically-relevant stimuli-responsive degradability for drug delivery applications. The specific focus, facilitated by a collaboration with a neuroscience research group, was on improving APD delivery to the brain by combining novel nanogel materials with the non-traditional yet advantageous minimally-invasive IN route of administration known to enhance drug bioavailability to the brain. The development of unique nanogel formulations that leverage the known advantages of nanogels for drug delivery (swelling and stimuli-responsiveness) while addressing their key limitations relative to APD delivery (hydrophilicity and poor degradability) represents the key novel contribution of this research. The findings within should significantly motivate the use of nanogel-based drug delivery systems for clinical applications not solely restricted to schizophrenia but extending into the delivery of other hydrophobic therapeutics.

Chapter 1 provides an overview of the motivation for this work, including the current disease state globally and the associated impacts of managing a chronic neuropsychiatric disorder. The present understanding of the etiology of schizophrenia is described, with emphasis placed on how the uncertainty associated with the widely accepted disease hypotheses limits clinical diagnosis and treatment options. The available animal models

used for validation of APDs in rodents, and both the benefits as well as the limitations of such models, are discussed. The two distinct classes of clinically prescribed APDs are presented; their particular mechanisms of action, therapeutic advantages, as well as the associated detrimental side effects are thoroughly reported. Current routes of administration of APDs are discussed, and the advantages of the non-conventional IN route explored within the thesis are presented. The end of the chapter describes the current nanoparticle-based drug delivery systems explored in literature to-date and identifies that a particular class of nanoparticle, the nanogel, is underutilized for APD delivery due to its perceived associated limitations based on previously-established state-of-the-art techniques for nanogel fabrication.

Chapter 2 utilizes conventional precipitation polymerization to synthesize POEGMA-based nanogels. Hydrophobic domains derived from the co-polymerization of BMA and MMA (0-15 mol %) are incorporated into the otherwise hydrophilic nanogel structure, and their effect on nanogel swelling and the uptake of the highly hydrophobic atypical APD lurasidone was determined. Incorporation of the hydrolytically-labile cross-linker EGDMA enables nanogel degradation over time. High cell viability was reported toward these nanogels, consistent with the POEGMA-based gels being known to have cytocompatible and non-toxic properties. The lurasidone-loaded nanogel system enabled the attenuation of hyperlocomotion in a rodent model of MK-801-induced schizophrenia

using 4× less drug than required for IP administration, confirming the enhanced lurasidone bioavailability provided by the intranasal route. Biodistribution showed continued retention of fluorescently-labelled nanogels in the nasal tissue for up to two days and little to no accumulation in any of the typical clearance organs. This hydrophobized nanogel drug delivery system shows potential to minimize the adverse side effects associated with systemic administration of APDs by minimizing the effective dose required for therapeutic intervention.

Chapter 3 expands on the work accomplished within the previous chapter. Nanogels containing BMA and MMA are similarly synthesized, although larger quantities (0-25 mol %) of hydrophobic co-monomer are co-polymerized into the nanogel. Introduction of a longer chain oligo(ethylene glycol methacrylate) is also introduced at varying mole fractions (0-30%) within 10% BMA nanogels. These modifications were utilized to expand our understanding of how the hydrophilic/hydrophobic balance governs nanogel stability and affects swelling as well as drug uptake. It was determined that both sufficient hydrophobic domains to enhance drug affinity as well as the retention of nanogel swelling are necessary to promote high drug uptake; the incorporation of ≥ 15 mol% hydrophobic co-monomer causes nanogel collapse and a decrease in swelling and porosity that prevents drug diffusion into the matrix and thus reduces drug encapsulation. The cross-linking architecture of the nanogels was also modified to include a covalent, redox

responsive disulfide bridge to enhance nanogel degradability, which can be facilitated through a bioorthogonal reaction using endogenous glutathione. The dose-dependent response of the degradable haloperidol-loaded nanogels was quantified by assessing two behavioural changes in rodents. A low 0.3 mg/kg dose was necessary to decrease rodent locomotion, considered to be a therapeutic benefit; a higher 1 mg/kg dose was required for the onset of catalepsy, a side effect considered comparable to EPS in humans. Such cataleptic responses were induced at a drug dose half of the 2 mg/kg free HLP drug solution administered IP previously reported. The enhanced bioavailability of IN administered APDs is reinforced by this work, as is the potential for this drug delivery system to be employed to deliver a variety of hydrophobic therapeutics requiring CNS access.

Chapter 4 pivots to examining a different nanogel synthesis technique developed in the Hoare research group. Aqueous nanogel self-assembly, made possible by thermoresponsive precursor polymers of aldehyde and hydrazide functionalized POEGMA, is explored. A systematic approach to nanogel self-assembly is investigated by interchanging the core and cross-linking polymers and varying the quantity of core polymer, ratio of cross-linking to core polymer, and temperature at which the self-assembly reaction is conducted relative to the core polymer's LCST. Multivariate statistics are used to analyze the effect of the process parameters on nanogel size and

polydispersity, identifying a non-linear relationship between the self-assembly variables and nanogel properties that suggests a complex chemical process that cannot be adequately modeled by a linear function. The scalability of a colloidally stable nanogel formulation with a moderate nanogel size (~280 nm) and low polydispersity ($PD < 0.15$) with the potential for biomedical applications was identified for further investigation. Large-scale self-assembly (50 mL) produced nanogels with properties comparable to the small-scale batch (6.5 mL), indicating the potential of this method to produce nanogels with tunable sizes for drug delivery and other clinical applications.

Chapter 5 implements the self-assembly strategies established in Chapter 4 to synthesize self-assembled nanogels containing hydrophobic domains of OLAMA. The hydrazide-functionalized POEGMA polymer is modified to include 20 mol% of short chain (4 or 8 repeats) OLAMA. Drug uptake of the atypical APD olanzapine is investigated both during and after self-assembly. The limited aqueous solubility of olanzapine prevented high loading capacity during the self-assembly reaction; however, drug incorporation post-synthesis via passive diffusion enabled encapsulation of therapeutically-relevant quantities of the APD, albeit with significant changes in nanogel size. The acid-catalyzed hydrolysis of the cross-linking hydrazone bond was investigated under acidic physiological conditions (pH 4) as well as accelerated conditions (pH 1) to demonstrate degradability. Drug release kinetics showed linear, sustained release with <15% of the total drug

released within 2 weeks, indicating that prolonged release using these nanogel formulations is possible. PPI behavioural studies in rodents treated with MK-801 revealed the time-dependent response associated with drug release. Restoration of PPI was not produced until 6 hours post-IN administration, indicating a lag in therapeutic onset not previously shown by the other nanogel formulations; however, following that lag, PPI was retained for 24-48 hours depending on the nanogel formulation. As these nanogels are larger, we hypothesize that the lag in onset can be attributed to both slower permeation of the nanogels into the nasal epithelium and the slow rate of drug release shown by the *in vitro* release kinetics. This chapter outlines that newer techniques for nanogel synthesis can produce viable materials for drug delivery that encompass the key advantageous parameters of nanogels.

6.2 Future Work

The research presented within this thesis utilizes novel, hydrophobized nanogel formulations with tunable chemical compositions, swelling, and externally-triggerable degradability coupled with the minimally invasive nose-to-brain delivery route to improve the bioavailability of various clinically prescribed APDs. The drug delivery systems presented herein have the potential to form a platform for the delivery of hydrophobic drugs to the central nervous system by exploiting the minimally-invasive IN route of administration. The ability to select materials that tailor nanogel chemistry to enhance

the affinity for hydrophobic drugs by improving their solubility, as well as the opportunity to exploit the unique swelling and elastic properties of nanogels to deliver larger particles encapsulating bigger payloads of drugs through biological barriers typically accessible only with smaller nanoparticles, are design considerations that can be widely applied to strategically deliver other types of hydrophobic drugs. As such, other currently prescribed APDs as well newly-developed APDs that are increasingly hydrophobic can be explored for their encapsulation and delivery potential using the described systems. Utilization of these nanogel systems to deliver therapeutics for the treatment of other CNS diseases such as Alzheimer's, Parkinson's and Huntington's as well as depression and anxiety also has potential. Alternately, the incorporation of drugs with anti-cancer activity for the treatment of glioblastoma, such as doxorubicin and paclitaxel that are also known to be poorly water-soluble, could benefit from the proposed targeted method of delivery as it can avoid the systemic circulation of cytotoxic drugs.

Additional future work that can be explored related to Chapter 2 is the completion of drug release studies. The low solubility of lurasidone in the majority of solvents makes it very difficult to detect using high-throughput methods relying on column separation such as HPLC and LC-MS/MS. Considerable effort was put forth to optimize detection methods using these systems; however, drug accumulation in columns caused carry-over into subsequent samples (despite substantial washing between) that led to unreliable data

collection and also introduced significant pressure problems. As a result, while UV-visible spectrophotometry could be effectively utilized for drug loading quantification, its limit of detection was not sensitive enough to quantify the low levels of lurasidone release in aqueous media. Further probing of alternate quantification methods is suggested. In addition, the biodistribution studies revealed that sustained levels of nanogel were retained in the nasal tissue for at least two days. This indicates that longer chronic time points need to be examined to determine when and how the nanogel is eventually cleared. This also motivates the investigation of additional behavioural study time points to determine if nanogel retention correlates with sustained drug release or if the two components decouple and only the nanogel persists.

The locomotor data presented in Chapter 3 revealed that IN administration of the 10% BMA 100:0 and 10% MMA 100:0 non-drug loaded nanogels could attenuate locomotor activity. We hypothesize that the presence of nanogel within the nasal cavity could prevent some of the sensory-stimulated movement that typically drives locomotion; however, further investigation is warranted on this point. Receptor binding assays could be probed to determine if there are meaningful interactions occurring. Histology on the nasal tissue and brain could also be conducted to determine if there is any inflammation or cytotoxicity concerns that could cause this outcome.

When methods for self-assembly scale up were proposed for inclusion in Chapter 4, increasing the polymer concentration was also proposed as an alternative to increasing the self-assembly volume. As shown in the published journal article, increasing the volume was selected as we felt this method more clearly implemented engineering solutions that were most relevant to the topic of the publication. However, the synthesis of high concentrations of self-assembled nanogels was executed and determined to be possible. Over time, these samples were also observed to transition from stable colloidal suspensions of nanogels to form macroscale hydrogels due to the transient nature of the hydrazone bonds and the excess unreacted hydrazide groups. This has only ever occurred in nanogel samples synthesized at high 10 wt% concentrations; the 0.5 and 1 wt% formulations reported in Chapters 4 and 5 have never produced macroscopic gelation over the many months they have been stored. Although not yet further characterized, this transition could be exploited as an alternate formulation for depot LAI. As the current limitations associated with IM LAIs are due to the pain and irritation caused by the oil-based deep tissue injections, the aqueous self-assembled nanogels could provide a more tissue-compatible alternative. Essentially, the transition from nanogels to macroscopic hydrogel represents an example of *in situ* gelation to create a different mesh-like polymer structure. As the drug release kinetics from the nanogels alone are slow, the formation of the macroscopic hydrogel could impart additional barriers to drug release, possibly resulting in a biphasic yet sustained drug release pattern. As this could be viewed as a

novel composite material as it transitions from nanogel to macroscopic hydrogel, possible investigation as a drug delivery vehicle could reveal unique characteristics.

The promising findings reported in Chapter 5 could be supplemented with additional behavioural studies. The focus of the presented PPI data was to determine the minimal effective dose required IN to elicit a significant therapeutic behavioural response. The next level of beneficial therapeutic efficacy would be to determine if a larger IN dose can be provided that enables a substantial difference in drug dosing frequency (i.e. transition from daily to weekly). Complementary biodistribution studies could also accompany this data. As the conventional nanogels in Chapter 2 show surprising long-term retention in the nasal tissue, comparable investigations should examine if this is characteristic of hydrophobized POEGMA nanogels regardless of their synthetic route.

Finally, the APDs employed in this thesis are all FDA approved and are currently clinically prescribed for the treatment of schizophrenia. As such, the pharmacokinetics studied within this thesis focused on the nanogel material, as it is the novel component of the drug delivery system. In order to facilitate clinical translation of these drug delivery systems, simultaneous examination of the biodistribution of both the drugs and the nanogels in preclinical models would be useful to gain a greater understanding of the observed behavioural responses and further substantiate and validate controlled release

kinetics *in vivo*. Cross-species translation of drug dosing information is also challenging due to the metabolic differences between rodents, primates (the typical clinical model), and humans. As such, using more advanced screening techniques, such as *ex vivo* tissue studies or organ-on-a-chip technology, would enable the evaluation of pertinent tissue interactions such as inflammation and receptor binding that could provide valuable safety and toxicity information to reinforce the pursuit of clinical translation and/or identify additional considerations to address prior to pursuing more involved studies. The introduction of nanogels facilitating controlled release adds additional complexity to translation as biodegradable moieties affect nanogel erosion and also influence drug release kinetics. As drug dosing frequency is known to effect maintenance of steady-state plasma levels of therapeutics and also plays a significant role in the risk of adverse side effects, elucidating the frequency and minimal effective APD dose is an additional, significant portion of work that can improve the safety and efficacy of these nanogel systems.